Micromolecular approaches to protein binding

Azrah Abdul Aziz

Department of Chemistry
The University of Sheffield

Submitted to the University of Sheffield
In fulfilment of the requirements for the degree of
Doctor of Philosophy

June 2019

ACKNOWLEDGEMENTS

Alhamdulillah, all praise to the Lord, the one that created me and made my dream come true. First and foremost, I would like to express my utmost gratitude and special appreciation to my supervisor, Dr Lance Twyman for his priceless guidance, encouragement, support, invaluable advice, kindest suggestion and constructive comments in completing this thesis. I would also like to thank the entire Twyman research group who presented a wonderful atmosphere to work and helped me through this journey as one family, notably Dr Muhammad Azrul Zabidi, Dr Alaa Kadhim, Dr Devanshi Singh, Dr Fatema Aboshnaf, Dr Hamza Qasem, Dr Jawad K Abaies, Dr Greg Clixby, Miss Samira Hussein, Mr Ibrahim Althobaiti, Mr Bunian Shareef, Mr Talal Alghassab, Mr Fan Meng and all my previous Mchem students that involved in this project.

A tribute to my late mum and dad; Muntamah and Abdul Aziz. How this thesis can be dedicated to you? Because you mean more than this! Thank you for giving me families and caring sisters that are teaching me what the meaning of being strong. To my sisters (informal mum assistant); Aziah, Azlin, Azmin and Azah, perfect sister I am not, but I am so thankful for the ones I have got. I would like to convey my sincere appreciation to my in-laws that give a precious gift from heaven, my caring and a lovely husband; Azhari Abd Aziz. To you love, I can't begin to explain how important it has been to have your support. You have been by my side from the start and this is all our relationship has ever known. For my beautiful and genius daughters; Arriessa Batrisyia and Naaila Kheesya Khayra, this is for you! Thank you because you still love your grumpy mummy, and I am deeply sorry because our journey was not as beautiful as we imagined.

Last but not least, I would like to thank everyone who has helped me directly or indirectly towards completing this research project.

ABSTRACT

This research described in this thesis examined two main macromolecules as ligands for protein binding, namely dendrimers and graphene oxide. The architecture of these materials was exploited and functionalised with amino acid to moderate protein binding and recognition.

The first area studied involved dendrimers that had been functionalised using non-covalent methods. Specifically, the amino acid was added to the end of a hydrophobic linear chain that could bind to the interior of the dendrimer using hydrophobic and hydrogen bonding interactions. A number of different linear chains were synthesised and added to various dendrimers to give a surface functionalised system. The dendrimers included an anionic dendrimer that was functionalised with linear chains in order to provide secondary interactions that could bind to the positively charged surface of α-chymotrypsin (Chy). Neutral dendrimers that could not bind to the positive surface were also studied. In this case, binding could only occur if the dendrimers were functionalised with the linear chains.

The results showed that the highest affinity occurred for the G3.5COOH-Tyr, with the inhibition constant (K_i) of 0.17 µM, which compares to the K_i for non-functionalised dendrimer of 0.31 µM . When the non-binding dendrimer (G3.5-OH) was functionalised with different amino acids (tyrosine, phenylalanine and valine), the G3.5-OH-Tyr was found to bind the most strongly via polyvalent interactions between the amino acids and the surface of the Chy. All the inhibitors studied were found to be competitive inhibitors, with the exception of the valine functionalised dendrimer, which did not bind. Circular Dichroism **(**CD) spectroscopy confirmed that denaturation of the protein did not occur during dendrimer binding.

The next area of study focused on cytochrome- c. The same non-covalent methodology used for α-chymotrypsin binding was utilised for this area. Binding could be measured directly using encapsulated Tetrahydroxyphenyl Porphyrin (THPP) as an internal quench. To coordinate THPP to the dendrimer, this was strengthened by inserting zinc, which could coordinate the dendrimer's internal amines. The results showed that the G3.5COOH-Tyr was bound with a dissociation constant (K_d) of 5.55 nm. CD spectroscopy showed that the dendrimer-porphyrin-chains did not cause denaturation of the protein during binding.

The final area focused on the use of functionalised graphene oxide (GO). This material was synthesised with amino acids to form a monomeric and an oligomeric functionalised surface of GO. The effects of functionalisation on the binding of GO to Chy was also studied. The binding of the functionalised GO was compared with the binding of the unfunctionalised GO and the results showed an inhibition constant (K_i) of 0.14 µg/mL for the monotyrosine, which was higher than either the oligomeric system or GO alone. In all cases, competitive inhibition was observed. CD spectroscopy confirmed that GO does not induce structural changes within the protein when bound and the spectroscopy also demonstrated that the GO inhibitors had no effect on the thermal stability of the enzyme.

ABBREVIATIONS

PAMAM Poly(amido amine)
PAMAM-OH Neutral Hydroxyl Terminated PAMAM
PAMAM-COOH Acid Terminated PAMAM
DCC Dynamic combinatorial chemistry
DCLs Dynamic combinatorial libraries
DCM Dichloromethane
DCCI Dicyclohexyl carbodiimide
DCU Dicyclohexyl urea
DMSO Dimethylsulphoxide
EDA Ethylenediamine
EDC 1-Ethyl-3-(3-dimethylaminopropyl)carbodiimide
DMAP 4-Dimethylaminopyridine
MA Methyl Acrylate
BTNA N-benzoyltyrosine-p-nitroanilide
^{1}H NMR Proton Nuclear Magnetic Resonance Spectrometry
^{13}C NMR Carbon-13 Nuclear Magnetic Resonance Spectrometry
IR/FTIR Infra Red/Fourier Transfer Infra Red Spectrometry
ES-TOF MS Electron Spray Time-Of-Flight Mass Spectrometry
MALDI-TOF MS Matrix Assisted Laser Desorption Ionisation Time of Flight
SEM Scanning Electron Microscopy (SEM)
EDX-SEM Energy Dispersive X-Ray Analysis-SEM
GO Graphene Oxide
XPS X-ray photoelectron spectroscopy
XRD X-Ray Diffraction
Chy α-chymotrypsin
Cyt-c cytochrome-c
NaOH Sodium Hydroxide
K_2CO_3 Potassium Carbonate
TRIS Tris(hydroxymethyl)aminomethane
UV/Vis Spectrometry Ultra Violet/Visible Spectrometry

NMR Abbreviations

δ Chemical Shift
ppm Parts Per Million
s Singlet Peak
sept Septet Peak
d Doublet Peak
t Triplet Peak
q Quartet Peak
m Multiplet Peak

Table of Contents

Chapter 1

Introduction

1.0 Introduction

Protein-protein complexes originate from interactions between proteins and are differentiated as homocomplexes, which typically display stability and endurance, and heterocomplexes, which display the property of formation or breakdown by extrinsic factors, besides being enduring as well. Given their characteristics, heterocomplexes present the necessary condition of participation of a protein capable of autonomous existence. Among the various biological processes that are reliant on such protein aggregates are signal transduction, cytoskeletal remodelling, cell regulation, immune response, and viral self-assembly.[1] Disease processes (e.g. homodimeric complex HIV-1 protease, Alzheimer's, different types of rheumatoid arthritis) [2] may arise, however, if proteins do not interact in a normal way. Furthermore, specific protein-protein complexes are disrupted in several cancer treatment strategies. For instance, in cancers associated with prolonged cMyc activation, c-Myc inhibitors play a key role. [3] The development of plaque molecules may be hindered through targeting and disruption of such interactions, thus potentially contributing to disease treatment (Figure 1).

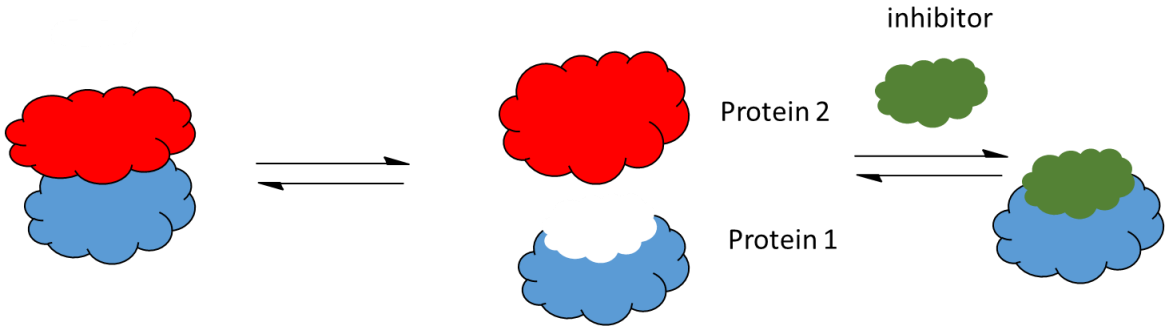

Figure 1: Suppression of protein binding.

1.1 Understanding protein protein interactions

A wide variety of primary structures emerge from the combination of the 20 existing natural amino acids in particular sequences, and in turn fold into proteins with tertiary and quaternary structures that differ considerably. It is this variety that enables proteins to perform a multitude of different roles.[4] There are numerous proteins that produce protein-protein complexes with typically non-covalent binding of at least two proteins to give rise to active compounds as illustrated in Figure 2.

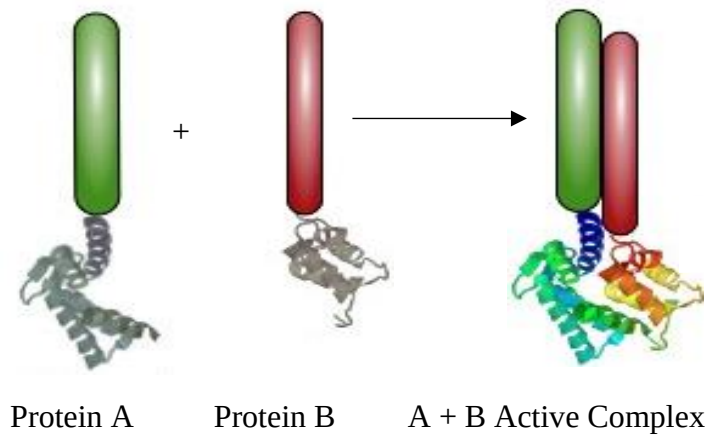

Figure 2: Representation of a combined active complex

Owing to cooperative binding that endows molecule-molecule interactions with stability, these forces gain a strength collectively that they lack on their own.[5] Various biochemical and biological processes can unfold on the basis of cooperative binding. Increase in apparent affinity reflects positive cooperation, enhancing the probability of binding of a second molecule. It is possible to interpret this as a significant rise in the relative concentration of the ligand for the second binding.[6] The outcomes of cooperative binding are illustrated in Figure 3. The formation of the initial bond occurs between the ligand and the original binding site at a rate K_1. After the formation of this bond, the formation of the second interaction not only occurs significantly quicker but also exhibits greater strength, since the relative concentration of the second ligand exceeds that of other molecules. K_1 is substantially smaller than K_2 so this effect is non-additive, while cooperative binding has a markedly more additive effect.

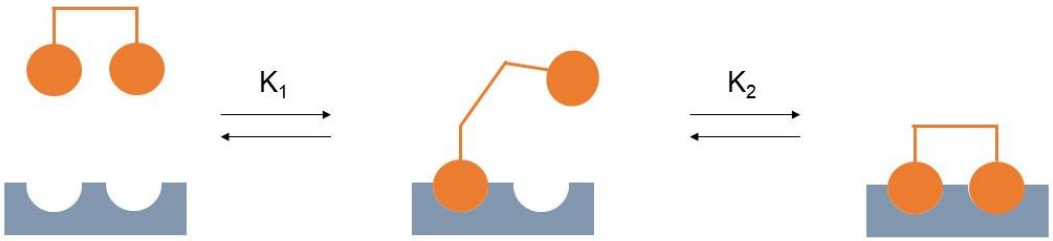

Figure 3: The effects of cooperative binding, with K_1 considerably smaller than K_2

Specific amino acids are much denser within the binding interfaces than in the other parts of the protein molecule. By comparison to the molecule exterior, these amino acids exhibit a higher degree of hydrophobicity, so binding interactions between proteins could be enhanced by taking advantage of hydrophobic interactions. Furthermore, aromatic amino acids of large size tend to be preferred at the binding interfaces, and a binding surface is the most probable part of the protein where amino acids like tyrosine occur.[7-8] Potential target proteins for assessing the binding capacity of the polymers as well as their ability to differentiate among protein surfaces in the same enzyme family are provided in Table 1. Disruption of interactions between proteins with synthetic inhibitors is based on the mechanism of formation of robust affiliated synthetic subunit complexes of molecules and proteins to hinder protein subunits from interacting with each other.

Mechanism	Protein	Amino acid residue	Inhibitor	Cleavage site
Serine protease	Elastase	240	*α*-anititrypsin	Ala, Gly
	α-chymotrypsin	241	Aprotinin	Phe, Tyr, Trp
	Trypsin	233	*p*-amino-benzamidine	Arg, Lys
	Kallikrein	619	Aprotinin	Arg
	Thrombin	308	Argatroban	Arg
Zinc protease	Carboxypeptidase A	307	Benzomercapto-propanoic acid	Phe, Trp, Leu
Aspartate protease	Cathepsin D	346	Pepstatin A	Phe-Phe

Table 1: Enzymes according to their customary inhibitor and cleavage site. Summarised table taken from Gilles et al., Biomacromolecules, 18(6), pp. 1772–1784, 2017.

1.2 Hot spots and interfacial area

However, it is important to gain insight into protein-protein recognition site interfaces and manner of binding prior to application of that approach. Among the key facets of protein-protein interfaces that need to be taken into account are size, shape, structure and qualities of amino acid residues, conformational modifications engendered by the development of complexes, the interrelation of reciprocity among surfaces that come into contact, as well as forces of interaction. [5, 7, 9] When protein-protein complexes are formed, solvent can no longer reach the extensive interfacial area on a protein, which largely displays hydrophobicity and has polar groups around it.[8] The interface surface area in the majority of proteins is between 500 and 5000 Å^2, as shown in Figure 4. [10 -11] For instance, cytochrome c and its analogue cytochrome- c peroxidase have an interfacial area of about 1150 Å^2, while chymotrypsin and its protein analogue have an interfacial area of about 2200 Å^2. At first, it was believed that the hydrophobic binding between contact amino acid groups was the reason for the free energy of binding and a series of intermolecular interactions across the whole interfacial area characterised by lack of strength and poor affinity yielded the interactions between proteins. [12]

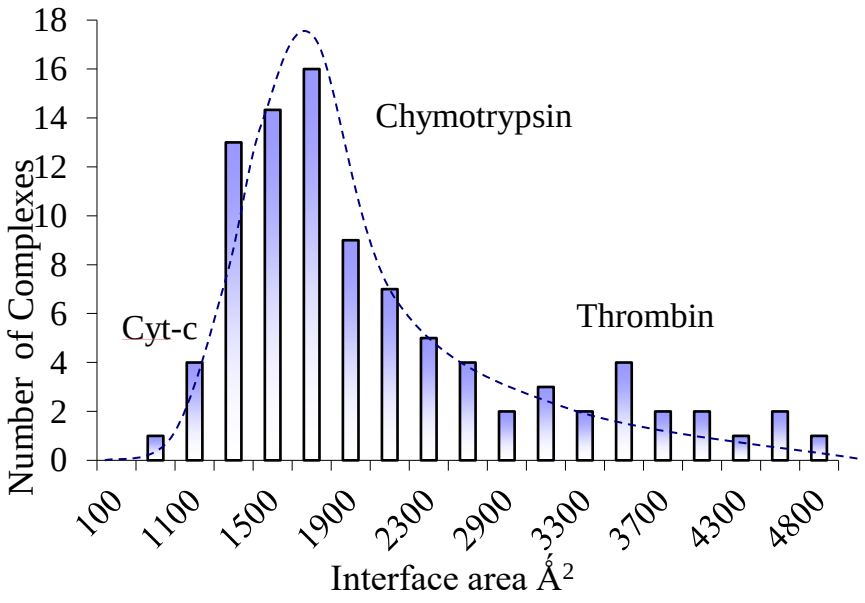

Figure 4: Illustration of the manner in which interfacial areas from typical protein-protein complexes are distributed

In the case of interactions between proteins, binding involves a couple of interactions of great strength and high affinity across a surface area of more limited proportions, was recognised by Wells and Clarkson known as the 'hot spot'.[9, 13] As evidenced by Bogan and Thorn, the hot spot represents a pre-organised surface of small dimensions on the surface of the protein supplemented with amino acids (e.g. tyrosine, tryptophan, arginine).[12] Furthermore, the fitting of complementary proteins is frequently possible due to the depressions and concavities it presents. Although it is possible for a protein to have more than one hot spot on its surface, the emerging complex must demonstrate stability and low energy for binding to occur through a particular hot spot.[21] Moreover, specific amino acids are preferred, since hot spots do not contain arbitrary compositions of amino acids.[12]

Given the above considerations, binding between proteins may be prevented via two distinct mechanisms, namely, targeting of the protein inner active site that is inaccessible to bulk solvent and targeting of the protein external surface that is accessible to bulk solvent.[14]

1.3 Small molecule inhibitor

Development of small molecules as possible inhibitors has garnered considerable attention. In general, interaction with the active site or a particular site of an enzyme is the purpose driving the development of small molecules. Hydrogen bonding, electrostatic interactions and salt bridges are the main types of interactions in the active site of a protein. Hence, such interactions could benefit from small 'drug-like' molecules demonstrating hydrophilicity and hydrogen bond donor groups.[15] Nonetheless, the creation of synthetic agents customised for targeting interactions between proteins is no easy task. One difficulty for small molecule inhibitors is that a relatively large area is necessary for recognition (700-1500Å^2 per protein).[9] Moreover, selective targeting is challenging because interacting surfaces take the form of shallow depressions without distinctive characteristics. The non-contiguous nature of the binding area of two interacting proteins is also problematic in terms of replication with basic synthetic peptides.[15] Furthermore, protein-protein interaction surfaces exhibit greater complexity than interaction surfaces between enzymes and ligands, which interferes with inhibitor development due to the fact that both proteins can present projections and pockets, rather than merely providing and filling a pocket, respectively.[16]

Additionally, the *in vivo* effectiveness of small molecules considered for use as possible drug molecules must be confirmed, and besides being highly effective against a particular protein, they must be minimally toxic and adequately bioavailable as well.

Figure 5 illustrates an existing commercially available inhibitor called Maraviroc, which represents a chemokine CCR5 receptor antagonist designed to target the viral reverse transcriptase or protease enzymes in the context of human immunodeficiency virus (HIV) therapy.[17]

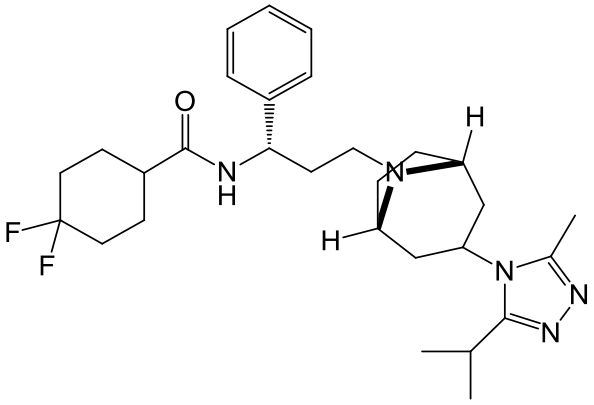

Figure 5: The chemical structure of Maraviroc

The chemical structures of certain inhibitors, such as Nutlins, are unlike those of the pharmacophores in other families of drugs that are known.[18] Nutlin-3 was chemically optimised and created as shown in Figure 6, exhibiting the ability to suppress *h*DM2-p53 complexes with an IC_{50} of 90 nM, as well as *in vivo* effect against xenografts.

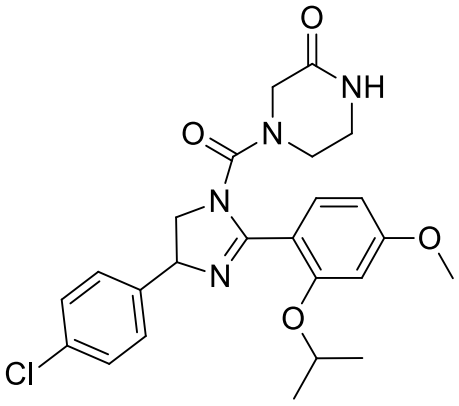

Figure 6: The chemical structure of the cis-imadazoline Nutlin

Inducible nitric oxide synthase (iNOS) is a major protein target. Produced by the dimeric enzyme nitric oxide synthase, the molecule nitric oxide plays a critical role in signal transduction. The enzyme presents the inducible isoform iNOS, which is believed to contribute to tissue damage in different autoimmune diseases. Hence, inhibitors selectively targeting iNOS could be beneficial for therapy. Combinatorial chemistry was employed by McMillan and colleagues to design an iNOS inhibitor (Figure 7). Disruption of the substrate binding site and dimerization interface was validated by X-ray crystallography studies. The action mechanism of the inhibitor involves interference with dimer formation. The inhibitor was shown by *in vivo* research on rat models to have activity with ED_{50} values of less than 2 mg/kg, confirming it as a promising therapeutic agent.[16,19]

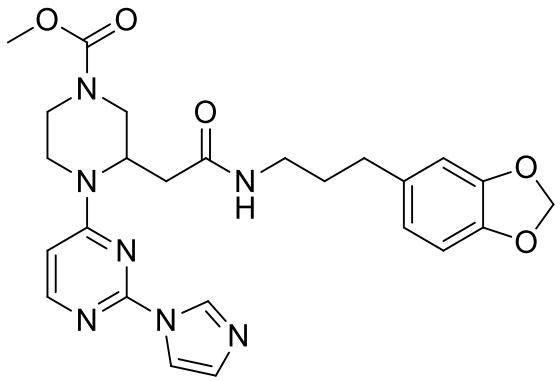

Figure 7: The chemical structure of iNOS inhibitor 86

Belonging to the family of cytokines, tumour necrosis factor alpha (TNF-α) contributes to systematic inflammation and therefore it is a key target as well. Enbrel, Remicade and Humira are just some of the inhibitors created to directly suppress TNF-α and proven to be efficient in treating rheumatoid arthritis.[16] However, these developments do not detract from the desirability of small molecule inhibitors, which are beneficial because they are cost-effective and easy to administrate. Figure 8 illustrates the strong TNF-α inhibitor that has been developed.[20] Its action mechanism involves development of an inactive dimer through displacement of a subunit of the trimer with biological activity.

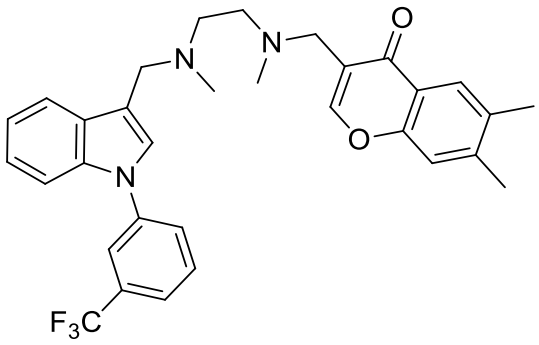

Figure 8: The chemical structure of TNF-α

1.4 α-Helix Mimetics

Peptides demonstrating stability (conformational robustness) and particular secondary structures have been designed as well. The achievement of suitable conformation stability requires over 15 amino acid residues. Recently, attention has been focused on the potential of stable β-turns and α-helices restricted by hydrogen-bond surrogate [21] and β-sheet systems for use in the treatment of various conditions, including cancer and HIV.[22]

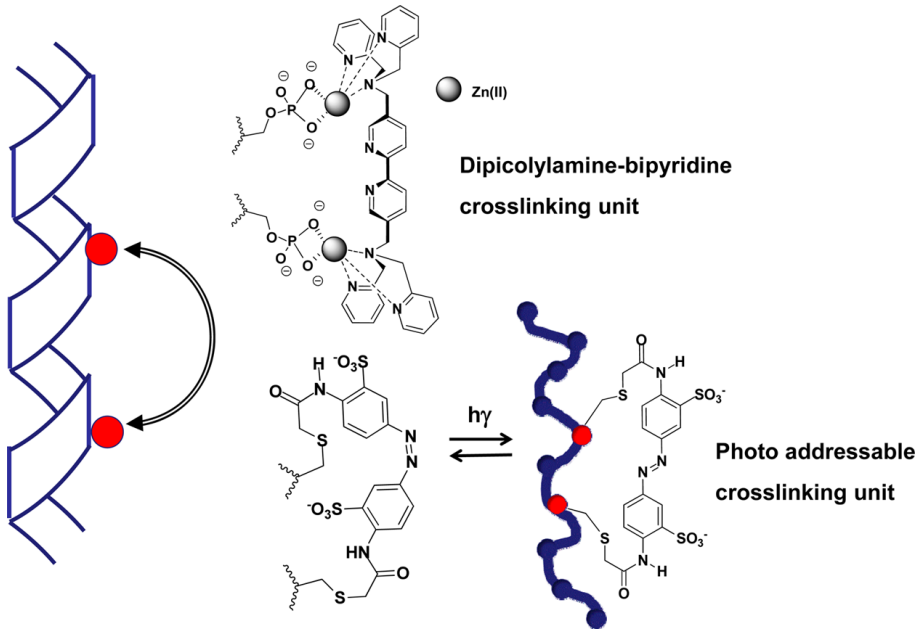

Figure 9: Cross-linking units of azobenzene and dipicolylamine-bipyridine

Peptide stabilisation has been attempted with azobenzene photoaddressable[23] and dipicolylamine-bipyridine[24] cross-linking units (Figure 9). These β-peptides are comparable to α-helices in terms of the side chains they exhibit along one face, although not all of them

have the same three-dimensional orientation. These systems are advantageous primarily because they are conformationally highly stable as well-defined protein secondary structures, whilst also being proteolytically stable.

A range of β-cyclodextrin dimers (β-CD) were employed by Breslow and colleagues [25] to show how protein aggregation was selectively disrupted (Figure 10). It was observed that protein aggregation was disrupted solely by β-CD compounds with depressions facing one another and adequately divided by a linker. This implies that inhibition depends on the character of the linker.

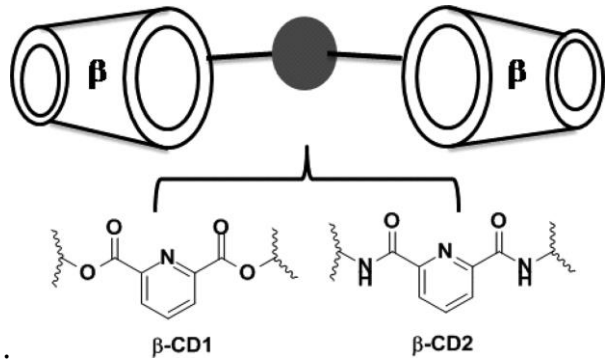

Figure 10: β-CD compounds facing one another and adequately divided by a linker

Terephthalamides and alkylidene cycloalkanes are also scaffold-type α-helix mimetics that have been suggested as possible α-helical mimetics.[26] A α-helical conformation was employed by Reymond and colleagues to develop peptide dendrimers. [27] Furthermore, significant attention has also been paid to the development of non-peptidic small molecule α-helical mimics as inhibitors of interactions between proteins. Meanwhile, a new pyrrolopyrimadine-based receptor was proposed by Lee and colleagues, as shown in Figure 11. [28] The capability of this scaffold as a α-helical mimic was assessed by monitoring the extent to which it could disrupt the interaction between p53 and MDMX. This involved screening the scaffold against a library comprising 900 compounds, followed by selection of primary amines comprising hydrophobic groups. The latter played a key role in replicating the side chains of the three amino acids contained in p53. Thus, the scaffold was confirmed to be conformationally rigid, highly soluble in water and cellularly permeable.

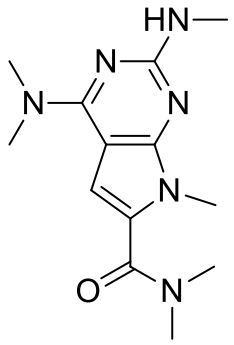

Figure 11: The chemical structure of the pyrrolopyramidine-based α-helix mimic

Small molecule inhibitors remain challenging to develop, [29] so other approaches for replicating selective mechanisms of interactions between proteins have been considered, involving interference with these interactions through attachment to the protein surface near rather than straight in the active site of the protein. No two proteins have the same peripheral surface, which is made up of areas of hydrophobicity, areas of hydrophilicity and charged areas. Furthermore, the interface between two interacting proteins includes not only electrostatic interactions, but also hydrogen bonding and π- π stacking interactions.[15]

The mechanism of most examined molecules involves binding within active depressions on proteins in order to inhibit interaction. By contrast, knowledge is limited regarding the mechanism of synthetic molecules that bind to the external surface to disrupt protein function. Thus, investigation of such molecules could lead to the discovery of new potential therapeutic agents as well as afford greater insight into protein periphery and surface recognition. [14]

1.5 Supramolecular protein scaffold

Self-assembled systems were used by Rotello for the purpose of surface recognition. The approach involved mixed-monolayer protected gold clusters (MMPCs) functionalised with terminal anionic groups binding to a-chymotrypsin surface with positive charge to suppress enzymatic activity via a two-step mechanism entailing rapid reversible suppression and subsequently a slower irreversible process of gradual enzyme breakdown. (Scheme 1). [30]

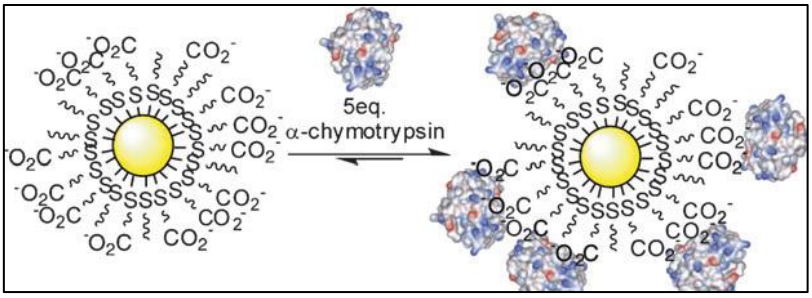

Scheme 1: Use of MMPCs for surface recognition

The developed electrostatic interactions were proven to be effective as the process displayed selectivity by comparison to elastase. The high efficiency of the interaction between the gold nanoparticle and *α*-chymotrypsin was confirmed through circular dichroism spectroscopy, with 10 nM K_i(app) and stoichiometry comprising five protein molecules to one MMPC. Furthermore, the inhibitory mechanism showed higher selectivity towards *α*-chymotrypsin than towards β-galactosidase.

An inhibitor derived from graphene oxide (GO) layers has elicited interest as well. The surface carboxylate group served as both a synthetic receptor and inhibitor of *α*-chymotrypsin activity, demonstrating a higher *α*-chymotrypsin suppression based on dose response (by weight) than the rest of the synthetic inhibitors that have been proposed.[31] Meanwhile, Wang and colleagues provided evidence that a nanocomposite material could be developed by integrating GO and iron oxide (IO) and could aid the development of novel drugs for treating Alzheimer's Disease.[32]

Other potential protein inhibitors of note are dendrimers, which have terminal groups that improve their interaction with hot spot residue. Due to their similar size and contours of key proteins, dendritic polymers are frequently called artificial globular proteins. [33] Two distinct dendrimeric peptide mimics were proposed by Fassina; those mimics were underpinned by four copies of the tripeptide Arg-Thr-Tyr (L-amino acids) or a partial-retro-inverso (Arg-Thr-Tyr, D-amino acids) connected to a polysine core characterised by lack of symmetry.[34] A natural amino acid series yielded the highest effectiveness. Meanwhile, evidence was brought forth by Twyman that dendrimers could be used to suppress chymotrypsin and cytochrome-c, and therefore they had potential for development of a binding mechanism

with size selectivity. Figure 12 shows the PAMAM dendrimers that were employed.

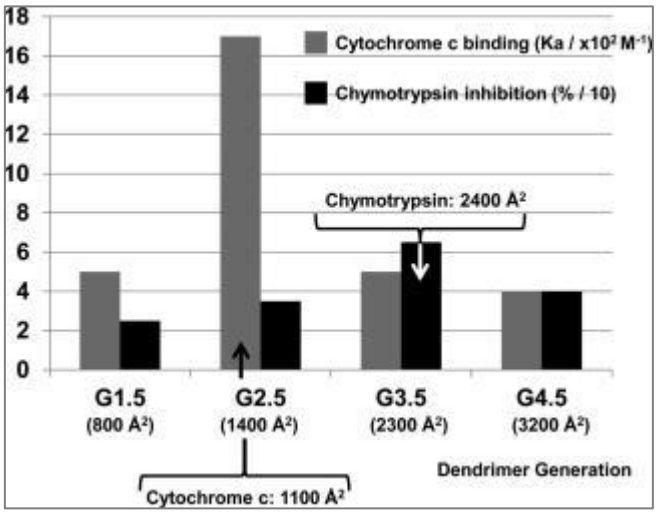

Figure 12: Binding and inhibition studies of PAMAM dendrimers

In other words, for a given protein, the dendrimer with an addressable area of similar size to the interfacial area of the protein in question is capable of most efficient binding. Enzymatic function is suppressed as a result of interaction between a large ligand and the enzyme active site, which basically obstructs the active site. This is why the dendrimers with the highest inhibition potency are the ones showing most effective binding.[35]

The approach of dendrimer-supported dynamic combinatorial chemistry (DCC) proposed by Ronald involves using dendrimers as soluble supports. DCC is distinguished by solution phase chemistry, homogeneous purification, routine characterisation of intermediates, and high support loadings. According to the findings obtained, combinatorial libraries can be effectively produced via DCC. Hence, since they facilitate molecular network accessibility, dynamic combinatorial libraries (DCLs) can be argued to have potential for the development and investigation of chemical complexity.[36]

1.6 Dynamic Combinatorial libraries

Aggregations of molecules in constant and reversible equilibrium are known as DCLs. By employing covalent or non-covalent interactions, these molecules are capable of assembling themselves into complexes and are controlled thermodynamically.[37] The relative stability of every constituent determines the DCL structure and in turn it is determined by exposure to extrinsic factors or templates, like a protein (Figure 13).[38]

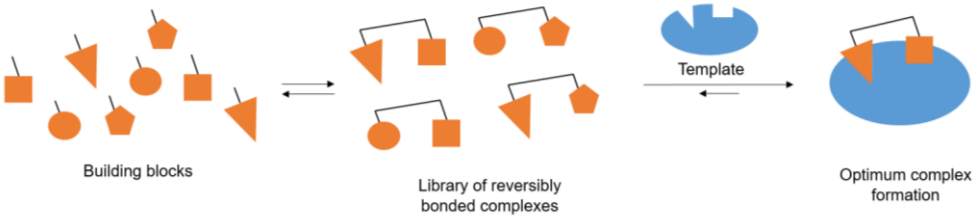

Figure 13 : Dynamic Combinatorial libraries

Based on the use of DCLs, a template molecule can be added to the reaction to drive it to the product exhibiting the most potent affinity for the template according to size and non-covalent effects. The implication of this is that it is possible to target optimum dendrimer-chain complexes for employing proteins as template molecules to identify the arrangement having the greatest affinity for binding. Thus, the usually protracted process of identification of new drugs can be sped up by developing DCLs for medicinal chemistry.[39]

Chapter 2

Non-covalent functionalised dendrimers to inhibit α-chymotrypsin

2.0 Introduction

There is widespread agreement that collaborative partnerships with other proteins is the basis of operation for the majority of proteins, despite a lack of clear understanding of these partnerships. There is basically no biological function that does not rely on protein-protein complexes, [40] which is why interaction between two proteins does not happen arbitrarily or in an uncoordinated manner, but is closely regulated towards the achievement of a specific goal. [41] Accumulations of proteins give rise to amyloid plaques and may be the result of impaired interactions between proteins. Therefore, conditions associated with amyloid plaques could potentially be treated by hindering the development of such plaques through disruption of protein-protein interactions.

As mentioned before, the binding or interfacial area of a protein, which is referred to as the hot spot, is usually 500-5000 $Å^2$. [7,42] Such interacting surfaces typically have a high charge and simple (polyvalent) electrostatics underpin interactions on the whole. Charged assemblies of polymers represent favourable structures for binding to external protein surfaces, as the majority of the ones without membranes present charged external surfaces. Macromolecular scaffolds exhibit a number of advantageous structural features for binding protein surfaces and binding is made more efficient by multiple polymer-protein surface contacts. [43-44] Furthermore, an extensive surface area for contact with the desired proteins is offered by polymers owing to their size and flexibility, which is greatly useful in identification of protein external surfaces.

The targeting of protein surfaces can be applied to a number of applications. One of which is enzyme inhibition. The protease family of enzymes contains a large number of proteins that can hydrolyse various amides and esters. Also, a large family of natural protein inhibitors is known to bind to the surface regions and the active sites of different serine proteases (elastase, chymotrypsin and trypsin). [45] The majority of protein inhibitors known and characterised so far are directed towards serine protease, α- chymotrypsin. Chy was the target employed in the present work to test effective inhibition using an artificial protein receptor. We have attempted to develop inhibitors that target the active sites, however, their active sites are very similar, which makes it difficult to identify a specific inhibitor for each

protease enzyme. Hence, the creation of inhibitors for surface binding is a novel approach. In terms of structure, Chy presents a ring of residues with positive charges surrounding its active pocket and scattered surface "hot spots"[12] (Figure 14).

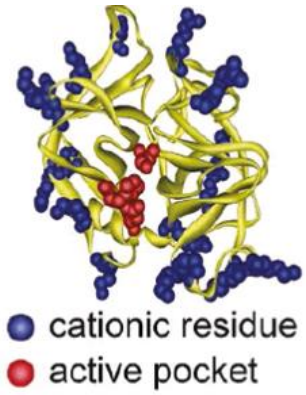

Figure 14: The surface of α-chymotrypsin (Chy). Image reprinted with permission from [De, M., Chou, S. S. and Dravid, V. P. J. Am. Chem. Soc. 133, 17524–17527 (2011)][31]

These hot spots can be targeted when developing a surfacebased inhibitor. Chy uses its cationic residues to establish connections with anionic synthetic receptors and inhibitors (e.g. polymeric micelles, [45] dendrimers, [46] porphyrins, [47] gold nanoparticles[48] and recently graphene oxide [49]) and consequently, substrate activity is suppressed. However, owing to extra noncovalent interactions afforded by the functionality of amino acids, protein binding is specific and has high affinity, despite the electrostatic nature of the main interactions. In a study that investigated the contribution of amino acid functionality and preferences in hot spots and interfacial areas, it was observed that tryptophan, tyrosine and arginine were likely found with hot spots when present. [12] Despite the low frequency of these amino acids in the structure of proteins.[50] The above-mentioned amino acids are ones that can provide a number of non-covalent, including that interactions.

Early work in this area used functionalised porphyrin and calixarene scaffolds that supported various amino acids. There demonstrated high-affinity for various groups binding to a set of proteins. [14] Meanwhile, Gilles and colleagues proposed the use of functionalised linear copolymers to bind enzymes with improved selectivity through screening co-monomers with different type of amino acid. [51] A library of inhibitors for binding to a variety of serine protease was created with selectivity dependent on the functionalised co-

monomers. Complementing the surface structure of the target proteins. The interaction between co-monomers and amino residues did not only occur on the protease surface, but also within its active site (Figure 14). Meanwhile, the manner in which various functionalised groups could collaborate is illustrated in Figure 14b. Bisphosphate co-monomers bind to elastase surface and an anchor monomer directs an alanine terminal group to dip in the active site and fill the elastase pocket.

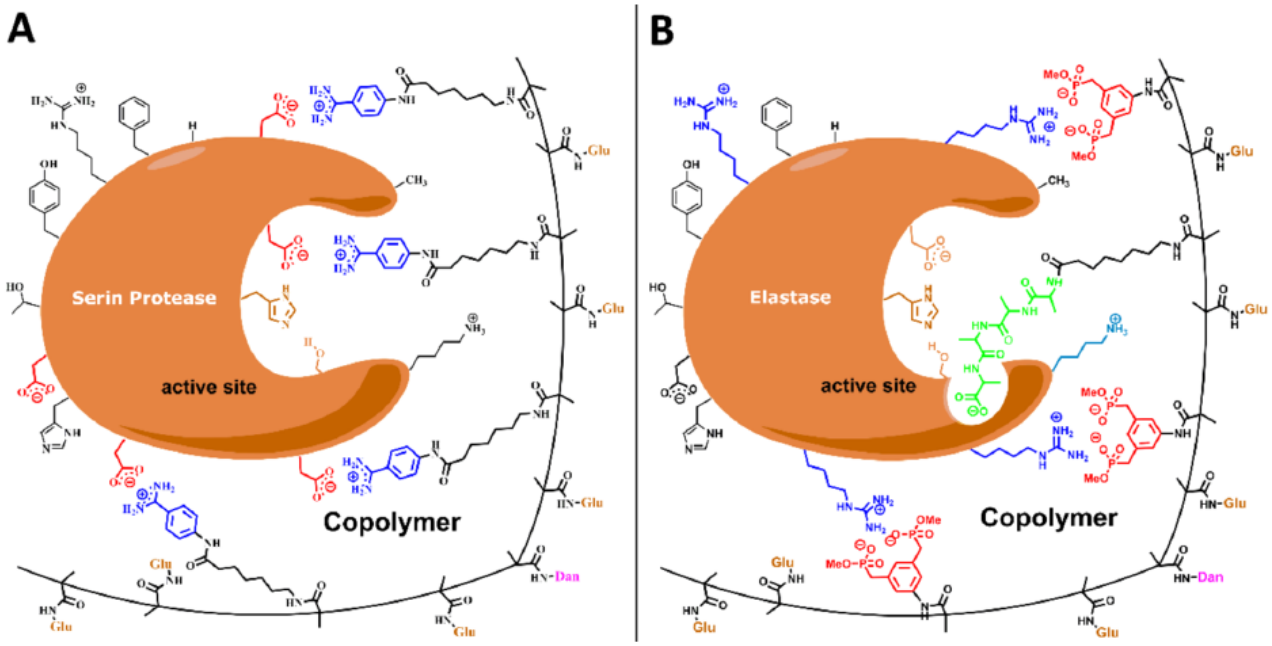

Figure 15: Representation of how serine protease (A) and elastase (B) interact with enzyme-targeting copolymers. Binding monomers were shown for acidic amino acids, aromatic amino acids (red) and histidine. Adapted with permission from [Gilles, P. et al. Biomacromolecules 18, 1772–1784 (2017).[51]

A range of essential functions are fulfilled by protein. The binding of functionalised linear copolymers to protein is made possible by the fact that complementarity exists between the functional groups of the two interacting sides. Hence, the intention is to create a linear chain polymer of key functionality to interact cooperatively with a protein with positive charge, namely, α-chymotrypsin. At the same time, the importance of the charged areas on the protein surface must also be considered. For instance, interaction is possible between the protein porcine pepsin with negative charge and ligands with positive charge, [52] as well as between the hot spot serine protease with positive charge and ligands with negative charge. Therefore, both functional group interactions and targeting charge are significant.

Linear polymers exhibit excessive dynamicity and flexibility. Polyvalent effects are the reason why proteins and linear polymers interact. Since linear polymers can enhance binding by altering their shape without restriction, no size specificity exists, so the strength of the binding increases with the number of existing charges. Consequently, the linear polymer-protein interactions are largely considered to lack specificity.[53] Therefore, we propose to use the rigid polymer as a scaffold to functionalised linear chain, that probably would increase the binding affinity.

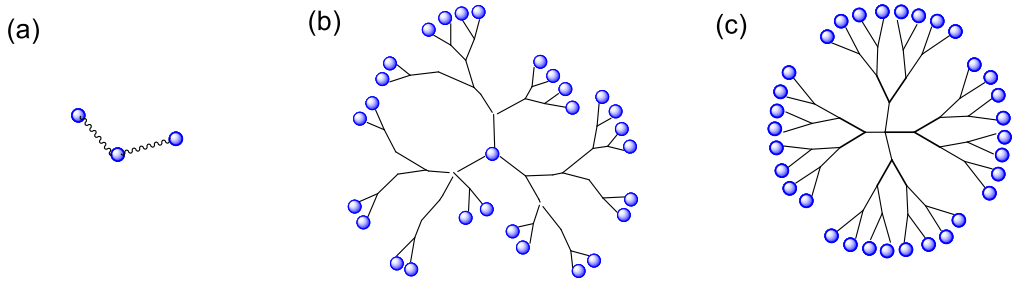

Figure 16: Illustration the structural of (a) linear polymer, (b) hyperbranched polymer and (c) dendrimer.

Unlike hyperbranched polymers (Figure 16), which can be easily and rapidly synthesised, dendrimers are less popular due to being synthetically challenging. [54] Their particular qualities are necessary solely in specific circumstances that justify the performance of a more difficult synthesis. The spherical structure created by the highly organised and repetitive character of the branches is useful particularly for replication of protein binding partners. Furthermore, the structure of dendrimers is significantly less flexible, so binding is only maximised when the position of the complimentary functional groups match on the dendrimer and protein. As such, dendrimer binding is entropically more cost-effective than linear polymer binding. This is beneficial in the context of molecule design as it enables binding energy enhancement. Moreover, dendrimers also differ from polymers in that their surface groups exhibit high-density.[55] Also, generational synthesis yields quantised sizes that aid the design of molecules for binding to particular protein binding sites, with improved binding affinity and a certain level of selectivity being made possible through selection of a dendrimer of complementary size with respect to protein binding areas. Given

the above considerations, dendrimers were selected as our synthetic inhibitors while Chy was the chosen protein target.

Nevertheless, dendrimers can bind to the surface of protein, but, dendrimers often lack specificity. Although some degree of selectivity can be achieved through selection of a molecule with a size that complements the target binding site. Addition of targeting groups (e.g. amino acids) to their surface can increase specificity. However, adding this targeting groups to specific sites on the inhibitor that are complementarity with those present on the surface of the established binding site, is very difficult. As such, we need methods that can generate large inhibitors that possess the correct functionality positioned at precise 3D locations (Figure 17). If this can be achieved, then we will be able to develop macromolecules that could be used to bind specifically inhibit enzymes, bind and purify proteins, as well as in the delivery drugs. These molecules could eliminate issues related to drug specificity and physical properties because they can encase and transport a small active molecule to a specific protein. [41]

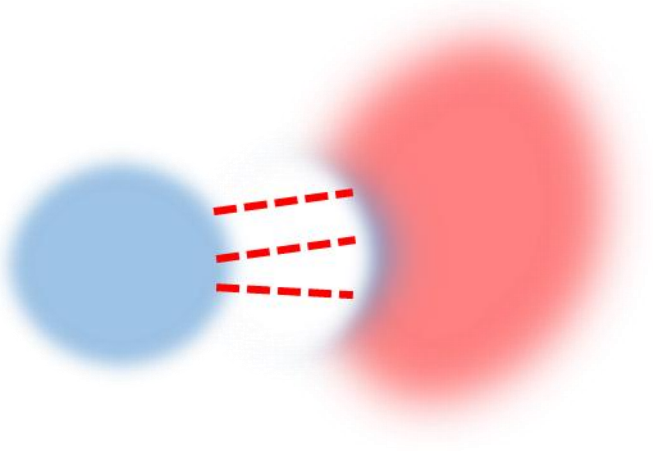

Figure 17: Targeted protein binding of molecules of large size between the protein and synthetic molecule, depicted in pink and blue, respectively

2.1 Aims and objectives

As previously mentioned, the protein binding advantages presented by dendrimers warrant their investigation in terms of potential protein-protein binding inhibitors. Nevertheless, to use dendrimers for targeted binding, it is necessary to address the extents of their selectiveness for particular proteins. Our group has previously reported selective binding of various proteins by distinct generations of dendrimer, according to size fit.[56] We have also shown that it is possible for particular amino acids to be covalently attached to the dendrimer surface, which could influence the binding in a positive or negative way.

Although this was progress towards a specific dendrimer/protein interaction, it was far from optimum. One of the problems was the limitation with respect to adding a combination of different amino acids in a controlled way. Specifically, how to control the exact position of each amino acid and its relative geometry with respect to neighbouring amino acids. To overcome this problem, we proposed a non-covalent approach where the target protein was a template for its own optimised and specific dendrimer ligand. To achieve this, we adopted the concepts of dynamic combinatorial chemistry.

The exact process would use non- functionalised dendrimers with either carboxylic acid or amine terminal groups depending on the specific surface charge on the target protein. These are simple to make and are even commercially available. The targeting groups would be incorporated non-covalently, based upon the ideas and results generated from our previous work on drug delivery. Specifically, the amino acids that could bind to the interior of the dendrimer using hydrophobic and hydrogen bonding interactions would be added to the end of a hydrophobic linear chain. A number of these functionalised linear chains can be synthesised and added to a dendrimer to give a functionalised system. The concept is shown in Scheme 2.

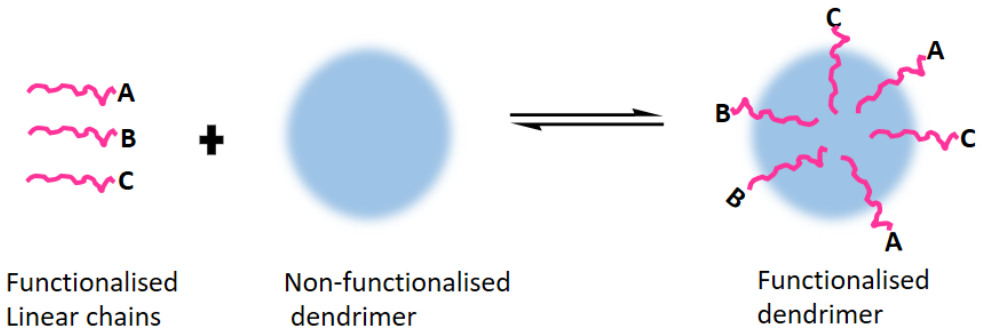

Scheme 2: The concept adopted from dynamic combinatorial chemistry

2.2 Results and discussion

2.2.1 Synthesis of dendrimers

The earlier stage was to synthesise the PAMAM; the divergent method was preferred because this technique is straightforward and simpler than the convergent method. The preparation of PAMAM dendrimers using the divergent method enables minimal generations to be formed. This method was introduced by Donald Tomalia and co-workers in 1985.[57] Commencing at G0.5 **1** successive reactions lead to higher generations, producing large G4.5 **9** dendrimers. The process involves two simple reactions that are repeated: 1) 1,4 Michael addition, which forms ester-terminated PAMAM dendrimers; 2) by an amination reaction at the amine termini of PAMAM dendrimers as depicted in Scheme 3.Therefore, the main objective can be achieved as generations are built up steadily to assemble a combinatorial library of different sized of dendrimers.

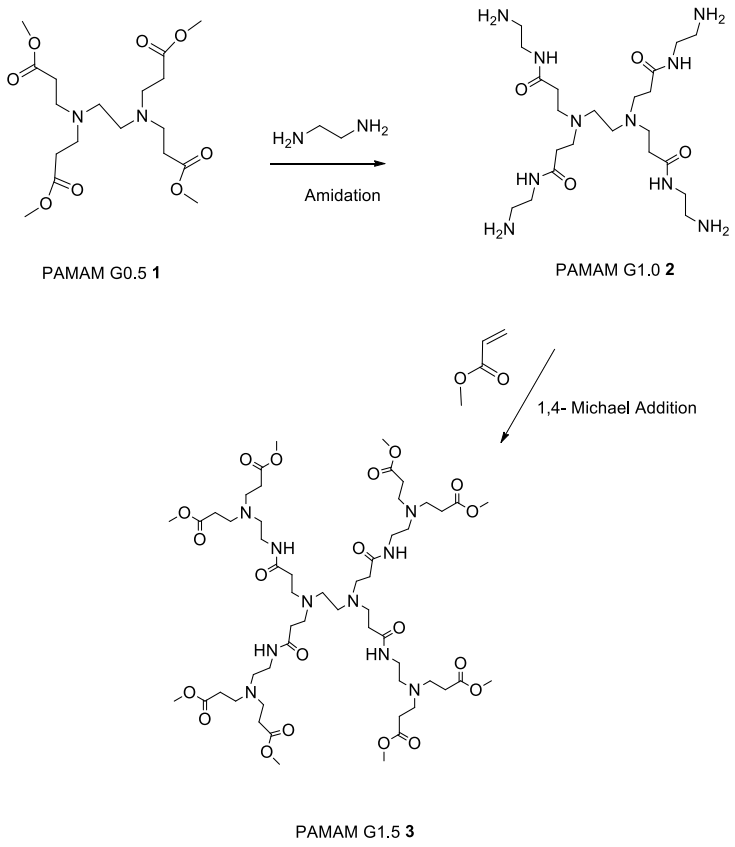

Scheme 3: Route of the half and full generation of PAMAMs.

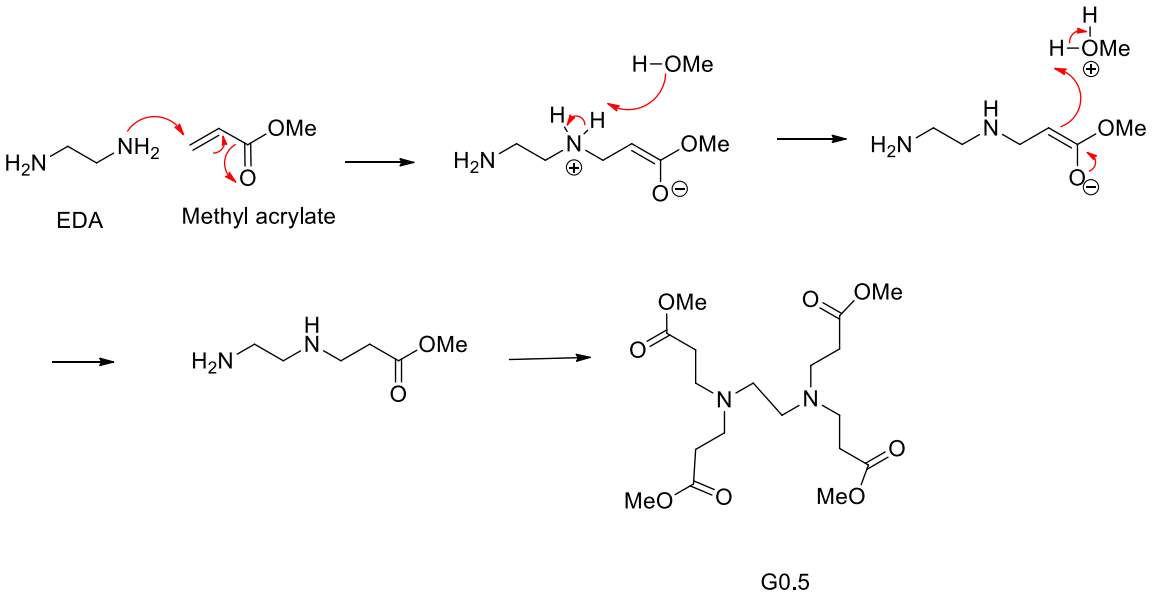

Scheme 4: Reaction mechanism to synthesise half-generation dendrimers (ester-terminated PAMAM).

Scheme 4 shows the first step of the 1,4-Michael addition for the creation of half generation PAMAM. G0.5 **1** was prepared in methanol using ethylene diamine (EDA) and methyl acrylate in methanol. The methyl acrylate was used in excess to avoid an incomplete Michael addition and preventing dendrimer destruction. The nucleophilic amine in EDA attacks the electrophilic terminal β-carbon in methyl acrylate using 1,4-Michael addition. The completion reaction was confirmed using ^{1}H NMR analysis as shown in Figure 18. The methoxy peak (ester group) at 3.68 ppm and the singlet at 2.53 ppm (a) integrated 4H was assigned to the core EDA. There is no peak at ≈ 5-6 ppm, indicating that the excess of methyl acrylate was completely removed. ^{13}C NMR and FTIR spectra, showed ester C=O at 172 ppm and 1735 cm^{-1} for the ^{13}C and FTIR respectively. Mass spectrometry also confirmed the mass, with a molecule ion at 405 (MH^{+}), indicating the product obtained.

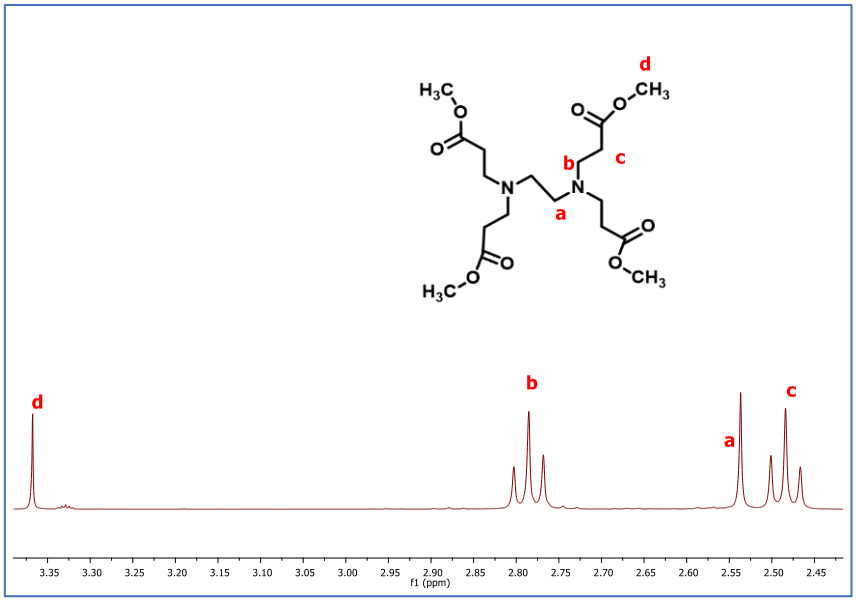

*Figure 18: [1] H NMR spectrum of half generation (G0.5 **1**) PAMAM and signal interpretation.*

The second step was an amidation reaction to produce a full generation. The reaction mechanism is shown in Scheme 5. The nitrogen's lone pair (EDA) attacks the electrophilic carbon ester (C=O) and the intermediate is formed. The amine from a second terminal protonates this intermediate, and the methoxy group leaves. The cation is eliminated by deprotonation to yield a full generation dendrimer.

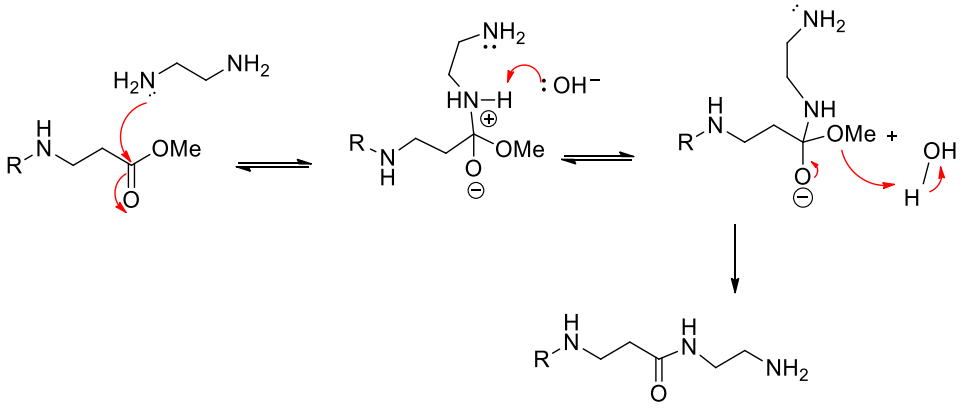

Scheme 5: Mechanism of amidation reaction of full generation PAMAM (amine terminated).

G1.0 was prepared by adding G0.5 **1** in methanol with an excess of EDA. The excess of EDA was purified with an azeotropic mixture (9:1 ratio) of toluene and methanol. The purified G1.0 **2** dendrimer was confirmed by ^{1}H NMR spectroscopy, which showed an absence of single peak of EDA at 2.67 ppm. The FTIR peak at 1735 cm^{-1} and ^{1}H NMR at

3.68 ppm that represents a C=O ester, was no longer visible. The Electrospray ionisation mass spectrometry (ES-MS) was used to analyse a smaller generation (less than 1000). A molecular ion at 517, which is equal to an MH^+ ion for G1.0 **2** obtained. These steps were repeated successively to create G4.5 **9** dendrimers and examined by Matrix-assisted laser desorption ionisation (MALDI) To confirm the characterisation of half and full generation PAMAM dendrimers is summarised in Table 2**.**

Dendrimer Generation	Molecular Formula	Molecular weight (g/mol)	Terminal groups	Ester methyl NMR peak (∂ ppm, integration)	Mass ion (MH^+) obtained
G0.5 **1**	C_{18} H_{32} N_2 O_8	406	CO_2Me (4)	3.68, 12H	405
G1.0 **2**	C_{22} H_{48} N_{10} O_4	516	NH_2 (4)	-	517
G1.5 **3**	C_{54} H_{96} N_{10} O_{20}	1205	CO_2Me (8)	3.69, 24H	1206
G2.0 **4**	C_{62} H_{128} N_{26} O_{12}	1429	NH_2 (8)	-	1430
G2.5 **5**	C_{126} H_{224} N_{26} O_{44}	2807	CO_2Me (16)	3.69, 48H	2806
G3.0 **6**	C_{142} H_{288} N_{58} O_{28}	3256	NH_2 (16)	-	3257
G3.5 **7**	C_{270} H_{480} N_{58} O_{92}	6014	CO_2Me (32)	3.69 ,96H	6014
G4.0 **8**	C_{302} H_{608} $N_{122}O_{60}$	6913	NH_2 (32)		6913
G4.5 **9**	$C_{558}H_{992}N_{122}O_{188}$	12411	CO_2Me (64)	3.69,192 H	12410

*Table 2: Analysis of PAMAMs generated (**1**-**9**).*

2.2.2 Synthesis of anionic PAMAM dendrimer

To confirm the dendrimer can bind with positively charged protein molecules, negatively charged terminated PAMAMs were selected. The ester group of half generation of the PAMAM dendrimers was hydrolysed using sodium hydroxide to produce carboxylate groups.

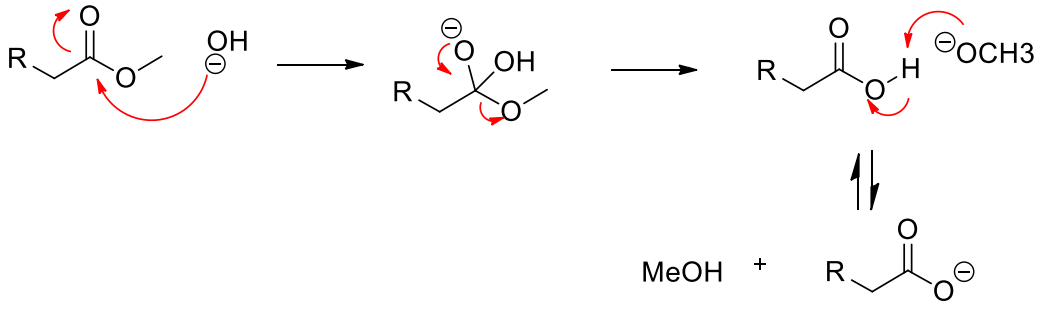

Scheme 6: Hydrolysis of ester groups/half generation of PAMAM.

As shown in Scheme 6, a tetrahedral intermediate was produced when the hydroxide ion attacked the electrophilic carbon ester (C=O). The methoxy anion is basic and therefore, deprotonates the carboxylic acid. Formation of the final product of G1.5COOH **(10)** was confirmed by ^{1}H NMR. The methyl ester peak at 3.69 ppm was no longer visible and the new methylene protons showed as a triplet at 2.28 ppm ($\underline{CH_2}CO$). The important functional groups were confirmed by ^{13}C NMR, showing two peaks at 174.5 ppm (C=O) and at 181.4 ppm (C=O for carboxylate group), and FTIR at 3255 cm^{-1} (N-H stretch) and 1645 cm^{-1} (C=O). The completion of the reaction was also confirmed by mass spectra (MALDI-TOF MS); a molecular ion was identified at 2582 (MH^+). The same procedure and characterisation were repeated to synthesise anionic dendrimers up to G4.5-COOH **(4)**. The characterisations as summarised in Table 3.

Dendrimer Generation	Chemical Formula	Expected Molecular weight (g/mol)	Number Of carboxylate surface groups	Obtained Mass ion (MH^+)
G1.5-COOH **10**	$C_{46}H_{80}N_{10}O_{20}$	1092	8	1093
G2.5-COOH **11**	$C_{110}H_{192}N_{26}O_{44}$	2582	16	2582
G3.5-COOH **12**	$C_{238}H_{416}N_{58}O_{92}$	5562	32	5563
G4.5-COOH **13**	$C_{494}H_{864}N_{122}O_{188}$	11521	64	11522

*Table 3: Analysis of anionic PAMAM-COOH generated (**10**-**13**).*

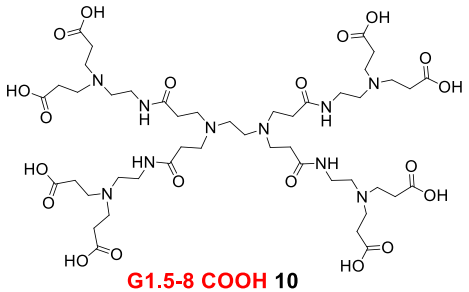

G1.5-8 COOH **10**

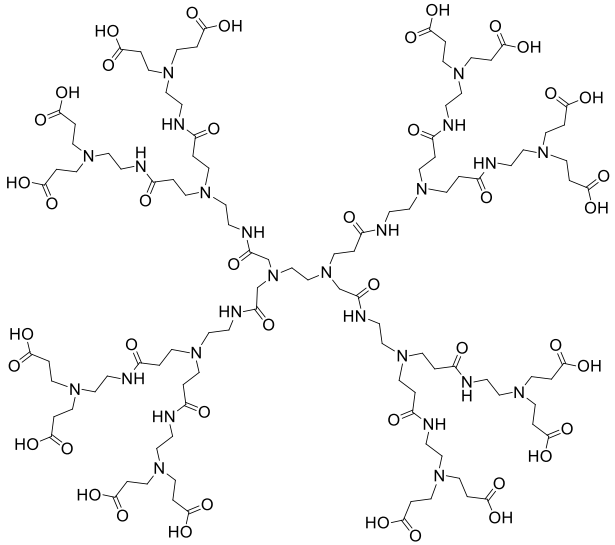

G2.5-16 COOH **11**

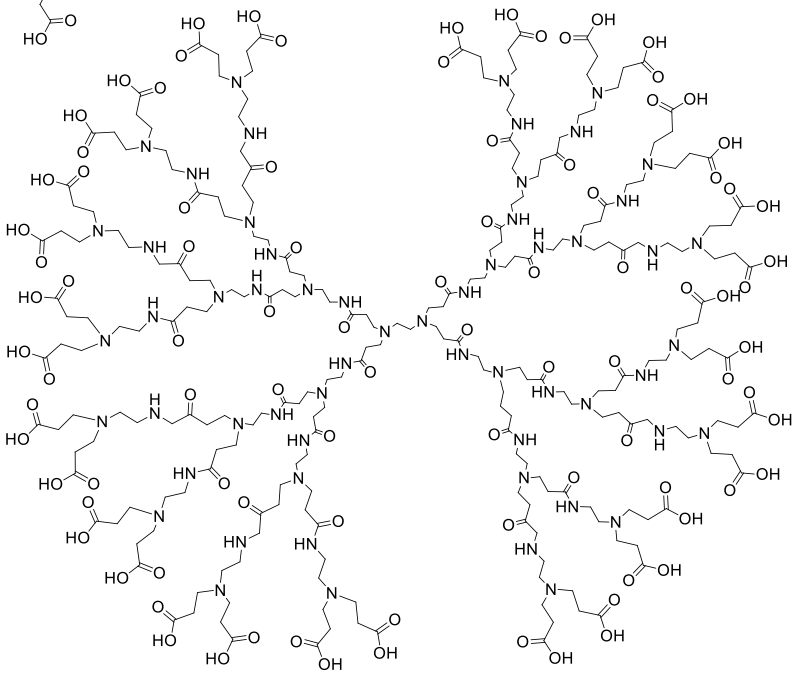

G3.5-32 COOH **12**

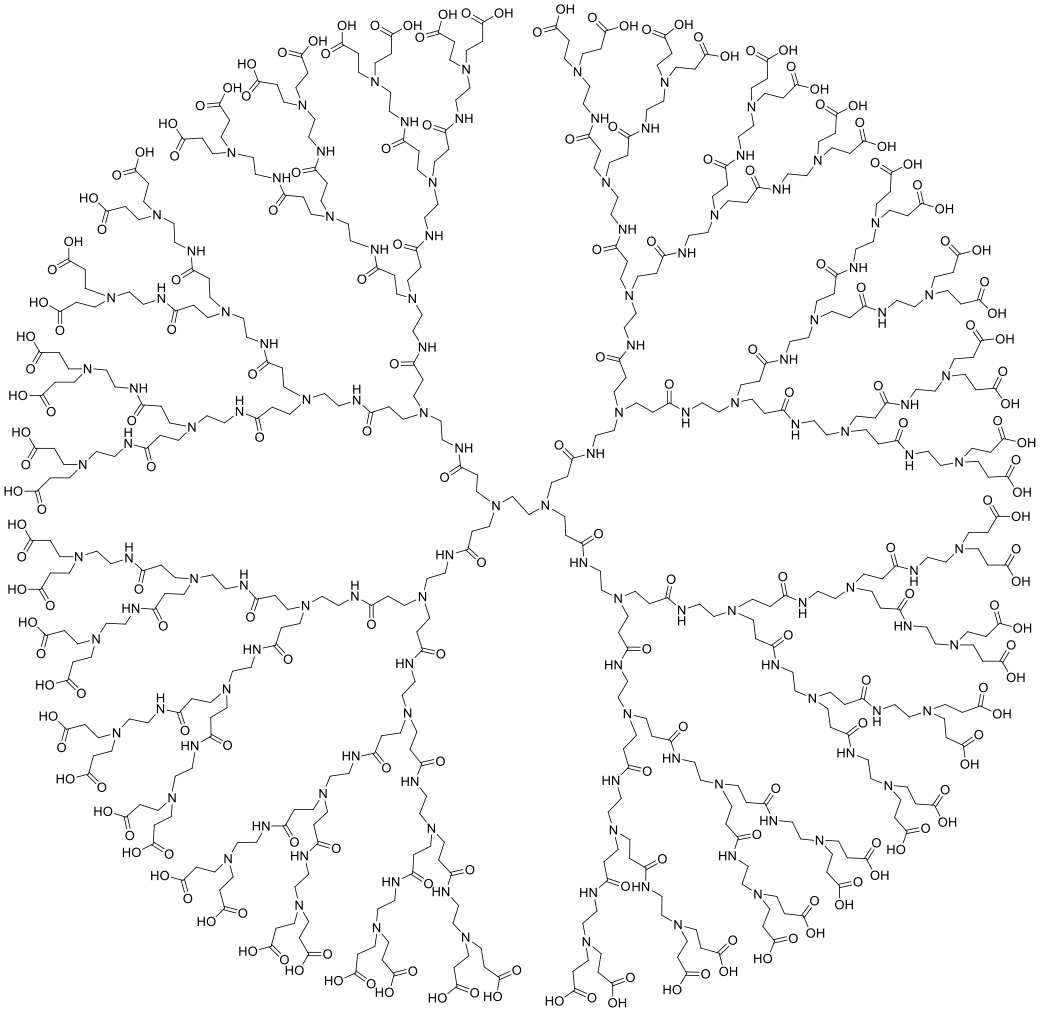

G4.5-64 COOH 13

*Figure 19: The anionic terminated PAMAM dendrimers (**10-13**) synthesised*

2.2.3 Synthetic strategies to design the linear chains

The next milestone was to synthesise the linear chain required to interact with the surface groups on the targeting proteins. Previous research by our group (Figure 20) studied a targeting group (guest) bound the dendrimer (host) using just hydrophobic interactions. [58] Unfortunately, the level of encapsulation of the hydrophobic guest within the dendrimer was very poor and ineffective as a targeting group. Therefore, we decided to improve the interactions between the dendrimer and the linear chain itself. To do this, we proposed to add hydrogen-bonding groups to the chain. These could then bind to the amides within the dendrimer and support any hydrophobic interactions.

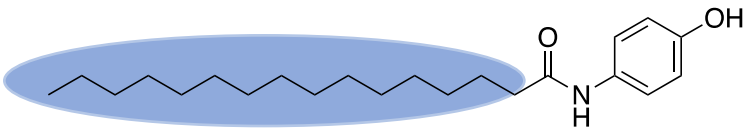

Figure 20: The structure of the hydrophobic linear chain with one hydrogen bond.

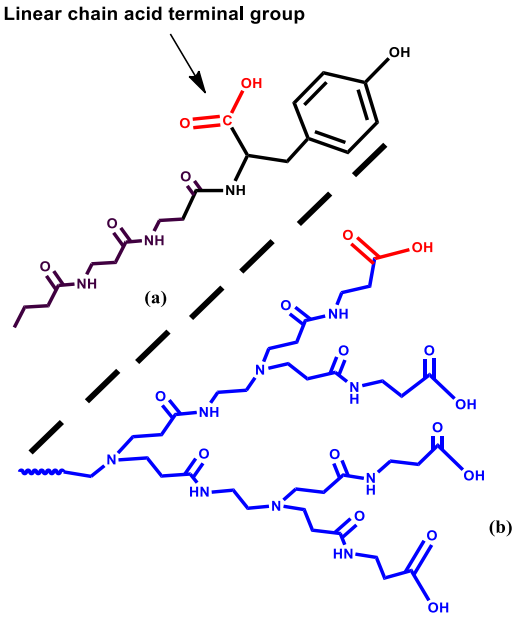

Figure 21. The linear chain was initially planned to incorporate(a) acid ending groups (b)to mirror the structure of dendrimer

To maximise the number of encapsulated chains, we designed a linear chain with three amide groups. Our preliminary plan was to have an acid terminal group (CO_2H) on the linear chain, as shown in Figure 21. We wanted an acid ended system, so that this chain

could bind to a target protein's positive surface. However, the intermediate molecules were insoluble, which meant an acid terminated chain was not possible and we decided to change the plan. The required negative charges can come from the carboxylate group of the G3.5-COOH **12** PAMAM dendrimer. The chain would then provide the tyrosine group to support these electrostatic interactions, with the amino acid added to the N-terminus of the chain, as shown in Scheme 7.

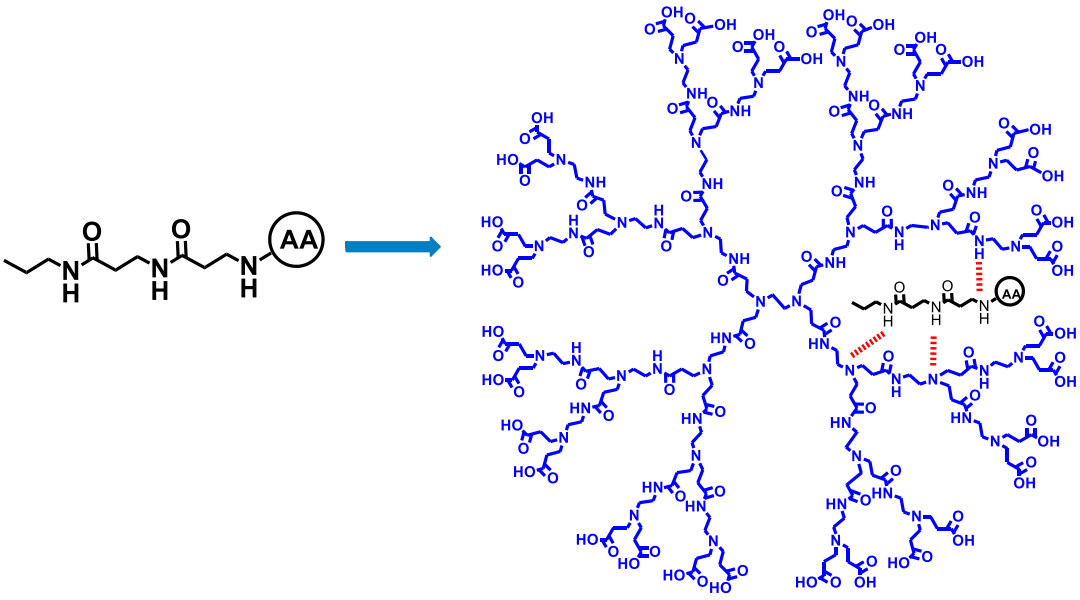

*Scheme 7: Possible interactions between an encapsulated chain and a G3.5-COOH dendrimer **12**.*

In this design, the linear chain can make three hydrogen bonds with the interior of the dendrimer. Furthermore, the amine would allow the dendrimer and the chain in the system to act as donors or acceptors to form hydrogen bonds. Retrosynthetic analysis of the target linear chain indicated that it was possible to synthesise the chain starting from an alkyl amine and extending the chain using β-alanine **14** repeat units (Scheme 8).

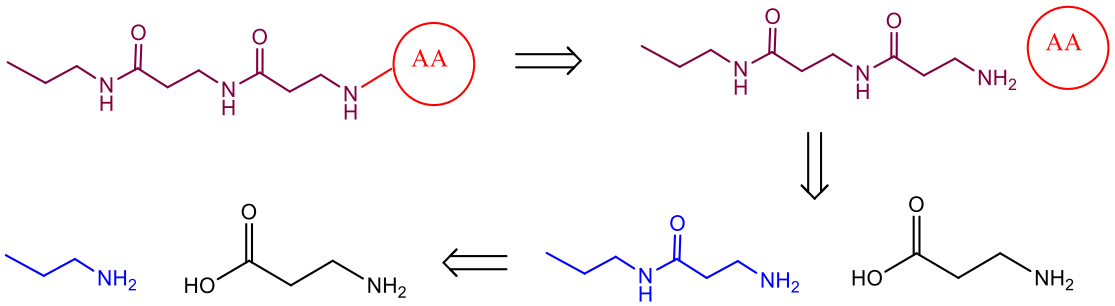

Scheme 8: Route of retrosynthesising the coupling of three amines.

2.2.4 Linear chain with three amide groups

Before going to the next stage of the proposed plan, to prevent self-polymerisation, it was essential to protect the amine group of β-alanine, which is a bi-functional molecule having carboxylic acid and amine terminal groups. Tert-butyloxycarbonyl (Boc) group was selected as it is relatively easy to add and remove.[59] The addition of the Boc group, which integrates as nine protons, was easy to recognise in the ^{1}H NMR as a sharp singlet around 1.40 ppm. The successful attachment of β-alanine was confirmed by integrating the broad singlets at 2.61 ppm and 3.42 ppm, which are assigned as the CH_2 protons, and comparing it to the Boc signal. Mass spectrometry confirmed the mass of with a molecule ion at 188 (MH^+) and 212 (MNa^+), indicating that Boc amide **15** had been created.

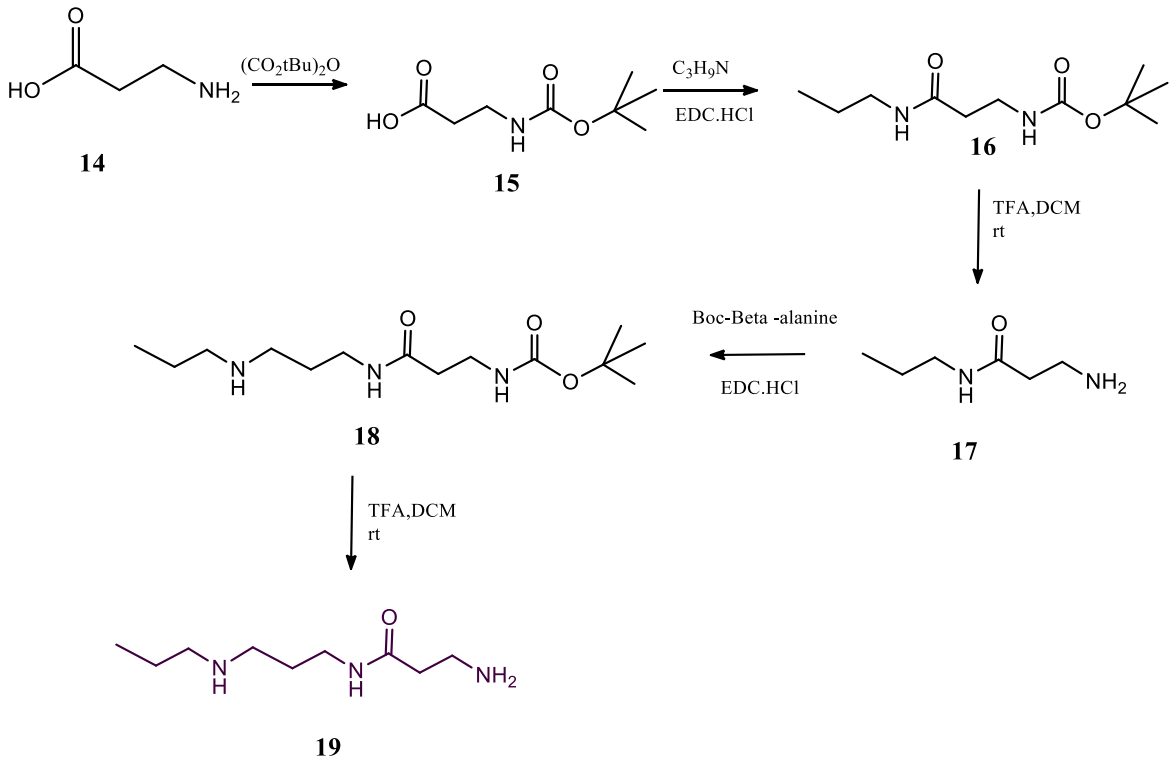

*Scheme 9: The synthetic route of the linear chains (**5-10**).*

The next reaction added propylamine to chain **15** (Scheme 9). However, the OH group of carboxylic acids are poor leaving groups. Therefore, to create a good leaving group, the acid was converted to an active ester using an amide-coupling agent, thereby enabling nucleophilic substitution. The carbodiimide family is commonly used to activate carboxylic acids towards ester or amide formation. The amine nucleophile can attack this carbonyl group because it contains a sufficiently good leaving group as shown in Scheme 10.[60] The reaction produces urea as a by-product, which must be removed at the end of the reaction.

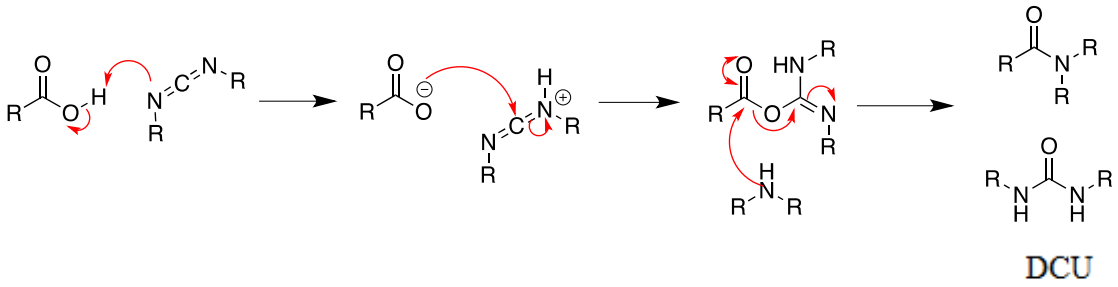

Scheme 10. Carbodiimide amide coupling mechanism.

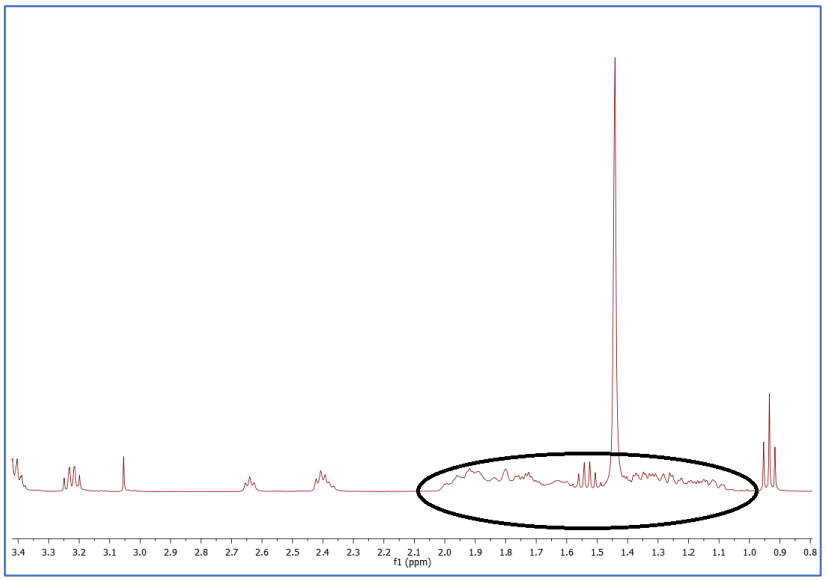

*Figure 22. ^{1}H NMR spectrum of chain **16** with impurities (in circle) when using dicyclohexyl carbodiimide as a coupling agent.*

The first attempted coupling used dicyclohexyl carbodiimide (DCCI); the ^{1}H NMR spectra is shown in Figure 22. Although, this indicates that the desired amide product was produced, there were impurities. These impurities are consistent with the urea by-product, dicyclohexyl urea (DCU), which can be seen around 1-2 ppm in the ^{1}H NMR. The crude product was rewashed with cold DCM, but the impurities were challenging to remove. However, as the next reactions would not be influenced by the impurities, we moved on to the next step without further purification. However, the Boc deprotection step lead to an impure product that still contained large amounts of urea. Unfortunately, we were unable to purify the product and needed an alternative method for the initial coupling.

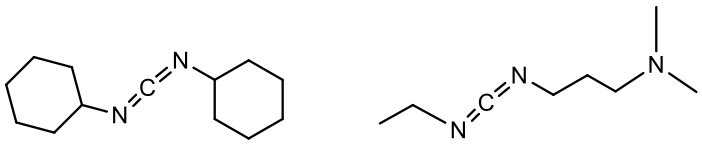

Figure 23: Structure of carbodiimide coupling agents.

To achieve this, ethyl-3-(3-dimethylaminopropyl) carbodiimide (EDC) was selected, as its water-soluble by-products are readily removed by solvent extraction. Specifically, the hydrochloride salt of EDC was chosen because it is cheaper than EDC. However, the hydrochloride could protonate the amine and decrease its nucleophilicity. Therefore, it was essential to neutralise the solution/reagents by adding triethylamine to act as a base. After the reaction, the ^{1}H NMR spectrum displayed the same peaks for the product, but without the peaks of urea impurities between 1 and 2 ppm (Figure 24). The integrated signals for the two protons at 3.41 ppm and 2.40 ppm were assigned as the $\underline{CH_2}N$ and $\underline{CH_2}CO$ respectively. The singlet at 1.45 ppm, which integrated 9H, was assigned to the Boc group. The ES-MS spectrum showed a signal at 231 for the MH^+ ion, indicating that synthesis of the pure protected chain **16** had been achieved.

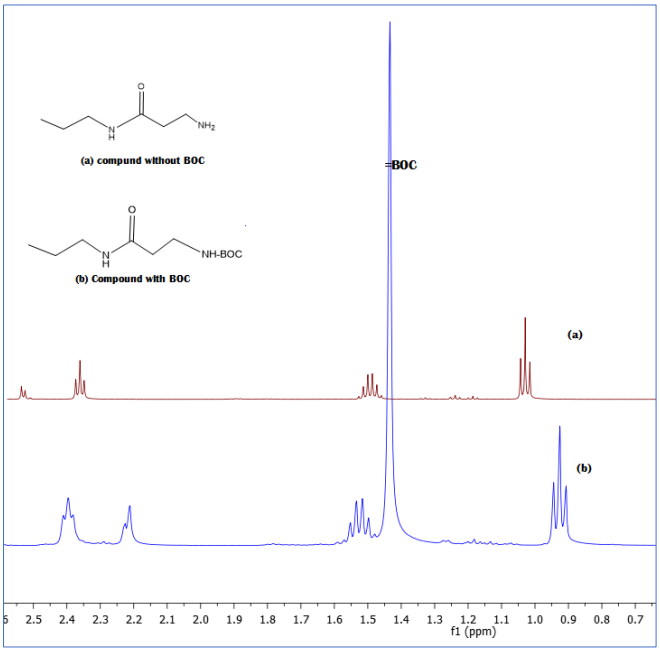

*Figure 24: ^{1}H NMR analysis using EDC as a coupling agent (a) chain **17** without BOC (b) chain **16** with Boc.*

Having successfully synthesised protected chain **16**, removal of the Boc group was the next step. The first attempt at deprotection failed when using stronger acids such as H_2SO_4 and HCl. However, TFA was found to remove Boc efficiently, as the carbon dioxide by-product could bubble away (Scheme 11). TFA was removed by evaporated and solvent extraction, resulting in the deprotected chain **17** (82%). The pH of the solution was also monitored to ensure that no TFA remained. An absence of the sharp singlet at 1.45 ppm for the Boc group in the ^{1}H NMR indicated successful removal of the Boc group.

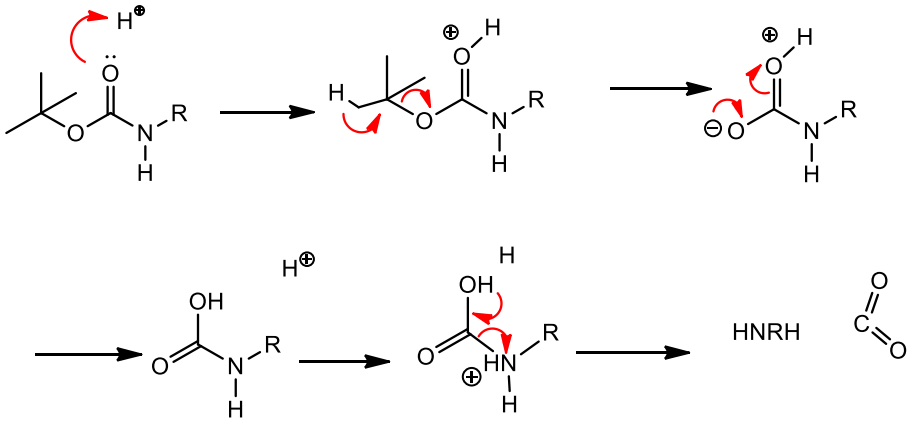

Scheme 11:Mechanism of Boc deprotection of the linear chain

The EDC procedure was repeated to attach a second Boc-β-alanine group to the chain. At this stage, DCM was not a good solvent as the deprotected compound was more polar and amide **17** was insoluble. Consequently, tetrahydrofuran (THF) was used to in place of DCM. The ^{1}H NMR spectrum displayed peaks consistent with the coupled product; a sharp singlet peak for the Boc group was present at 1.42 ppm and the terminal methyl group as a triplet at 0.93 ppm. Mass spectrometry analysis confirmed the mass of amide **18** with a molecular ion at 302 (MH^+). The compound was subsequently deprotected to give amine **19,** as previous shown in Scheme 9. A summary of the characterisation data is shown in Table 4. The next step was the attachment of tyrosine to the chain's terminal amine.

Linear chain	Chemical Formula	Molecular weight (g/mol)	Boc^{1}H NMR peak (∂ ppm, integration)	Mass ion (MH^+)	Mass ion (MH^+-Boc)
16	$C_{11}H_{22}N_2O_3$	230	1.45, H	231	131
17	$C_6H_{14}N_2O$	130	-	131	x
18	$C_{14}H_{27}N_3O_4$	301	1.42, H	302	202
19	$C_9H_{19}N_3O_3$	201	-	202	x

Table 4: The summary of characterisation of the linear chain.

2.2.5 Addition of tyrosine to the linear chain

Tyrosine was selected due to its UV active group (λ_{max}= 275 nm), but more importantly, due its ability to complement the amino acids on the binding site of protein. Binding studies using a dendrimer with covalently coupled tyrosine demonstrated a significant increase in affinity, because of the high abundance of tyrosine on protein-protein binding interfaces. [1,12] EDC coupling was used to attach the Boc-tyrosine with amine **19** (Scheme 12**)**. However, ^{1}H NMR analysis displayed extra peaks that were not anticipated. Tyrosine's UV activity facilitated analysis of the product mixture using thin layer chromatography. This revealed several spots, all of which were inconsistent with uncoupled tyrosine or linear chain.

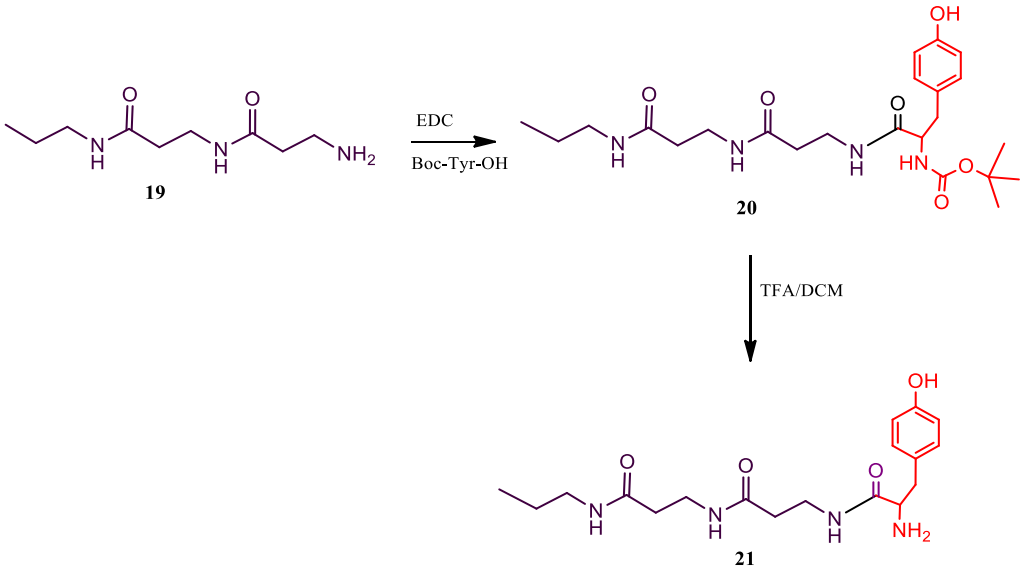

Scheme 12: Coupling of tyrosine (red) to the linear chain.

Therefore, the compound was purified by chromatography. Due to the polarity of the amine, amides and the tyrosine unit, 10% methanol was added to eluent DCM. As well as verifying the presence of tyrosine, the ^{1}H NMR analysis of the collected fractions showed that the impurity peaks, had been eliminated. The remaining complexity in the spectrum was due to the tert-butyl groups and bulky phenol groups that restricted rotation. As such, the Boc group was split into two overlapping peaks at 1.37 ppm with a combined integration equalling nine protons.

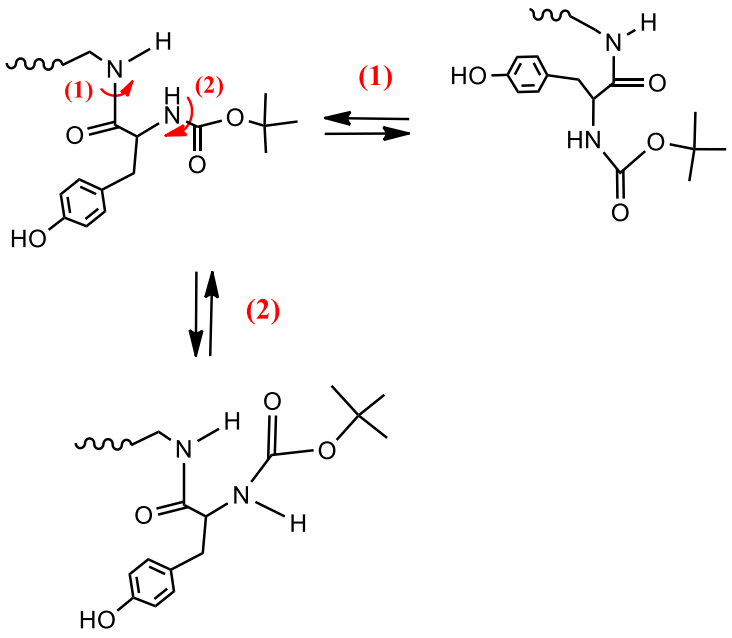

Scheme 13: Some of possible amide restricted rotation.

The tyrosine aromatic peaks were further complicated by the enantiomeric carbon, which meant other peaks were observed as a diastereotopic. As such, ^{1}H NMR showed two sets of doublets for each proton, which integrated for one hydrogen. For each the CH_2 protons adjacent to the aromatic ring are diastereotopic and are observed as two broad singlets (Scheme 14), each integrating as one proton.

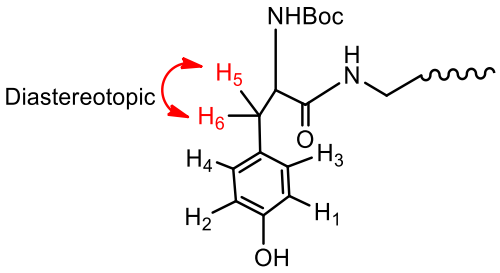

Scheme 14: The integration of a diastereotopic proton.

Further evidence from mass spectrometry confirmed the mass, with a molecular ion at 487.5 (MNa^+). Therefore, it was concluded that the protected tyrosine **20** had been successfully synthesised. The final tyrosine chain **21** was synthesised by removal of the Boc using the same deprotection techniques mentioned before. Targeting tyrosine chain **21** was now ready to encapsulate within a dendrimer, as shown in Figure 25.

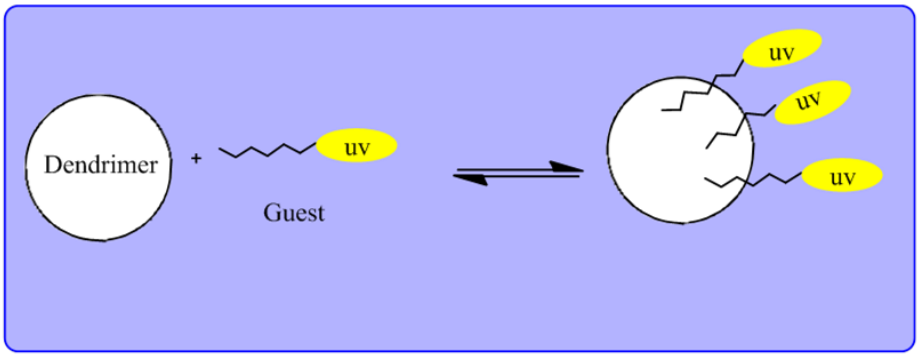

Figure 25: Planned encapsulation of the linear chain within the dendrimer.

2.2.6 Encapsulation tyrosine chain 21 with anionic PAMAM dendrimers

The initial intention was to use an anionic dendrimer as this would provide anionic carboxylate peripheral groups to bind with the cationic surface of the protein.[35] This could identify whether or not the size (or terminated charge) from the outside of the dendrimers affected the number of chains encapsulated. Specifically, G1.5 -8 COOH **22**, G2.5 -16 COOH **23**, G3.5 -36 COOH **24** and G4.5-64 COOH **25** were studied.

The encapsulation was carried out using a dendrimer to chain and an excess of chain was used to ensure a high loading efficiency. Therefore, 5.5 mg of dendrimer and 4.1 mg of Tyr chains **21** were dissolved in methanol. The mixture was shaken at room temperature to

ensure that everything had been dissolved. Methanol was removed under reduced pressure and 0.1 M Tris buffer solution (pH 7.46) was added. The final concentrations of dendrimer and tyrosine chain **21** were 1.0 x10^{-6} M and 1.12 x 10^{-5} M, respectively. The solutions were filtered to remove any undissolved chains and the filtrate analysed by UV spectroscopy. A control experiment to test the maximum solubility of the tyrosine chain **21** in the buffer was also carried out. A spectrum for the dendrimer alone showed a peak at 213 nm. However, at 270-300 nm (where the tyrosine could be seen) there was no significant peak. [61]

The proportion of encapsulated chains within the dendrimer were calculated (as shown in Table 5). Each absorbance was divided by the extinction coefficient (ε) of the tyrosine linear chains **21.** To measure the loading encapsulation, the concentration of the dendrimer was divided by the concentration of functionalised chain.

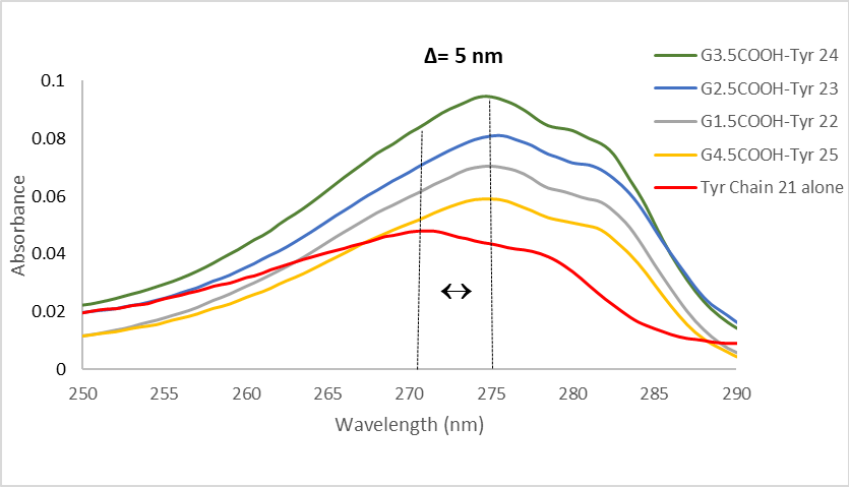

Figure 26: UV absorbance data before and after encapsulated tyrosine chain in different generations of anionic dendrimers.

Generation dendrimer	Absorbance	Concentration of Chains, **x**/ M	Ratio of chain to dendrimer	Chain(s) encapsulated* (x-y)/z
G1.5-COOH **22**	0.0703	8.31E-06	8.3	3 (± 0.31)
G2.5-COOH **23**	0.0807	9.54E-06	9.5	4 (± 0.33)
G3.5-COOH **24**	0.0944	1.12E-05	11.2	6 (± 0.30)
G4.5-COOH **25**	0.0539	6.37E-06	6.4	1 (± 0.35)
Concentration of Dendrimer, (**z**) / M =1E-06 Free tyrosine chain **21** in buffer (**y**) =5.13E-06 *subtracted with the background solubility of the tyrosine chains **21**				

*Table 5:Analysis the encapsulation of PAMAM-COOH with tyrosine chains **21***

In all cases, we observed a 5 nm bathochromic shift in tyrosine peak. This is good evidence for encapsulation and suggests the absorptions are from encapsulated chain. However, the background solubility of the chain was subtracted to allow for any non-encapsulate species.

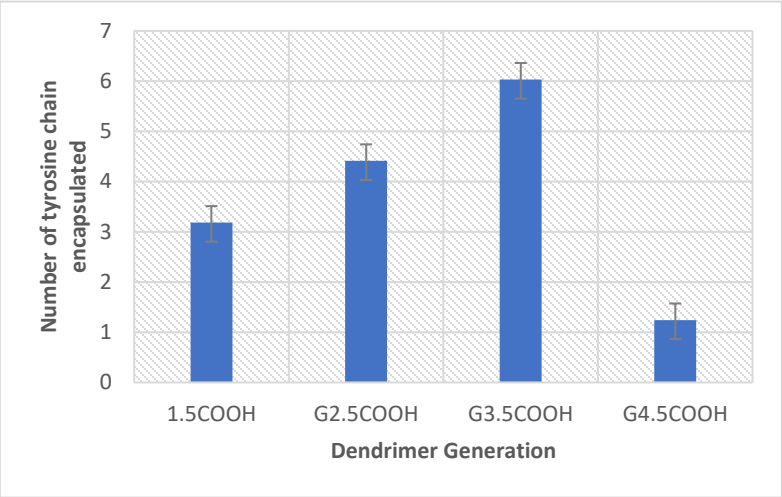

Figure 27: Trendline of the number of chains encapsulated in the different generation anionic PAMAM dendrimer.

The maximum number of chains used and all were dissolved in the G3.5 solutions. Overall, the results suggested that some of the chains were encapsulated well, as indicated by a significant improvement in the absorption λ_{max}. The efficiencies of encapsulation of the tyrosine chain **21** into PAMAM dendrimers were reasonable (Figure 27). As anticipated, the encapsulation number was lower in G1.5-COOH **10** and G4.5-COOH **13**. This is due to the lower generation effects and non-globular shape of G1.5-COOH **10**. However, for G4.5-COOH **13** because of the crowded and rigid surface. [33,62] Nonetheless, the G3.5-COOH **12** dendrimer had the optimum size for interaction with the binding area of Chy and encapsulated the highest number of chains.

2.2.7 Assay of G3.5-COOH 12 anionic PAMAM as an inhibitor using chymotrypsin by UV spectroscopy

De et al. have examined the enzyme activity of graphene oxide (GO) and demonstrated that GO is a very good inhibitor of α-chymotrypsin (Chy). As a result, we have used the same assay to study inhibition by the functionalised dendrimers. [31] Ciolkowski et al. reported that dendrimers with positive ends (G4 PAMAM-NH_2) and neutral ends (G4 PAMAM-OH) could interact with the negative charged surface of the protein porcine pepsin and could inhibit its enzymatic activity. It was also found that these dendrimers acted as mixed, partially non-competitive pepsin inhibitors. [52] However, no studies using acid terminated dendrimers as competitive inhibitors were reported.

As previously discussed, anionic dendrimers were selected for this study, as they have a negative surface charge that can bind to the positive surface of Chy. Furthermore, the interfacial binding area of Chy contains a large number of additional groups that strengthen any protein-protein or protein-ligand interaction. Thus, the G3.5-COOH **12** anionic dendrimer was used as the scaffold for the functionalised linear tyrosine chains **21**. This dendrimer has previously been shown to bind Chy by virtue of its size and anionic functionality. [35] Specifically, this new study will implement tyrosine chains as additional functionality which is known to be important for protein binding and recognition. The first experiment was a control that would allow a comparison between binding or inhibition before and after functionalisation with the tyrosine chain **21**.

BTNA **26 (**N-benzoyltyrosine-p-nitroanilide) is a chromogenic substrate which can be used to determine the rate of amide hydrolysis by UV spectrophotometry (Scheme 15). Chy prefers substrates with large hydrophobic side chains and aromatic amino units, denoting BTNA **26** as a suitable substrate. [48] When BTNA **26** is hydrolysed, nitronaniline **28** is generated, which is UV active, (λ_{max} = 410 nm).

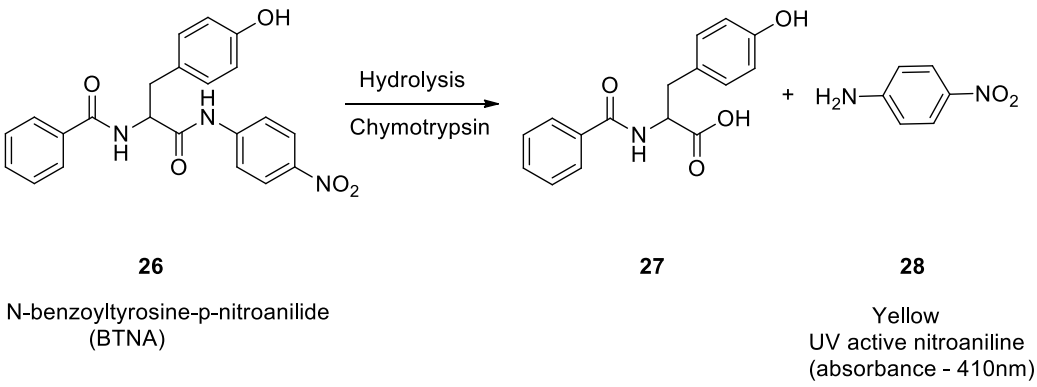

*Scheme 15: UV absorbent product from α-chymotrypsin enzyme catalysed hydrolysis of BTNA **26***

Prior to these studies, it was important to determine the conditions of the experiments. For example, the duration and optimum concentration for efficient yield. In addition, it is imperative to verify that there was no interaction or reaction between BTNA **26** and the inhibitor and all inhibition was a direct consequence of interaction between the inhibitor and the protein. Therefore, a control reaction in the absence of G3.5-COOH **12** is also required. In addition, controls must be conducted to determine the optimum amount of substrate to use.

If excessive substrate **26** is used, then surplus nitroaniline **28** will be generated. Also, if too little substrate is used, then insufficient nitroaniline **28** will be generated and detected. Therefore, it is important to establish the correct concentration of all specimens and the time required to complete the reaction. To verify whether the right concentration was selected for the experiment, a solution was formulated based on an enzyme to substrate ratio of 1:5 and an enzyme concentration of 0.4 μM. This was measured by adding BTNA **26** into a Chy solution (pH = 7.46 phosphate buffer). Hydrolysis of the BTNA **26** substrate was monitored by measuring the nitroaniline **28** absorbance at λ = 410 nm at 120 second intervals for a period of 40 mins.

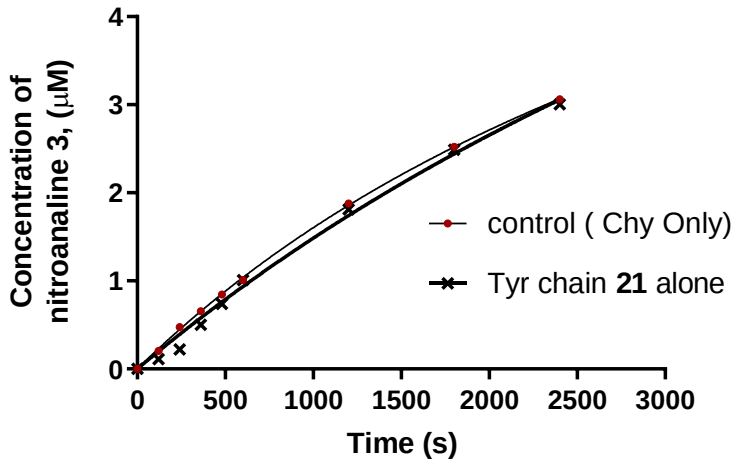

Figure 28: The rate of reaction plots for the hydrolysis of 2.0 μM BTNA 26 (substrate) with the Chy (enzyme) at 0.4 μM without inhibitor called control reaction.

For the control reaction, a typical reaction profile of nitroaniline **28** concentration (M) against time (s) was recorded in the absence of any inhibitor (Figure 28). The rate or initial velocity (V) was calculated by fitting a linear regression to the data using GraphPad Prism 7.03. [63] This initial velocity is not a constant rate and is dependent upon the substrate concentration [S] (as well other concentrations). To confirm that inhibition binding was not due to the tyrosine chains alone (i.e. without dendrimer). Therefore, we carried out a control using tyrosine chain **21** to see if it could inhibit Chy on its own. The experiment was carried out by adding BTNA **26** to a solution of Chy and chains (excess of 10eq). No difference were observed in the rate profile for the enzyme activity. Therefore, at the concentrations studied, the linear chains do not bind to the enzyme's active site or form large, self-aggregating structures that could bind to the surface of Chy.

The experiment was repeated in the presence of G3.5-COOH **12** (inhibitor), which was added at half the concentration of Chy, as this would avoid too much inhibition. This would allow the activity of the enzyme to be observed before the enzyme was completely bound to the inhibitor. The experiment was prepared by pre-incubating 1.0 μM Chy with 0.5 μM G3.5-COOH **12** in 0.1 M phosphate buffer (final concentration of Chy and G3.5-COOH **12**, 0.4 μM and 0.2 μM, respectively). The mixture was shaken for 24 hours prior to the assay. The reaction profiles are shown in Figure 29. The reaction rates were 1.38 x 10^{-9} Ms^{-1} and

9.24 x 10^{-10} Ms^{-1}, for the control and G3.5-COOH **12** system respectively. Thus, the presence of G3.5-COOH **12** slows the reaction rate and inhibits the reaction by 33% (with 50 inhibitor relative to Chy).

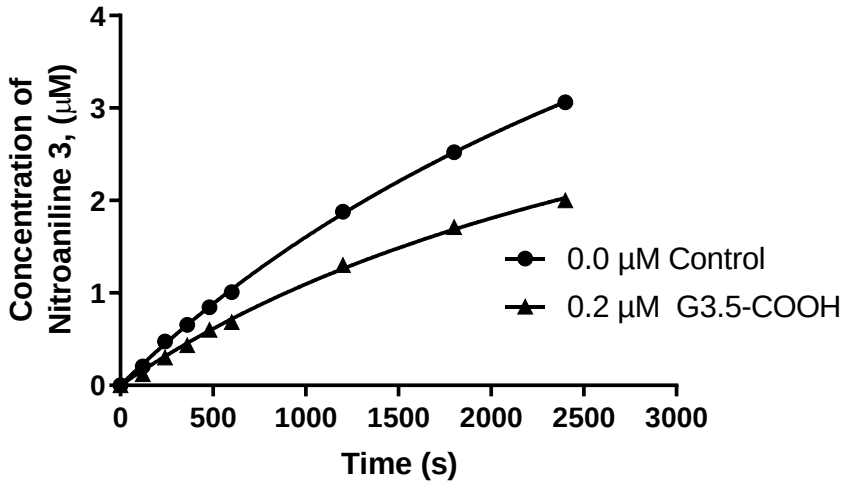

*Figure 29: Rate plots for the hydrolysis of 2.0 μM BTNA **26** (substrate leading to the formation of nitroaniline **3**) with the absence and presence of 0.2 μM G3.5-COOH **12** to find the initial velocity (V). Chy at 0.4 μM*

It would be expected that at higher concentrations of inhibitor, decreased rates would be observed. The ratio of enzyme and substrate was set at 1:5 with enzyme concentration at 0.4 μM. However, as the concentration of inhibitor was increased from 0.2 to 0.4 μM, the level of inhibition increased from 33% to 54%. The experiment was then carried out at inhibitor concentrations and the results are shown in Table 6. When the concentration of G3.5-COOH **12** increases, the initial velocity is reduced due to increased binding and inhibition.

BTNA **26** [S], μM	0.0 μM Control	0.2 μM G3.5-COOH **12**	0.4 μM G3.5-COOH **12**	0.8 μM G3.5-COOH **12**
	Initial velocity (V), nMs^{-1}			
2.0	1.380 (±0.571)	0.924 (± 0.035)	0.628 (±0.012)	0.348 (±0.010)
4.0	2.230 (±0.872)	1.65 (±0.155)	1.170 (±0.107)	0.690 (±0.018)

*Table 6: Initial velocity data for the hydrolysis of 2.0 μM and 4.0 μM BTNA **26** (substrate) with the absence (Chy only) and presence of G3.5-COOH **12** at different concentrations. Chy at 0.4 μM.*

Therefore, the three concentrations of G3.5-COOH **12** inhibitor shown in Table 6 were utilised as reference templates. In further studies, the substrate concentration was increased, and an enzyme: substrate ratio of 1:10 was used. The enzyme concentration remained at 0.4 μM. At this ratio, it was expected that the potential for collisions between enzyme and substrate would be increased, contributing to an increase in the rate of hydrolysis. This was confirmed by measuring the initial rates, which were 2.23 x 10^{-9} Ms^{-1} in the absence of G3.5-COOH **12**. Subsequently, this decreased gradually to 6.90 x 10^{-10} Ms^{-1} in the presence of G3.5-COOH **12** at the maximum concentration used (0.8 μM). To understand the mode of inhibition and to calculate the inhibition constant (K_i), enzyme initial velocities were collected as a function of substrate concentrations [S] and G3.5-COOH **12** inhibitor concentrations [I]. For accuracy in determining K_i, more data points were required at different substrate concentrations. Substrate solubility was poor, which limited the substrate concentration to a maximum of 8.0 μM. Therefore, these experiments were conducted at the same four concentrations of G3.5-COOH **12** (0, 0.2, 0.4, and 0.8 μM) and four concentrations of substrate (2.0, 4.0, 6.0 and 8.0 μM). All experiments were performed at an enzyme concentration of 0.4 μM. For each of the G3.5-COOH **12** concentrations, the initial rates were obtained (Figure 29). In each case, the reaction profiles and initial velocities were reduced when compared to the control reaction (without G3.5-COOH **12**). When the G3.5-COOH **12** inhibitor concentration increased (across the table), initial velocities were reduced. Also, as the substrate concentration increased (down the table), the initial velocities also increased. Therefore, at the concentrations studied, the initial rates did not saturate, which indicated that V_{max} had not been reached.

BTNA **26** [S], µM	0.0 µM Control	0.2 µM G3.5-COOH **12**	0.4 µM G3.5-COOH **12**	0.8 µM G3.5-COOH **12**
	Initial velocity (V), nMs^{-1}			
2.0	1.380 (±0.571)	0.924 (± 0.035)	0.628 (±0.012)	0.348 (±0.010)
4.0	2.230 (±0.872)	1.65 (±0.155)	1.170 (±0.107)	0.690 (±0.018)
6.0	2.780 (±0.109)	1.97 (±0.159)	1.62 (±0.157)	0.897 (±0.0267)
8.0	3.240 (±0.217)	2.301 (±0.211)	1.820 (±0.145)	1.090 (±0.100)

*Figure 30: The initial velocity data in the absence (Chy only) and presence of G3.5-COOH **12** to hydrolyse BTNA 26. Chy at 0.4 µM*

The data obtained was plotted and analysed using the mixed mode inhibition model by fitting the data to Equation 1 (using GraphPad). Equation 1 includes the actions of non-competitive, uncompetitive and competitive inhibitors to generate the α parameter, whose value can be used to define which one of three types of inhibition is occurring (Figure 30). [63]

$$V = \frac{V_{max}[\mathrm{S}]}{[\mathrm{S}]\left(1+\frac{[\mathrm{I}]}{\alpha K_i}\right)+K_m\left(1+\left(\frac{[\mathrm{I}]}{K_i}\right)\right)}$$

Equation 1

Non-competitive inhibition, is the condition in which the substrate binding to the enzyme is unaffected by the inhibitor and $\alpha = 1$. When $\alpha > 1$, binding of the substrate to the enzyme is prevented by the inhibitor, this condition is referred to as competitive inhibition. By contrast, uncompetitive inhibition for which $\alpha < 1$, the inhibitor binds to the enzyme-substrate complex preventing formation of product. [64]

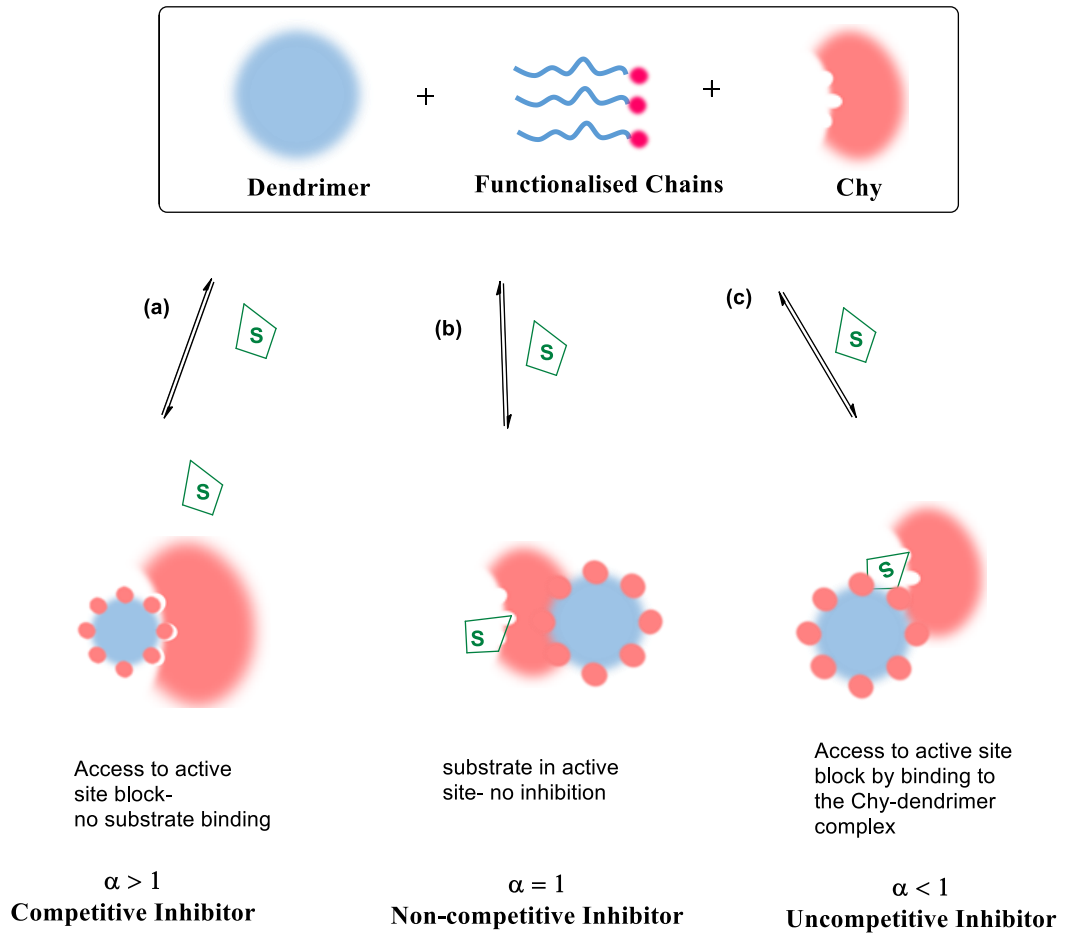

Figure 31: The type of inhibitor present can be defined by its effect on the degree of inhibition. a) When α > 1, binding of the substrate to the enzyme is prevented by the inhibitor, this condition is referred to as competitive inhibition; b) when α =1 is the condition in which the substrate binding to the enzyme is unaffected by the inhibitor called non-competitive inhibition; c) When α < 1, the inhibitor binds to the enzyme-substrate (ES) complex preventing formation of product corresponds to uncompetitive inhibitor.

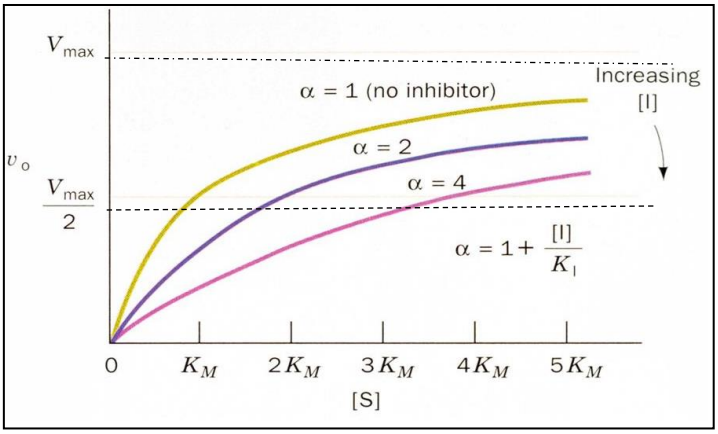

Figure 32: Illustration of the information from the degree of inhibition (α) dependent/related parameters with the V_{max}, K_m, [I] and K_i.

The α value can also be best described as the ratio between the rates of uninhibited and inhibited reactions ($V_{0\ (uninhibited)}$:$V_{i\ (inhibited)}$) [65] and this value is related to K_m (Michaelis constant) as shown in Figure 32. K_m measures the affinity of a substrate for an enzyme and shows how well a substrate and an enzyme bind. Using competitive inhibition as an example of how the inhibitor binds strongly to the enzyme, the substrate binds the enzyme weakly and this results in a higher K_m compared to the uninhibited enzyme.

The Michaelis constant K_m is found by halving the V_{max} (maximum velocity). If K_m changes from 100 μM (uninhibited) to 400 μM (inhibited), then α is 4. That is to say, higher K_m and higher α indicate stronger binding between enzyme and inhibitor. Figure 33(a) shows the variation in enzyme initial velocity with the substrate concentration by plotting a mixed-model inhibition. This data can be transformed into a Lineweaver-Burk or double reciprocal plot that describes the variation in the reciprocal of initial velocity with the reciprocal of substrate concentration (Figure 33(b).

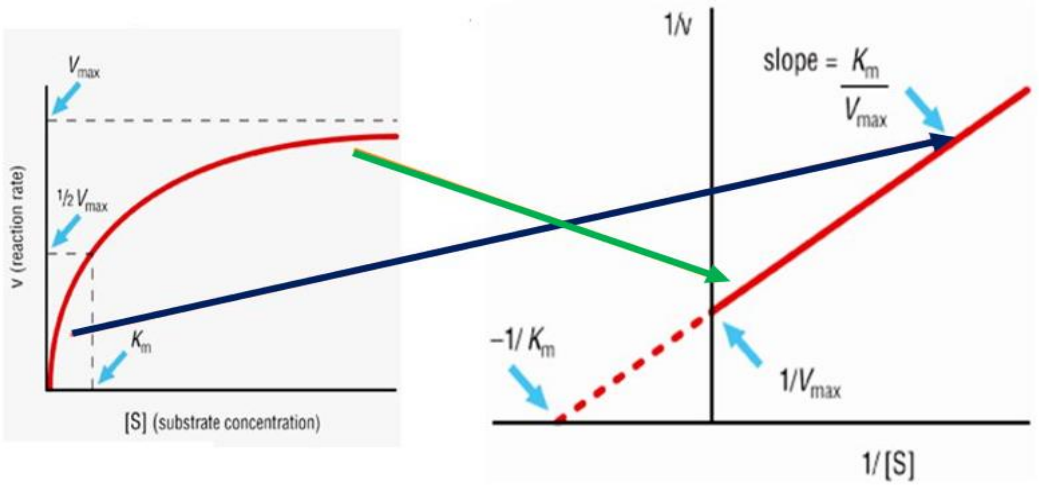

(a) Mixed-model inhibition (b) Transformed into Lineweaver-Burk

Figure 33: Mixed inhibition data transformed into double reciprocal Lineweaver-Burk analysis using GraphPad Prism 7.03

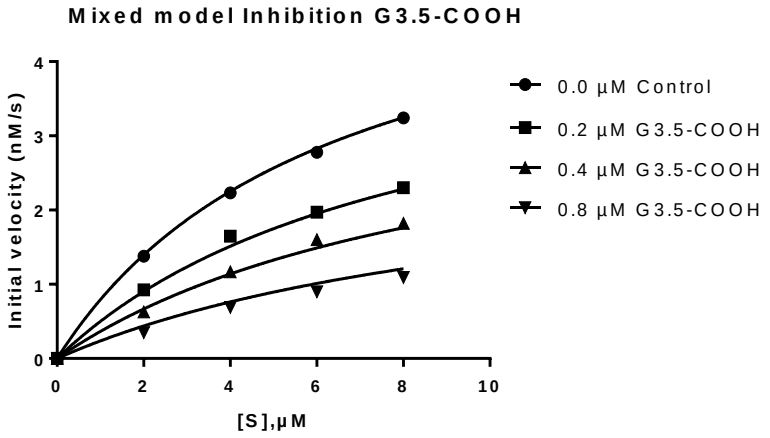

*Figure 34: The initial rate vs substrate (BTNA **26**) concentration at various concentration of G3.5-COOH **12**. Chy at 0.4 µM.*

Initial rates at various substrate and dendrimer concentrations were obtained and plotted to generate the graph in Figure 34. The best fit values of K_i and V_{max} and K_m were measured (Table 8). The Lineweaver-Burk plots were also employed to identify the inhibition mode. This information is based on the V_{max} value. If the V_{max} is unchanged and shows the same y-intercept (with or without the inhibitor), this indicates a competitive inhibition (Figure 35). The substrate and inhibitor compete to reach the active site. If the inhibitor binds first, the rate of the reaction slows down and this causes K_m to increase. As mentioned earlier, a

higher K_m means weak binding between enzyme and substrate (and vice versa for a lower K_m). Uncompetitive and non-competitive inhibitors change the V_{max} value. K_m values are reduced in uncompetitive inhibition and K_m the is unaffected in non-competitive inhibition. Further discussion on this is given in literature review. [65 - 66]

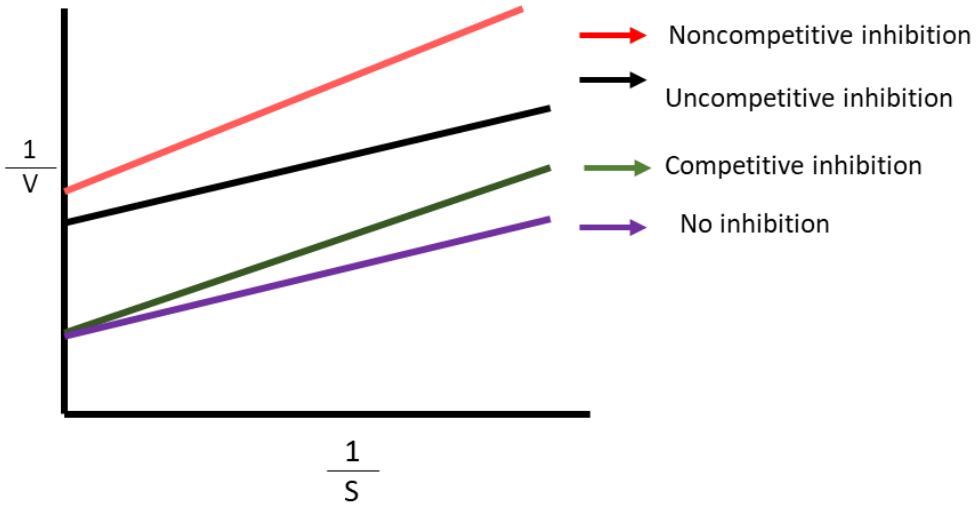

Figure 35: The Lineweaver-Burk plots to recognise three main categories of reversible inhibition

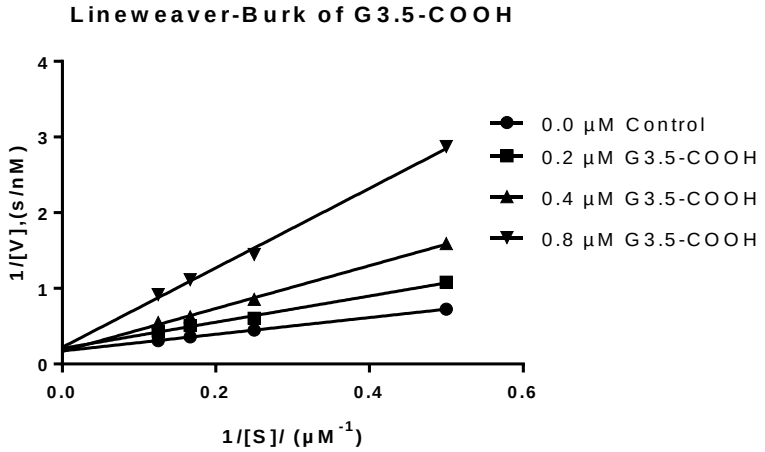

Figure 36: The data in Figure 34 transformed into a Lineweaver-Burk plot and demonstrating a common y-intercept. Chy at 0.4 µM.

The results obtained in Figure 36 show that there is a common y-intercept for different concentrations of the G3.5-COOH **12** inhibitor. This demonstrates the action of a competitive inhibitor. The values of V_{max}, K_m, and K_i as best-fit values from the G3.5-COOH **12** data set (obtained from Figure 34) are summarised in Table 8. A V_{max} of 6.0 nMs^{-1} and a K_m of 6.34 µM was determined. The α value was measured as 2.57, which indicates a strong competitive inhibition (more than 1). The Lineweaver-Burk plot also show a competitive inhibitor, as the data plots share the same y-intercept for each G3.5-COOH **12** concentration. The inhibitor can compete with the substrate and bind at the entrance of the enzyme active site. The K_i value is 0.31 µM, which provides information regarding the binding strength of the inhibitor and can be used as a reference to compare with other inhibitors (i.e. the functionalised G3.5-COOH dendrimer inhibitors).

Dendrimer / Kinetic inhibition data	Control Chy only	G3.5-COOH **12**
V_{max} , nMs^{-1}	applicable	6.00 (± 0.011)
Alpha, α		2.57 (± 0.002)
K_i , µg/mL		0.31 (± 0.020)
K_m , µM		6.34 (± 0.030)

*Table 7: Summary of kinetic parameters from a linear fit data for G3.5-COOH **12***

2.2.8 Inhibition with tyrosine functionalised G3.5-COOH 12 using a non-covalent method

This study examines whether a dendrimer (in the presence of a linear chain capped with tyrosine) is able to bind to Chy better than a dendrimer without the tyrosine chain (Figure 37). Analogous experiments and measurements of the non-functionalised G3.5-COOH **12** were used. This permitted identification of the dendrimer which had the most effective inhibition (i.e. with or without functionalisation).

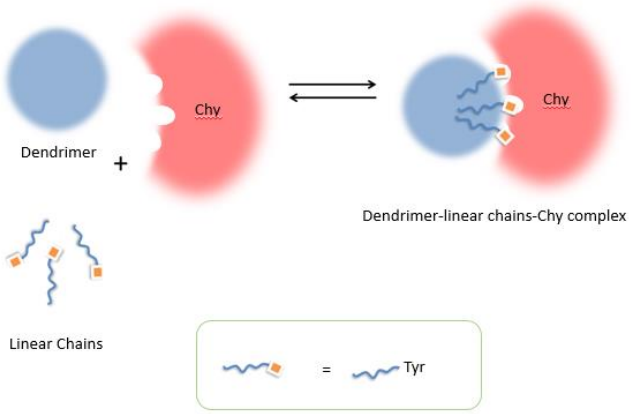

*Figure 37: Non- covalent G3.5-COOH **12** with tyrosine chain **21** to inhibit Chy*

The next step involved the encapsulation process, which was carried out using methanol and 0.5 µM concentrations of G3.5-COOH **12** with 5.0 µM linear chains **21**. The solvent was removed to yield a PAMAM dendrimer/linear chains co-precipitate. Phosphate buffer (pH 7.46, 0.1 M) was added to the precipitate and the solution filtered. The dendrimer-chain complex was then added to Chy solution (as previously described).

BTNA **26** [S], µM	0.0 µM Control	0.2 µM G3.5-COOH-Tyr **24**	0.4 µM G3.5-COOH-Tyr **24**	0.8 µM G3.5-COOH-Tyr **24**
	Initial velocity (V), nMs^{-1}			
2.0	1.380 (±0.571)	0.683 (± 0.051)	0.468 (±0.040)	0.251 (±0.043)
4.0	2.230 (±0.872)	1.163 (±0.841)	0.820 (±0.060)	0.480 (±0.066)
6.0	2.780 (±0.109)	1.503 (±0.914)	1.150 (±0.977)	0.673 (±0.051)
8.0	3.240 (±0.217)	1.771 (±0.132)	1.280 (±0.121)	0.876 (±0.022)

*Table 8: The summary of initial velocity data in the absence (Chy only) and presence of G3.5-COOH-Tyr **24**. Chy at 0.4 µM.*

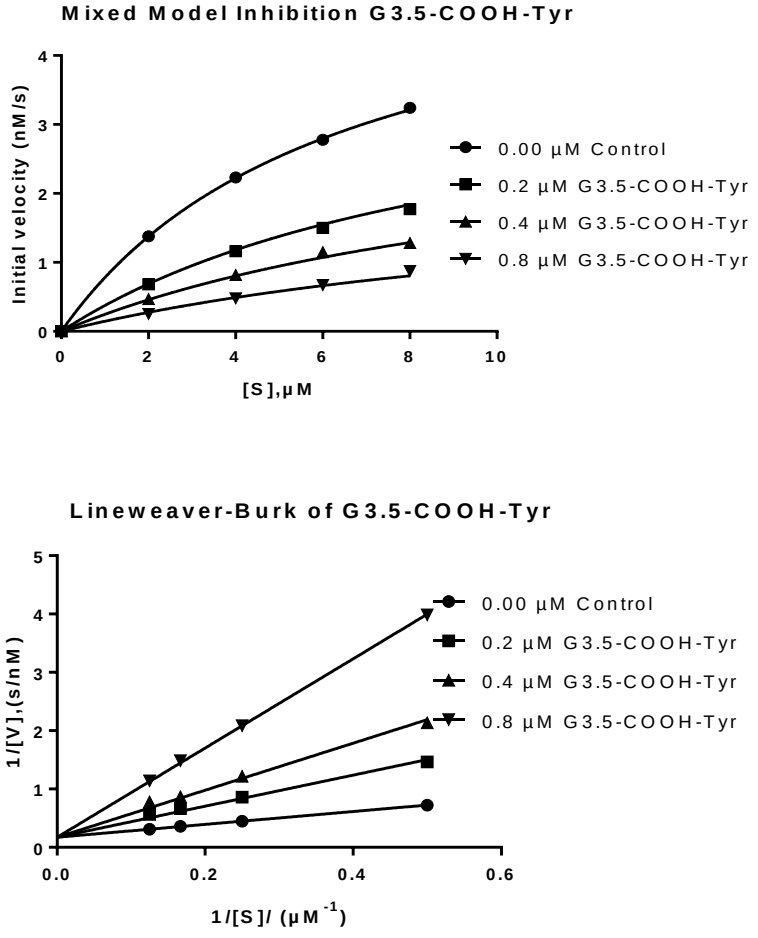

*Figure 38: Mixed mode inhibition and Lineweaver-Burk plots of G3.5-COOH-Tyr **24**. Chy at 0.4 µM.*

Dendrimer / Kinetic inhibition data	3.5-COOH **12**	G3.5-COOH-Tyr **24**
V_{max} , nMs^{-1}	6.00 (± 0.011)	6.00 (± 0.005)
Alpha, α	2.57 (± 0.002))	3.02 (±0.002)
K_i , µg/mL	0.31 (± 0.020)	0.17 (±0.004)
K_m , µM	6.34 (± 0.030)	6.41 (±0.022)

*Table 9: Summary of parameters obtained from a linear fit of data for a control, non-functionalised G3.5-COOH **12** and functionalised G3.5-COOH-Tyr **24**.*

The data for experiments with various substrate and G3.5-COOH-Tyr **24** concentrations are in Table 9. The Lineweaver-Burk plot (Figure 38) shows a common y-intercept, indicating competetive inhibition. If the tyrosine chain did not affect the binding affinity, G3.5-COOH **12** should bind with equal strength as the functionalised PAMAM and the kinetic data would be the same as reported for the G3.5-COOH **12** on its own. The results in Table 10 show that with incorporated linear chains binds and inhibits better than the dendrimer alone. The V_{max} obtained was the same as at 6.00 nMs^{-1}, however, the K_m value increased from 6.34 µM (for non-functionalised G3.5-COOH **12**) to 6.41 µM (for G3.5-COOH-Tyr **24**) because of weaker binding between the BTNA **26** and the Chy. Furthermore, it can be concluded from the α value and Lineweaver-Burk plots that both inhibitors demonstrate competitive inhibition. The α value increased from 2.57 (for non-functionalised G3.5-COOH **12**) to 3.02 when the tyrosine chain was present (G3.5-COOH-Tyr **24**), confirming that binding inhibition was much stronger.

As such, G3.5-COOH-Tyr **24** is a better inhibitor than the non-functionalised G3.5-COOH **12** dendrimer. This is also demonstrated by K_i which is much lower for the functionalised dendrimer. The results confirm that G3.5-COOH-Tyr **24** has a greater binding affinity (and therefore inhibits the activity of Chy at a much lower concentration) than the non-functionalised dendrimer. Specifically, the K_i value for the functionalised system was 45% lower than K_i for the non-functionalised dendrimer (0.17 uM and 0.31 uM, respectively). Therefore, both systems bind to the interfacial area using their carboxylate groups but binding is improved by secondary interactions between the tyrosine functional groups and specific sites on the protein's binding surface.

The dendrimer-chain system is dynamic and the chains can move to maximise any interaction. Therefore, the protein will establish an equilibrium where the most stable species may be a protein-dendrimer complex involving the linear chains encapsulated within the dendrimer. However, as previously mentioned, although the orientation of chains encapsulated within the dendrimer is unknown, it would be reasonable to assume that the tyrosine-targeting group is on the outside of the dendrimer and the hydrophobic amides chain hydrogen bond to the amides within the dendrimer as shown in Figure 39 (a). However, it is possible that the tyrosine units are inside the dendrimer and the hydrophobic amide chains are outside, binding to the hydrophobic patches on the surface of Chy, to provide a more stable complex (Figure 39b). There is another possibility involving a mixture of orientations as shown in Figure 39 (c). In each scenario, the complexes would slow down or inhibit the reaction. Overall, the use of a non-covalent method has shown that strong binding is possible and indirectly advocates its suitability as a simple method for functionalisation compared to the covalent method.

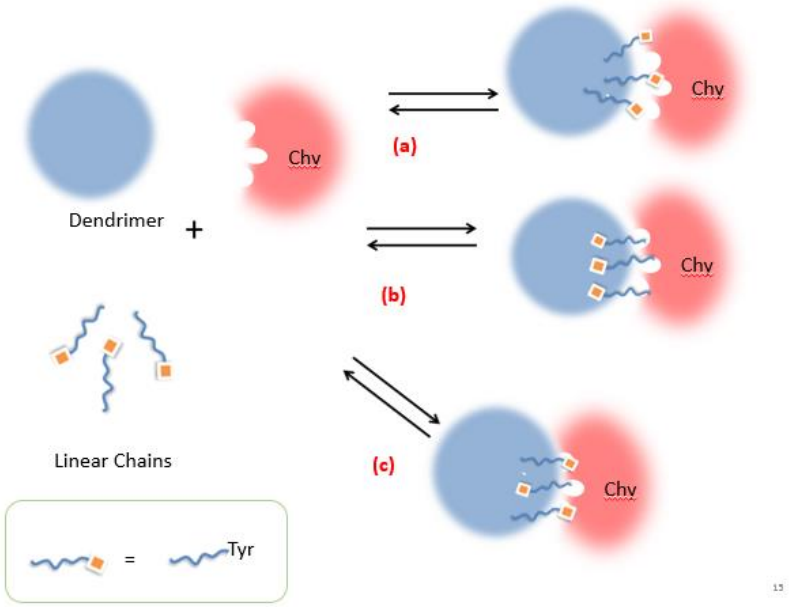

Figure 39: The possible reaction that can inhibit the activity of Chy a) desirable interaction in which functional terminal group bind to the surface of Chy b) non-desirable hydrophobic amide linear chain bind to the surface of Chy and c) the mixed orientation of chains on the surface dendrimer.

2.3 The polyvalent interaction of amino acids binding to the surface of Chy

We have sucessfully demonstrated that a dendrimer functionalised with a non-covalent tyrosine chain can inhibit Chy and function as a competitive inhibitor. However, acid dendrimers can bind on their own (unselective). The amino acid chains improve binding, but the acid interactions are dominant, thus the binding may lack selectivity. Therefore, neutral dendrimers that are unable to bind were chosen for our next study. This would allow us to establish the strength of the tyrosine-protein interactions in the absence of the dominat anionic interactions. If binding takes place, then must arise from the amino acids on the linear chain binding in a cooperative, polyvalent manner to the protein.

2.3.1 Functionalised neutral dendrimers with different functionality as inhibitors of protein interactions

The study by the Twyman group found by that a covalently functionalised dendrimer (tyrosine, phenylalanine and valine) could affect binding in a positive or negative way, depending upon the terminal group functionality. [67] Wenck et al. also reported that molecular recognition of characteristic amino acid residues on the surface of lysozyme leads to efficient enzyme inhibition, which can be switched on and off by non-covalent interactions. [68] Giles et al. demonstrated that functionalised linear copolymers could bind enzymes with improved selectivity. [51] Following that, we decided to incorporate the same key amino acids into our linear chain and use a neutral dendrimer that cannot bind.

2.3.2 Synthesis of neutral dendrimer for non-binding interactions

To achieve our aim, we needed to synthesise a neutral PAMAM dendrimer. This was achieved by converting the ester/half generation PAMAM into PAMAM-OH using ethanolamine via nucleophilic substitution. [69] The reaction is analogous to the EDA reaction. However, as ethanolamine is not very reactive, the conditions used were different to those used in EDA substitution. Nevertheless, the mechanism was comparable. This method was performed using potassium carbonate as a base, as shown in Scheme 16 and a minimum quantity of dimethylsulphoxide (DMSO) as a solvent. The crude product was

initially purified by filtration to give the neutral PAMAM dendrimer in DMSO. Acetone was used to precipitate the crude product as a thick paste. The product was dissolved in the minimum amount of water and the purification process repeated twice to give the neutral PAMAM dendrimer product as a paste in 40% yield.

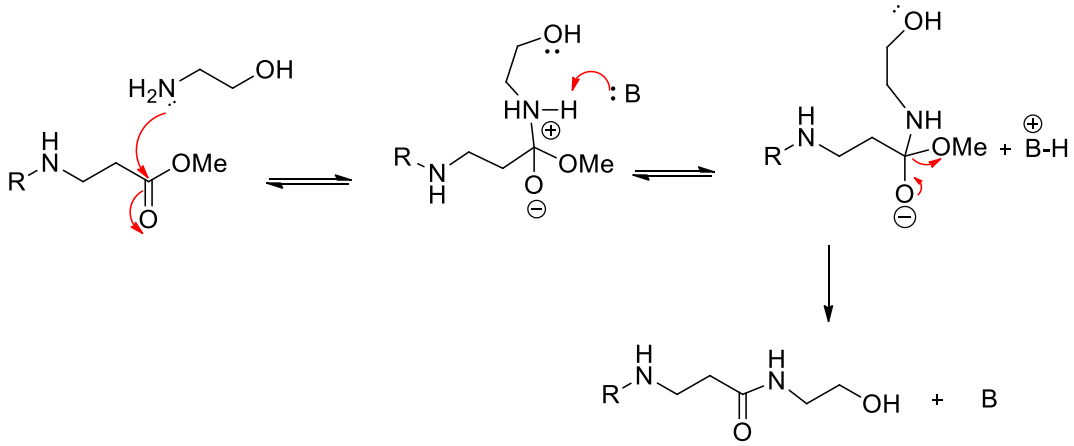

Scheme 16. Addition of ethanolamine groups with potassium carbonate (B) to produce neutral dendrimers.

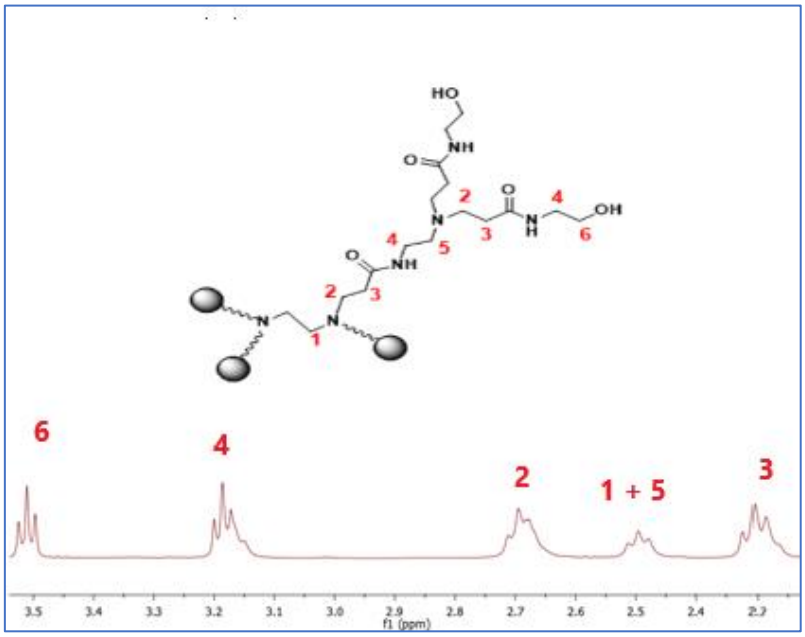

*Figure 40. [1]H NMR spectrum of G1.5 PAMAM-OH **29** after purification (one arm of dendrimer is presented)*

In ^{1}H NMR of the G1.5-OH **29** confirmed the reaction had worked (Figure 40), as the ester methyl peak at 3.69 ppm was no longer visible, and new peaks for the methylene protons (adjacent to the terminal hydroxyl groups) were visible as a triplet at 3.58 ppm. These protons shifted to slightly higher chemical shift compared to other methylene groups due to their proximity to the electronegative oxygen. The success of the reaction was also confirmed by ^{13}C NMR and FTIR spectra, which showed no visible peaks for the ester C=O at 175 ppm and 1735 cm^{-1} for the ^{13}C and FTIR respectively. The MALDI spectrum had a molecular ion at 1438, which is equal to MH^{+} ion. The same procedure and characterisation strategy was used to synthesise neutral dendrimers up to G 3.5 with 32 OH **31**. The data for all dendrimers is shown in Table 10.

Dendrimer Generation	Chemical Formula	Expected Molecular weight (g/mol)	Number Of OH surface groups	Obtained Mass ion (MH^{+})
G1.5-OH **29**	$C_{62}H_{120}N_{18}O_{20}$	1438	8	1438
G2.5-OH **30**	$C_{142}H_{272}N_{42}O_{44}$	3272	16	3272
G3.5-OH **31**	$C_{302}H_{576}N_{90}O_{92}$	6940	32	6941

*Table 10. Analysis of characterisation of generation neutral PAMAM-OHs (**29-31**)*

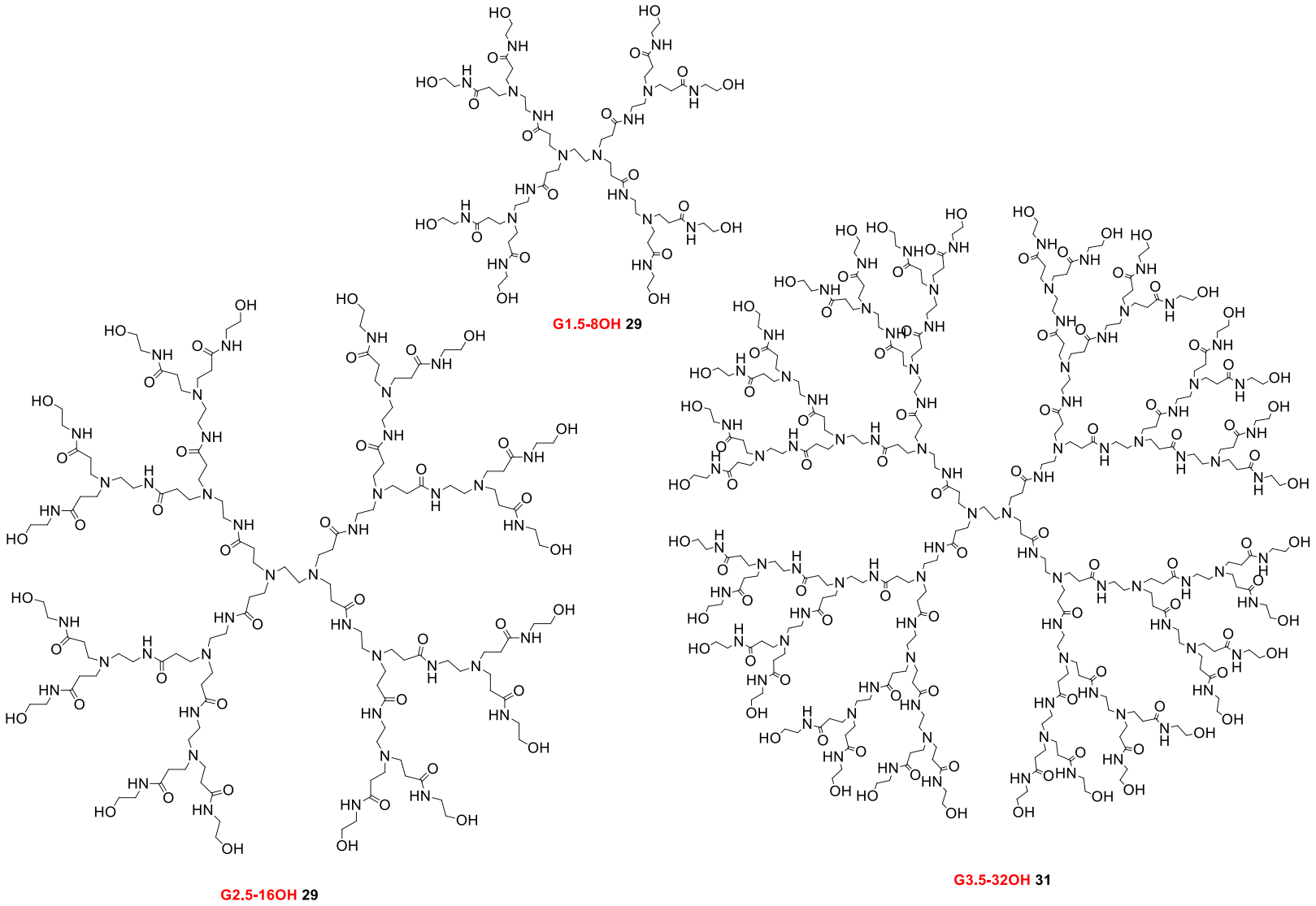

*Figure 41: Prepared neutral terminated PAMAM-OHs (**29-31**).*

2.3.3 Synthesis of linear chains functionalised with phenylalanine and valine

To test the effect of different amino acids on the binding, we selected phenylalanine and valine as alternative capping groups for our linear chain. Phenylalanine is another amino acid known to be important with respect to protein binding. However, due to lack of hydrogen binding function, we expected it to bind weaker than tyrosine. Valine is an amino acid known to have little or no effect on biding. Therefore, when encapsulated into dendrimer we expect to see very little inhibition.

To convert the amino chain **19** into the phenylalanine **33** and valine chain **35,** the same general method and purification were carried out as previously described for tyrosine (*refer section 2.3.5, page 44*). The synthesis route is shown in Scheme 17**.** The phenyl protons were observed between 7.27 ppm and 7.40 ppm for *meta*, *ortho* and *para* respectively. In the DEPTQ ^{13}C NMR spectrum, peaks were attributed to the aromatic group at 128.0 ppm and 129.4 ppm. The mass spectrum showed a molecular ion at 347 (MH^+). Furthermore, FTIR showed peaks 2923 cm^{-1}, 3035 cm^{-1}, corresponding to the C-H and N-H respectively, and at 1528 cm^{-1} from the aromatic C-C bands. For valine, the ^1H NMR showed peaks at 5.28 ppm for the N-H and a peak at 3.55 ppm for the stereogenic CH. Also, a doublet around 1-0.98 ppm and septet at 2.26 ppm for the isopropyl group. The mass spectrum had a molecule ion at 299 (MH^+) and a peak at 323 (MNa^+) indicating that valine **35** had been successfully prepared.

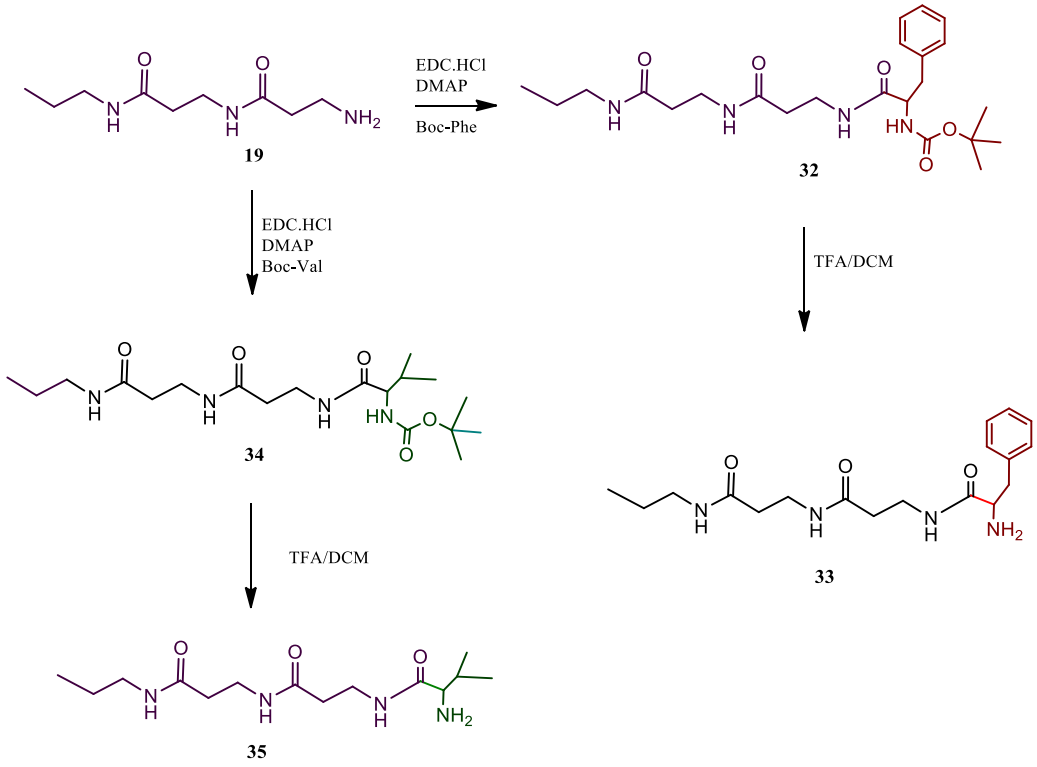

*Scheme 17. Synthesis of phenylalanine **33** and valine **35** from the amino chain **10.***

2.3.4 Encapsulation of the functionalised linear chain with PAMAM-OH dendrimer

In order to evaluate the potential of the non-covalently methodology using neutral PAMAM-OH dendrimers, we needed to establish that the encapsulation of chains could occur. Hence, different generations of neutral PAMAM dendrimers were studied for their encapsulation ability. Specifically, G1.5-8OH **29**, G2.5-16OH **30** and G3.5-36 OH **31** were studied. A large excess of the amino acid chain was added to a methanol solution of dendrimer, and the same procedure and calculation used to encapsulate the tyrosine chain **21** (*refer section 2.2.6, page 46*) was also applied here and the resulting UV spectrum shown in Figure 42.

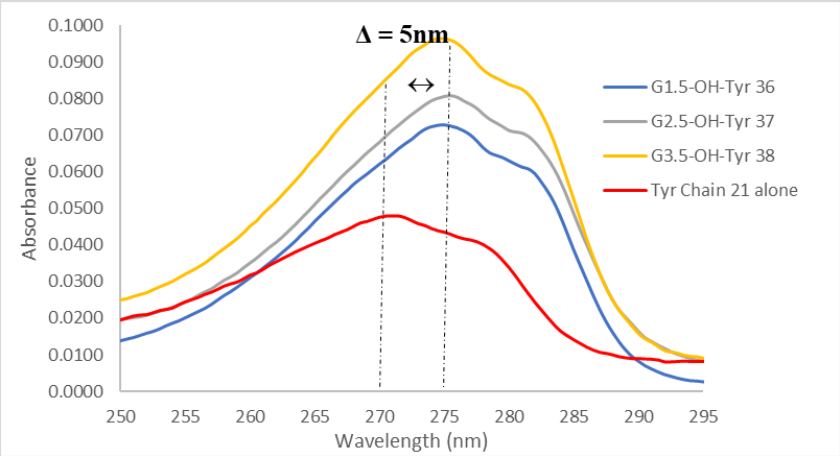

*Figure 42. UV absorbance data before and after encapsulation of tyrosine **21** in different generation of neutral dendrimer (representative graph).*

a) Encapsulation data for Tyrosine **21**

Generation dendrimer	Absorbance	Concentration of Chains, **x**/ M	Concentration of Dendrimer, **z** / M	Ratio of chain to dendrimer	Chain(s) encapsulated* (x-y)/z
G1.5-OH **29**	0.0727	8.60E-06	1E-06	8.6	3 (±0.30)
G2.5-OH **30**	0.0805	9.52E-06		9.5	4 (± 0.25)
G3.5-OH **31**	0.0964	1.14E-05		11.4	6 (±0.41)
Free tyrosine chain **21** in buffer (y) =5.13E-06 *subtracted with the background solubility of the tyrosine chains **21**					

b) Encapsulation data for Phenylalanine **33**

Generation dendrimer	Absorbance	Concentration of Chains, **x**/ M	Concentration of Dendrimer, **z** / M	Ratio of chain to dendrimer	Chain(s) encapsulated* (x-y)/z
G1.5-OH **29**	0.0591	6.82E-06	1E-06	6.8	3 (±0.28)
G2.5-OH **30**	0.0712	8.22E-06		8.2	4 (± 0.22)
G3.5-OH **31**	0.0845	9.76E-06		9.8	6 (±0.42)
Free phenylalanine chain **33** in buffer (y) =4.18E-06 *subtracted with the background solubility of the phenylalanine chains **33**					

c) Encapsulation data for Valine **35**

Generation dendrimer	Absorbance	Concentration of chains, **x**/ M	Concentration of Dendrimer, **z** / M	Ratio of chain to dendrimer	Chain(s) encapsulated* (x-y)/z
G1.5-OH **29**	0.1200	9.23E-06	1E-06	9.2	3 (±0.27)
G2.5-OH **30**	0.1325	1.02E-05		10.2	4 (± 0.22)
G3.5-OH **31**	0.1564	1.20E-05		12.0	6 (±0.43)
Free valine chain **35** in buffer (**y**) =5.87E-06 *subtracted with the background solubility of the valine chains **35**					

*Table 11. Analysis of the encapsulation of PAMAM-OH with linear chain of a) tyrosine **21**, b) phenylalanine **33** and c) valine **35** at 0.1 µM Tris buffer.*

Table 12, the effect of size generation of dendrimer on the solubility of the functionalised chains can be seen. Where G1.5 had eight OH groups, only 3 chains could be incorporated into the dendrimers' hydrophobic void. Furthermore, for the G2.5 with 16 OH groups, four chains were encapsulated, and for the G3.5 with 36 OH group, 6 chains were encapsulated inside the dendrimer. The data is summarised in Figure 43

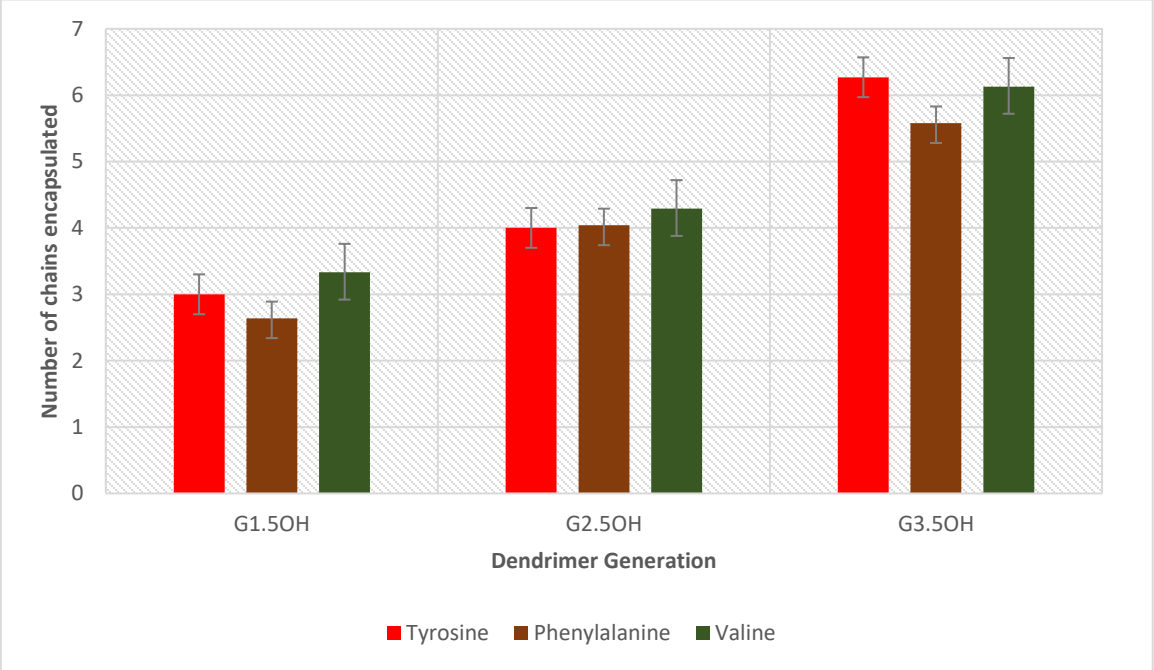

Figure 43: Trend line of the number of chains encapsulated in the different generations of PAMAM-OH.

The increasing trend line in encapsulation is due to the number of hydrogen bonding sites and the increased hydrophobic and globular structure of the higher generation of PAMAM dendrimers. Though the loading increased for the largest dendrimer studied, there was no significant difference between the G1.5-8OH **29** and G2.5-16OH **30**. This is probably due to the relatively open structures for these smaller dendrimers, resulting in a poor hydrophobic cavity being formed. This is a known effect and is linked to the lack of a densely packed structure for these small dendrimers. [70-71]

We already knew that the G3.5 dendrimer was the optimum size for interacting with the binding area of Chy,[67] but G3.5 (32 end groups) is also the best-sized dendrimer for encapsulating the maximum number of targeting chains. After studying the effect of dendrimer size on encapsulation capacity, the study continued by investigating the spectra of the complex in Figure 45. Due to the different environment within the dendrimer, we can see a clear shift in tyrosine λ_{max} after encapsulation. However, for the other chains, λ_{max} did not change. We are not sure why, but one possibility is a difference in the orientation of the encapsulated chains. For tyrosine **21**, it could be that the amino acid end group is within the dendrimer. For the other amino acids, the head group could be orientated "out", with the amino acid groups being solvated by bulk water. This needs further investigation. However, all bonding is non-covalent. The tyrosine linear chains could re-orientate themselves so that their head group points out and interacts with the protein (Figure 44).

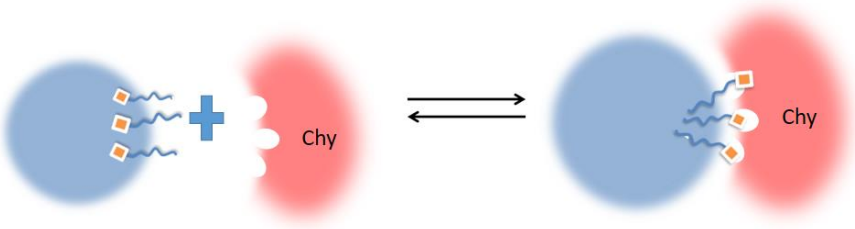

Figure 44: The possible situation when the linear chains re-orientate and interact with the Chy.

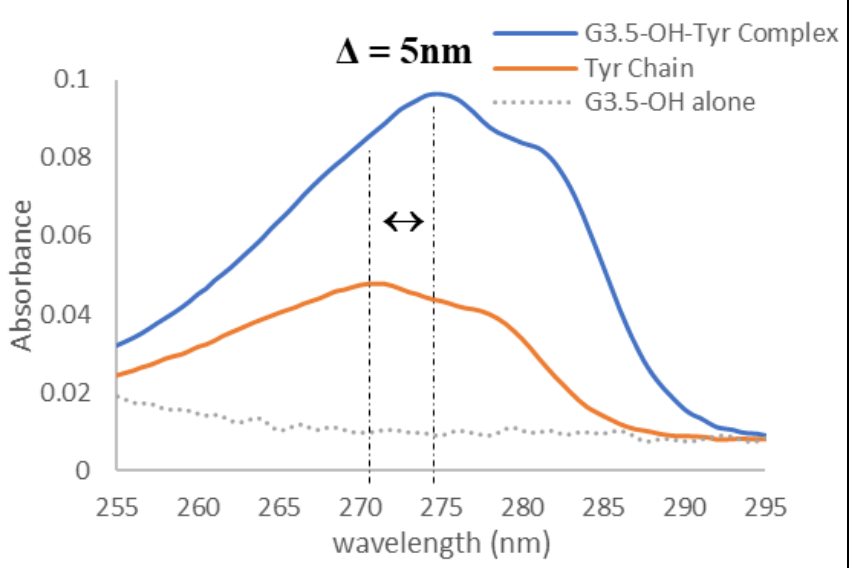
Δ = 5nm
G3.5-OH-Tyr Complex
Tyr Chain
G3.5-OH alone
Absorbance
0.1
0.08
0.06
0.04
0.02
0
255
260
265
270
275
280
285
290
295
wavelength (nm)

(a)

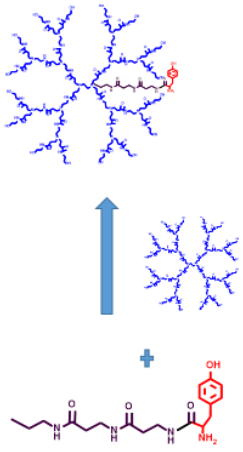

21

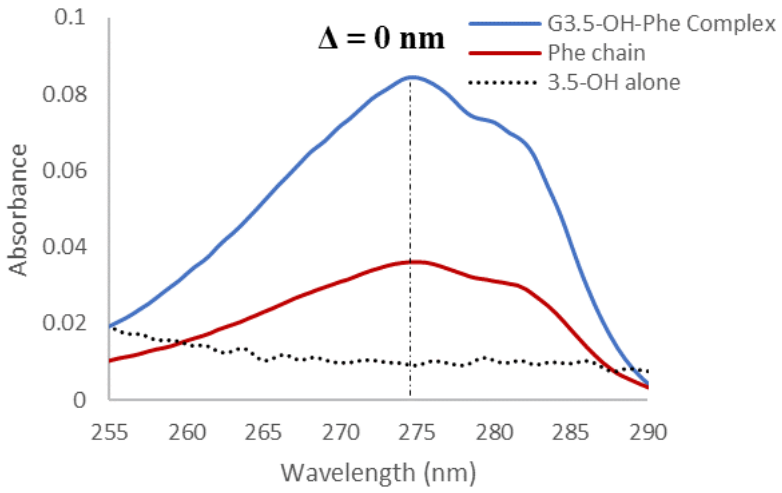
Δ = 0 nm
G3.5-OH-Phe Complex
Phe chain
3.5-OH alone
Absorbance
0.1
0.08
0.06
0.04
0.02
0
255
260
265
270
275
280
285
290
Wavelength (nm)

(b)

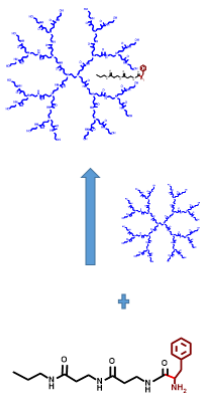

33

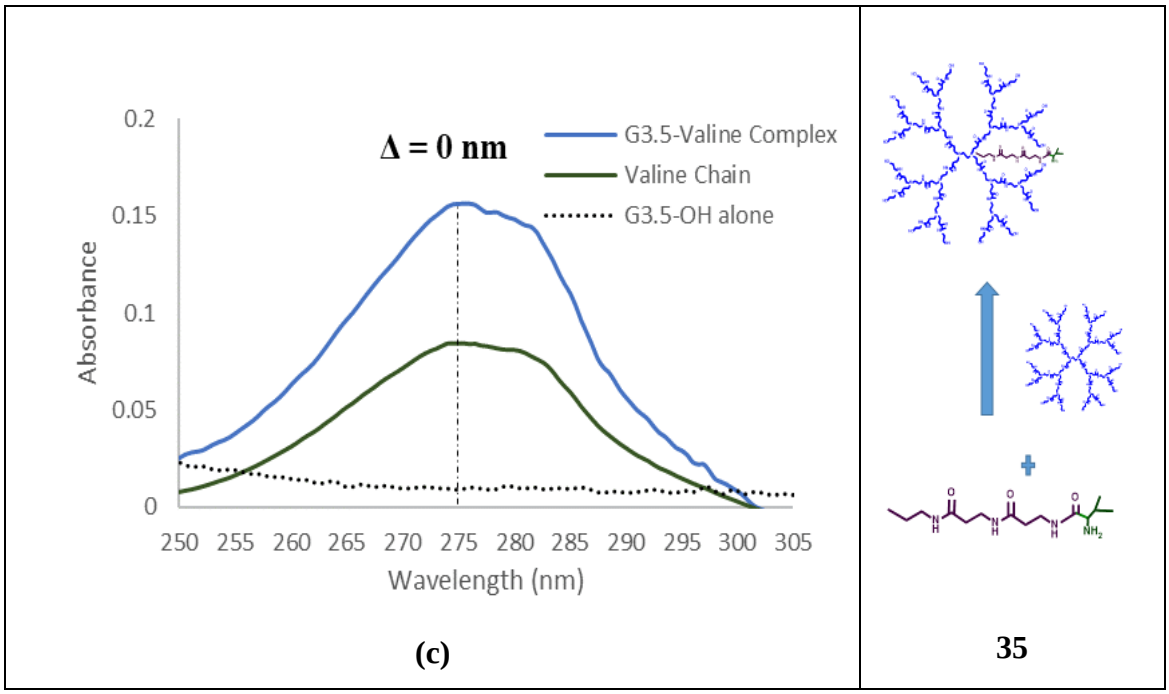

*Figure 45: UV absorbance before and after encapsulation of G3.5-OH **31** with different terminal chains a) tyrosine **21** b) phenylalanine **33** and c) valine **35** in the TRIS buffer 0.1 µM.*

Generation dendrimer	Baseline Corrected Absorbance at λ_{max}	Molar absorption coefficient (ε) / M^{-1} cm^{-1}	Concentration of chain (s) / M	Ratio of chain to dendrimer	Chain (s) encapsulated*
G3.5-OH-Tyr **38**	0.0964	8456	1.14E-05	11.4	6 (±0.41)
*Free Tyr **21** Chain	0.0434		5.13E-06	5.1	n/a
3.5-OH-Phe **39**	0.0845	8660	9.76E-06	9.8	6 (±0.42)
*Free Phe **33** Chain	0.0362		4.18E-06	4.2	n/a
G3.5-OH-Val **40**	0.1564	14400	1.20E-05	12.0	6 6 (±0.43)
*Free Val **40** Chain	0.0845		5.87E-06	5.9	n/a
Concentration of Dendrimer, M = 1.00E-06 *Background solubility subtracted					

*Table 12: UV absorbance data of chains before (free) and after encapsulation by G3.5-OH **31**.*

The data summarised in Table 12 indicates that G3.5-32 OH **38** solutions can solubilise 11 linear chains with at least 6 being encapsulated within the dendrimer through supramolecular/non-covalent interactions. It also confirms that a neutral dendrimer can act as a scaffold for the linear chain. The next step was to test the inhibition properties of these complexes.

The intention of this part of the study is to determine how important and strong the polyvalent interactions from the amino acids are when binding proteins. If this methodology is valid, then the dendrimers functionalised with amino acids known to be involved in protein-protein binding, should bind well to the surface of α-chymotrypsin and inhibit its function. On the other hand, a dendrimer functionalised with valine, which is not associated with protein binding, would result in weaker binding and less inhibition. This is the same hypothesis used in the previous work described by Bogan[12] and Twyman.[35] If polyvalent interactions are not observed or if the orientation of the chains is not compatible with binding, then there will be no change in binding. In that instance, the kinetic inhibition data would be the same as that measured in the G3.5-OH **31** control reaction/experiment.

2.3.5 Assay of neutral G3.5 and tyrosine complex as an inhibitor to α- Chymotrypsin

The experiment used the same method as the anionic PAMAM dendrimers when determining the inhibition and kinetic data. The first experiment was a control only using BTNA **26** and Chy in buffer (pH 7.46). This provided the initial rate of nitroaniline **28** production.

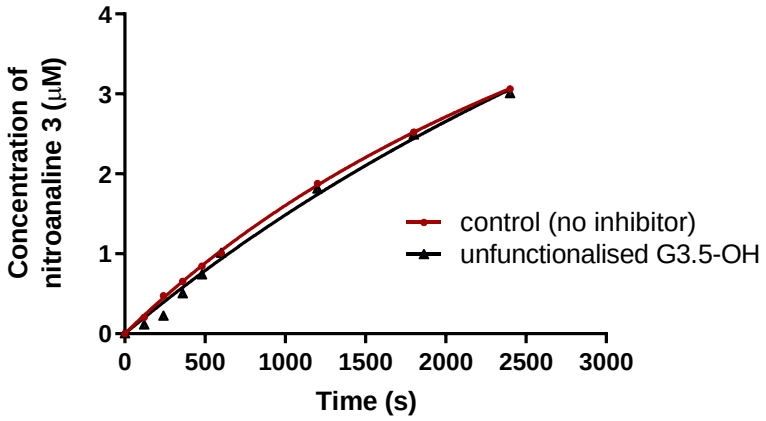

*Figure 46. Rate plot for hydrolysis of 2.0 μM BTNA **26** in 0.4 μM of Chy in the absence and presence of unfunctionalised G3.5-OH **31**, leading to the formation of nitroaniline **28**.*

The data is shown in Figure 46 and is similar to the profile observed earlier for PAMAM-COOH system (*refer Figure 29*). Analysis confirmed an initial rate of reaction 1.38 x 10^{-9} Ms^{-1}. To test whether or not the neutral dendrimer could bind, the reaction was repeated using G3.5-OH **31** at a final concentration equivalent to the enzyme (0.4 μM). As expected the profile did not change and confirms that the G3.5-OH **31** PAMAM does not bind to the protein or inhibit the reaction. This is because the dendrimer does not have any groups that can interact with charged surface or any other groups present on the protein, as depicted in Figure 47. This means that any binding following the addition of the functionalised chains could be associated with polyvalent interactions between the amino acids and the protein surface.

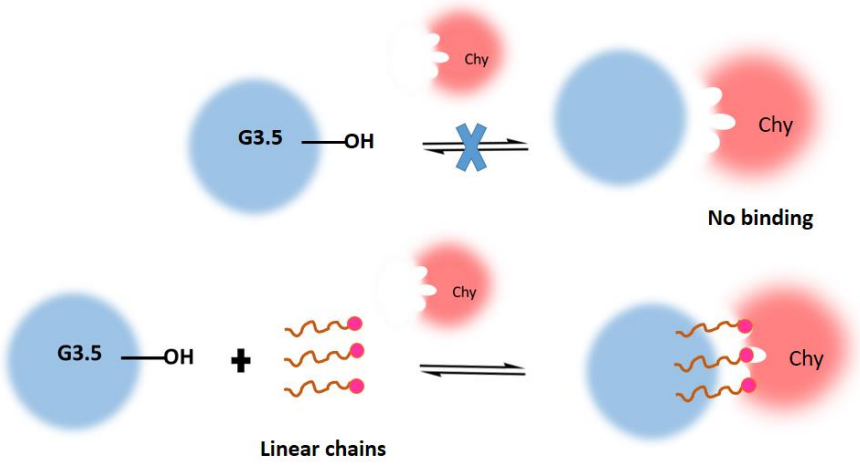

Figure 47: Cooperative interactions of the amino acid with the Chy's surface.

The next step was to prepare the complex between the neutral dendrimer and the linear chains. Encapsulation was carried out using concentration of 0.4 µM of G3.5-OH **31** and 4.0 µM linear chains-Tyr **21** (10 eq excess) in methanol. The solvent was removed to yield a PAMAM dendrimer/linear chain co-precipitate. Phosphate buffer (pH 7.46, 0.1M) was then added to the precipitate. A solution of Chy was then added and the mixture pre-incubated for 24 h.

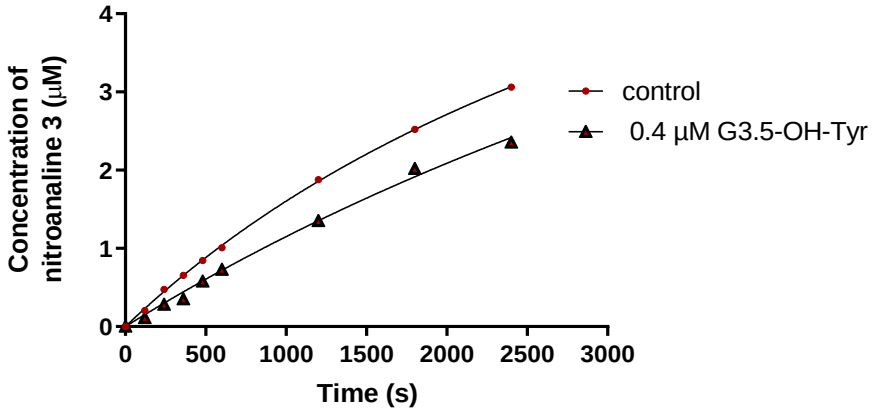

*Figure 48: Rate plot for hydrolysis of 2.0 µM BTNA 26 for a control and G3.5-OH-Tyr **38**. Chy at 0.4 µM.*

A reduced reaction profile was obtained, indicating a slower rate (Figure 48). For the G3.5-OH-Tyr **38** complex, the initial rate was 1.025 nMs^{-1}, which compares to 1.38 $nMs^{-1}$for the control or non-functionalised neutral G3.5-OH **31** alone. Functionalisation of the neutral G3.5-OH can therefore, inhibit Chy by 26% at 0.4 µM. We anticipated that the tyrosine targeting groups were on the outside of the dendrimer and these were capable of binding to complementary groups and hydrophobic patches on the surface of Chy to blocks substrate access to the active site. Further experiments were performed, repeating the reaction using a twice the concentration (0.8 µM) of inhibitor. If our hypothesis of binding/inhibition was correct, we predicted that ≈50% inhibition would occur and the initial rate would be halved (assuming saturation was not reached). However, the results obtained with the G3.5-OH-Tyr **38** concentration of 0.8 µM, showed 41% inhibition (0.820 nMs^{-1}). Although the inhibition did not quite double, it was significantly increased. In order to determine the mode of inhibition, the experiments were repeated using various inhibitor and substrate concentrations.

BTNA **26** [S], µM	0.00 µM Control	0.4 µM G3.5-OH-Tyr **38**	0.8 µM G3.5-OH-Tyr **38**	1.6 µM G3.5-OH-Tyr **38**
	Initial velocity (V), nMs^{-1}			
2.0	1.380 (±0.571)	1.025 (± 0.443)	0.820 (±0.0231)	0.643 (±0.0154)

*Table 13: Initial velocity data of 2µM BTNA **26** (substrate) at different concentration of G3.5-OH-Tyr **38**. Chy at 0.4 µM.*

The concentration of inhibitor was systematically doubled again increasing it from 0.8 to 1.6 µM (concentration and ratio of enzyme and substrate remained constant in all experiments). The initial rate for a1.6 µM inhibitor was 0.643 nMs^{-1}, indicating a 54% level of inhibition. At this concentration, we did not see such a large increase in the initial rate or level of inhibition. This is probably due to saturation with respect to the enzyme and inhibitor concentration. In addition, we decided not to use more than 5.0 µM of G3.5-OH **31**, as the neutral PAMAM has a tendency to form large aggregates. [52] For the next experiments, the substrate concentration was increased but the enzyme concentration was kept the same. Specifically, the substrate (BTNA **26**) concentration was doubled to 4.0 µM and the enzyme kept at 0.4 µM (1:10). The initial rate in the absence of inhibitor was 2.230 x 10^{-9} Ms^{-1}.

The experiments were then repeated using 0.4, 0.8 and 1.6 uM concentrations of inhibitor (G3.5OH-Tyr **38**). The initial rates gradually decreased to 1.18 x 10^{-9} Ms^{-1} in the presence of inhibitor at the maximum concentration used (1.6 μM). The data for all concentrations is shown in Table 14. The experiment was continued using the same concentration of enzyme, but the substrate ratios were increased to 1:15 and 1:20 (6.0 and 8.0 μM BTNA **26**). These experiments were conducted using the same four concentrations of inhibitor G3.5-OH-Tyr **38** (0, 0.4, 0.8, and 1.6 μM). For each concentration of the inhibitor G3.5-OH-Tyr **38**, the initial velocities were obtained (Table 14). In all cases, the reaction profiles and initial velocities were reduced when compared to the control reaction(s). Overall, as the concentration of G3.5-OH-Tyr **38** inhibitor increases, the initial velocities are reduced. When the substrate concentration increases then the initial velocities increase.

BTNA **26** [S], μM	0.00 μM Control	0.4 μM G3.5-OH-Tyr **38**	0.8 μM G3.5-OH-Tyr **38**	1.6 μM G3.5-OH-Tyr **38**
	Initial velocity (V), nMs^{-1}			
2.0	1.380 (±0.571)	1.025 (± 0.443)	0.820 (±0.023)	0.643 (±0.015)
4.0	2.230 (±0.872)	1.710 (±0.666)	1.410 (±0.523)	1.180 (±0.411)
6.0	2.780 (±0.109)	2.100 (±0.821)	1.840 (±0.786)	1.421 (±0.622)
8.0	3.240 (±0.217)	2.511 (±0.922)	2.162 (±0.843)	1.680 (±0.771)

*Table 14. The summary of initial velocity data in the absence and presence of G3.5-OH-Tyr **38**. Chy at 0.4 μM*

To determine the mode of inhibition, the initial rate data obtained was plotted (Figure 49a) using a mixed inhibition model. In addition, Lineweaver-Burk plots (Figure 49b) were analysed to confirm whether or not the inhibition was competitive or non-competitive. From these plots, a common y-intercept was obtained, indicating competitive inhibition. The values of V_{max}, K_m and K_i, as best-fit values, are summarised in Table 17. The value of α = 1.95, which is more than 1, confirming and enzyme-inhibitor complex had formed. We assumed that binding was via the secondary interactions of tyrosine, as the dendrimer did not bind on its own. These interactions can arise from aromatic π-π, H-bonding and hydrophobic interactions with the surface of Chy. The K_i was 1.23 μM, indicating the

concentration required to inhibit the enzyme (0.4 µM) completely. The K_i and α values of tyrosine functionalised G3.5-OH **31** can be used as a reference to compare with phenylalanine and valine to show the effect of terminal group functionality in inhibiting Chy.

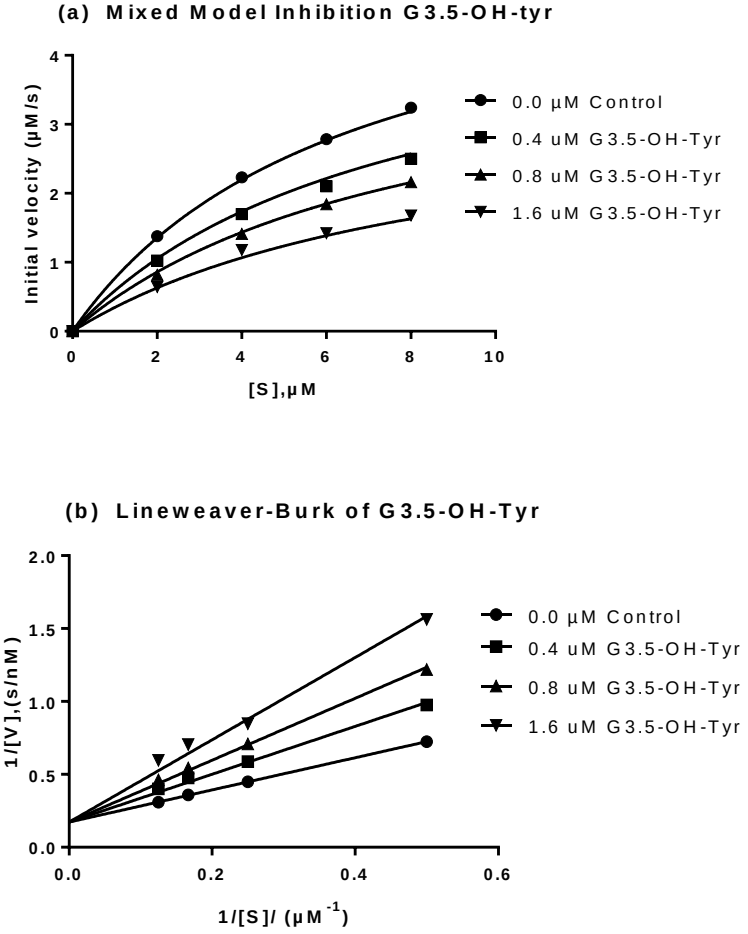

*Figure 49: (a) Mixed mode inhibition and (b) Lineweaver-Burk plots for G3.5-OH-Tyr **38** at 0.4 µM of Chy.*

Dendrimer / Kinetic inhibition data	Control/ non-Functionalised G3.5-OH **31**	G3.5-OH-Tyr **38**
V_{max} , nMs^{-1}	Not applicable	6.00 (± 0.013)
Alpha, α		1.95 (± 0.021)
K_i , µg/mL		1.23 (± 0.017)
K_m , µM		6.56 (± 0.015)

*Table 15. Summary of parameters obtained from a linear fit of data for a control (or non-functionalised G3.5-OH **31**) and functionalised G3.5-OH with tyrosine **38**.*

2.3.6 Assay of neutral PAMAM dendrimers functionalised with linear chain-phenylalanine 33

To demonstrate the influence of ligands on binding ability, we turned our attention to the use of different amino acids on the terminal group. Initially, we studied phenylalanine **33** and performed measurements analogous to those used for G3.5-OH-Tyr **38**. This permitted investigation into the effectiveness of the amino acid and allowed us to compare the results from the previous study using covalently attached amino acids; these found that phenylalanine bound slightly less strongly than the tyrosine dendrimer.[67] Experiments using different amino acids also allowed us to determine whether or not the amino acids are on the periphery of the dendrimer complex. For example as illustrated in Figure 50, if the amino acids were inside the dendrimer then the same inhibition result would be obtained for all amino acids. If this were the case, then it confirms that binding to the enzyme occurs via the hydrophobic ends of the linear chain, and not the amino acid head group.

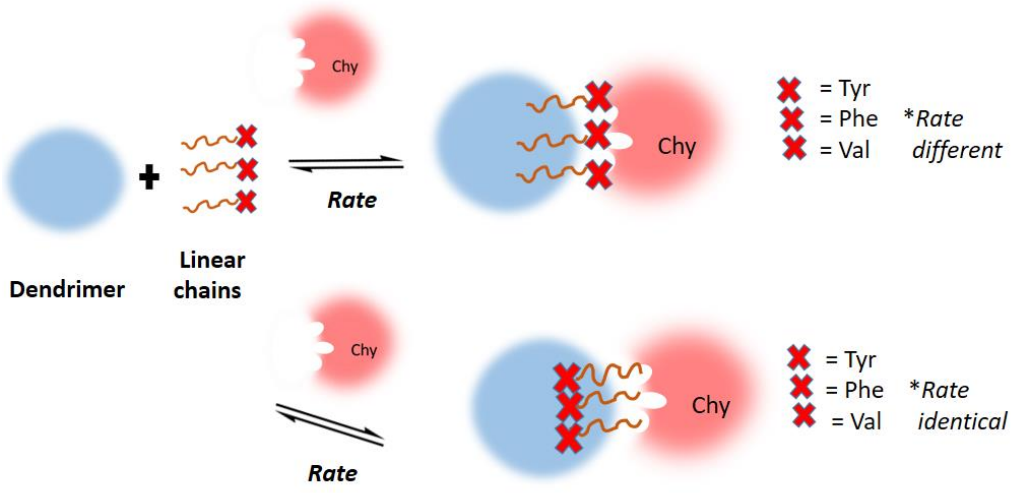

Figure 50: Possible orientations of amino acid chains in the dendrimer. If the head is on the surface, the rates will be significantly different when X= Tyr/Val. However, if rates are the same, then head groups are probably buried in the dendrimer.

The kinetic data for experiments with substrate and various concentrations of G3.5-OH-Phe **39** is shown in Table 16. The Lineweaver-Burk plot (Figure 51) confirms competitive inhibition, and the data is summarised in Table 17. The V_{max} obtained for G3.5-OH-Tyr **38** and G3.5-OH-Phe **39** gave the same value of 6.00 nMs^{-1}. The K_m value for the Phe was 6.31 µM, which is slightly lower than the value for G3.5-OH **31** (6.56 µM). This indicates that the Phe interacts similarly to the Tyr, and the slight decrease is due to Phe not having the extra H bond provided by tyrosine phenol. This is confirmed by K_i of 1.933 µM, which is slightly higher than G3.5-OH-Tyr **38**. Overall, we are sure that Tyr performs better due to the additional hydrogen bonding provided by the phenolic OH. This additional interaction contributes to the better stability of the G3.5-OH-Tyr **38** complex.

BTNA **26** [S], µM	0.00 µM Control	0.4 µM G3.5-OH-Phe **39**	0.8 µM G3.5-OH-Phe **39**	1.6 µM G3.5-OH-Phe **39**
	Initial velocity (V), nMs^{-1}			
2.0	1.380 (±0.571)	1.161 (± 0.555)	0.998 (±0.042)	0.720 (±0.041)
4.0	2.230 (±0.872)	1.970 (±0.783)	1.680 (±0.550)	1.281 (±0.328)
6.0	2.780 (±0.109)	2.440 (±0.853)	2.051 (±0.704)	1.741 (±0.688)
8.0	3.240 (±0.217)	2.790 (±0.982)	2.350 (±0.877)	1.890 (±0.765)

*Table 16: The summary of initial velocity data, in the absence and presence of G3.5-OH-Phe **39** at 0.4 µM of Chy.*

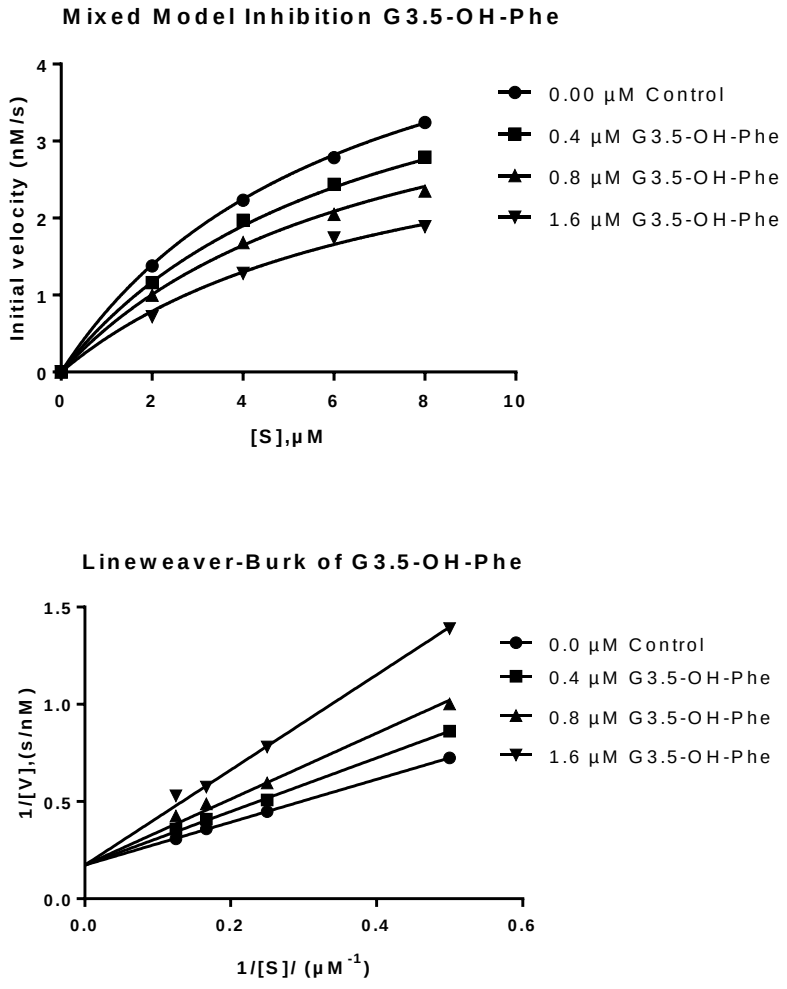

*Figure 51: Mixed mode inhibition and Lineweaver-Burk for G3.5-OH-Phe **39** at 0.4 µM of Chy..*

Dendrimer / Kinetic inhibition data	G3.5-OH-Tyr **38**	G3.5-OH-Phe **39**
V_{max} , nMs^{-1}	6.00 (± 0.013)	6.00 (±0.011)
Alpha, α	1.95 (± 0.021)	1.45 (±0.015)
K_i , µg/mL	1.23 (± 0.017)	1.93 (±0.012)
K_m , µM	6.56 (± 0.015)	6.31 (±0.022)

Table 17: Summary of kinetic parameters obtained from a linear fit.

2.3.7 Assay of neutral PAMAM functionalised with linear chain-valine 35

In contrast to tyrosine and phenylalanine, valine is known to be a bad amino acid with respect to protein binding. As such, if attached to the linear chain and encapsulated within the dendrimer, assuming orientation is with the head group out it should be a poor inhibitor. Therefore, we repeated the inhibition experiments using a linear chain with a terminal valine. From our overall results (Table 18), we see a set of data that indicates poor inhibition and therefore, poor binding. The valine initial rates for all the substrate and concentrations used were very similar to those obtained for the control data. It is clear from Figure 52 that the valine dendrimers do not bind or inhibit chymotrypsin. The Lineweaver-Burk plot shows that there is no common y-intercept, but also the α value is very low (no binding).

BTNA **26** [S], µM	0.00 µM Control	0.4 µM G3.5-OH-Val **40**	0.8 µM G3.5-OH-Val **40**	1.6 µM G3.5-OH-Val **40**
	Initial velocity (V), nMs^{-1}			
2.0	1.380 (±0.571)	1.367 (± 0.568)	1.30 (±0.487)	1.299 (±0.432)
4.0	2.230 (±0.872)	2.190 (±0.866)	2.111 (±0.873)	2.100 (±0.621)
6.0	2.780 (±0.109)	2.700 (±0.111)	2.600 (±0.987)	2.590 (±0.887)
8.0	3.240 (±0.217)	3.100 (±0.231)	3.001 (±0.543)	2.995 (±0.321)

*Table 18. The summary of initial velocity data in the absence and presence of G3.5-OH-Val **40**. Chy at 0.4 µM*

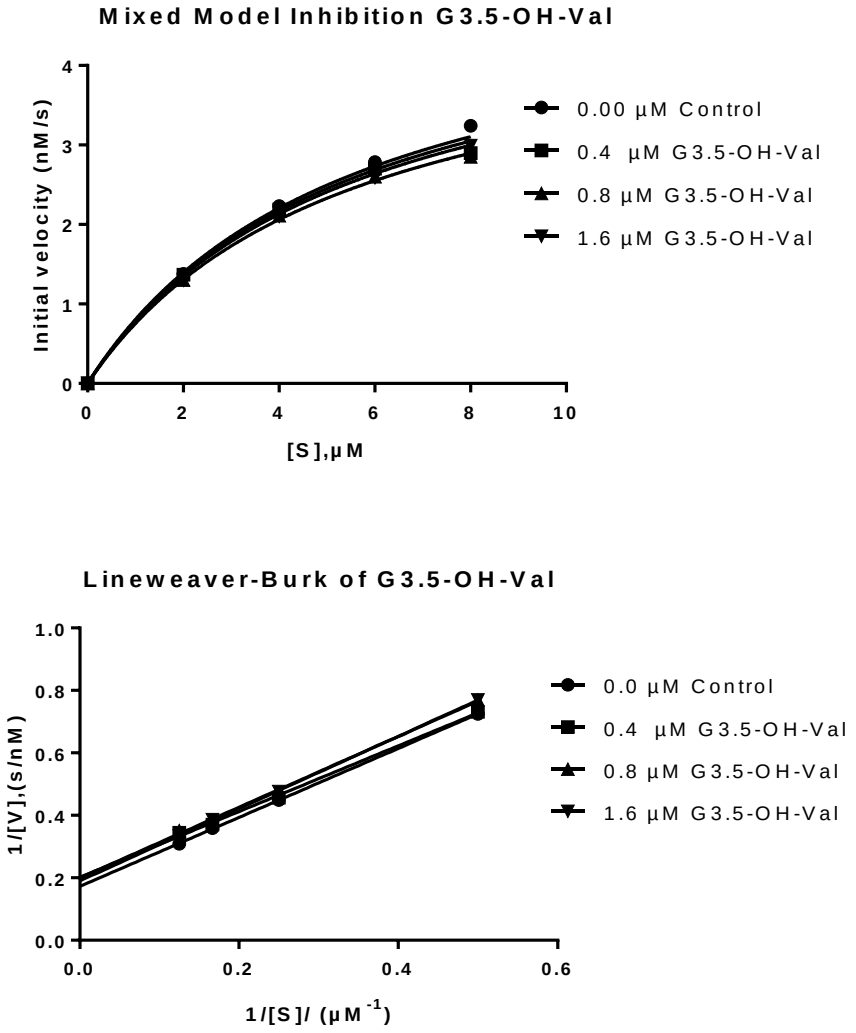

*Figure 52. Mixed mode inhibition and Lineweaver-Burk plots of [BTNA **26**] at various concentrations of G3.5-OH-Val **40** at 0.4 µM of Chy.*

Dendrimer / Kinetic inhibition data	G3.5-OH-Val **40**
V_{max} , nMs^{-1}	5.24 (± 0.182)
Alpha, α	0.85 (± 0.012)
K_i , µg/mL	24.60 (± 0.500)
K_m , µM	5.50 (± 0.004)

*Table 19.Summary of kinetic parameters obtained for functionalised G3.5-OH-Val **40.***

2.3.8 Comparison of functionalised G3.5-OH dendrimer with tyrosine, phenylalanine and valine

Overall, the data confirmed our predictions with regard to amino acid availability and populations at interfacial/binding areas. In particular, the binding affinity of dendrimers functionalised with tyrosine and phenylalanine for chymotrypsin was high. In contrast, valine-functionalised dendrimers demonstrated the lowest inhibition and therefore weakest binding. Valine is occurs commonly in protein structures, but its availability is low at their binding/interfacial areas. Table 20 shows the initial rates at the highest substrate concentrations, which shows that the tyrosine and phenylalanine systems inhibit 48%, and 42% respectively, confirming good binding. However, the valine systems bind very weakly only inhibiting 8 % (± 5%).

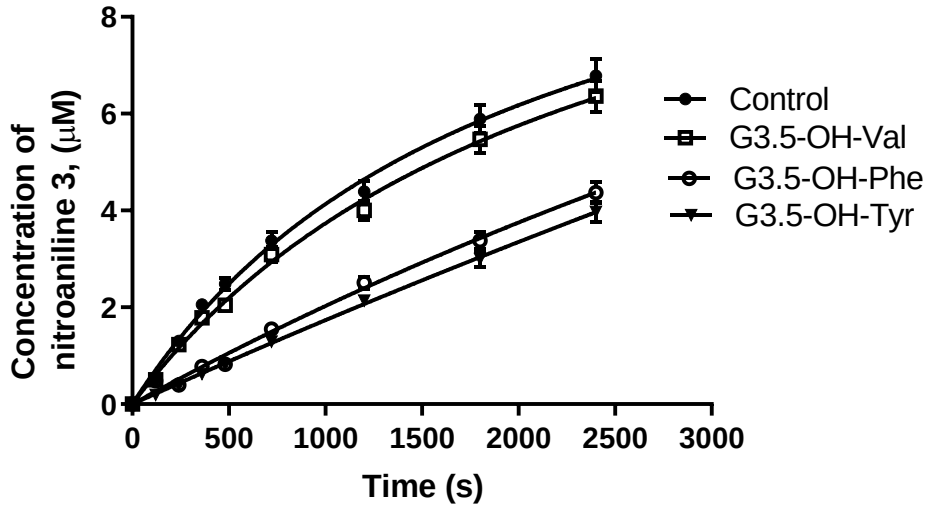

Figure 53: The rate plots of 8.0 μM BTNA 26 (substrate) in the presence and absence for all functionalised G3.5-OH (1.6 μM) during hydrolysis at 0.4 μM of Chy.

Kinetic inhibition data \ Dendrimer	Control / non-functionalised G3.5-OH	G3.5-OH-Val **40**	G3.5-OH-Phe **39**	G3.5-OH-Tyr **38**
Initial velocity (V), nMs^{-1}	3.240 (±0.217)	2.995 (±0.321)	1.890 (±0.765)	1.680 (±0.771
Percentage Inhibition (%)	0	8	42	48

Table 20: Initial velocity translated into percentage inhibition from Figure 53

Dendrimer / Kinetic inhibition data	G3.5-OH-Val **40**	G3.5-OH-Phe **39**	G3.5-OH-Tyr **38**
V_{max} , nMs^{-1}	5.24 (± 0.182)	6.00 (±0.011)	6.00 (± 0.013)
Alpha, α	0.85 (± 0.012)	1.45 (±0.015)	1.95 (± 0.021)
K_i , µg/mL	24.60 (± 0.500)	1.93 (±0.012)	1.23 (± 0.017)
K_m , µM	5.50 (± 0.004)	6.31 (±0.022)	6.56 (± 0.015)

Table 21. Summary of kinetic parameters obtained for all functionalised G3.5-OH

One of the aims was to study the possibility of using a neutral, dendrimers that cannot bind protein or induce inhibition. The aim was to functionalise the dendrimers non-covalently with amino acids known to be good and bad for protein binding and use inhibition as a method to assess binding. Table 21 summarises the kinetic and inhibition results. The V_{max} obtained for the functionalised G3.5-OH showed a V_{max} of 6.00 nMs^{-1} when functionalised with tyrosine and phenylalanine, and slightly lower for valine. The K_m values were also smaller with G3.5-OH-Val **40**, indicating stronger binding between the enzyme and substrate. From the α values and Lineweaver-Burk plots, we confirmed that the tyrosine and phenylalanine ligands demonstrated competitive inhibition. It also can be observed that α was higher for tyrosine **38** (1.95 vs 1.45 for phenylalanine **39**).

Dendrimers functionalised with valine, showed weak binding and uncompetitive inhibition (α = 0.85). The result was confirmed through a Lineweaver-Burk plot, which did not show a common y-intercept. Valine does not contain suitable functionality that can interact (electrostatically, H-bonding, aromatic π-π etc) and is only capable of weak hydrophobic binding, which is very weak, giving a high K_i of 24.60 µM. In contrast, Tyr and Phe had K_i values of 1.93 µM and 1.23 µM respectively. As discussed above, tyrosine bound most strongly, as it has the extra hydrogen bond contributed by the OH on the aromatic group. The results indicate the importance of functionality on molecular interactions with respect to binding to the protein surface of Chy.

In addition, the results show that the head group of the linear chain is important. Specifically, that tyrosine's and phenylalanine aromatic groups results in stronger binding than valine. As such, we have shown that the orientation of linear chain is almost certainly with the head group pointing out (interacting with the protein) and the hydrophobic tail

inside the dendrimer. If this was not the case, then all of the amino acid chains would have bound the same and given similar rates and levels of inhibition.

2.3.9 The effect of the dendrimer terminal's charge and the ligand's functionality

We could compare the results so far and determine whether the dendrimer's terminal charge or the functionality contributes the most to the interactions. This was achieved by comparing the neutral dendrimer (G3.5-OH **31**) with tyrosine ligands with the results from the G3.5-COOH **12** dendrimers with and without the tyrosine linear chains **21**. By comparing the results from these experiments, which are shown schematically in Figure 54, we will be able to determine the extent of any cooperative interactions for the various dendrimer/system.

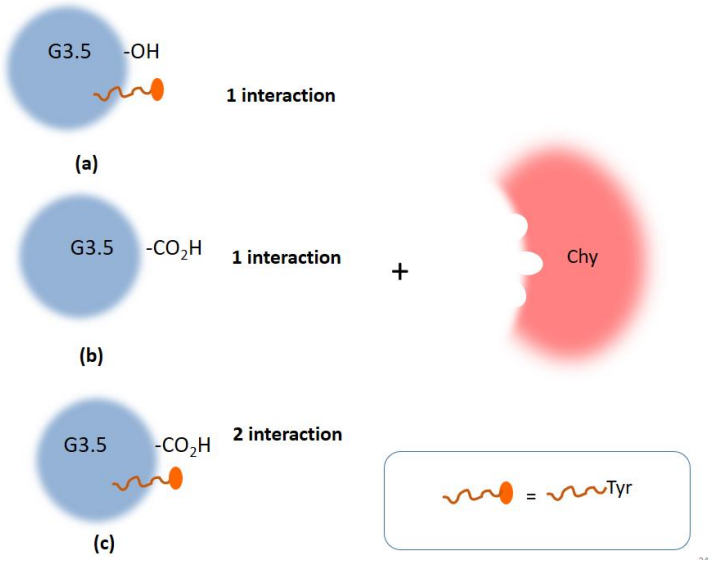

*Figure 54: Illustration to determine whether it is the dendrimer's terminal charge or the functionality of the ligand that contributes the most to the secondary interactions. One interaction when a) G3.5-OH-Tyr **38** is functionality tyrosine binding is important and b) G3.5-COOH **12** possesses dendrimer's terminal charge (carboxylate group) predominantly. Two interactions from c) G3.5-COOH-Tyr **24** which is cooperative interaction between carboxylates and tyrosine ligand.*

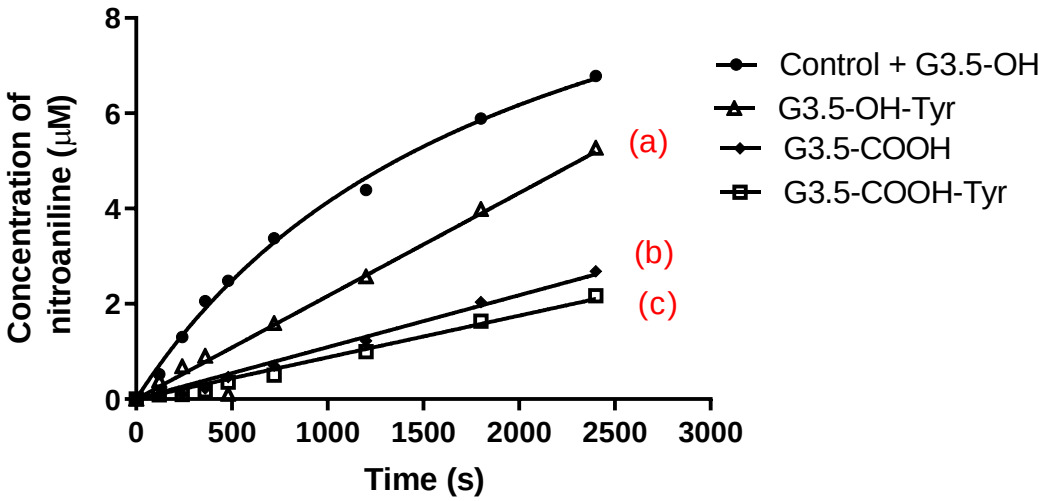

*Figure 55 : Rate plots of 8.0 μM BTNA **26** (substrate) in the presence and absence of dendrimer inhibitors (0.8 μM) during hydrolysis at 0.4 μM of Chy.*

Dendrimer / Kinetic inhibition data	Control/ 3.5-OH **22**	G3.5-OH-Tyr **38**	G3.5-COOH **12**	G3.5-COOH-**Tyr 24**
Initial velocity (V), nMs^{-1}	3.240 (±0.217)	2.162 (±0.843)	1.090 (±0.100)	0.876 (±0.022)
Percentage Inhibition (%)	0	33	66	73

Table 22 :Initial velocity translated into percentage inhibition from data obtained in Figure 55.

Figure 55 shows all of the data. The neutral G3.5-OH **31** dendrimer does not bind to Chy, but can bind when it encapsulates the tyrosine linear chain, giving a relative binding value of 33%. When the anionic G3.5-COOH **12** binds to the positive surface of Chy, there is stronger relative binding of 66%, whilst the G3.5-COOH-Tyr **24** system has a relative binding affinity of 73%.

Overall, the data tells us that the neutral dendrimer with encapsulated aromatic amino acids resulted in reasonable binding, with an α of 1.95 and a K_i = 1.23 μM. However, the K_i decreased significantly when the carboxylate dendrimer was used (0.31 μM). In comparison, the strongest binding occurred with the carboxylic acid dendrimers encapsulated with tyrosine chain (K_i is 0.19 μM and α = 3.02) (Table 23). However, although binding is strongest for the carboxylic acid/tyrosine dendrimer complex, the

increase in binding between dendrimer and dendrimer /chain complex is modest. In contrast, the difference for the neutral system was relatively high (33%)

In addition, the binding of the carboxylic acid dendrimer/tyrosine complex was less than the predicted binding by adding the neutral dendrimer tyrosine complex to the carboxylic acid dendrimer (no tyrosine). That is, if the binding was additive then the carboxylic acid dendrimer/tyrosine complex should have had a relative binding of at least 99% (33% for neutral-Tyr dendrimer plus the 66% for the carboxylic acid dendrimer). This tells us that binding is dominated by charge-charge interactions, with the weaker tyrosine ligand only reinforcing the binding where it can. As such, the use of charge can result in strong non- selective binding, with selectivity being provided by different functionalities on the linear chain. Therefore, to get more selectivity, dendrimers and/ or linear chains with less charge may need to be used.

Dendrimer / Kinetic inhibition data	G3.5-OH Tyr **38**	G3.5-COOH **12**	G3.5-COOH Tyr **24**
V_{max} , nMs^{-1}	6.00 (± 0.013)	6.00 (± 0.011)	6.00 (± 0.005)
Alpha, α	1.95 (± 0.021)	2.57 (± 0.002)	3.02 (±0.002)
K_i , µg/mL	1.23 (± 0.017)	0.31 (± 0.020)	0.17 (±0.004)
K_m , µM	6.56 (± 0.015)	6.34 (± 0.030)	6.41 (±0.022)

*Table 23: Summary of kinetic parameters obtained from a linear fit of data for the enzyme catalysed hydrolysis BTNA **26** including a control, G3.5-OH-Tyr **38**, non-functionalised G3.5-COOH **12**, and functionalised G3.5-COOH-Tyr **24**.*

In order to validate any cooperative/additive binding, we compared our results to those in the literature. Work by Gilles et al. reported a functionalised copolymer that could inhibit a 0.5 µM solution of chymotrypsin with an IC_{50} = 0.44 µM. [51] The kinetic data obtained for G3.5-COOH-Tyr **24** complex translated into the percentage of enzyme activity shown in Table 24 and an IC_{50} value of 0.23 µM was obtained from a plot of [BTNA **26**] vs [G3.5-COOH-Tyr **24**] (0.4 µM solution of chymotrypsin). We cannot compare our results directly with work of Gilles, because the substrate and concentration of the enzymes used were different. However, if we normalise for the enzyme then we get an IC_{50} of 0.28, which is significantly better than the IC_{50} of the copolymers studied by Gilles.[51] This supports our earlier assumption that the organised shape dendrimer acts as a scaffold to present its terminal charges in a size-controlled manner and present the functionalised linear chains in an organised arrangement, so as to maximise binding.

Enzyme Activity (%)

[G3.5-COOH-Tyr **24**], µM	2.0 µM BTNA **26**	4.0 µM BTNA **26**	6.0 µM BTNA **26**	8.0 µM BTNA **26**
0.0 (control)	100	100	100	100
0.2	49.50	52.15	54.07	54.63
0.4	33.91	36.77	41.37	39.51
0.8	18.19	21.53	24.21	27.04

*Table 24 : Data of the enzyme activity obtained from the previous data (Table 9: G3.5-COOH-Tyr **24**) at 0.4 µM of Chy.*

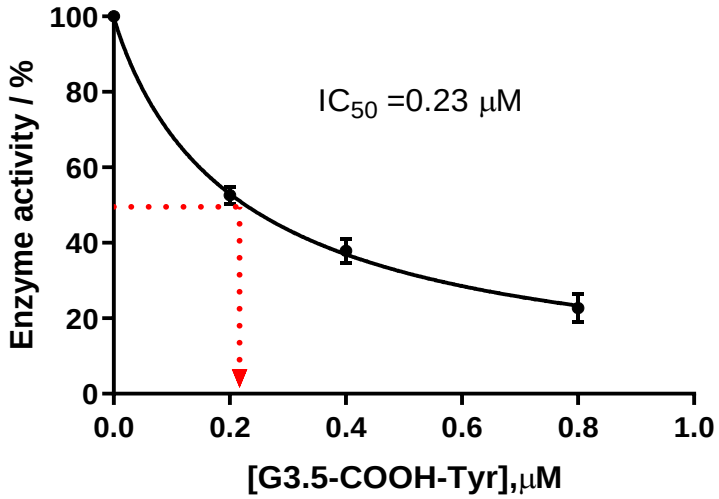

Figure 56. Determination of the IC_{50} value from the data in Table 9

In our case, the value of IC_{50} (0.23 µM) is greater than K_i (0.17 µM), which is another indicator of competitive inhibition. An IC_{50} is traditionally used in medical applications to allow comparisons to be made between various systems. However, recent studies tend to compare K_i values, as these reflect the binding affinity, with the IC_{50} telling us more about the functional strength of the inhibitor (as a drug). [68,72] Nevertheless, in establishing non-covalent interactions with Chy, we do not know if complex formation has altered or denatured the structure of the proteins. This can be studied using circular dichroism (CD) and looking for changes in spectra before and after binding to the dendrimer systems.

2.3.10 Circular dichroism (CD)

This technique can identify denaturation on the secondary structures of protein and polypeptides. The measurement was carried out at pH 7.46 (phosphate buffer 0.1 M) and 37°C. Two characteristic minima conformations of Chy occur in the CD spectra at 232 and 204 nm.[73] The experiment was conducted by comparing the CD spectra of Chy with the spectra obtained for the dendrimer species. The results attained for the dendrimer, with and without chains, do not denature Chy and this concurs with the literature. In this case, the dendrimer systems are sufficiently dynamic/flexible and can change shape to maximise binding, through a process known as the induced fit mechanism. [67,74] The results are shown in Figure 57.

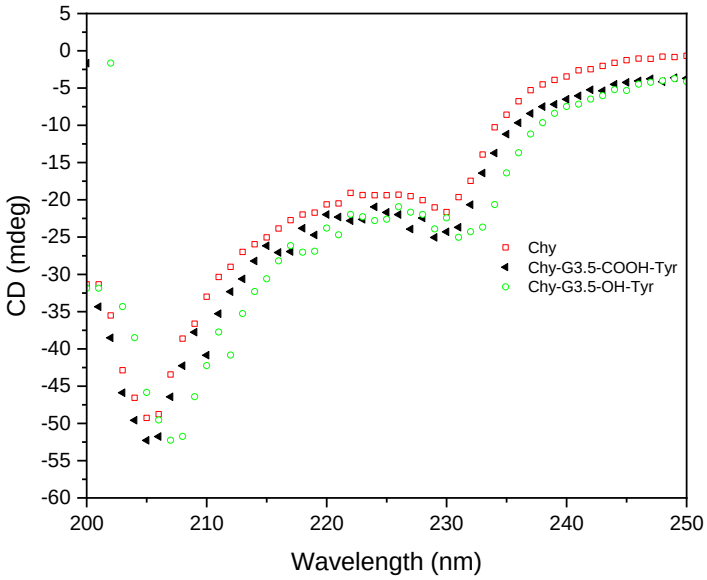

Figure 57. CD spectra for chymotrypsin alone and when bound functionalised dendrimer in phosphate buffer.

The same technique was also used to determine the effect of binding upon protein stability at various temperatures, specifically, to establish whether the dendrimer-chain/protein complex would be more or less stable when subjected to an increase in temperature. Although the functionalised dendrimer did not denature the protein, it may have weakened its structure and made more susceptible to small changes in temperature. As a result, dendrimer binding may make it easier to denature, and changes in the CD spectrum would be seen at lower temperatures (compared to unbound protein).

Alternatively, binding may strengthen the structure and make it resilient to large changes in temperature. In this case, changes in the CD spectrum would occur at higher temperatures (relative to unbound protein).

Therefore, Chy and the protein/dendrimer complexes were heated from 37°C to 65°C with interval time 1°C per minute. Figure 59 shows the change in intensity relating to the denatured protein plotted against temperature at 230 nm. The results obtained for the functionalised dendrimers and Chy were similar as those obtained for Chy alone.

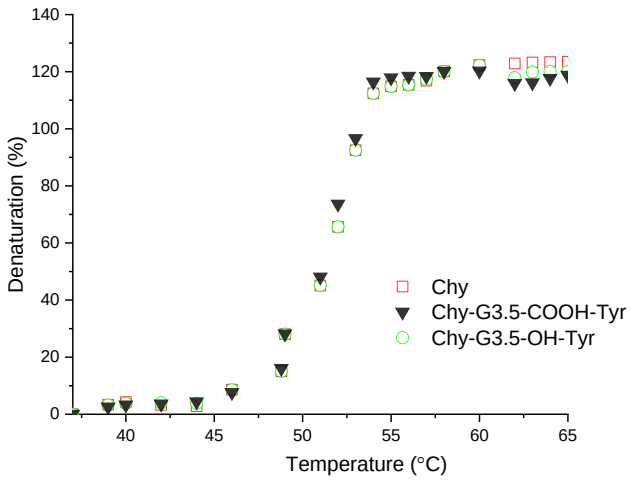

Figure 58. Temperature profiles of percentage denaturation of chymotrypsin when bound to a functionalised dendrimer at 230 nm in phosphate buffer.

Therefore, the protein structure does not change with the presence of the dendrimers system. As such, any effect on the protein function is not caused by structural changes to the protein (as a result of binding).

2.4 Conclusion

Our aim was to use non-functionalised dendrimers and incorporate targeting and binding groups non-covalently into the surface of the dendrimer. A number of linear chains were synthesised and encapsulated within the dendrimer to give the functionalised system. The dendrimers act as a scaffold for the linear chain, which bind to the protein. The functionalised systems that were used confirmed the importance of the charge at the dendrimer's terminal to binding. We also demonstrated that neutral dendrimer functionalised with a different amino acid chain could also bind well to the protein. This confirms that although charge is important, the terminal functionality is key with respect to binding. The next step was to investigate if the same methodologies could be applied to other proteins.

2.5 Future works

Future work relating to this project, would involve developing new multivalent dendrimer-chain complexes that contains a number of different amino acids, which can be presented at their surface (Figure 59). In addition, we will develop a dynamic combinatorial approach, to synthesise functionalised dendrimers using different amino acids chains that can form cross-links to template together or with the dendrimer, in the presence of a protein. This would allow optimum ligand binding opportunities at its binding surface.

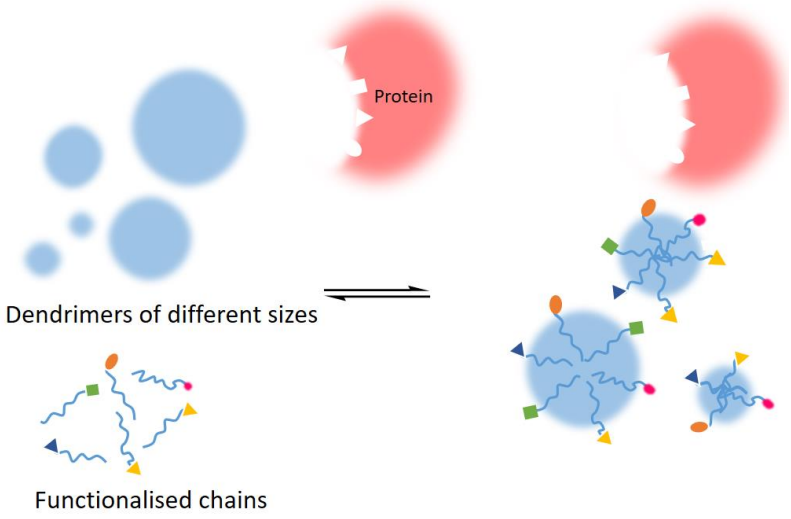

Figure 59: Dynamic Combinatorial Library to self-selected dendrimer-protein complex.

2.6 Experimental

2.6.1 Instrumentation

NMR Spectroscopy
^{1}H NMR and ^{13}C NMR spectra were measured using Brucker AVX400 MHz, Brucker HD400 MHz and Brucker AV1400 MHz.

Infrared (FTIR) Spectroscopy
FT-IR Spectrometer was used, and the spectra was analysed by a Perkin Elmer.

Mass Spectrometry
Matrix Assisted Laser Desorption Ionisation Time of Flight (MALDI-TOF) Spectrometry and Electrospray Ion Mass (ESI-MS) and were performed to analyse the sample.

UV/Vis spectroscopy
The measurement was carried out by Analytik Jena AG Specord S600 and recorded by the Software (WinASPECT).

Circular Dichroism Spectrometer (CD)
The protein solution was analysed by a Jasco (Model J-810) at the wavelength 200-250°C. The result obtained was studied using origin software.

2.6.2 Synthesis of PAMAM dendrimers

Synthesis of PAMAM G0.5 (4 OMe) 1
Ethylenediamine , EDA (10 mL, 150 mmol) in methanol (150 mL) and methyl acrylate (57 mL g, 630 mmol) was added in droplets over 30 minutes. The reaction mixture was allowed to stir at room temperature for 24 hours. The excess solvent and unreacted methyl acrylate were removed and purified. The product (50 g, 98 %) G0.5 **1** obtained as a yellow oil.
FTIR (ν_{max}/cm^{-1}), 2954 ($O\underline{CH_3}$, stretch), 1730 (C=O, ester), 1440 (CH_2, bend),1174 (C-O), 1124, 1039 (C-N); ^{1}H NMR (400 MHz, MeOD), 3.68 (12H, *s*, $O\underline{CH_3}$), 2.77 (8H, *t*, J 7.0 Hz, $N\underline{CH_2}CH_2CO$), 2.53 (4H, *s*, $\underline{CH_2}N$), 2.48 (8H, *t*, J 7.0 Hz, $NCH_2\underline{CH_2}CO$); ^{13}C NMR (100 MHz, MeOD), 174 (C=O),52.0, 51.0 (CH_3), 48.5 , 32.0 (CH_2); Mass spec (ES) 405 (MH^+), 427 (MNa^+) ,ES-MS C_{18} H_{32} N_2 O_8 = 406 (calculated)

Synthesis of PAMAM G1.0 (4 NH_2) 2
A PAMAM G0.5 **1** (49.40 g, 0.12 mol) in methanol (120 mL) was stirred and EDA (309.26 g, 5.14 mol) was added drop-wise for 45 minutes. The mixture was allowed to react at room temperature for 3 days. Methanol and the excess of EDA were removed at 45 ^{o}C at reduced pressure and purified with an azeotropic solution (1.0 L mixture of 9:1 toluene: methanol) and washed again with methanol (100 mL). The purification process was carried out several times until the EDA was completely removed and dried at reduced pressure. The final product (60g, 95 %) obtained G1.0 **2** as a yellow oil:
FTIR (ν_{max}/cm^{-1}), 3286 (N-H, stretch), 2937 (C-H, stretch),1646 (C=O), 1560 (N-H, bend), 1462, 1442 (C-H, bend); ^{1}H NMR (400 MHz, MeOD), 3.27 (8H, *t*, J 6.5 Hz, $CONH\underline{CH_2}$), 2.76 (8H, *t*, J 7.0 Hz, $CH_2N\underline{CH_2}$), 2.74 (8H, *t*, J 6.5 Hz, $CH_2\underline{CH_2}NH_2$), 2.55 (4H, *s*,$\underline{CH_2}N$), 2.38 (8H, *t*, J 7.0 Hz, $\underline{CH_2}CONH$); ^{13}C NMR (100 MHz, MeOD),

174.0 (C=O), 52.0, 50.0 , 42.0, 40.5, 32.5 (CH_2); Mass spec (ES), 517 (MH^+), 539 (MNa^+), ES-MS C_{22} H_{48} N_{10} O_4 = 516 (calculated)

Synthesis of PAMAM G1.5 (8 OMe) 3

A PAMAM G1.0 **2** (30.72 g, 59.46 mmol) in methanol (100 mL) was stirred at 0 ºC and methyl acrylate (103.24g, 1.20 mol) was added in droplets for 45 minutes. The mixture was allowed to react at room temperature for 3 days. After completion of the reaction, the solvent was concentrated at reduced pressure at 45 ºC. The product was dried and (63 g, 89%) G1.5 **3** obtained as a yellow oil:

FTIR (ν_{max}/cm^{-1}), 3312 (N-H, stretch), 2952 (C-H, stretch), 2876, 1735 (C=O, ester), 1650 (C=O), 1537(N-H), 1436 (CH_2, bend); ^{1}H NMR (400 MHz; MeOD) 3.68 (24H, *s*, O$\underline{CH_3}$), 3.27 (8H, *t*, J 6.5 Hz, NH$\underline{CH_2}$), 2.80 (24H, *t*, J 7.0 Hz , N$\underline{CH_2}$), 2.57 (12H, *t*, J 6.5 Hz, $\underline{CH_2}$N), 2.48 (16H, *t*, J 7.0 Hz, $\underline{CH_2}$CO), 2.41 (8H, *t*, J 7.0 Hz, $\underline{CH_2}$CO); ^{13}C NMR (100 MHz, MeOD), 172.5 (C=O),171.5 (C=O), 53.0 , 52.0 (CH_3), 51.5, 50.5, 49.5, 38.0, 33.5, 33.0 (CH_2); Mass spec (ES), 1205 (M),1227 (MNa^+), ES-MS $C_{54}H_{96}N_{10}O_{20}$ = 1205 (calculated)

Synthesis of PAMAM G2.0 (8 NH_2) 4

A PAMAM G1.5 **3** (40.70 g, 33.76 mmol) in methanol (100 mL) and EDA (325.4 g, 5.42 mol) was added dropwise for 45 minutes. The mixture was allowed to react at room temperature for 6 days. The purification process was carried out with an azeotropic solvent (2.0 L mixture of 9:1 toluene: methanol) and washed with methanol again (100 mL) until the EDA was completely removed. The product was dried and (47 g, 97 %) G2.0 **4** achieved as a sticky yellow oil:

FTIR (ν_{max}/cm^{-1}), 3286 (N-H, stretch), 2938 (C-H, stretch), 1646 (C=O, amide), 1561 (N-H) ; ^{1}H NMR (400 MHz, MeOD), 3.27 (24H, *t*, J 6.0 Hz, NH$\underline{CH_2}$), 2.81 (24H, *t*, J 7.0 Hz, N$\underline{CH_2}$), 2.74 (16H, *t*, J 6.0 Hz, $\underline{CH_2}NH_2$), 2.60 (12H, *t*, J 7.0 Hz, $\underline{CH_2}$N), 2.35 (24H, *t*, J 6.5 Hz, $\underline{CH_2}$CO); ^{13}C NMR (100 MHz, MeOD), 174.0 (C=O), 173.5 (C=O), 52.5, 51.0 , 50.0, 42.0 , 41.0, 37.5, 33.2, 32.5 (CH_2); Mass spec (ES), 1430 (MH^+), ES-MS C_{62} H_{128} N_{26} O_{12} = 1429 (calculated)

Synthesis of PAMAM G2.5 (16 OMe) 5

A PAMAM G2.0 **3** (29.18 g, 20.42 mmol) in methanol (100 mL) was stirred and methyl acrylate (70.74 g, 0.82 mol) was added dropwise for 45 minutes. The mixture allowed to react at room temperature 5 days. Methyl acrylate and the excess solvent were removed at 45 ºC at reduced pressure. The product was dried under a high vacuum to yield G2.5 **5** (42 g, 72 %) as a sticky yellow oil:

FTIR (ν_{max}/cm^{-1}), 3298 (N-H stretch), 2952 (C-H stretch), 1735 (C=O, ester), 1645 (C=O, amide), 1552 (N-H, amide bend), 1435 (CH_2); ^{1}H NMR (400 MHz; MeOD) 3.69 (48H, s, O$\underline{CH_3}$), 3.28 (24H, *t*, J 6.5 Hz, NHCH2), 2.82 (24H, *t*, J 7.0 Hz, N$\underline{CH_2}$), 2.79 (32H, *t*, J 7.0 Hz, N$\underline{CH_2}$), 2.62 (12H, *t*, J 7.0 Hz, N$\underline{CH_2}$), 2.58 (16H, *t*, J 6.5 Hz, $\underline{CH_2}$N), 2.49 (32H, *t*, J 7.0 Hz, $\underline{CH_2}$CO) ;^{13}C NMR (100 MHz, MeOD), 173.0 (C=O), 172.5(C=O), 171.5 (C=O), 53.0 , 52.5 , 52.0 (CH_3), 50.0 ,49.7, 49.5 , 37.5, 37.0 ,34.0, 33.5, 32.0 (CH_2);

Mass spec (ES), 2806 (MH^+), ES-MS C_{126} H_{224} N_{26} O_{44} = 2807 (calculated).

Synthesis of PAMAM G3.0 (16 NH_2) 6

A PAMAM G2.5 **5** (24.78 g, 8.82 mmol) in methanol (100 mL) was stirred. EDA (104.28 g, 1.74 mol) was added dropwise for 45 minutes. The mixture was allowed to

react at room temperature for 10 days. The crude product was purified with azeotropic solution (2.0 L mixture of 9:1 toluene: methanol) to remove EDA at 45 ^{o}C. The final product washed with methanol (100 mL) and EDA was completely removed by repeating the purification process. The product was dried to give a G3.0 **6** (28 g, 97 %) as a yellow oil:
FTIR (ν_{max}/cm^{-1}), 3290 (N-H, stretch), 3090 (C-H stretch), 1639 (C=O), 1562 (N-H), 1487 (CH_2); ^{1}H NMR (400 MHz, MeOD), 3.27 (24H, *t*, J 7.0 Hz, NH$\underline{CH_2}$), 2.82(32H, *t*, J 6.0 Hz, $\underline{CH_2}$N), 2.70 (56H, *t*, J 7.0 Hz, $\underline{CH_2}$N), 2.59 (32H, *t*, J 6.0 Hz, N$\underline{CH_2}$), 2.38 (56H, *t*, J 7.0 Hz, $\underline{CH_2}$CO); ^{13}C NMR (100 MHz, MeOD), 175.0 (C=O), 174.6 (C=O), 174.4 (C=O), 51.4, 49.1, 41.64 , 39.9 , 36.8 , 33.8 (CH_2); Mass spec (ES), 3257(MH^+), ES-MS C_{142} H_{288} N_{58} O_{28}= 3256(calculated).

Synthesis of PAMAM G3.5 (32 OMe) 7
A PAMAM G3.0 **6** (24.98 g, 7.68 mmol) in methanol (100 mL) and stirred. Methyl acrylate (51.62g, 0.60 mol) was added dropwise for 45 minutes. The mixture was allowed to react for 4 days. Methyl acrylate and the excess solvent were removed at 45 ^{o}C at reduced pressure. The product of G3.5 **7** (38 g, 81 %) obtained as a sticky yellow oil:
FTIR (ν_{max}/cm^{-1}), 3296 (N-H stretch), 2952 (C-H stretch), 2832, 1736 (C=O, ester), 1642 (C=O, amide), 1550 (N-H bend), 1440 (CH_2); ^{1}H NMR (400 MHz, MeOD), 3.69 (96H, *s*, O$\underline{CH_3}$), 3.29 (24H, *t*, J 5.0 Hz , NH$\underline{CH_2}$), 2.86 (32H, *t*, J 6.0 Hz, N$\underline{CH_2}$), 2.78 (56H, *t*, J 7.0 Hz ,N$\underline{CH_2}$), 2.65 (64H, *t*, J 7.0 Hz, N$\underline{CH_2}$), 2.58 (32H, *t*, J 6.0 Hz, $\underline{CH_2}$N), 2.49 (64H, *t*, J 7.0 Hz , $\underline{CH_2}$CO), 2.40 (56H, *t*, J 7.0 Hz, $\underline{CH_2}$CO);^{13}C NMR (100 MHz, MeOD), 173.5(C=O), 53.0, 52.5, 49.8, 49.5 , 49.0 (CH_3), 37.4, 36.5 , 33.5, 31.5 (CH_2); Mass spec (ES), 6014 (M), ES-MS C_{270} H_{480} N_{58} O_{92} = 6014 (calculated).

Synthesis of PAMAM G4.0 (32 NH_2) 8
A PAMAM G3.5 **7** (19.44 g, 3.24 mmol) in methanol (100 mL) was stirred. EDA (93.5 g, 1.56 mol) was added dropwise for 45 minutes. The mixture was allowed to react for 10 days at room temperature. The crude product was purified with an azeotropic solution (2.5 L mixture of 9:1 toluene: methanol) at 45 ^{o}C to ensure the EDA was completely removed. The crude product was washed with methanol (100 mL) and concentrated. The product of G4.0 **8** (21 g, 92 %) obtained as a yellow oil:
FTIR (ν_{max}/cm^{-1}), 3282 (N-H, amide stretch), 3088, 2945 (C-H stretch), 1645 (C=O), 1558 (N-H bend), 1468 (CH_2 bend); ^{1}H NMR (400 MHz, D_2O), 3.25 (56H, *t*, J 6.0 Hz, NH$\underline{CH_2}$), 3.15 (64H, *t*, J 6.0 Hz, NH$\underline{CH_2}$), 2.74 (120H, *t*, J 7.0 Hz, N$\underline{CH_2}$), 2.63 (64H, *t*, J 6.0 Hz,$NH_2\underline{CH_2}$), 2.54 (60H, *t*, J 6.5 Hz, NH$\underline{CH_2}$), 2.34 (120H, *t*, J 6.50 Hz, $CH_2\underline{CH_2}$); ^{13}C NMR (100 MHz, D_2O), 175.0 (C=O), 51.5, 50.0, 42.0 , 40.0, 36.5, 33.0, 32.5 (CH_2); Mass spec (ES), 6913 (M), ES-MS C_{302} H_{608} $N_{122}O_{60}$ = 6913 (calculated).

Synthesis of PAMAM G4.5 (64 OMe) 9
A PAMAM G4.0 **8** (13.38 g, 1.94 mmol) in methanol (60 mL) was stirred. Methyl acrylate (33.04 g, 0.38 mol) was added dropwise for 45 minutes. The mixture was allowed to react at room temperature for 7 days. Methyl acrylate and the excess solvent were removed at 45 ^{o}C at reduced pressure. The product of G4.5 **9** (22 g, 91 %) obtained as a sticky yellow oil:
FTIR (ν_{max}/cm^{-1}), 3415 (N-H stretch), 2933 (C-H stretch), 1724 (C=O, ester), 1645 (C=O), 1568 (N-H bend), 1436 (CH bend); ^{1}H NMR (400 MHz, MeOD), 3.69 (192H, *s*, O$\underline{CH_3}$), 3.29 (120H, *q*, J 5.5 Hz, NH$\underline{CH_2}$), 2.85 (128H, *t*, J 7.0 Hz, N$\underline{CH_2}$), 2.79

(120H, t, J 7.0 Hz, N$\underline{CH_2}$, 2.63 (60H, *t*, J 6.0 Hz, $CH_2\underline{CH_2}$), 2.58 (64H, *t*, J 6.0 Hz, $CH_2\underline{CH_2}$N), 2.49 (128H, *t*, J 7.0 Hz, $CH_2\underline{CH_2}$), 2.41 (120H, *t*, J 7.0 Hz, $CH_2\underline{CH_2}$CO); ^{13}C NMR (100 MHz, MeOD), 173.5 (C=O), 173.0 (C=O), 53.0, 52.5, 51.0, 50.0, 49.5, 38.0, 37.5, 34.0 , 33.0 (CH_2); Mass spec (ES), 12410 (MH^+), ES-MS $C_{558}H_{992}N_{122}O_{188}$= 12411 (calculated).

2.6.3 Synthesis of PAMAM-COOH dendrimers

Synthesis of PAMAM G1.5-COOH (8 COOH)

A PAMAM G1.5 **3** (28.86 g, 23.94 mmol) was dissolved in 60 mL of methanol and water (ratio 10:1). Sodium hydroxide (8.16 g, 0.20 mol) was added and the mixture was stirred and refluxed for 4 days at 45 ^oC. The excess solvent was removed at 45 ^oC at reduced pressure. The product of G1.5-COOH **10** (7.0 g, 27 %) obtained as a white sticky solid:

FTIR (ν_{max}/cm^{-1}) , 3266 (N-H stretch), 2819, 1645 (C=O), 1559 (N-H bend), 1403 (CH_2 bend), 1317, 1155, 1117, 1036, 946; ^{1}H NMR (400 MHz, D_2O), 3.25 (8H, *t*, J 6.0, NH$\underline{CH_2}$), 2.72 (24H, *m*, N($\underline{CH_2}CH_2$), 2.54 (12H, *t*, J 7.0 Hz,$CH_2\underline{CH_2}$N), 2.35 (8H, *t*, J 7.5 Hz, $CH_2\underline{CH_2}$CO), 2.28 (16H, *t*, J 8.0 Hz, $CH_2\underline{CH_2}$C); ^{13}C NMR (100 MHz, D_2O), 182.0 (C=O, carboxylic acid), 173.5 (C=O), 51.0 , 50.5, 50.0 , 49.0, 36.5, 34.0, 32.5 (CH_2); Mass spec (ES), 1093(M^+), 1115 (MNa^+), ES-MS $C_{46}H_{80}N_{10}O_{20}$ = 1092 (calculated).

Synthesis of PAMAM G2.5-COOH (16 COOH) 11

A PAMAM G2.5 **5** (30.56 g, 10.88 mmol) in 88 mL of methanol and water (ratio 10:1) and stirred. Sodium hydroxide (6.98 g, 0.174 mol) was added and refluxed at 45 ^oC for 3 days. The excess solvent was removed at 45 ^oC at reduced pressure and dried under a high vacuum. The product of G2.5-COOH **11** (26 g, 92 %) obtained as a pale yellow solid:

FTIR (ν_{max}/cm^{-1}) , 3255 (N-H stretch), 3095, 2942, 2838, 1645 (C=O), 1555 (N-H bend), 1398 (CH_2 bend); ^{1}H NMR (400 MHz, D_2O), 3.25 (24H, *t*, J 6.0 Hz, NH$\underline{CH_2}CH_2$), 2.73 (56H, *m*, N($\underline{CH_2}CH_2$), 2.55 (28H, *t*, J 7.0 Hz , $CH_2\underline{CH_2}$), 2.35 (24H, *t*, J 7.0 Hz, $CH_2\underline{CH_2}$CO), 2.28 (32H, *t*, J 8.0 Hz, $CH_2\underline{CH_2}$CO); ^{13}C NMR (100 MHz, D_2O), 181.5 (C=O, carboxylic acid), 174.5 (C=O), 52.0, 51.5, 50.0, 49.0 , 36.5, 34.5 , 33.0, 32.5 (CH_2); Mass spec (ES), 2582 (M), ES-MS $C_{110}H_{192}N_{26}O_{44}$ = 2582 (calculated).

Synthesis of PAMAM G3.5-COOH (32 COOH) 12

A PAMAM G3.5 **7** (8.82 g, 1.46 mmol) in 44 mL of methanol and water (ratio 10:1). Sodium hydroxide (1.94 g, 48.40 mmol) was added and stirred. The mixture was refluxed for 3 days at 45 ^oC. The product was concentrated at reduced pressure at 45 ^oC and dried under a high vacuum. The product of G3.5-COOH **12** (8.0 g, 97 %) obtained as a yellow solid:

FTIR (ν_{max}/cm^{-1}) , 3265 (N-H stretch), 1638 (C=O), 1560 (N-H bend), 1398 (CH_2), 1318, 1205, 1155, 1029, 875; ^{1}H NMR (400 MHz, D_2O), 3.23 (56H, *t*, J 7.0 Hz, NH$\underline{CH_2}$CH), 2.75 (120H, *m*, N($\underline{CH_2}CH_2$), 2.56 (60H, *t*, J 6.0 Hz, $CH_2\underline{CH_2}$N), 2.37 (56H, *t*, J 7.0 Hz, $CH_2\underline{CH_2}$CO), 2.30 (64H, *t*, J 8.0 Hz, $CH_2\underline{CH_2}$CO); ^{13}C NMR (100 MHz, MeOD),179.0 (C=O, carboxylic acid), 173.5 (C=O), 52.0, 51.0 , 50.0, 37.5 , 35.5 , 33.5 (CH_2); Mass spec (ES), 5563 (MH^+), ES-MS $C_{238}H_{416}N_{58}O_{92}$ = 5562 (calculated).

Synthesis of PAMAM G4.5-COOH (64 COOH) 13

A PAMAM G4.5 **9** (8.71 g, 0.70 mmol) in methanol and water (ratio 10:1, 35 ml) and stirred. Sodium hydroxide (1.67 g, 41.70 mmol) was added and refluxed at 45 ^{o}C for 3 days. The excess solvent was removed at 45 ^{o}C at reduced pressure and dried under a high vacuum. The product G4.5 PAMAM-COOH (8.0 g, 98 %) obtained as a yellow sticky oil:

FTIR (ν_{max}/cm^{-1}) , 3255 (N-H, amide stretch), 3074, 2945, 2819, 1645 (C=O), 1558 (N-H, amide bend), 1402 (CH_2, bend); ^{1}H NMR (400 MHz, D_2O), 3.23 (120H, *m*, NH$\underline{C}H_2$), 2.74 (248 H, *m*, N$\underline{CH_2}CH_2$), 2.56 (124H, *t*, J 7.0 Hz, CH_2CH_2), 2.35 (120H, *t*, J 7.0 Hz, $CH_2\underline{CH_2}CO$), 2.26 (128H, *t*, J 8.0 Hz, $\underline{CH_2}COOH$); ^{13}C NMR (100 MHz, D_2O), 181.5 (C=O, carboxylic acid), 173.5 (C=O, amide), 52.0 , 51.1 , 50.0 , 48.5 , 36.5 , 34.5 , 32.0 (CH_2); Mass spec (ES), 11522 (MH^+), ES-MS $C_{494}H_{864}N_{122}O_{188}$ = 11521 (calculated).

2.6.4 Synthesis of PAMAM-OH dendrimers

General procedure to synthesis neutral PAMAM dendrimer

To a solution of half generation dendrimer in DMSO was added with potassium carbonate and ethanolamine in droplets. The mixture was stirred and refluxed for 3 days at 50 ^{o}C. The crude product was filtered at reduced pressure to remove any solid residues. The filtered product was washed with acetone (2 x 600 mL) using a large conical flask. The oil product was observed, and which was allowed to settle at the bottom of the flask. The upper layer (acetone) was decanted off and 4.0 mL of distilled water was added to dissolve the product. The product was precipitated in acetone and allowed to settle and the upper layer (acetone) was decanted off. Traces of solvent were removed at reduced pressure. The product was dried to yield PAMAM-OH dendrimer

Synthesis of PAMAM G1.5 OH (8 OH) 29

A PAMAM G1.5 **3** (28.62 g, 0.024 mol) was dissolved in 14 mL of DMSO. Potassium carbonate (32.82 g, 0.24 mol) and ethanolamine (14.50 g, 0.24 mol) were added portion wise to the mixture and was stirred and refluxed for 3 days at 50 ^{o}C. The purification was followed as mentioned above. The product was dried to yield G1.5-OH **29** (14 g, 40 %) as a concentrated yellow oil:

FTIR (ν_{max}/cm^{-1}) , 3295 (N-H stretch), 3097, 2948, 2845, 1643 (C=O), 1560 (N-H), 1445 (CH_2), 1363, 1315, 1223, 1066; ^{1}H NMR (400 MHz, D_2O), 3.58 (16H, *t*, J 5.5 Hz, $CH_2\underline{CH_2}OH$), 3.24 (24H, *m*, NH$\underline{CH_2}CH_2$), 2.76 (24H, *m*, N($\underline{CH_2}CH_2$), 2.56 (12H, *t*, J 7.0 Hz, $CH_2\underline{CH_2}N$), 2.37 (24H, *t*, J 7.0 Hz, $CH_2\underline{CH_2}CO$);^{13}C NMR (100 MHz, D_2O), 175.0 (C=O), 173.5 (C=O), 60.0, 52.0 , 50.0 , 49.0 , 41.5 , 37.0, 33.0, 33.0 (CH_2); Mass spec (ES), 1438 (MH), 1460 (MNa^+), ES-MS $C_{62}H_{120}N_{18}O_{20}$ = 1438 (calculated).

Synthesis of PAMAM G2.5 -OH (16 OH) 30

A PAMAM G2.5 **5** (14.06 g, 5.02 mmol) was dissolved in 14 mL of DMSO. ethanolamine (6.30 g, 0.104 mol) and potassium carbonate (14.14 g, 0.102 mol) were added portion wise with continuously stirring and was refluxed at 50 ^{o}C for 3 days. The purification was followed as mentioned above. The product was dried to give G2.5-OH **30** (15 g, 94 %) as an orange oil:

FTIR (ν_{max}/cm^{-1}) , 3395 (N-H stretch), 2955, 1640 (C=O), 1564 (N-H), 1445(CH_2), 1315, 1072, 1026; ^{1}H NMR (400 MHz, D_2O), 3.56 (32H, *t*, J 5.5 Hz, $CH_2\underline{CH_2}OH$), 3.23

(56H, *m*, NH$\underline{CH_2}CH_2$), 2.76 (56H, *t*, J 7.0 Hz, N($\underline{CH_2}CH_2$), 2.53 (28H, *t*, J 7.0 Hz, $CH_2\underline{CH_2}$N), 2.34 (56H, *t*, J 7.0 Hz, $CH_2\underline{CH_2}$CO); ^{13}C NMR (100 MHz, D_2O), 175.5 (C=O), 174.5 (C=O), 60.0 , 51.5 , 49.0 , 41.5, 39.0 , 36.5 , 33.0 (CH_2); Mass spec (ES), 3272 (MH), ES-MS $C_{142}H_{272}N_{42}O_{44}$ = 3272 (calculated).

Synthesis of PAMAM G3.5-OH (32 OH) 31

A PAMAM G3.5 **7** (11.08g, 1.84 mmol) was dissolved in 8 mL of DMSO. Ethanolamine (4.42 g, 0.072 mol) and potassium carbonate (9.00 g, 0.066 mol) were added portion wise. The reaction mixture was refluxed for 3 days at 50 ºC. The crude product was filtered under vacuum to remove any residues. The purification was followed as mentioned above. The final product was dried to obtain G3.5-OH **31** (12 g, 99 %) as an extremely sticky orange solid:

FTIR (ν_{max}/cm^{-1}) , 3265 (N-H), 3072, 2918, 2826, 1640 (C=O), 1549 (N-H), 1438 (CH_2), 1364, 1295, 1030, 958, 885, 824; ^{1}H NMR (400 MHz, D_2O), 3.56 (62H, *t*, J 5.5 Hz, $CH_2\underline{CH_2}$OH), 3.25 (120H, *m*, NH$\underline{CH_2}CH_2$), 2.75 (120H, *m*, N($\underline{CH_2}CH_2$), 2.55 (60H, *t*, J 6.0 Hz, $CH_2\underline{CH_2}$N), 2.36 (120H, $CH_2\underline{CH_2}$N); ^{13}C NMR (100 MHz, D_2O), 175.1 (C=O), 174.5 (C=O), 61.5, 60.0, 52.0 , 49.0, 44.0, 42.0 , 37.0 , 33.0 (CH_2) ; Mass spec (ES), 6941 (MH^+), ES-MS $C_{302}H_{576}N_{90}O_{92}$ = 6940 (calculated).

2.6.5 Synthesis of Linear Chain

Synthesis of methyl-3-butyramidopropanoate

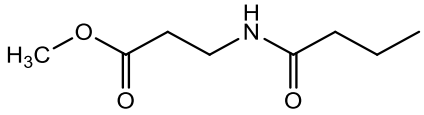

The mixture of butyric acid chloride (1.31g, 12.3 mmol) and beta alanine methyl ester hydrochloride (1.885g, 13.5 mmol) were dissolved and stirred in dried DCM (50 mL) at 0ºC. Dried triethylamine (3.75g, 36.8 mmol) was added dropwise under nitrogen condition. The reaction mixture was allowed to cool at room temperature and refluxed at 60ºC for 24 hours. The crude product was washed with sodium hydrogen carbonate solution. The solution was combined and dried with Mg_2SO_4 and filtered. The organic solvent was removed at reduced pressure and the final product (1.92g, 65%) was obtained as a viscous dark yellow oil:

FTIR (ν_{max}/cm^{-1}) , 2935 and 2875(C-H stretch), 1685 and 1640 (C=O stretch), 1540 (N-H bend), ^{1}H NMR(400 MHz; MeOD) 3.79 (2H, *m*, CH_2), 3.60 (3H, *s*, CH_3), 2.58 (2H, *t*, J 7.0 Hz, CH_2), 2.32 (2H, *t*, J 7.0 Hz, $CH_2\underline{CH_2}$), 1.39 (2H, *m*, CH_2), 0.92 (3H, *t*, J 7.5 Hz, $\underline{CH_3}$ CH_2); ^{13}C NMR (100 MHz; MeOD) 173.6, (C=O), 51.9 (CH_3), 40.8, 35.5, 35.3, 22.2 (CH_2), 13.1 (CH_3); Mass spec (ES) 174 (MH^+), ES-MS $C_8H_{15}NO_3$ = 173 (calculated).

Hydrolysis of methyl-3-butyramidopropanoate

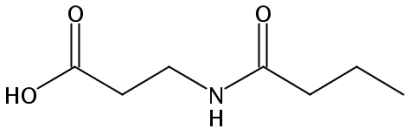

Methyl-3-butyramidopropanoate (2.0 g) was added with KOH (2 ml, 2M) in THF (10 mL) and 1.0 mL of water. The mixture was refluxed at 70 ºC for 24 hours. The solvent was removed at reduced pressure and washed with sulfuric acid (2 mL, 2.0 M) followed by sodium hydrogen carbonate (2 mL, 2.0 M), and water. The solution was combined and

dried with Mg_2SO_4 and filtered and dried under a high vacuum. The product (2.0 g, 96%) obtained as a white powder:
FTIR (ν_{max}/cm^{-1}), 3550 - 3200 (broad, s),2935 and 2872 (C-H stretch), 1680 and 1640 (C=O stretch), 1540 (N-H bend).

Boc protected chain (16)

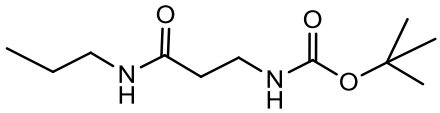

n-propylamine **14** (1.0 g, 0.0169 mol), Boc-β-alanine **15** (3.41 g, 0.018 mol) and DMAP (4.40 g, 0.036 mol) were dissolved in DCM (100 mL). EDC.HCl (3.45 g, 0.018 mol) and triethylamine (5.17 g, 0.0507 mol) were added to the mixture. The mixture was allowed to react under nitrogen condition. The crude product was washed with brine solution (100 mL x 3), and the aqueous layers were backwashed with DCM and the phases separated. The organic layers were collected and dried with Mg_2SO_4. The solvent was concentrated at reduced pressure and dried under a high vacuum to give boc chain **16** (4.0 g, 96 %) as a white powder:
FTIR (ν_{max}/cm^{-1}) , 3335 (N-H stretch), 2968 (C-H), 1682, 1645 (C=O), 1528 (N-H bend); ^{1}H NMR (400 MHz; $CDCl_3$) 5.85 (1H, *s*,$CH_2\underline{NH}$), 5.25 (1H, *s*, $CO\underline{NH}$), 3.45 (2H, *q*, $NH\underline{CH_2}$ CH_2), 3.25 (2H, *q*, J 6.0 Hz $NH\underline{CH_2}$ CH_2), 2.45 (2H, *t*, J 6.0 Hz, $\underline{CH_2}CO$), 1.55 (2H, *m*, $CH_2\underline{CH_2}CH_3$), 1.45 (9H, *s*, $CH_2\underline{CH_3}$), 0.95 (3H, *t*, J 7.5 Hz, 3x $\underline{CH_3}$); ^{13}C NMR (100 MHz; $CDCl_3$); 172.5 (C=O), 155.8 (C=O), 80.5 ($COCH_3$), 41.5, 37.0, 36.5, 29.0 (CH_3), 23.0 (CH_2); Mass spec (ES) 230 (MH^+), ES-MS $C_{11}H_{22}N_2O_3$= 231 (calculated).

Boc deprotection chain (17)

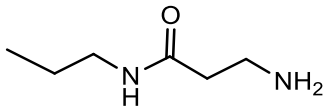

Boc protected chain **16** (3.0 g, 0.013 mol) in DCM (25 mL) and TFA (25 mL) was added and stirred for 24 hours under nitrogen condition. The crude product was washed with water (5 x 25 mL) and concentrated under vacuum. The final product was dried under a high vacuum to yield amide chain **17** (1.4 g, 82 %) as a yellow oil:
FTIR (ν_{max}/cm^{-1}) , 2978 (N-H) , 1645 (C=O), 1558 (N-H); ^{1}H NMR (400 MHz; D_2O) 3.10 (2H, *t*, J 6.98 Hz, $CH_2\underline{CH_2}$), 2.98 (2H, *t*, J 7.0 Hz, $CH_2\underline{CH_2}$), 2.51 (2H, *t*, J 7.0 Hz, $\underline{CH_2}CH_2$), 1.36 (2H, *m*, $CH_3\underline{CH_2}$), 0.75 (3H, *t*, J 7.0 Hz, $CH_2\underline{CH_3}$); ^{13}C NMR (100 MHz; D_2O) 171.5 (C=O), 43.0, 41.5, 36.0, 32.0 (CH_2), 21.5 (CH_3); Mass spec (ES) 131 (MH^+), ES-MS $C_6H_{14}N_2O$ = 130 (calculated).

Amide chain (18)

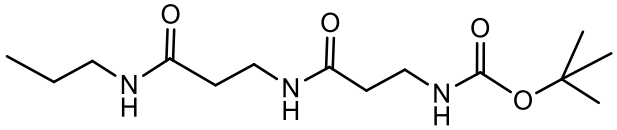

Boc deprotection chain **17** (2.65 g, 0.020 mmol) in THF (50 mL) and was added with Boc-β-alanine (3.85 g, 0.020 mol), DMAP (4.89 g, 0.04 mol), EDC.HCl (3.83 g, 0.020 mol) and triethylamine (6.11 g, 0.06 mol). The mixture was allowed to react for 24 under nitrogen condition. The crude product was washed with brine (100 mL x 3), diluted HCl, and the aqueous layers were backwashed with DCM. The organic layers were combined

and dried with Mg_2SO_4 and the solvent was removed at reduced pressure. The final product was dried under a high vacuum to yield **18** (4.5 g, 78 %) as a cream coloured powder:
FTIR (ν_{max}/cm^{-1}) , 3306 and 2965 (N-H),2935 and 2875 (C-H), 1689 and 1635 (C=O), 1538 (N-H); ^{1}H NMR (400 MHz; $CDCl_3$) 6.83 (1H, *s*), 6.28 (1H, *s*), 5.32 (1H, *s*, NH), 5.18 (1H, *s*, NH), 3.55 (2H, *q*, J 6.0 Hz), 3.37 (4H, *m*, $\underline{CH_2}CH_2$), 3.24 (2H, *q*, J 7.0 Hz), 2.55 (2H, *m*, $\underline{CH_2}CH_2$), 2.43 (4H, *m*, $\underline{CH_2}CH_2$), 1.55 (2H, *m*, $\underline{CH_2}CH_3$), 1.42 (9H, *s*, 3 x CH_3), 0.95 (3H, *t*, J 7.0 Hz,$CH_2\underline{CH_3}$); ^{13}C NMR (100 MHz; $CDCl_3$) 175.6 (C=O),156.0, 79.5,37.2, 37.9,42.5, 36.1, 39.8, 23.1, 28.4 (CH_2), 12.0 (CH_3); Mass spec (ES) 302 (MH^+), 324 (MNa^+), 202 (MH^+ - Boc). ES-MS $C_{14}H_{27}N_3O_4$= 301 (calculated).

Amine chain (19)

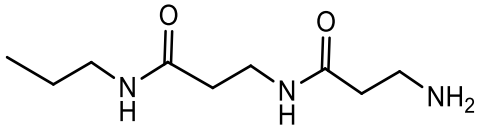

Amide chain **18** (4.5 g, 0.016 mol) in DCM (25 mL) and TFA (25 mL) was added and stirred. The mixture was allowed to react for 24 hours under nitrogen condition. The DCM was removed at reduced pressure at 50 ºC, purified with water (2 x 100 mL) and dried to give a dark brown oil. The crude product was purified again with DCM (2 x 100 mL), diluted HCL(2 mL) and with water (100 mL). The excess solvent was removed at 50 ºC at reduced pressure and dried under high vacuum. The product contained impurities and was used to the next step. The crude product (3.0 g, 93%) obtained as a dark brown oil:
FTIR (ν_{max}/cm^{-1}) , 2938 (N-H stretch), 1645 (C=O, stretch), 1555 (N-H bend), 1178 and 1130 (C-N); ^{1}H NMR (400 MHz; $CDCl_3$), 7.86 (2H, *t*, J 6.0 Hz), 7.75 (2H, *s*), 3.26 (2H, *dd*, J 13.0 Hz, 7.0 Hz, CH_2), 3.18 (4H, *s*), 2.96 (6H, *m*), 2.54 (2H, *t*, J 7.0 Hz), 2.45 (4H, *m*, $CH_2\underline{CH_2}NH_2$), 1.38 (2H, *m*, $\underline{CH_2}CH_3$), 0.90 (3H, *t*, J 7.0 Hz, $CH_2\underline{CH_3}$); ^{13}C NMR (100 MHz; $CDCl_3$) 172.5, 170.5, 170.0 (*C*=O), 40.5, 36.0, 35.5, 35.0, 33.0, 32.0, 23.0 (CH_2), 12.0 (*C*H_3); Mass spec (ES) 202 (MH^+), 223 (MNa^+) ES-MS $C_9H_{19}N_3O_2$= 201(calculated).

Boc-protected tyrosine chain (20)

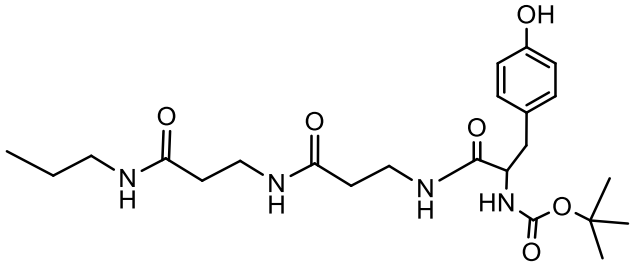

Amide chain **19** (1.0 g, 4.98 mmol) was dissolved in THF (40 mL) and Boc-Tyrosine-OH (1.4 g, 4.98 mmol), DMAP (1.21 g, 9.96 mmol) were added followed by triethylamine (1.52 g, 0.015 mol) and EDC.HCl (0.78 g, 4.0 mmol). The reaction mixture was allowed to react 24 hours under nitrogen condition. The crude product was washed with brine (100 mL x 3), and the aqueous layers were backwashed with DCM and the phases were separated. The organic layers were collected and dried and concentrated to yield a yellow oil which crystallised into a yellow powder. Silica chromatography was used to purify the crude product (gradient of 10 % methanol) in

DCM. The fractions collected, and the solvent was removed at reduced pressure. The product of Boc chain **20** (1.5 g, 65%) obtained as a white powder:
FTIR (ν_{max}/cm^{-1}) , 3305 and 2968 (N-H, stretch), 2935 and 2878 (C-H), 1688 and 1639 (C=O stretch), 1536 (N-H bend), 1168 (C-N); ^{1}H NMR (400 MHz; MeOD) 7.04 (2H, *d*, J 8.5 Hz, *m*-C$\underline{H}_{Ar}$), 6.72 (2H, *d*, J 8.5 Hz, *o*-C$\underline{H}_{Ar}$), 4.18 (1H, *t*, J 7.0 Hz, $CH_2\underline{CH}$), 3.42 (4H, *m*, $CH_2\underline{CH_2}$), 3.15 (2H, *t*, J 7.0 Hz, $CH_2\underline{CH_2}$), 2.98 (1H, *dd*, J 14.0 Hz, 6.0 Hz, diastereotopic CH_2), 2.75 (1H, J 14.0 Hz, 9.0 Hz, diastereotopic CH_2), 2.38 (2H, *t*, J 7.5 Hz , N$H\underline{CH_2}$), 2.31 (2H, *q*, J 6.0 Hz, NH$\underline{C}H_2CH_2$), 1.55 (2H, *m*, $CH_3\underline{CH_2}$), 1.38 (9H, *s*, 3x CH_3), 0.95 (3H, *t*, J 7.5 Hz, $CH_2\underline{CH_3}$); ^{13}C NMR (100 MHz; MeOD) 174.5, 173.5 (C=O), 132, 128.5, 115.5, 49.0, 41.0, 36.0, 35.0, 23.0 (CH_2), 28.5 (CH_3); Mass spec (ES) 487.5 (MNa^+), 387.4 (MNa^+-Boc), ES-MS $C_{23}H_{36}N_4O_6$ = 464 (calculated), UV Absorbance (MeOH) λ_{max} (nm) 278, 225.

Tyrosine chain (21)

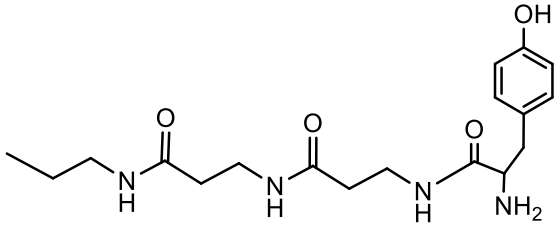

Boc-protected tyrosine chain **20** (1.0 g, 2.15 mmol) in DCM (20 mL) and TFA (10 mL) was added and stirred. The mixture was allowed to react for 24 hours under nitrogen condition. The crude product was washed with water (4 x 25 mL) and purified with DCM (4x 25 mL) and concentrated under vacuum. The product dried under high vacuum for overnight. The product of tyrosine chain **21**(1.5 g, 65%) as a white powder. FTIR (ν_{max}/cm^{-1}) , 3288 and 3086 (N-H), 2936 (C-H), 1634 (C=O), 1536 and 1512 (N-H), 1185 and 1138 (C-N); ^{1}H NMR (400 MHz; MeOD) 7.08 (2H, *d*, J 8.5 Hz, *m*-CH_{Ar}), 6.78 (2H, *d*, J 8.5 Hz, *o*-CH_{Ar}), 3.96 (1H, *t*, J 7.0 Hz, $CH_2\underline{CH}$), 3.42 (4H, *m*, $CH_2\underline{CH_2}NH$), 3.15 (2H, t, J 7.0 Hz, $CH_2\underline{CH_2}$), 3.05 (1H, *dd*, J 14.0 Hz, 7.0 Hz, diastereotopic $C\underline{H_2}$), 2.95 (1H, *dd*, J 14.0 Hz, 8.0 Hz, diastereotopic $C\underline{H_2}$), 2.40 (2H, *t*, J 7.0 Hz, $CH_2\underline{CH_2}$), 2.35 (2H, *q*, $NH\underline{C}H_2CH_2$), 1.55 (2H, *m*, $CH_3\underline{CH_2}$), 0.92 (3H, *t*, J 7.5 Hz, $CH_2\underline{CH_3}$); ^{13}C NMR (100 MHz; MeOD) 173.5, 173.5, 171.0 (C=O), 133.0, 126.0, 117.0 (Ar*C*), 60.0, 43.0, 38.0, 37.5, 37.5, 36.8, 36.5 (*C*H_2), 24.0, 12.0 (*C*H_3), Mass spec (ES) 365 (MH^+), ES-MS $C_{18}H_{28}N_4O_4$ = 364 (calculated).; UV Absorbance (MeOH) λ_{max} (nm) 275, 227 .

Boc-protected phenylalanine (32)

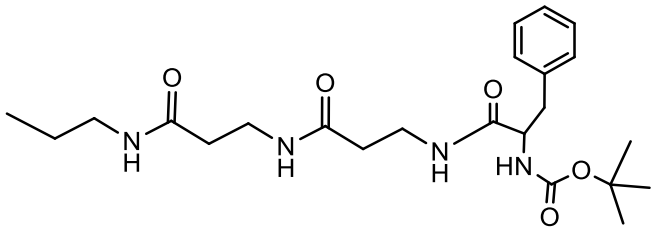

ν_{max}/cm^{-1} (FTIR) 3048 (N-H), 2928 (C-H), 1638 (C=O), 1529 (C=C aromatic) and 1514 (N-H), 1180 and 1136 (C-N); ^{1}H NMR (400 MHz; MeOD) 7.40 (2H, *t*, J 9.0 Hz, *m* -$\underline{CH}$*Ar*), 7.29 (2H, *d*, J 8.5 Hz, *o*-$\underline{CH}$*Ar*) , 7.27 (1H,*t*, J 9.0 Hz, *p*-$\underline{CH}$*Ar*), 3.98 (1H, *t*, J 7.0 Hz, $CH_2\underline{CH}$), 3.45 (4H, *m*, $CH_2\underline{CH_2}$), 3.15 (2H, *t*, J 7.0 Hz,CH_2 $C\underline{H_2}$), 3.05 (1H, *dd*, J 14.0 Hz, 8.0 Hz, diastereotopic CH_2), 2.95 (1H, J 14.0 Hz, 8.0 Hz, diastereotopic CH_2), 2.42 (2H, *t*, J 7.5 Hz, $CH_2\underline{CH_2}$), 2.38 (2H, *q*, J 7.0 Hz, $CH_2\underline{CH_2}$NH), 1.58 (2H, *m*,

$CH_3\underline{CH_2}CH_2$), 1.44 (9H, *s*, 3x CH_3), 0.95 (3H, *t*, J 7.5 Hz, $CH_2\underline{CH_3}$); ^{13}C NMR (100 MHz; MeOD) 173.5, 172.5, 170.2 (C=O), 130.0, 122, 120.6 (C_{Ar}), 57.0, 43.0, 38.0, 38.0, 37.5, 35.5, 24.0, 12.0 , 82% yield; Mass spec (ES) 447 (MH^+), ES-MS $C_{23}H_{36}N_4O_5$ = 448 (calculated);UV Absorbance (MeOH) λ_{max} (nm) 275, 227 .

Phenylalanine chain (33)

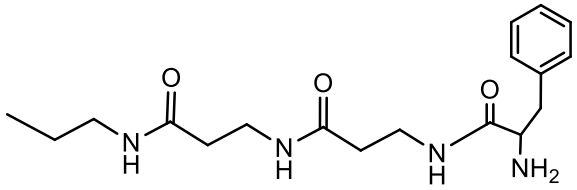

FTIR (ν_{max}/cm^{-1}) , 3035(N-H), 2923 (C-H), 1634 (C=O), 1528 (C=C aromatic) and 1515 (N-H) and 1330 (C-N); ^{1}H NMR (400 MHz; MeOD) 7.40 (2H, *t*, J 9.0 Hz, *m* - C<u>H</u>*Ar*), 7.29 (2H, *d*, J 8.5 Hz, *o*-<u>CH</u>*Ar*) , 7.27 (1H,*t*, J 9.0 Hz, *p*-<u>CH</u>*Ar*), 3.96 (1H, *t*, J 7.2 Hz, $CH_2\underline{CH}$), 3.45 (4H, *m*, $CH_2\underline{CH_2}NH_2$), 3.15 (2H, *t*, J 7.0 Hz,CH_2 C<u>H</u>$_2$), 3.09 (1H, *dd*, J 14.0 Hz, 8.0 Hz, diastereotopic CH_2), 2.95 (1H, *dd*, J 14.0 Hz, 8.0 Hz, diastereotopic CH_2), 2.40 (2H, *t*, J 7.0 Hz ,$\underline{CH_2}$NH), 2.35 (2H, *q* J 7.0 Hz, $CH_2\underline{CH_2}$), 1.58 (2H, *m*, $CH_3\underline{CH_2}CH_2$), 0.98 (3H, *t*, J 7.0 Hz, $CH_2\underline{CH_3}$); ^{13}C NMR (100 MHz; MeOD) 173.5, 172.5, 171.5 (C=O), 129.4, 128, 120.6 (Ar*C*), 55.4 (*C*), 38.0 (*C*H_2), 25.0, 12.0 (*C*H_3), 65% yield; Mass spec (ES) 347 (MH^+), ES-MS $C_{18}H_{28}N_4O_3$= 348 (calculated); UV Absorbance (MeOH) λ_{max} (nm) 275, 227 .

Boc-protected valine chain (34)

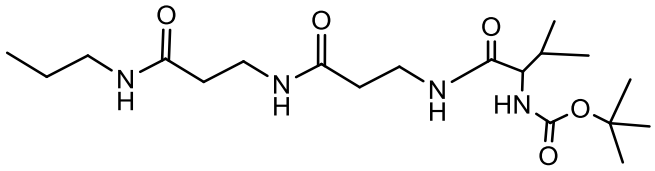

FTIR (ν_{max}/cm^{-1}) , 2932 (N-H stretch), 1640 (C=O, stretch), 1552 (N-H, bend), 1324, 1170 and 1131 (C-N); ^{1}H NMR (400 MHz; MeOD), 4.55 (1H, *d*, J 5.5 Hz, <u>CH</u>), 3.45 (4H, *m*, $CH_2\underline{CH_2}NH_2$), 3.10 (2H, *t*, J 7.0 Hz,CH_2 C<u>H</u>$_2$), 2.66 (1H, *sept*, <u>CH</u>$(CH_3)_2$), 2.40 (2H, *t*, J 7.0 Hz ,$\underline{CH_2}$NH), 2.35 (2H, *q* J 7.0 Hz, $CH_2\underline{CH_2}$), 1.58 (2H, *m*, $CH_3\underline{CH_2}CH_2$), 1.44 (9H, *s*, 3x CH_3), 1-0.98 (6H, *d*, CH($\underline{CH_3}$)$_2$), 0.95 (3H, *t*, J 7.5 Hz, $CH_2\underline{CH_3}$); ^{13}C NMR (100 MHz; MeOD) 173.0, 172.0, 160.5 (C=O), 80.0 (C), 64.0, 41.0, 37.0, 34.5, 32.0 , 29.0 (CH_3), 19.5 (CH_3),12.0 (CH_3); 72% yield ; Mass spec (ES) , 399 (MH^+), 299 (MH^+ - Boc) ES-MS $C_{19}H_{36}N_4O_5$ = 400 (calculated); UV Absorbance (MeOH) λ_{max} (nm) 275, 227.

Valine chain (35)

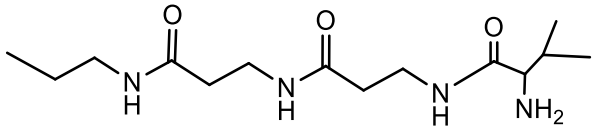

FTIR (ν_{max}/cm^{-1}) , 2940 (N-H stretch), 1657 (C=O stretch), 1566 (N-H bend), 1280 and 1130 (C-N); ^{1}H NMR (400 MHz; MeOD), 5.28 (1H, *s*, NH), 3.55 (1H, *d*, J 5.5 Hz, <u>CH</u>), 3.45 (4H, *m*, $CH_2\underline{CH_2}NH_2$), 3.10 (2H, *t*, J 7.0 Hz,$CH_2C\underline{H_2}$), 2.40 (2H, *t*, J 7.0

Hz ,$\underline{CH_2}NH$), 2.35 (2H, *q* J 7.0 Hz, $CH_2\underline{CH_2}$), 2.26 (1H, *sept*, $\underline{CH}(CH_3)_2$), 1.58 (2H, *m*, $CH_3\underline{CH_2}CH_2$), 1-0.98 (6H, *d*, $CH(\underline{CH_3})_2$), 0.91 (3H, *t*, J 7.5 Hz, $CH_2\underline{CH_3}$); ^{13}C NMR (100 MHz; MeOD) 172.5, 170 (*C*=O), 41.0, 38.0, 35.0, 32.0, 29.0 (CH_2), 18.5 (CH_3),13.0 (CH_3); 55% yield; Mass spec (ES) 299 (MH^+), 323 (MNa^+), ES-MS $C_{14}H_{28}N_4O_3$= 300 (calculated).; UV Absorbance (MeOH) λ_{max} (nm) 275, 227 .

2.6.6 Encapsulation of the chains within the PAMAM dendrimer

Preparation of TRIS buffer solution

Tris(hydroxymethyl)aminomethane (**TRIS**) (6.05 g, 0.05 mol) was added into 500 mL of distilled water. The pH of the solution was monitored and adjusted with hydrochloric acid until the pH of the solution was reached 7.46. The TRIS buffer solution obtained had a concentration of 0.1 M.

General procedure for the encapsulation

Dendrimer and the chain (excess 10 eq) were dissolved in methanol. The solutions were combined and stirred for 24 hours in room temperature. The solvent was removed at reduced pressure and the residue was dissolved in TRIS buffer. The solutions were filtered to remove the excess insoluble chains before being analysed via UV.

.

2.6.7 *α*-Chymotrypsin for Binding Assay

Preparation of phosphate buffer

Disodium hydrogen phosphate (14.48 g) and monosodium dihydrogen phosphate (1.75 g) were dissolved in 1.0 L distilled water. The pH adjusted to 7.46 with HCl or NaOH and the buffer solution obtained with the concentration 0.1 M.

Preparation of functionalised dendrimer (Z)

Dendrimer and linear chain (excess 10 eq) in methanol and was stirred for 24 hours at room temperature. Methanol was removed at reduced pressure to yield a dendrimer/linear chains co-precipitate. The co-precipitate produced was dissolved in phosphate buffer and filtered.

Preparation of 4 nitroaniline solution (Beer -Lambert)

A series of 4-nitroanaline **28** in DCM solution with different concentrations was prepared. The Δ absorption values were used at 410 nm and Beer- Lambert was shown the relationship between absorbance and concentrations of 4-nitroanaline **28**.

Preparation of *α*-chymotrypsin solution

α-chymotrypsin (5 mg) was dissolved in 200 mL of phosphate buffer (pH=7.46, 0.1 M) to give 1.0 x 10^{-6} M solution. Protein solution was added to the dendrimer/functionalised dendrimer (**Z**) in equal volume and the solution was shaken for 24 hours prior to assay.

The binding experiment for anionic dendrimer G3.5 COOH 12

General procedure:

All of the specimens were dissolved in 0.1 M of phosphate buffer (pH 7.46) at 25 ºC. Dendrimer prepared with different concentration (0.5, 1.0, and 2.0 μM), and were incubated with 1.0 x 10^{-6} M α-chymotrypsin for 24 hours prior to assay. For control experiment, the cuvette began with α-chymotrypsin and buffer solution (1.0 mL α-chymotrypsin and 1.0 mL phosphate buffer) or 2.0 mL protein-dendrimer/functionalised solution and was added with 0.5 mL BTNA **26**. Hydrolysis of the BTNA **26** substrate was monitored by recording the 4-nitroaniline absorbance at λ = 410 nm at 120 second intervals for a period of 2400 s.

Assay of Dendrimer-Chymotrypsin Activity

For each final concentration of dendrimer (0.2, 0.4, and 0.8 μM), the initial velocity was measured at BTNA **26** (substrate) concentrations of 2 μM, 4 μM, 6 μM, and 8 μM. All experiments were performed at an enzyme concentration of 0.4 μM. Initial velocity for each dendrimer/substrate combination was obtained by linear fittings of 4-nitroaniline production over the time using Graphpad prism 7.0. Initial velocity conditions were observed in all cases. All measurements were recorded at least three times. The data obtained was plotted and analysed using the mixed mode inhibition model and transformed into Lineweaver-burk plot.

For G3.5-OH **31 with concentration (0.4 , 0.8 and 1.6 μM) and the linear chain was used excess of 10 eq respectively.*

Chapter 3

Functionalised Dendrimer For

Measuring Binding To Cytochrome- C

3.0 Introduction

An electron transport protein of great significance for electron transfer as well as apoptosis, cytochrome-c constitutes an appealing target. Otherwise referred to as mitochondrial protein, cytochrome-c is made up of 104 amino acids and one heme group, with the latter serving as electron transporter in energy transduction because it can shift between ferrous (Fe^{2+}) and ferric oxidation states (Fe^{3+}).[75] There are two minor and three major helices constituting the cytochrome-c structure and they give rise to a heme pocket by folding in a round shape. [76] Cationic lysine residues and hydrophobic domains are arranged along the border of the heme edge surface. This is indicative of strong dependence electrostatic interactive with its protein partner, cytochrome- c peroxidase (Figure 60). The interaction happening in the protein active site can be accommodated by targeting the residues to take advantage of non-covalent interactions.

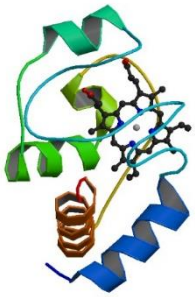

Figure 60: The ribbon structure of cytochrome-c with a heme moiety

Scaffold macromolecules, including bipyridine metal complexes,[77] fullerenes,[78] dendrimers, [74] fullerene dendrimers [79] and anthracene,[80] can bind to compete with its protein partner of cytochrome-c. As argued in the second chapter (*page 22*), dendrimers provide a suitable platform to match interface of protein. Meanwhile, in a different approach, Tetracarboxyphenyl porphyrin (TCPP) can serve as a basis for the development of ligands capable of targeting protein surfaces because they present a relatively large surface characterised by hydrophobicity. Also, binding can be detected by fluorescent emission spectrocopy, which simplies the binding studies. Fisher first reported the binding of TCPP to cytochrome-c, with 0.05-5 mM K_d.[81] In a different study, Hamilton and colleagues produced cytochrome-c ligands of higher affinity using

anionic functionalised calix[4]arene. [14, 82] The number and position of the cationic sites on the protein surfaces determines the binding affinities, given that the multi-anionic site of the synthetic receptors was fixed on to rigid macrocyclic scaffolds. A supramolecular complex resulted from the interaction between the terminal carboxylate anions surrounding the heme depression and the cytochrome-c cationic surface.

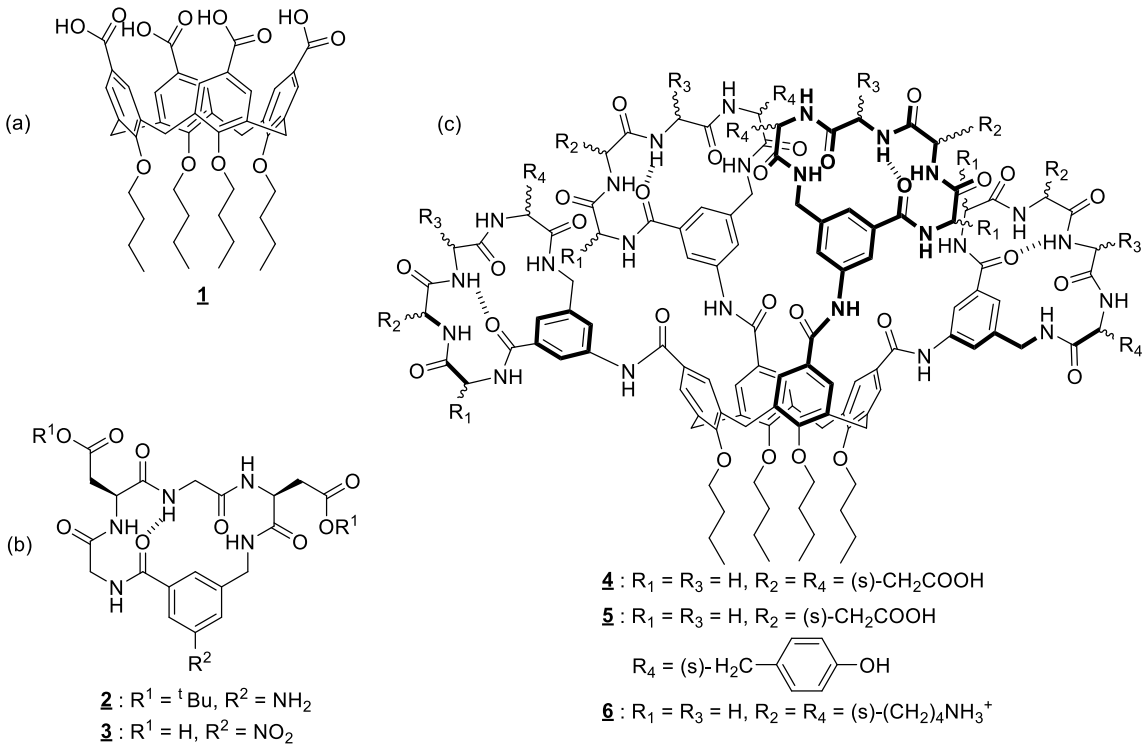

Figure 61 : Chemical structures of (a) Calix [4]arene (b) Cyclic Peptide Loops, and (c) Calix[4]arene attached to four peptide loops for the surface recognition to Cyt-c. Adapted with permission from Hamilton and co-worker. [83-,84]

The interaction between cytochrome-c and the apoptopic protease activating factor (APAF1) has been validated by earlier research.[85] Such an interaction may induce apoptosis. The calix[4]arene scaffold could disrupt the cytochrome-c- APAF1 complex, with a K_d of 30 nM.[86] Furthermore, Hamilton also showed that an amino acid functionalised TPP was capable of recognising cytochrome-c. Moreover, as the amino acid and peptide derivatives surrounding the external edge perturbed fluorescent quenching to differing extents, then differing proteins could be recognised by the different fluorescence quenching (Scheme 18).[87]

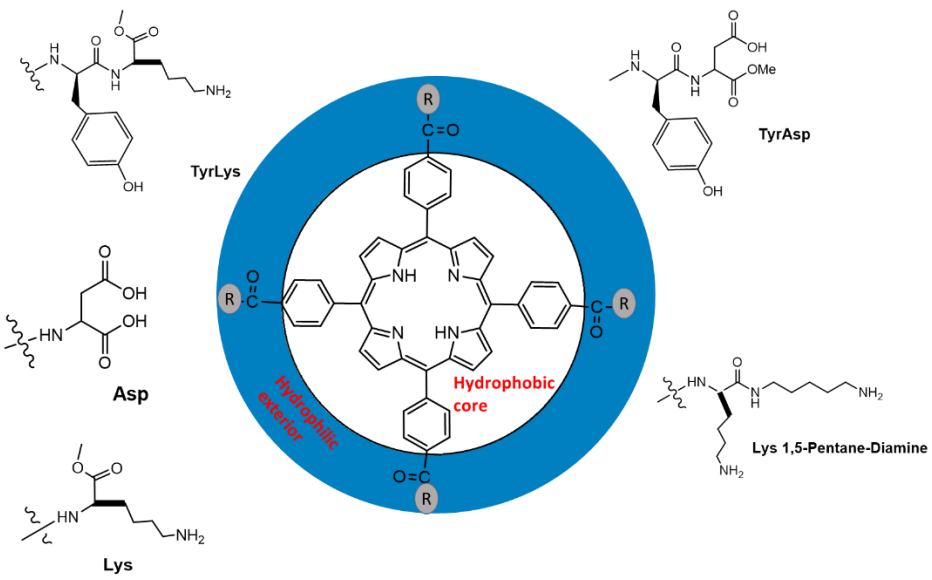

Scheme 18: A tetraphenyl porphyrin with amino acids

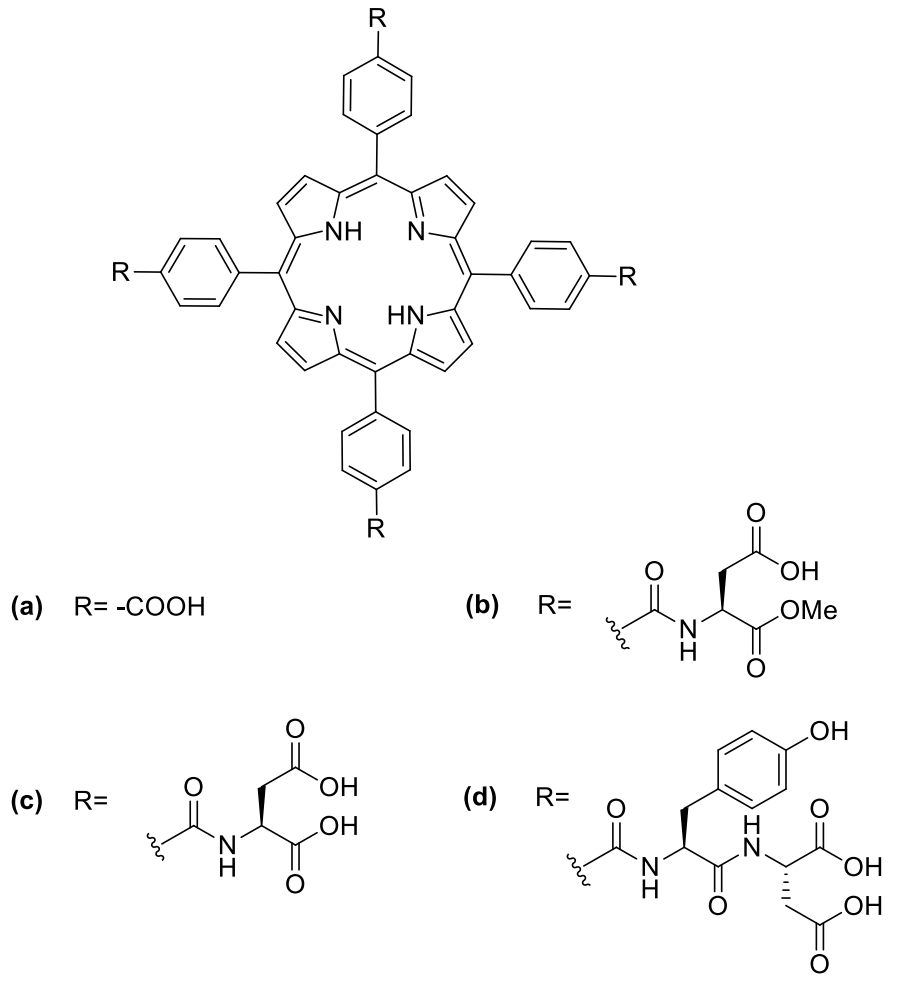

Figure 62: Scaffolds of tetraphenyl porphyrin with the hydrophobic and anionic groups

Another observation derived from the tetraphenyl porphyrin studies, was the number of existing hydrophobic and anionic groups determines the relative affinity of a receptor to the surface of a protein, as shown in Figure 62. Such a receptor exhibits high-affinity binding in a liquid environment. The receptor with the greatest affinity for the cytochrome-c surface (20 nM K_d) is receptor (d) due to the highest number of carboxylic acid and phenyl groups. These groups bind cytochrome-c by electrostatic and hydrophobic interactions as illustrated in Scheme 19. Such a finding suggests that this may not only have an ability for protein surface recognition but may also have promising qualities of medicinal relevance. [14]

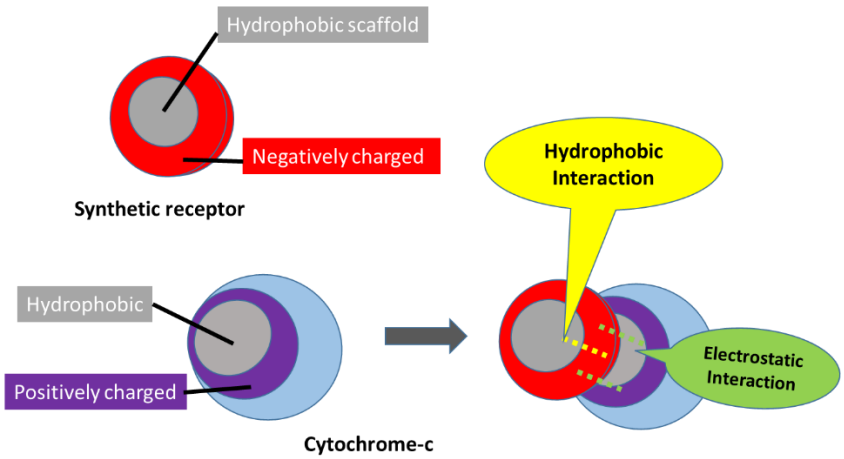

Scheme 19: The binding mechanism of cytochrome-c

Evidence was provided by Crowley and colleagues about the occurrence of a dynamic assembly of porphyrin interactions displaying energetic similarity taking up a number of distinct patches on the surface.[88] Furthermore, it was observed that a decrease of up to 50°C in the melting temperature of cytochrome-c was achieved by porphyrin with appropriate functionality. By contrast, the melting temperature of cytochrome-c was unaffected by porphyrin, highlighting that the "denaturing" effect depended on charge complementarity. [40] The applied assumption was that the preferential binding of porphyrin to protein in its unfolded state was what caused the effect. Meanwhile, in a different study, Hamilton provided proof that a 25°C decrease in the melting temperature of cytochrome-c was triggered by a receptor based on tetrabiphenyl porphyrin, suggesting preference for negative cooperative binding to cytochrome-c in its unfolded state.[89]

By comparison to free-base counterparts, metalloporphyrins exhibit quicker aggregation in a liquid environment owing to improved π-π stacking.[90-91] Hence, proteins could possibly be detected through interactions between metals and ligands, since binding displaying selectivity and high affinity could be achieved with fewer interactions. This led to the development of dendrimers based on zinc (II) porphyrin, with binding to cytochrome-c being achieved based on the hydrophobic metalloporphyrin core and the electrostatic binding, leading to a stable porphyrin/cytochrome-c complex. Meanwhile, Tsukube and colleagues undertook the creation and synthesis of proteo-dendrimers (1a−4a) as synthetic receptors, comprising a polyanionic heptaglutamic acid unit, with four lysines and each with 2 carboxylic acid (at the surface) for each dendrimer, hydrophobic dendrons (benzyl ether groups), a hydrophilic polyether surface ensuring solubility in water, and a fluorescent zinc porphyrinate as core serving as signalling device (Scheme 20). Competitive inhibition disrupted the interaction between APAF1 and cytochrome-c.[92]

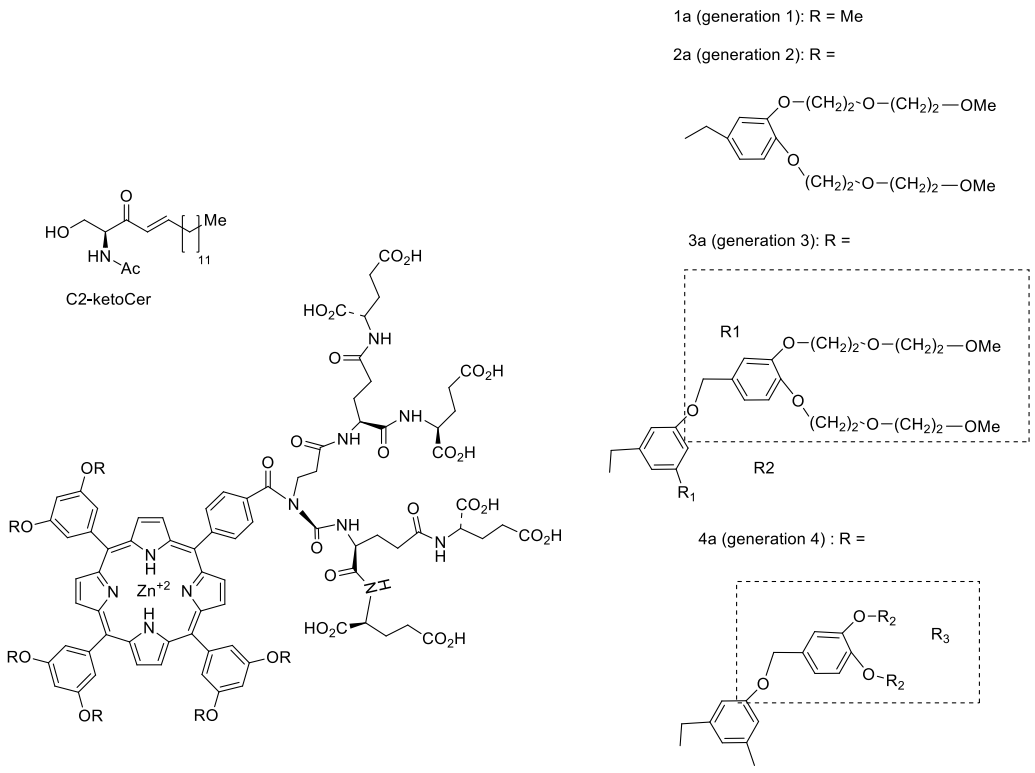

Scheme 20: The chemical structure of proteo-dendrimers (1a-4a)

The present assay demonstrated that 2a was the proteo-dendrimer with the highest potency, being the least cytotoxic and the most soluble. Interaction occurred between the proteo-dendrimer's polyanionic patch and the cytochrome-c polycationic patch (four

protonated lysines), the interfacial area being around 1000 $Å^2$. Description of the interactions of polyanionic G1.5−G4.5 PAMAM dendrimers was provided by Twyman and colleagues as well. Cytochrome-c quenching was achieved by those dendrimers based on G1.5−G4.5 CO_2H terminal groups and binding non-covalently using TCPP as a competitive (Hot) ligand .[35] Hence, this type of interaction between proteins could be disrupted with the help of this category of receptors.[47]

3.1 Aims and Objectives

In addition to *α*-chymotrypsin, cytochrome-c (Cyt-c) was also selected as a target protein to assess dendrimer binding and the potency of the functionalised dendrimers. The same non-covalent methodology for adding the targeting groups to *α*-chymotrypsin was used. Cyt-c was specifically chosen as its binding surface is well documented. In addition, it has a porphyrin moiety that is capable of quenching chromophoric ligands bound to the interfacial/hotspot area. Therefore, fluorescence spectroscopy can be used to quantitatively measure binding. This feature was developed by Hamilton as a method to directly measure the binding of Tetracarboxyporphyrins (TCP) to Cyt-c.[14]

Recent studies undertaken within the Tywman group have found that a porphyrin cored dendrimer could bind to the surface of Cyt-c and quench its fluorescent signal.[35] These dendrimers possessed a simple negatively charged surface. However, the use of covalent chemistry to add the porphyrin core was difficult. The difficulty would be made worse if covalent chemistry was also used to add targeting groups to the surface. To overcome this limitation, the group initially studied a non-covalent system, where the signaling porphyrin was encapsulated within a sample dendrimer Scheme 21(a).

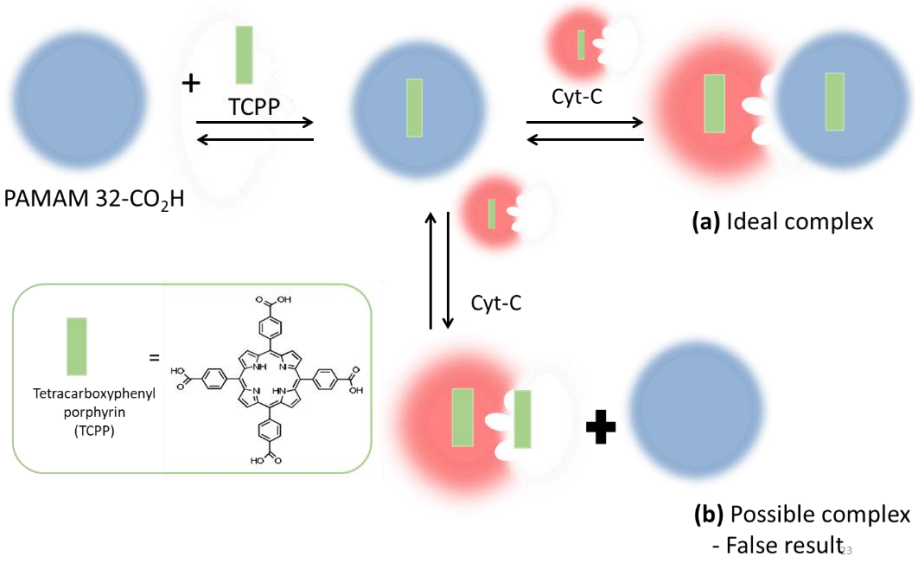

Scheme 21: Possible binding complexes that could form when the TCPP/dendrimer complex is added to the protein. Both results are quenching. a) Ideal complex between dendrimer and protein b) complex between TCPP and protein that results in a quenched signal, but no dendrimer binding.

The method used an insoluble porphyrin chromophore that could be complexed via hydrophobic effects to the interior of the dendrimers. If this complex bound, then quenching of fluorescence would be observed. The method worked and quenching was observed, but there were other possibilities that could have generated the same result. TCPP is encapsulated within the dendrimer via hydrophobic and electrostatic interactions. However, it is possible for TCPP to be released and bind independently to the protein (via electrostatic interactions). This would generate a false result Scheme 21(b).

To overcome this problem, Tetraphenyl porphyrin TPP, which is insoluble and could not bind to the protein was studied. However, this failed as TPP was not encapsulated very well. The problem was solved using the phenolic porphyrin (Figure 63). The phenolic group is acidic enough to bind electrostatically to the amines within the dendrimer, but also not the protein. In addition, when the porphyrin was metallated, it could also coordinate to the internal nitrogens of the dendrimer and help strengthen binding (via a cooperative binding effect).

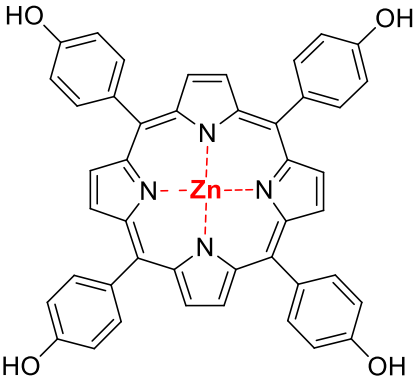

Figure 63: The compound of 3-hydroxyphenyl porphyrin (phenolic porphyrin)

The aim of this project was to extend the above-mentioned approach by incorporating binding groups non-covalently to the dendrimer, as shown in Scheme 22.

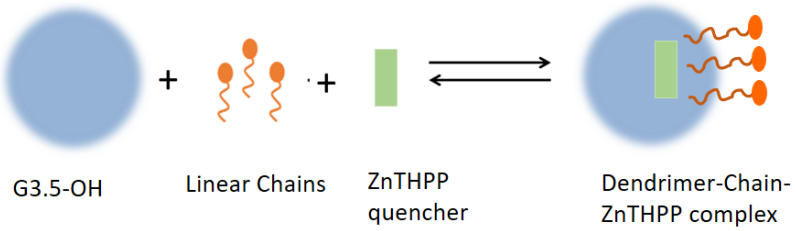

Scheme 22: A ZnTHPP-dendrimer-chain complex formed when the dynamic system was established

3.2 Results and discussion

3.2.1 Synthesis of Zinc Tetrahydroxyphenyl Porphyrin (ZnTHPP) 44

In order to coordinate with the dendrimer and help strengthen binding, zinc was inserted into the porphyrin. ZnTHPP **44** was synthesised using a two-step process, which involved the synthesis of THPP **43**, which was obtained (Scheme 23) from the reaction of pyrrole **41** and 4-hydroxy benzaldehyde **42** in refluxing propionic acid for 3 hours. The mixture was cooled to -5 ºC and the solid obtained collected by filtration. The solid was washed with a mixture of propionic acid and ethanol before it was dissolved in methanol and concentrated in a vacuum, yielding purple crystals. [93]

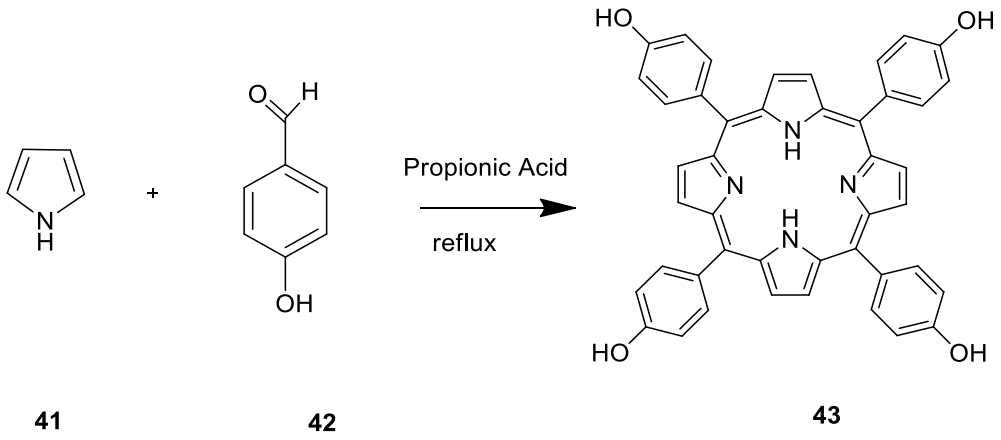

*Scheme 23:Synthesis of Tetrahydroxyphenyl Porphyrin (THPP) **43***

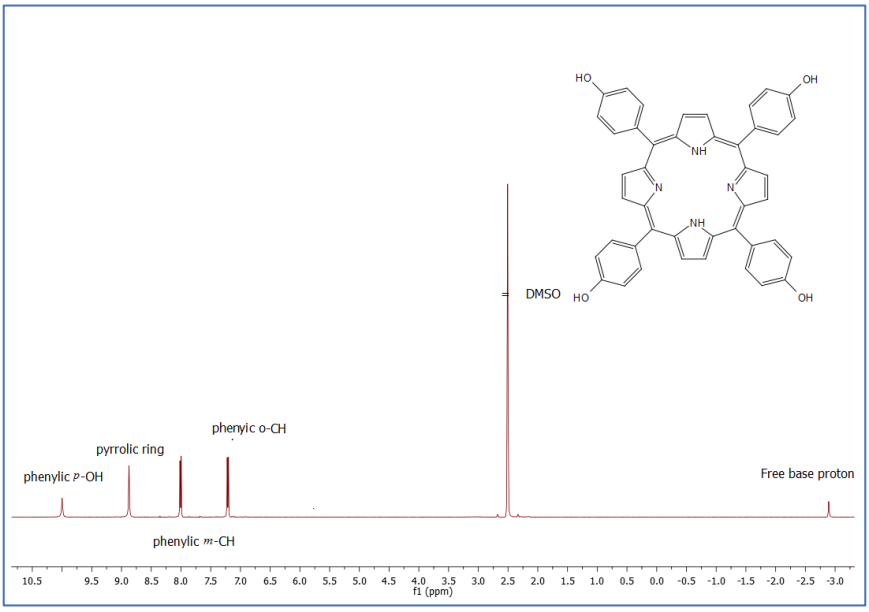

*Figure 64: [1]H NMR spectrum of Tetrahydroxyphenyl Porphyrin (THPP) **43** in DMSO solvent*

The structure was confirmed by ^{1}H NMR (Figure 64), which showed peaks at 8.85 ppm corresponding to the pyrrolic *β*-H of the porphyrin ring. Two doublets were also observed, which corresponded to resonances of the phenylic protons at 7.18 ppm and 7.97 ppm (*ortho* and *meta* respectively). Further signals were observed with a chemical shift of 9.99 ppm, related to the hydroxyl groups. The free base protons (inner NH) were observed at -2.92 ppm due to strong shielding by the porphyrin macrocycle. The UV spectrum showed an intense absorption at 418nm corresponding to the Soret band. Four-Q bands, at 520 nm, 560 nm, 595 nm and 655 nm, were also observed. FTIR spectra showed signals for OH, NH and C=N groups, at 3248 cm^{-1}, 2924 cm^{-1} and 1609 cm^{-1}, respectively. Mass spectrometry analysis confirmed the mass of the product with a molecular ion at 679 (MH^{+}).

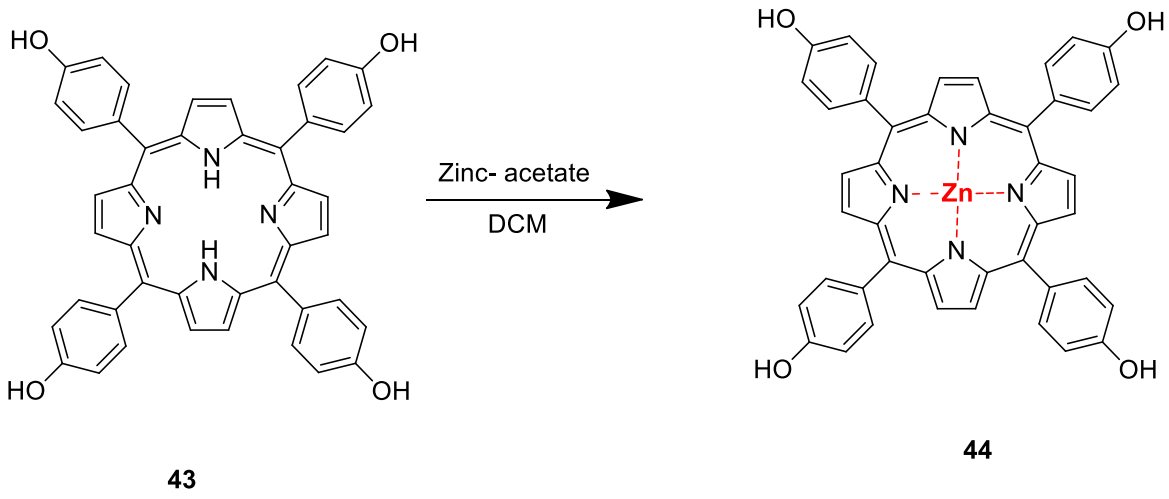

43 **44**

*Scheme 24: Synthesis of Zinc Tetrahydroxyphenyl Porphyrin (ZnTHPP) **44***

Zinc was inserted into the porphyrin by refluxing THPP **43** with zinc-acetate in dichloromethane (DCM) for 30 minutes in Scheme 24. The product was filtered to remove unreacted zinc-acetate. The ^{1}H NMR spectrum showed that zinc had been inserted, as the peak for the free base protons was no longer visible at -2.92 ppm. Mass spectrometry confirmed insertion with a molecular ion peak observed at 743 (MH^{+}). The UV-Vis spectrum exhibited a Soret band at 425 nm and only two Q bands at 596 nm and 661 nm; a reduction from the four bands of the free base porphyrin. The next step was to encapsulate ZnTHPP **44** within a dendrimer via coordination.

3.2.2 Complexation of ZnTHPP 44 with functionalised PAMAM

To form the dendrimer-chain porphyrin complex in Figure 65, a solution of ZnTHPP **44** with a concentration of 1.0 x 10^{-6} M in a phosphate buffer solution was prepared. A dendrimer-chain complex solution was prepared using 5.5 mg of G3.5-OH **31** PAMAM dendrimer and 3.6 mg of Tyr chains **21** dissolved in methanol. Methanol was removed under reduced pressure and 1.0 L of the ZnTHPP **44** porphyrin buffer solution was added. The final concentrations of G3.5-OH-Tyr **38** were 1.0 µM of dendrimer and 9.76 µM of the linear chain, respectively. UV/Vis spectroscopy was used to confirm the encapsulation. We observed that when ZnTHPP **44** was added to the dendrimer solution, the absorption of the porphyrin soret band shifted to a new signal at 430 nm (Figure 66). The change was due to coordination binding between ZnTHPP **44** and the nitrogens within dendrimer (Figure 67).

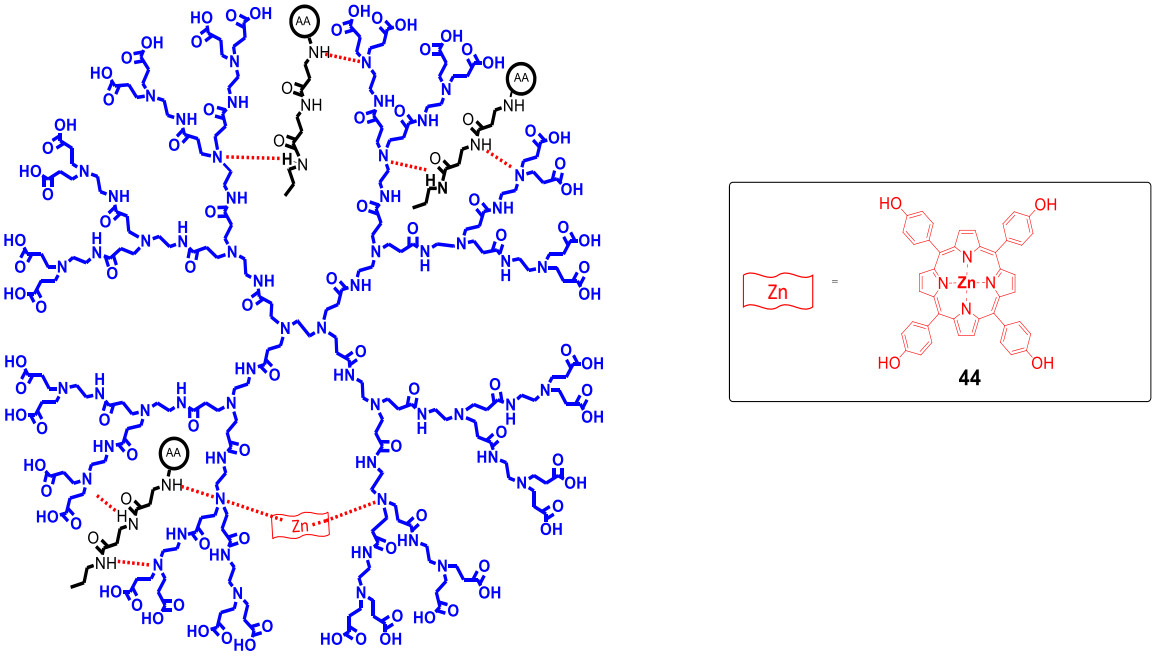

Figure 65: The additional interaction provided by coordination of ZnTHPP

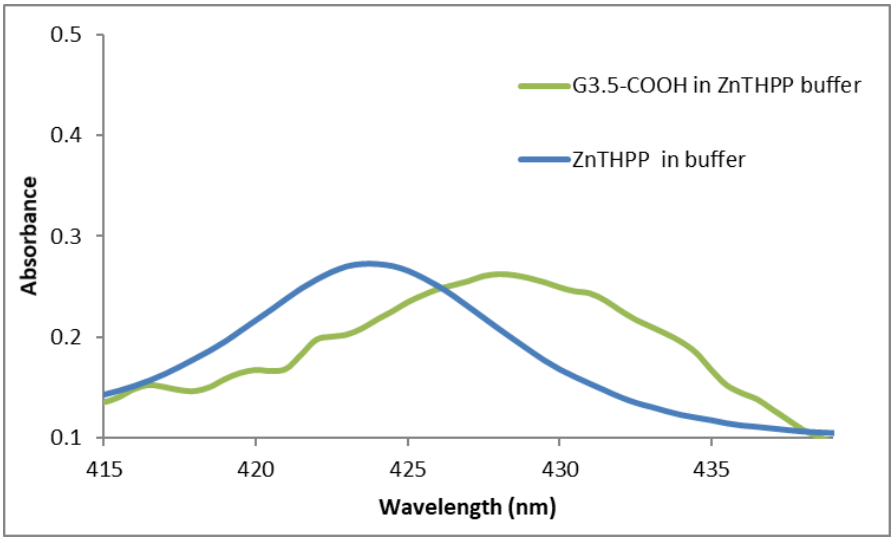

Figure 66: The UV spectrum of ZnTHPP buffer alone and 1.0 µM functionalised G3.5-COOH ***12*** *added to ZnTHPP buffer solution (1.0 µM).*

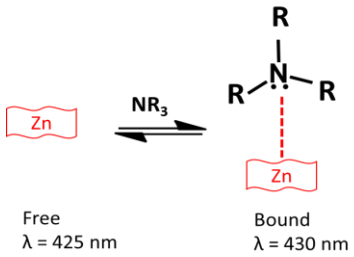

Figure 67: The coordination binding made the absorption of the porphyrin soret band shifted from 425 nm to 430 nm

3.2.3 Assessment of binding between dendrimer and Cyt-c using non-covalent targeting and non-covalent signaling.

The aim for this study was to confirm how important and how strong the polyvalent interactions from the amino acids were to the binding of Cyt-c. Therefore, our initial step was to incorporate binding groups non-covalently to a dendrimer that could not bind Cyt-c. Our main target was to bind to the surface of Cyt-c as shown in Figure 68.

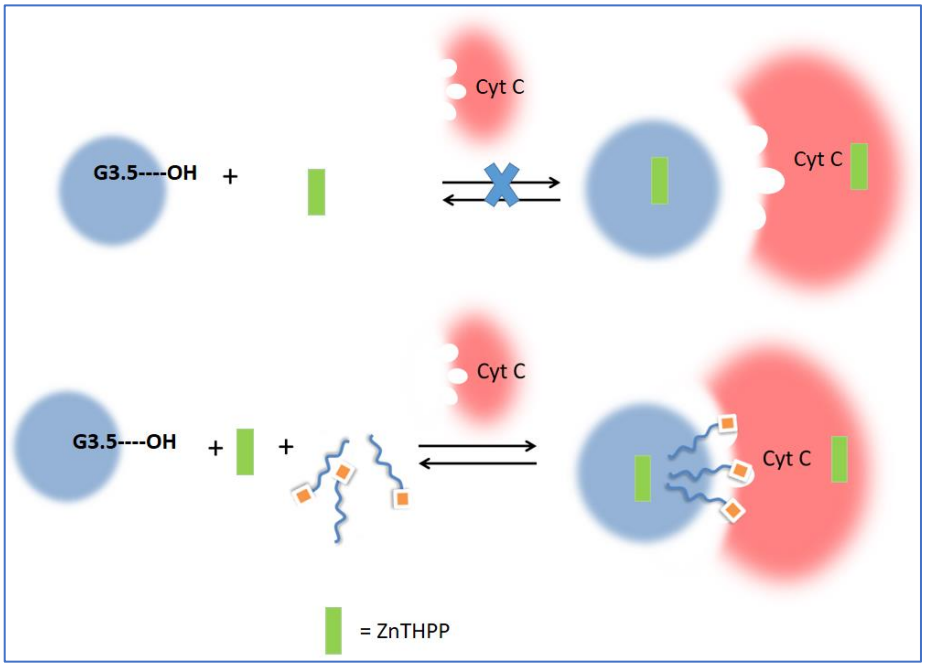

Figure 68: A functional group from the chains provide binding to active site of Cyt-c.

Our first experiment was carried out to measure any reduction in porphyrin emissions, when a solution of Cyt-c (1.0 µM) was titrated into a solution of ZnTHPP buffer (1.0 µM). No change in intensity occurred on the fluorescent reading confirming that the porphyrin did not bind to Cyt-c. The next control was undertaken to determine if there was any effect on intensity when 9.76 µM (maximum for encapsulation control) of the targeting chains was added to the ZnTHPP buffer solution without dendrimer. No change in the intensity of porphyrin fluorescence was observed during these experiments. Therefore, we concluded that the linear chains did not bind to ZnTHPP **44**. To confirm that G3.5-OH **31** did not bind to the protein, a control experiment was carried out up by adding a solution of dendrimer in ZnTHPP buffer to the protein (at constant

porphyrin concentration). Again, no effect on Cyt-c fluorescence was observed. The experiment was repeated with the addition of the tyrosine chain **21**. The encapsulation of experiment was carried out as previously described in section 3.2.2 (*page 118).* Cytochrome-c (0.3 mg) was incubated in dendrimer-chain solution to give a final concentration of 1.0 µM.

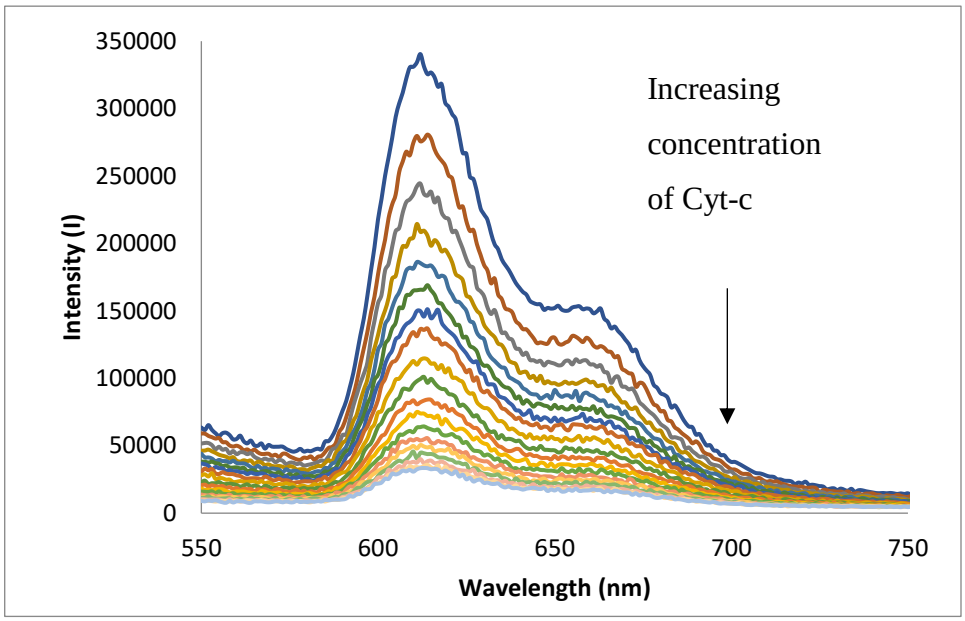

*Figure 69:Emission spectra reduced after each titration of 20 µL of Cyt-c to a solution of G3.5-OH **31** (1.0 µM) in the presence of chains in ZnTHPP buffer.*

This solution was then added in aliquots to a solution of the ZnTHPP/tyrosine/ dendrimer complex. As can be seen in Figure 69, the intensity of the porphyrin peak decreased as the solution of Cyt-c was added. This confirms that binding occurred, as the intensity of the ZnTHPP peak was only quenched when chromophore (Cyt-c) was very close. The intensity at 610 nm was plotted against the concentration of Cyt-c and the plot fitted to a 1:1 binding model using Graphpad Prism. The data and fit are shown in Figure 70.

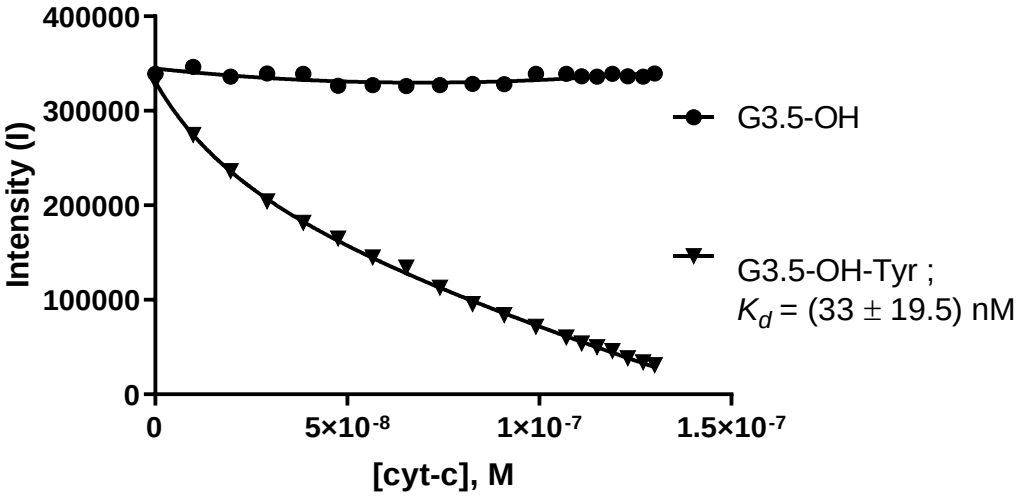

*Figure 70: A binding plot of intensity of the emission against the concentration of Cyt-c titrated with the absence and presence of chains in neutral G3.5-OH **31** dendrimer at 1.0 µM ZnTHPP buffer.*

The data generated a dissociation constant, K_d, for G3.5OH-Tyr **38** of 33 nM (K_a = 3.00 x 10^7 M^{-1}). This was similar to the research undertaken by Hamilton and colleagues, who obtained a K_d for Tetraphenylporphyrin of 20±5 nM. [47]

Our data showed that binding was lower than the above-mentioned study, but our ligand was neutral and lacked the strong electrostatic interaction of TCPP. Therefore, we proposed to use the G3.5-COOH **12** anionic dendrimer in the next stage in an effort to improve binding. The addition of a tyrosine chain to the dendrimer may lead to an enhanced protein binding (and recognition).

We predicted that, if the chain functionalised dendrimer did not bind, or the chains orientation was not compatible, the same dissociation constant would be obtained for the dendrimer/ Tyr complex and G3.5-COOH **12** alone. Therefore, binding studies were initially carried out with G3.5-COOH **12** dendrimer and the experiment was then repeated using the tyrosine chains **21**. In both cases ZnTHPP was encapsulated as the probe. The data is shown in Figure 71 and clearly demonstrates increased binding strength for the dendrimer/ Tyr complex.

(a)

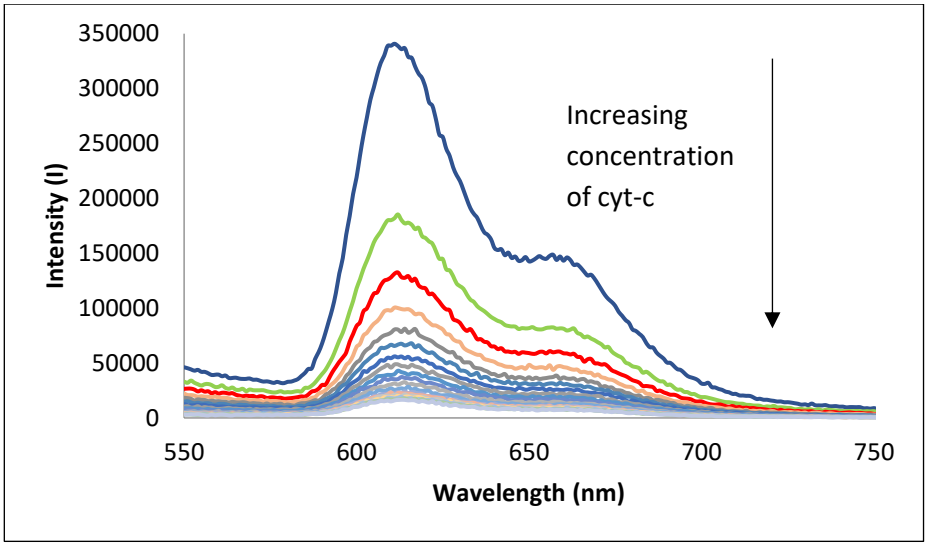

(b)

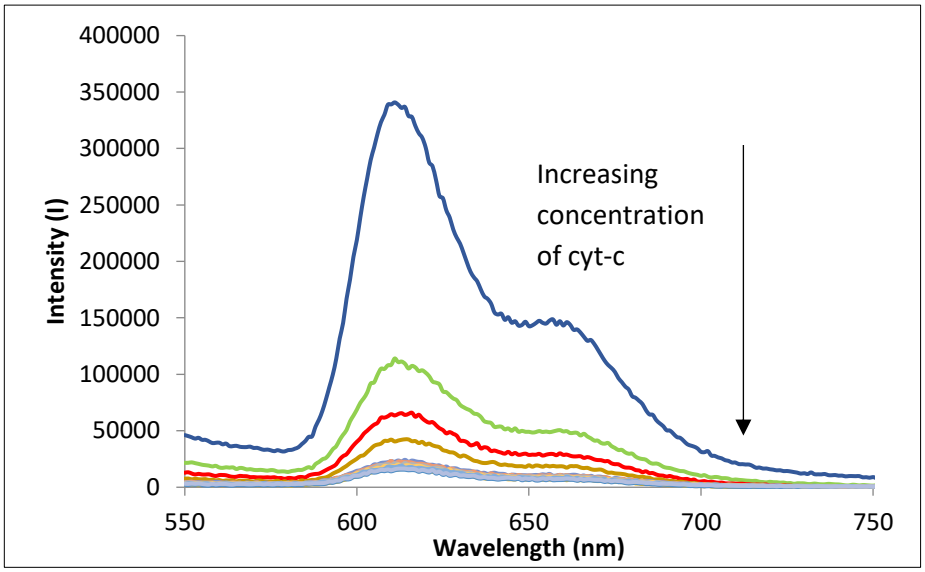

*Figure 71:Emission spectra reduced after each titration of 20 µL of Cyt-c to a solution of (a) 1.0 µM of G3.5-COOH **12** alone and (b) 1.0 µM of G3.5-COOH- Tyr **24** in ZnTHPP buffer.*

The emission for G3.5-COOH-Tyr **24** was quenched to a greater extent than with G3.5-COOH **12** alone. Plotting the intensity vs [Cyt-c] and fitting the data to a 1:1 model (graphpad) allowed us to calculate K_d for G3.5-COOH **12** of 10.85 nm (K_a = 9.22 x 10^7 M^{-1}) and a K_d of 5.55 nM (K_a = 18.00 x 10^7 M^{-1}) for the G3.5-COOH-Tyr **24** system. Therefore, both bind well to the interfacial area using their carboxylate groups, but binding is significantly improved by the polyvalent interactions and functionality of the dendrimer/Tyr complex. The chains are held non-covalently, therefore, the dendrimer-chain system is dynamic, and the chains can move to maximise any interactions. As

such, the protein will establish an equilibrium where the most stable species are in solution. Specifically, the protein-dendrimer complexes.

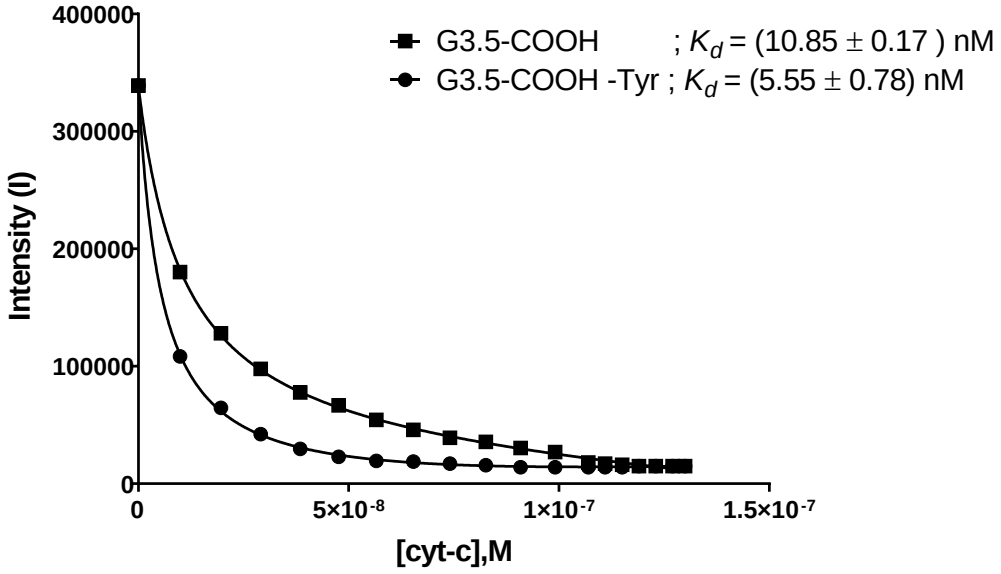

Figure 72: A binding plot of intensity of the emission against the concentration of Cyt-c titrated in the absence and presence of chains

Although we have demonstrated that non-covalent interactions can form a complex that can bind and detect Cyt-c, it remains unknown as to whether or not binding between proteins and dendrimer alters or denatures the structure of the proteins. A previous study within the group showed that the dendrimer did not denature Cyt-c and Chy.[35] We therefore wanted to test the effect of dendrimer binding on protein structure.

3.2.4 Circular Dichroism (CD)

Changes in protein structure can be examined using CD, so any structural differences can be identified by comparing the CD spectra of Cyt-c in the presence and absence of the functionalised dendrimer. The control experiment was carried out using Cyt-c (1.0 µM) as the buffer. This was then repeated using a dendrimers-chain/protein complex, with the final concentration of the dendrimer and tyrosine chain being 1.0 µM and 10 µM respectively. The measurements were carried out at 230 nm in the ZnTHPP buffer (pH= 7.46) at 37°C. As can be seen, the CD spectra for the two systems are similar. The results are shown in Figure 73 and indicate that the CD spectra of the dendrimer without a chain, or unfunctionalised dendrimer, concurs with the published data, and does not denature Cyt-c. [35,52]

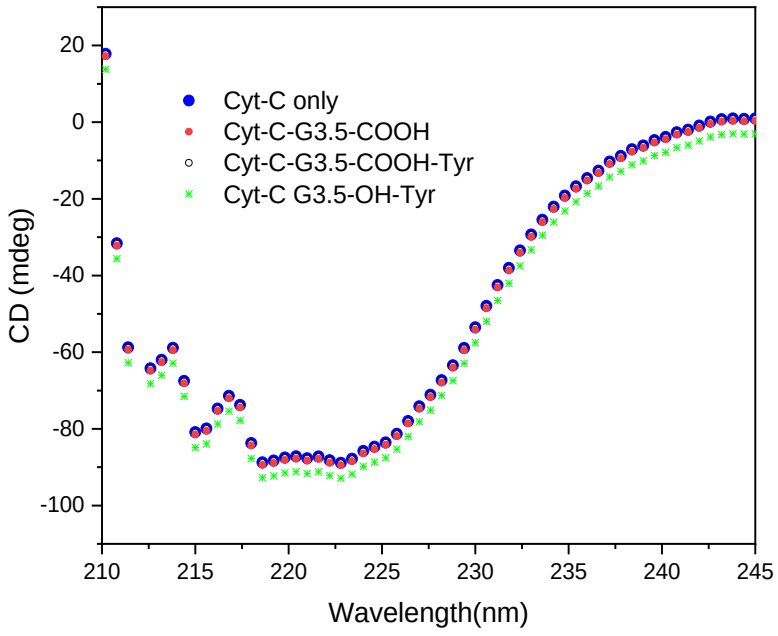

Figure 73: CD spectra of Cyt-c when bound to nonfunctionalised and functionalised dendrimer (with tyrosine) in the ZnTHPP buffer.

Hamilton et al. reported that tetrabiphenyl porphyrin-based receptors could bind with high affinity towards the surface of Cyt-c (K_d = 0.6 nM) and demonstrated how binding could affect the melting temperature of the protein using circular dichroism. [89] For this study, we were interested to see whether the same technique could also be used to determine any effect of binding upon protein stability using the dendrimer system that

they had established. In effect, we aimed to establish whether the dendrimer /protein would be more or less stable with regard to changes in temperature when bound to the dendrimer. As such, the dendrimer protein complexes were heated from 37°C to 75°C, at 1°C per minute. The results for the functionalised dendrimers bound to Cyt-c at 230 nm were the same as those obtained for Cyt-c alone, as shown in Figure 74. Therefore, it can be concluded that the dendrimers system does not change the protein structure and that any effect on the protein function is not caused by a simple denaturation process, as the dendrimer binds to the protein.

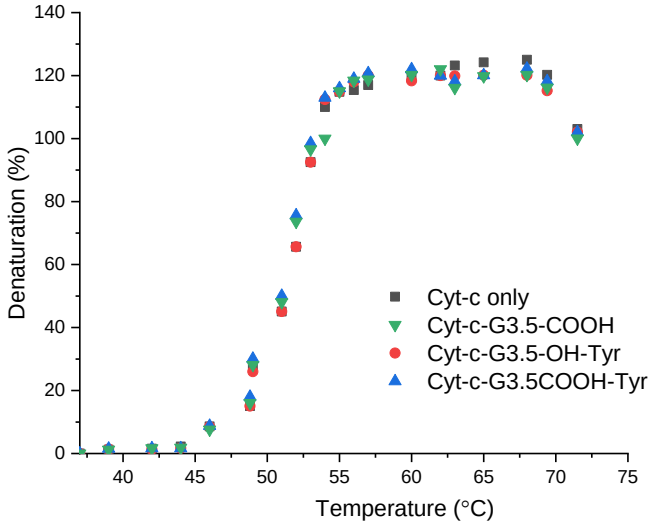

Figure 74: Temperature profiles of denaturation (unfolding) of Chy and when bound to a functionalised dendrimer in the ZnTHPP buffer at 230 nm.

3.3 Conclusion

In conclusion, the binding potency of the functionalised dendrimers was successfully measured using non-covalent methods. The study also confirmed that no binding took place between the neutral G3.5-OH **31** and Cyt-c, due to a lack of terminal functionality that could bind to the protein surface. However, the same neutral dendrimer could bind to Cyt-c if the tyrosine chains were encapsulated. The binding affinity for the tyrosine functionalised system was 3.00 x10^7 M^{-1} to the surface protein. The data is presented in Table 25.

Cytochrome-c	K_d (Dissociation constant), nM	$K_a = 1/K_d$ (Association constant), 10^7 M^{-1}
ZnTHPP	0.00	not applicable
*TCPP alone	20.00	5.00
G3.5OH-Tyr **38**	33.00	3.00
G3.5 COOH **12**	10.85	9.22
G3.5-COOH-Tyr **24**	5.55	18.00

*Table 25: Comparison dissociation and association constant (K_d and K_a) with inhibitor to bind Cyt-c in 0.3µM porphyrin buffer system. *TCPP without inhibitor (as reported by Hamilton[47])*

When the G3.5-OH **31** system was used, the ligands were neutral and lacked any strong electrostatic interaction. Therefore, the next stage of the study investigated the G3.5-COOH **12** anionic dendrimer in order to determine the binding affinity from the terminal electrostatic interaction and thus to establish the contribution to binding from the tyrosine chain. Therefore, a baseline experiment was carried out using G3.5-COOH **12** and the data was compared to that obtained from the functionalised dendrimer tyrosine (G3.5-COOH-Tyr **24**). The binding affinity of the G3.5-COOH **12** dendrimer was 9.22 x 10^7 M^{-1}. When tyrosine was added, the binding of G3.5-COOH-Tyr **24** increased by almost 100% to 18 x 10^7 M^{-1}. Therefore, this clearly shows the importance of the terminal groups on binding.

We assumed that the orientation of the linear chain in the complex had the ‘head’ group pointing out, thus enabling it to interact with the protein surface; however, it is also possible that the ‘tail’ of the linear chain points out and can therefore bind the protein.

It is suggested that future work is required to confirm this with other amino acids. This study has concentrated on just one amino acid (tyrosine) and due to this narrow focus, future work is needed to investigate other functional groups, as well as complexes that possess a number of different functionalities. This could enhance both selectivity and recognition.

3.4 Experimental

**Dendrimers were synthesis as previously reported (page 95)*

Synthesis of Tetrahydroxyphenyl Porphyrin (THPP) 43

Freshly distilled pyrrole **41** (12.51 g, 180 mmol) and 4-hydroxylbenzaldehyde **42** (30.0 g, 120 mmol) were added and refluxed in propionic acid (500 mL) for 24 hours at 142 ºC. The mixture was allowed to cool at room temperature and placed for 2 hours at -5ºC. The crude product was washed with the mixture of propionic acid and ethanol (1:1), and chloroform repeatedly. The organic layer was concentrated in a vacuum, yielding (2.0 g, 2.5%) purple crystals.
ν_{max}/cm^{-1} (FTIR) 3248 cm^{-1} (OH broad band), 2924 cm^{-1} (NH stretch) ,1609 cm^{-1} (C=N) , 1463, 1378, 1172, 964,798, ^{1}H NMR (400 MHz; DMSO) 9.99 (s , 4H phenylic *p*-OH), 8.84 (s, 8H,β-pyrrole), 7.97 (d, J 8.50 Hz , 8H phenylic *m* -CH), 7.18 (d, J 8.50 Hz , 8H, phenylic-*o*-CH), -2.92 (s,2H, NH-pyrrole); ^{13}C NMR (100 MHz; $CDCl_3$) 134.5, 127.6, 126.5, 120.4 (CH_2), 11.8 (CH_3); Mass spec (ES) 679 (MH^+) , ES-MS $C_{44}H_{30}N_4O_4$ = 678 (calculated), UV Absorbance (MeOH) λ_{max} (nm) 418;Q bands 520 nm, 560 nm, 595 nm, 655 nm

Synthesis of Zn inserted to THPP 44

A Tetrahydroxyphenyl Porphyrin **43** (2.0 g, 2.0 mmol) was refluxed in 100 mL of DCM and excess zinc acetate was added for 10 minutes. The solution was then filtered and evaporated. The crude product was dried to give ZnTHPP **44** (250 mg, 47%) as a purple crystal.

ν_{max}/cm^{-1} (FTIR) 2923(s), 3245 cm^{-1} (OH broad band), 2924 cm^{-1} (NH stretch) ,1609 cm^{-1} (C=N) , 1465, 1379, 1175, 968,792; ^{1}H NMR (400 MHz; DMSO) 9.97 (s, 4H phenylic p-OH), 8.84 (s, 8H,β-pyrrole), 7.96 (d, J 8.50 Hz , 8H phenylic *m* -CH), 7.18 (*d*, 8H, J 8.50 Hz , phenylic-o-CH); ^{13}C NMR (100 MHz; $CDCl_3$) 134.5, 127.6, 126.5, 120.4 (CH_2), 11.8 (CH_3); Mass spec (ES) 743 (MH^+) , ES-MS $C_{44}H_{28}N_4O_4Zn$ = 742 (calculated), UV Absorbance (MeOH) λ_{max} (nm) 425 ;Q bands 596 nm, 661 nm

3.4.1 Preparation for Cytochrome c (Cyt-c) binding assay

Preparation of ZnTHPP buffer solution

A porphyrin buffer solution was made from (0.022 g, 3 $x10^{-5}$ mol) ZnTHPP **44** to give final concentration of 1.05 µM in phosphate buffer (pH=7.4).

Preparation of dendrimer (or dendrimer-chain) solution (Z)

The PAMAM dendrimer solutions (**Z**) were made up to 1.0 µM using porphyrin buffer solution and was shaken for 2 hours at room temperature. This was in order to keep the porphyrin concentration constant as the PAMAM were titrated.

Preparation of cytochrome- c solution

Cytochrome-c (0.3 mg, $3.4x10^{-7}$ mol) was added in dendrimer (**Z)** (if functionalised; dendrimer-chain) solution and shaken for 2 hours in room temperature to give a final concentration of 1.0 µM

Assay of Cytochrome-c activity

Cytochrome-c solution (50 µL) was added to 2.0 mL of the dendrimer/chain solutions in porphyrin buffer (**Z**) by fluorescence spectroscopy (Total amount in cuvette = 2.5 mL). After each aliquot was added the cuvette was shaken for 2 minutes and a fluorescent emission reading was taken.

3.4.2 Protein Binding Assay for Circular Dichroism (CD) Spectroscopy

Preparation of dendrimer /chains solutions

Dendrimer/chain solution was made up in ZnTHPP buffer solution to give a stock solution of concentration $1.0\ x10^{-6}$ M.

Preparation of protein solutions

For native cytochrome-c was prepared in ZnTHPP buffer to give $1.0x10^{-6}$ M. Followed by dendrimer/chain protein with Cytochrome-c in ZnTHPPP buffer.

Chapter 4

Synthesis of oligomeric and monomeric functionalised graphene oxides, their application as improved protein ligands and as enzyme inhibitors using α-chymotrypsin as a model protein.

4.0 Introduction

Measuring the properties of graphene and its potential application has been widely studied and has piqued the interests of many scientists. There has been a rise of interest this field since 2010, when Geim and Novosolev were awarded the physics Nobel Prize for their trailblazing work in isolating graphene from bulk graphite. [94] A graphene oxide (GO) is a derivative of graphene and has a large surface area and is abundant with oxygen functional groups (alcohols, epoxides, carbonyls, and carboxylates)[49] in Figure 75a. GO is chemically versatile, and has been explored in many areas ranging, from biology, material science, and pharmacology. However, protein interactions have been less well studied.

Synthetic inhibitors of protein interactions can overcome the aggregation of protein that can be cause a range of diseases, including thromboembolism, [2] diabetes [2] and Alzheimer's disease. [95] The appeal of using a synthetic inhibitor lies largely in its tailorable features, that can be designed, synthesised, and functionalised according to the target protein. De and Dravid found unfunctionalised GO has been shown to bind the serine protease surface of protein in Figure 75; α-chymotrypsin (Chy) and to inhibit its function. [31]

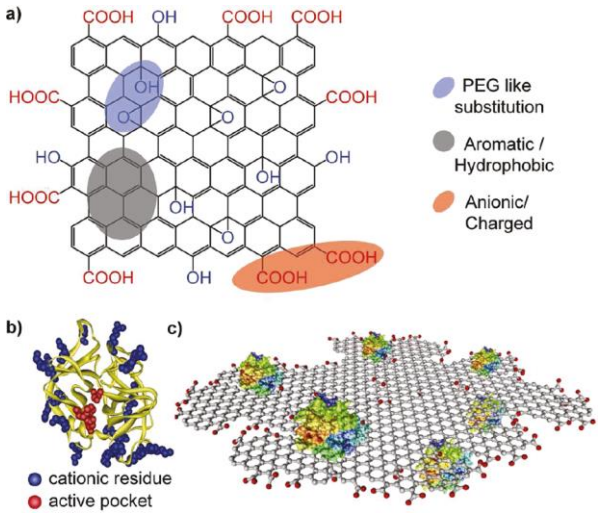

Figure 75:Illustration of a) Graphene oxide (unfunctionalised) b) The surface of α-chymotrypsin and c) GO and Chy complexation. Reprinted with permission from [De, M. J. Am. Chem. Soc. ***133,*** *17524–17527 (2011)].* [31]

However, in nature, protein-protein binding has functional group selectivity. There are several key amino acids which have been known to be important in terms of protein-protein interactions such as tyrosine, tryptophan and phenylalanine and they are primarily targeted for surface recognition.[12] Although there have been a number of reports describing the functionalisation of GO with amino acids, including a recent paper describing a magnetic nano-hybrid system for protein purification,[96] the methodology and characterisation is often over simplified. For example, the most common method of functionalisation describes the use of a coupling agent and an excess of amino acid in its non-protected form. The result of which is reported as a monomeric addition of the amino acid.[96-97] However, this method does not produce a GO surface functionalised with a monomeric layer of amino acid.[98-99] Instead, this methodology produces a surface functionalised with an oligomeric amino acid surface. Although coupling of the first amino acid will initially generate a monomeric functionalised surface, the amino acid is unprotected and therefore free to react with a second amino acid, which in turn can react with a third. Alternatively, an unprotected amino acid can react in solution and form dimers, trimers and oligomers, which in turn can add to the GO surface (where they are free to react further). Therefore, what is obtained is a GO surface with a random oligomeric layer of amino acids. Although this may be an advantage with respect to flexibility, which can lead to high affinity and strong binding, it can also result in a lack of selectivity. In addition, the aromatic amino acids important with respect to protein/enzyme binding are aromatic. These will simply lay down and bind strongly to the GO surface because of favourable and cooperative π-π interactions. As a result, these interactions must be overcome before GO can bind to the protein surface. In comparison, a single monomeric layer will not bind cooperatively to the surface of GO. Therefore, any monomeric interactions between the amino acid and the GO surface will be much weaker (than the cooperative interactions possible with the oligomers). This will make it much easier for the amino acid to interact with a protein surface. Nevertheless, a lack of flexibility and possible steric issues, may limit binding of the mono layered GO. Therefore, it is possible for either the monomeric or oligomeric system to bind strongest (with respect to each other, or GO). It is also possible that neither will bind particularly well, and the unfunctionalised GO remain the best ligand. To test this proposition, we proposed to functionalise the surface of GO with a monomeric and an oligomeric layer of amino acids and to assess binding affinities.

Binding of the mono and oligo layered systems will be assessed relative to their ability to inhibit the activity of the protein α-chymotrypsin. This is possible because the substrate entrance to the active site of α-chymotrypsin sits in the middle of its binding/interfacial area. Therefore, when GO binds, it blocks the active site entrance and the substrate cannot enter.[74] This will result in a reduction of the enzyme's activity, which can be used to assess relative binding efficiency.[68]

4.1 Aims and Objectives

The main aim of this project is to study the potential of functionalised GO as an inhibitor of protein-protein interactions. De et al. demonstrated GO inhibited the activity of *α*-chymotrypsin and displayed the highest inhibition when compared with all the other previously reported artificial inhibitors.[31] However, the limitations using GO (unfunctionalised) in this study are its non-selectivity and low affinity to the cationic surface of *α*-chymotrypsin. Therefore, we envisage to introduce surface recognition sites in GO by functionalising its surface with amino acids as proposed in (Figure 76). The layered GO will be utilised and its properties studied. To develop this strategy, we intend to react the terminal carboxylic acids in GO with tyrosine, which possesses a high affinity with "hot spot" areas on proteins. [86] We will repeat the same strategy using *α*-chymotrypsin as a model protein to bind with GO (unfunctionalised), [31] which will allow us to assess the potential of functionalised GO to inhibit proteins.

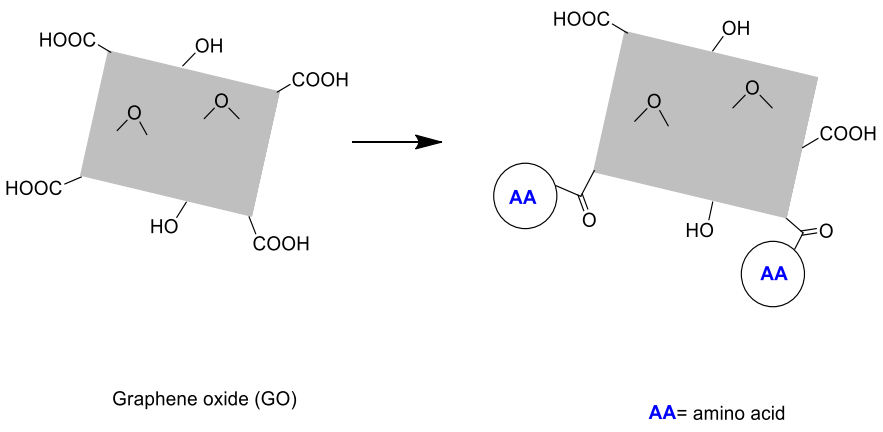

Figure 76: Proposed functionalised GO sheet with amino acids for protein binding study

To achieve our aim, our initial target is to synthesis GO from graphite powder. The Tour method is preferred because it will produce a higher yield of GO and importantly, it is a safe procedure with no toxic gas produced during the reaction when compared with the

other methods described in the literature. [100] Despite GO containing the same types of functional groups (alcohols, epoxides, carbonyls, and carboxylates), the relative and absolute abundance of carbon and oxygen (C/O) in the as-synthesised GO may vary significantly from one method to another. [49,100] However, the functional groups in GO are our main concern because this will allow us to use the same functional groups in GO to undergo the functionalisation process.

Two different approaches are used to functionalise GO with tyrosine. The first involves the covalent attachment of tyrosine to GO upon reacting the α-amine group in tyrosine methyl ester with the carboxylic groups in GO followed by hydrolysis of the methyl ester to give the carboxylic acid. Although this involves a two-step process that is difficult to prepare a monomeric system, it will, however, produce GO functionalised with a thin layer of tyrosine with a fixed spacer. The second approach is an effort to simplify the synthesis and will directly react non-protected tyrosine (-NH_2 and COOH) with GO. This will produce a GO surface with an oligomeric system/thicker layer of tyrosine, as shown in Figure 77.

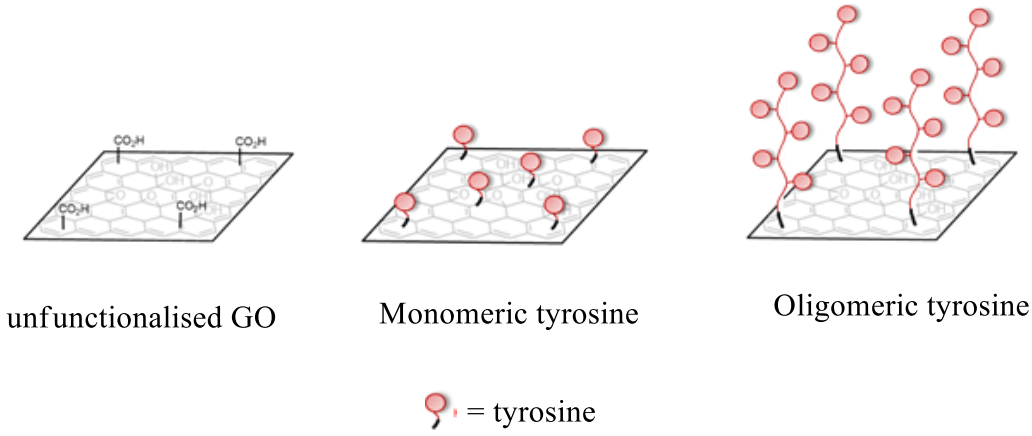

Figure 77: A schematic representation of the surface of GO attached to tyrosine in different ways.

We will investigate and compare of the effects of the two different surfaces on protein binding and inhibition. In addition, we will study a different aromatic amino acid, phenylalanine, which possesses the same structural flexibility as tyrosine and will allow us to measure the importance of selectivity on the hot spot area of α-chymotrypsin . These biofunctionalised nanomaterials will be prepared and characterised by FTIR, Elemental Analysis (EA), Thermogravimetric analysis (TGA), RAMAN Spectroscopy,

X-ray Photoelectron Spectroscopy (XPS), Scanning Electron Microscope (SEM) and X-ray Diffraction (XRD). Their potential to inhibit α-chymotrypsin using various substrate and GO concentrations will be used to determine K_m, K_i, V_{max} and α values, as well as to determine the mode of binding. As a further investigation, we will also examine the effects of protein binding on the structure and thermal stability of α-chymotrypsin using Circular Dichroism (CD).

4.2 Results and discussion

The initial aim was to synthesise GO from graphite. The physical and chemical properties of this receptor are well known, and the synthetic procedure is recognised [49] and making it a viable option for this study. However, a limitation of GO in dispersion agents and its bulk structure is that it is difficult to analyse by liquid phase NMR or any common measurement. Therefore, the analysis starts with FTIR and other material measurements that evaluate the structure and properties of materials.

4.2.1 Synthesis of unfunctionalised Graphene oxide (GO) 46

GO can be synthesised from the oxidation of graphite by various methods as reviewed in Brodie, Staudenmaier, and Hummers.[49] In 2010, the Tour method improved the Hummers' method by excluding the $NaNO_3$ from the reaction which makes the procedure safer as did not generate toxic gas. [100] Therefore, GO **46** was synthesised using a Tour method as illustrated in Scheme 25. Graphite powder **45** was added to the 9:1 mixture of cool concentrated H_2SO_4/H_3PO_4 and $KMnO_4$ was mixed (in droplets) to limit the potential hazards of exothermic reaction. The strong oxidising agent ($KMnO_4$ and H_2SO_4/H_3PO_4) was intercalated into graphite to yield GO **46** (Scheme 25).

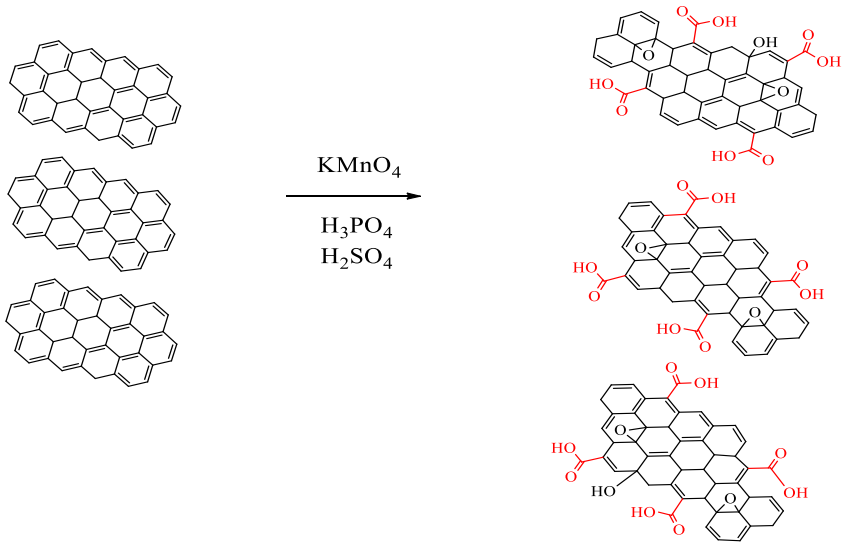

Graphite **45**

Graphene Oxide (GO) **46**

*Scheme 25: Schematic diagram to produce GO **46** sheets using the Tour method.* [100]

The structure of the GO **46** obtained was confirmed by comparing its characterisation data with published data.[100] The completion of the reaction was monitored using FTIR in Figure 78**.** No significant changes in the pure graphite observed and the indication of successful oxidation of the inert bulk carbon structure when their important functional group was visible. The broad peak was observed at 3400 cm^{-1}(OH), 1701cm^{-1} (C=O), 1200 cm^{-1} (C-OH), 1620 cm^{-1}(C=C) and 1050 cm^{-1} (skeletal C=O or C-C) corresponding to carboxylic and epoxy groups, confirming the presence of oxygen. [49,100-101]

(a)

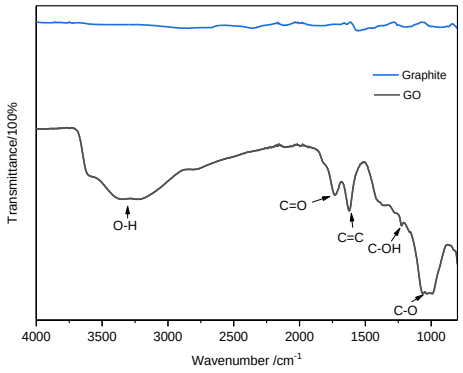

FTIR

(b)

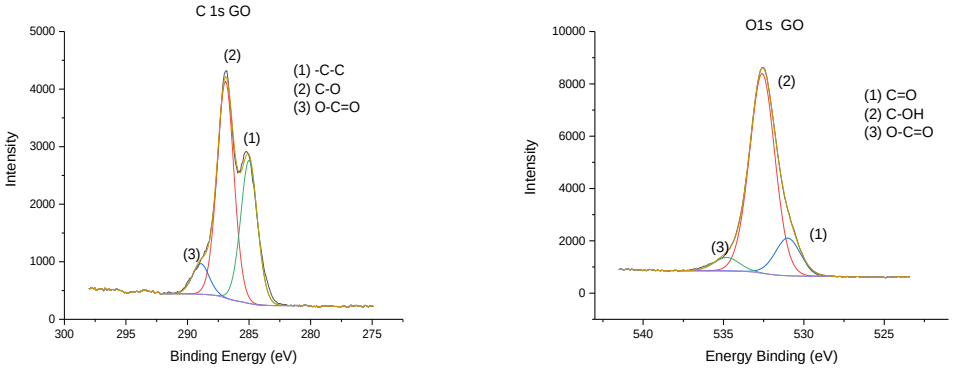

XPS (C 1s) **XPS (O 1s)**

*Figure 78: (a) FTIR spectra of graphite **45** and GO **46** and (b) The deconvoluted XPS spectra of the C1s and O1s of GO*

Nevertheless, the presence of oxidation in graphite also can be confirmed in C 1s XPS spectra. XPS was used to probe the electronic/bonding environment of various atoms. After deconvolution (Figure 78b), the spectrum of GO **46** shows three peaks at 285 eV, 286.99 eV , and 288.76 eV, corresponding to the carbon (sp^2), the epoxide, and the carboxyl, respectively. The O 1s peak binding energies were observed for C=O, C-OH and O-C=O group, at 531.0 eV , 532.59 eV and 534.80 eV respectively. [99-102].

RAMAN	SEM
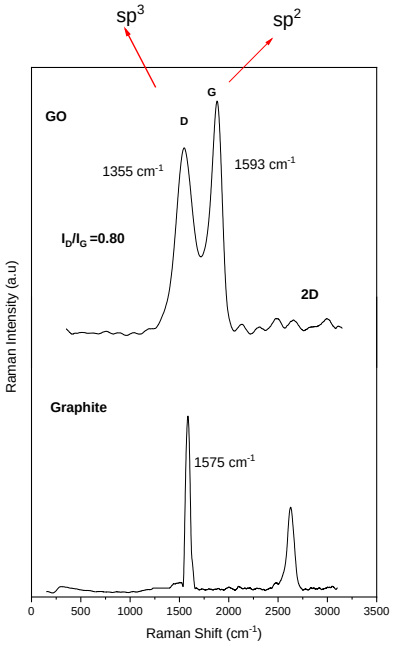	**Graphite** 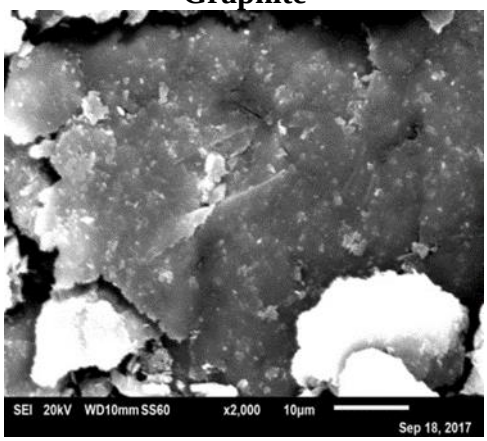 **GO** 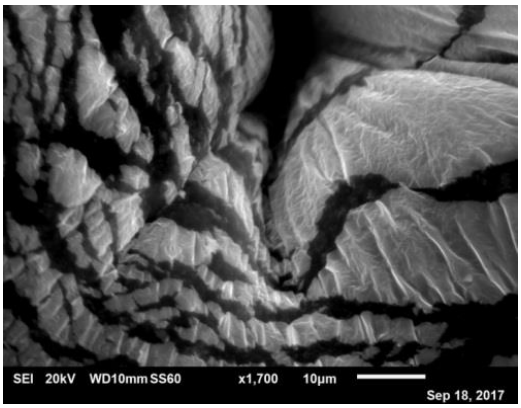

*Table 26: RAMAN spectra and SEM images of graphite **45** and GO **46***

RAMAN was used to identify the type of carbon on components and the band shape, (Table 26). The structure of GO **46** was confirmed by two strong peaks at 1355 cm^{-1} and 1593 cm^{-1}, corresponding to the D and G-bands. Graphite showed one sharp single peak at 1575cm^{-1}. The I_D/I_G of GO **46** is 0.80 indicated the sp^2 of a carbon bond was converted/modified to the sp^3-hybridized carbon on the surface of GO **46** due to the attachment of oxygen-containing functional groups. [103] The 2D band at 2500–3200 cm^{-1} can be observed broader and symmetrical, indicates the I_{2D}/I_G ratio shown a multilayer (with less than five layers) of GO **46** sheets formed. [104-105] This layers' presence has also been proven by X-ray diffraction (XRD) as a diffraction peak centred at 10° due to the a layer-to-layer distance attributed to inserted oxygen groups. [106]

4.2.2 Chemical functionalisation of GO

Having successfully synthesised GO, the next step was functionalisation with a monomeric and oligomeric layer of amino acid. As discussed, our aim is to study the effects of the two different surfaces upon functionalised GO. We need to confirm the structures synthesised (functional characteristics) are well characterised and desired functionalisation of GO is achieved.

4.2.3 Functionalisation GO using a monomeric system

The first method involved providing a monomeric tyrosine system on the surface of GO. The oligomeric system was synthesised by adding EDC and the methoxy ester of tyrosine to a suspension of the GO **46** in water and stirring for 24 hours at 70 °C to produce GO-Tyr (O_2Me) **47**. The process is illustrated schematically in Scheme 26. The completion of the reaction was confirmed by FTIR spectra, the carbonyl peaks at 1703 cm^{-1} observed and the OH groups broad peak was no longer visible. After isolation, the functionalised GO was resuspended in water and the ester group hydrolysed using potassium hydroxide. The experiment was conducted using ultrasonic oscillation for 2 hours to allow a multilayer of GO dispersed in water. A representation of the two-step procedure is shown in Scheme 26.

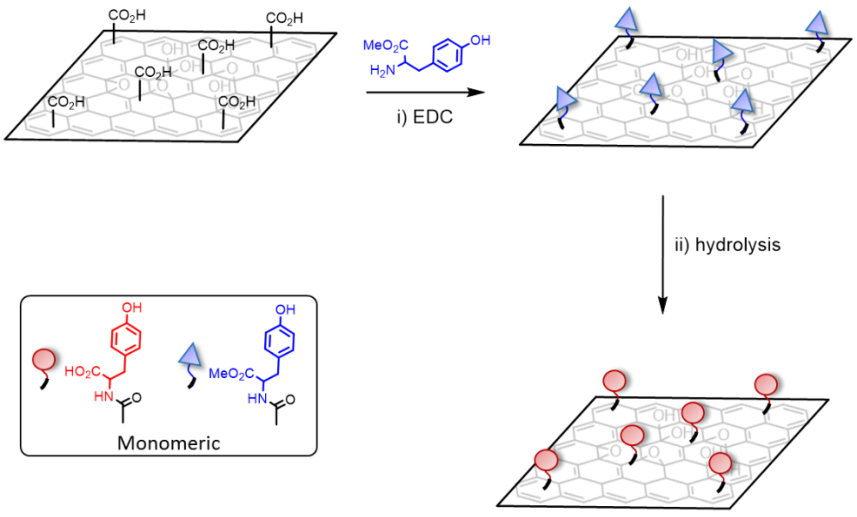

Scheme 26: Hydrolysis of GO methyl ester tyrosine to produce monomeric tyrosine (GO-Tyr Mono) ***47***

Subsequent to conversion into carboxylic acids, FTIR peak showed at 1703 cm^{-1} (C=O (carbonyl group), 1695 cm^{-1} (amide group) and 3032 cm^{-1} (OH group). The elemental analysis showed the percentage of carbon increased from 39.65% (unfunctionalised GO **46**) to 47.51% (Tyr-mono **48**) and no nitrogen was observed before functionalisation (same with XPS data). The RAMAN spectrum also confirmed the formation of multilayers of which showed broader and symmetrical in the 2D band as the comparison to the GO. As relative to the ratio of I_D/I_G, suggesting that the area of a layer containing moderate patches of tyrosine and a thin layer produced as the carbon sp^3 hybridized increased slightly from 0.80 to 0.86 nm.

4.2.4 Oligomeric method on the surface GO with tyrosine and Phenylalanine

As mentioned earlier, to simplify the preparation, we used non-protected tyrosine and phenylalanine ($-NH_2$). The aim to react directly carboxylate of GO with the amine. The oligomeric system was synthesised using the same initial step, except the non-protected of amino acids (L-tyrosine and L-phenylalanine respectively) were used instead. An excess of amino acid was added to produce amine-functionalised GO. The compound was sonicated in an ultrasonic bath during and after the reaction. This is because the ultrasound irradiation can cause the mechanochemical exfoliation of aggregated GO into multilayer GO sheets.

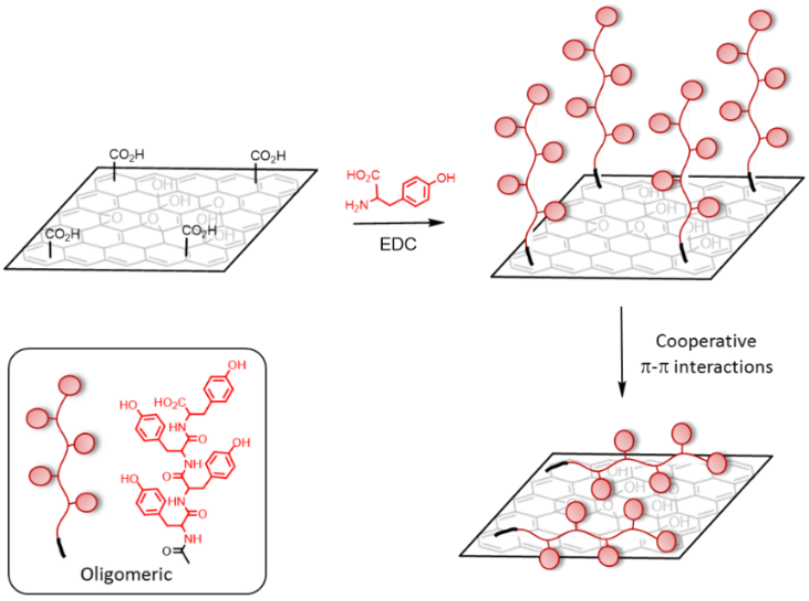

Scheme 27: Synthesis of oligomeric tyrosine and possible binding on the surface of GO.

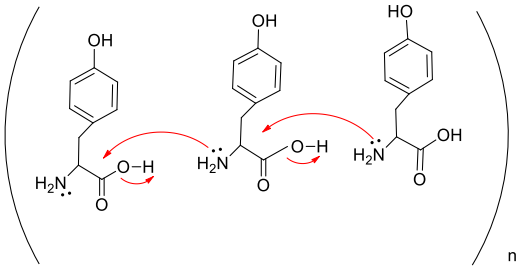

Scheme 28: Illustrated mechanism self-polymerisation of tyrosine that would be produced on the oligomeric system

However, using the excess of amino acid the possibility of self-polymerisation can occur as illustrated in Scheme 28. [20] Furthermore, we also considered the possibility that other pathways might be involved, such as epoxide-ring opening by terminal nucleophiles of tyrosine or acylation. [49, 99-102] These factors have been taken into consideration during structural characterisation studies. FTIR spectroscopy confirmed the efficacy of inserting amino acids on the surface of GO **46**. The peaks obtained for GO functionalised tyrosine and phenylalanine seems similar with their commercialised amino acid. Having successfully attached amine on the GO sheets, we analysed the composition elements of the compounds by elemental analysis and SEM-EDX. We knew these methods would provide different values due to the different surface and bulk chemical compositions of a sample; and also feature the method used. [36-39] Although not an appropriate tool alone for characterisation, therefore, we need to combine the information with other techniques. Nevertheless, the analyses are still reliable between the methods. The data confirmed the nitrogen was found after functionalisation and the nitrogen can only be derived from an amino acid in Table 27 .

ELEMENTAL ANALYSIS				
Compound	C (%)	H (%)	N (%)	C:N ratio
GO **46**	39.65	3.30	/	/
GO-Tyr (Oligo) **49**	47.51	3.55	2.87	1: 16
GO-Phe (Oligo) **50**	45.50	2.98	3.80	1:12
SEM-EDX				
Compound	C (%)	N (%)	O (%)	C:N ratio
GO **46**	52.87	/	47.13	/
GO-Tyr(Oligo) **49**	60.07	5.93	33.99	1:10
GO-Phe (Oligo) **50**	58.05	7.80	34.20	1:7

*Table 27: The elemental analysis and SEM-EDX data for GO, Oligomeric system, GO-Tyr **49** and GO-Phe **50** to identify the atomic ratio of C:N.*

Therefore, the surface of GO **46** has been functionalised as the amount of bound Tyr and Phe give reliable quantitative results. RAMAN spectrum (Figure 79) shows a comparison between the oligomeric system of tyrosine and phenylalanine. The data demonstrated that functionalisation of GO with phenylalanine shifted the G and D bands to 1591 and 1352 cm^{-1}, respectively. As expected, the D band of GO-Tyr (Oligo) **49** increased due to the functionality of tyrosine increased. The higher I_D/I_G ratio also indicated the bonding type of functionalised GO with tyrosine (1.02) was higher compared to GO-Phe **50** (0.93). This confirmed that the vibration sp^3-hybridized increased consequently to the more hydrophilic patches of tyrosine. This is also indicated that the compound was successfully attached with the oligomeric system, meaning more sp^3 bonds produced, due to the more covalently subunits of tyrosine bonding linked on the surface of GO.

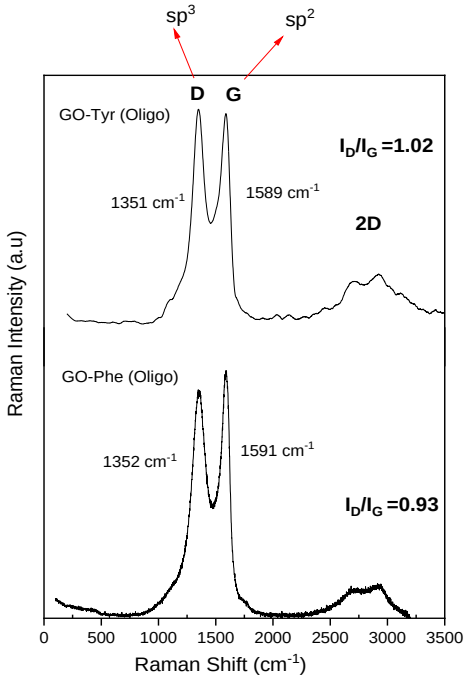

*Figure 79: RAMAN spectra of the oligomeric system of phenylalanine **50** and tyrosine **49***

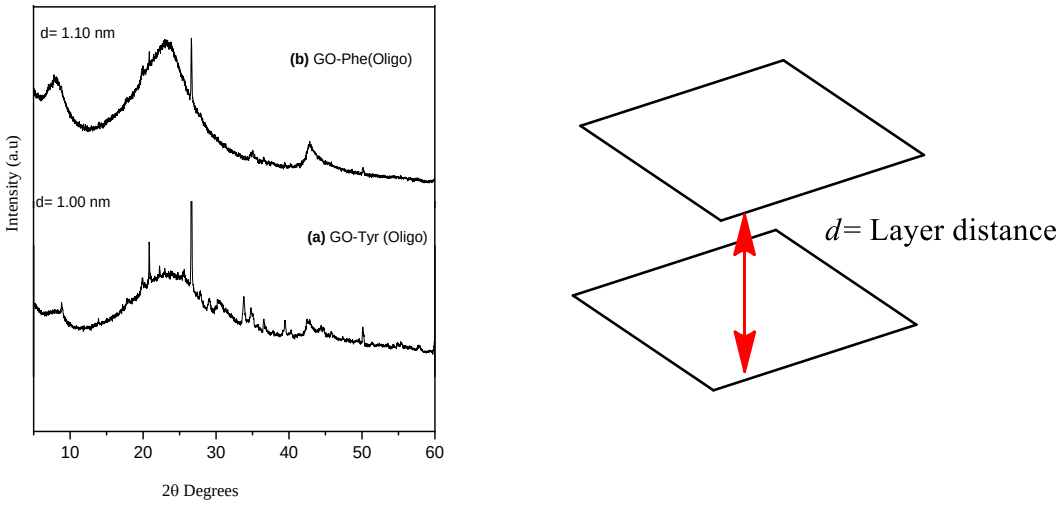

Figure 80: XRD patterns of functionalised of GO-Tyr (Oligo) ***49*** *and GO-Phe (Oligo)* ***50****.*

XRD spectra in Figure 80, showed the broad diffraction peaks at 26° because of inserted aromatic rings on the surface of GO **46**. [100] Chemical composition changes can be observed after functionalisation as the peak shifted from 10° to 8.78°. As we expected, d-spacing increased due to the oligomeric system inserted and produced the thicker layer. Furthermore, no a significant difference with oligomeric method in regards of the layer produced (1.0 nm for tyrosine and 1.1 nm of phenylalanine respectively). Therefore, we summarised that GO **46** samples were successfully functionalised with the flexibility of oligomeric amino acids for the entire volume.

4.2.5 Comparing Monomeric system and oligomeric system on the surface GO

Oligomeric and monomeric GO-Tyr was intensively studied in term of fixed and flexibility spacer produced on the surface of GO. This is important to compare their elements' content and the degree of amine, as we study the effect of these structures in the protein binding study. The elemental analysis and SEM-EDX were compared in Table 28. The carbon content increased from around 40% for GO **46**, to 45 and 48% for the monomeric **48** and oligomeric **49** systems respectively. This increase in carbon content with an increasing level of functionalisation is consistent with other reports. Elemental analysis also showed that nitrogen was present in both the monomeric and oligomeric systems, with a higher percentage observed for the oligomeric system (around 5.5 % and 3% for the oligo and monomeric systems respectively). On its own,

this does not necessarily indicate a higher level of functionalisation, as this is dependent on the relative amounts of the other elements present.

However, the carbon to nitrogen ratio can be used to assess qualitatively the relative levels of functionalisation. A lower ratio indicates a higher proportion of nitrogen, relative to the carbon content. The ratio for the two systems was 1:8 and 1:16 for the oligomeric and monomeric species respectively, confirming a higher level of functionalisation for the oligomeric system. SEM-EDX mapping of the GO **46** surface showed that only carbon and oxygen were present, whilst images for the monomeric and oligomeric samples also showed nitrogen in Figure 81. Furthermore, SEM-EDX analysis (Figure 81), indicated a carbon to nitrogen ratio of 1:4 for the oligomer and 1:10 for the monomer, which correlate reasonably well with elemental analysis. This data confirmed no impurities were involved in order to avoid undesired activity/reaction during protein binding study.

ELEMENTAL ANALYSIS				
Compound	C (%)	N (%)	H (%)	C:N ratio
GO **46**	39.65	/	3.30	/
GO-Tyr (Mono) **48**	45.11	5.49	4.18	1: 8
GO-Tyr(Oligo) **49**	47.51	2.87	3.55	1: 16
SEM-EDX				
Compound	C (%)	N (%)	O (%)	C:N ratio
GO **46**	52.87	/	47.13	/
GO-Tyr (Mono) **48**	58.40	16.82	24.77	1:4
GO-Tyr(Oligo) **49**	60.07	5.93	33.99	1:10

*Table 28 : The elemental analysis and SEM-EDX data for GO, GO-Tyr (Mono) **48** and GO-Tyr (Oligo) **49** to identify the atomic ratio of C:N.*

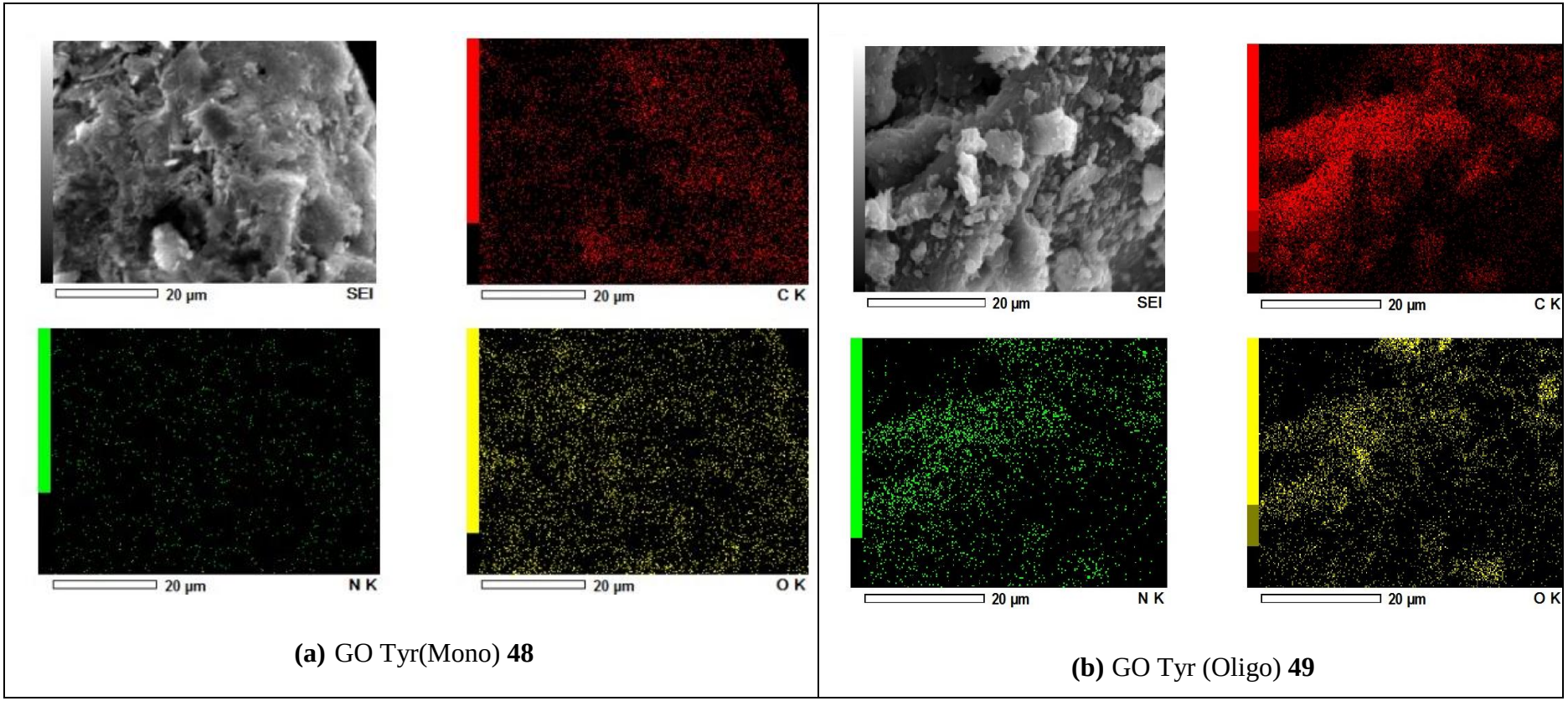

(a) GO Tyr(Mono) **48**

(b) GO Tyr (Oligo) **49**

*Figure 81: Quantitative SEM-EDX element mapping of GO-Tyr a) Mono **48** and (b) Oligo **49** of all elemental. The scale bar is 20 µm*

The N 1s XPS spectra showed two peaks, indicating two main bonding states of nitrogen (Figure 82). The first, at a binding energy of 400.35 eV, is attributed to the nitrogen in the amide bond, which form when the amino acid reacts with the carboxylates on the surface (or the growing oligomer). The second peak comes at 400.7 eV, and can be assigned to a nitrogen in an amine bond. [99,107] The ratio of amide and amine peaks in the oligomer is 1:0.33. However, more amine bonds appear to have formed in the monomeric system, where a ratio of 1:1.35 was observed. The disparity comes from the differences in the synthetic methods. During the synthesis of the oligomeric and monomeric systems, the N-terminus of the amino acid can react with the surface carboxylate groups to generate amides. The N-terminus can also react with the epoxides on the surface of GO, to give an amine and this is possible for both the oligomeric and monomeric synthesis. However, as a non-protected tyrosine is used in the oligomeric method, the N-terminus can also react with the C-terminus of another amino acid or a growing oligomer. Either will result in the formation of more amide bonds and fewer amines and this is the reason why the amide peak for the oligomeric system is much higher/more intense than the monomeric system.

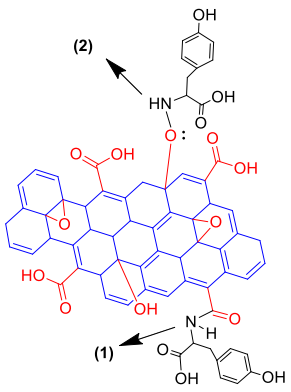

(a)

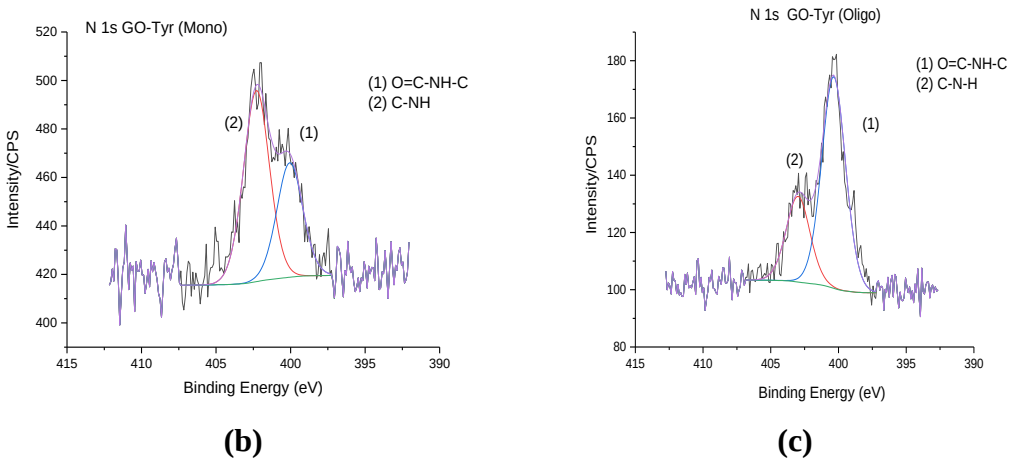

Figure 82: (a) Possible structure pathway functionalisation to present the deconvoluted of XPS spectra of the N1s of (b) GO-Tyr (Mono) ***48*** *and (c) GO-Tyr (Oligo)* ***49***

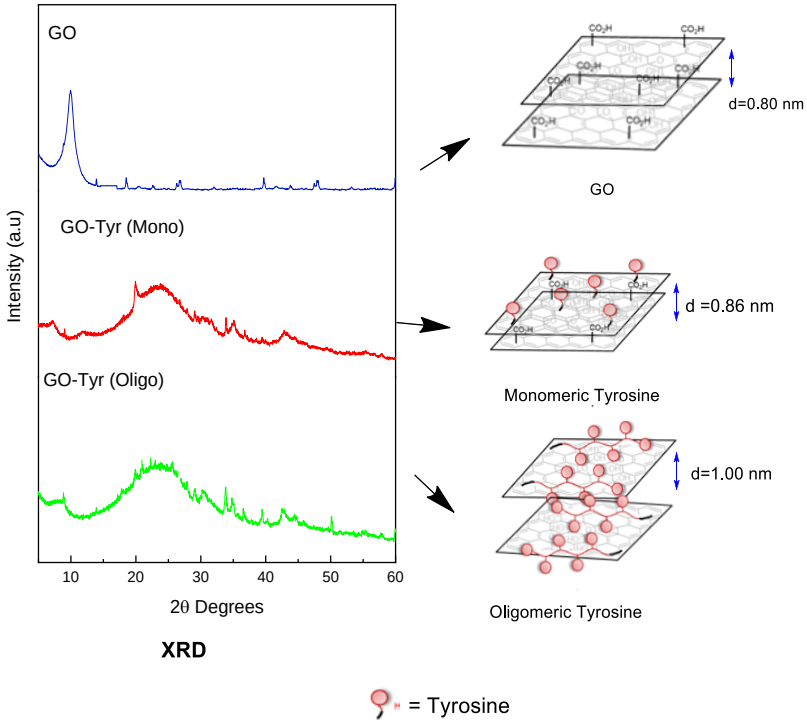

Figure 83: Interpretation of layer distance using XRD technique in functionalisation of GO

XRD showed that for the monomeric system was measured as 0.86 nm, which is slightly higher than the 0.80 nm recorded for GO **46**. This similarity is to be expected, as tyrosine is small and the aromatic functional group is probably lying flat on the surface and minimising the *d* spacing (as a result of π–π interactions). However, the *d* spacing for the oligomeric system was larger, at 1.00 nm, which is greater than either the GO, or the monomeric functionalised system. Again, this to be expected as the oligomeric system is longer/bigger and will take up more space on the surface. Although the aromatic rings can lay flat on the surface, it is not necessarily true that all of the aromatic rings will, or can lay flat. This is particularly true for longer oligomers, where it is likely that "kinks" or "bulges" may form on the surface, which would result in a higher *d* spacing (Figure 83).

TGA analysis (Figure 84) of GO **46** was similar to published data, [100] with decomposition taking place in three phases. Initially, around 25% weight loss occurred at 50–120°C, which was related to the loss of water. The second phase appeared from 120-440°C, which corresponded to the loss of oxygen-containing groups and accounted for around 30% weight loss. The final phase took place between 440 °C and 750 °C (when the measurement was stopped) and is due to the pyrolysis of oxygen and unstable carbons remaining in the structure to yield CO and CO_2.[100,108] The monomeric and oligomeric systems decomposed much faster with both showing an initial and fast degradation corresponding to loss of water. In the case of the monomer, this was followed by a fast decomposition from 100-600 °C (accounting for around 50% loss of weight). The oligomeric system was equally unstable, showing a continuous and fast decomposition from 120 °C to 450°C, which accounted for nearly 80% lost weight. For both systems, this was followed by a final pyrolysis stage from 600 °C to 750 °C. The faster degradation of the functionalised systems is a result of amino acid and oligomer degradation, which is reflected in the relative increases in weight loss.

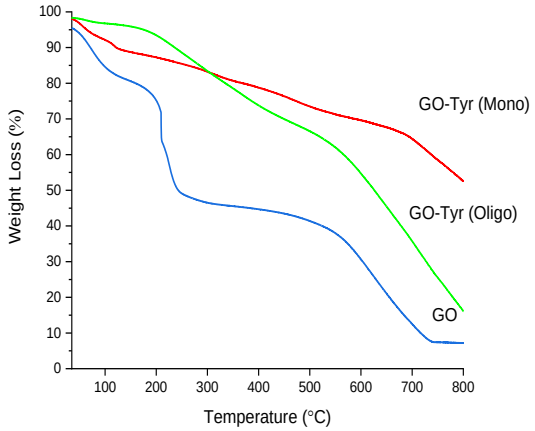

Figure 84: TGA curves of GO, GO-Tyr (Mono) ***48*** *and GO-Tyr (Oligo)* ***49****.*

We concluded that unfunctionalised GO **46**, GO-Tyr (Mono) **48** and GO-Tyr (Oligo) **49**, the carbon, oxygen, and nitrogen content increased significantly, the amount of sp^2 carbons decrease as effectively converted into sp^3 hybridized and the d-spacing layer increased respectively. This outcome indicated the functionalisation of GO with different spacer ability was achieved.

4.3 Using UV spectroscopy to assay Graphene Oxide inhibition of the enzyme *α*-Chymotrypsin

4.3.1 Unfunctionalised Graphene Oxide (GO)

Protein binding of the functionalised GO was assessed using an enzyme inhibition assay. The basic premise (with respect to protein binding) is based on the assumption that binding to the surface of an enzyme may prevent or reduce substrate access to the active site. This is particularly relevant for α-chymotrypsin, whose active site entrance is rich in positive charge.[109] We exploited this principle to demonstrate a size based relationship between dendrimers and protein binding.[35] De and Dravid also used the same premise to demonstrate how simple GO, which is rich in negative charge, could interact electrostatically with *α*-chymotrypsin.[31] However, electrostatics are not the only interactions involved in protein binding. The active site entrance of α-chymotrypsin also contains functionality capable of engaging in a number of other interactions (e.g. H-bonding, π–π, and hydrophobic interactions). [110] Therefore, addition of explicit functionality to the surface of GO should result in improved selectivity. To test this, we carried out the hydrolysis of the enzyme substrate N-benzoyl tyrosine p-nitroanilide (BTNA **26**), using *α*-chymotrypsin.

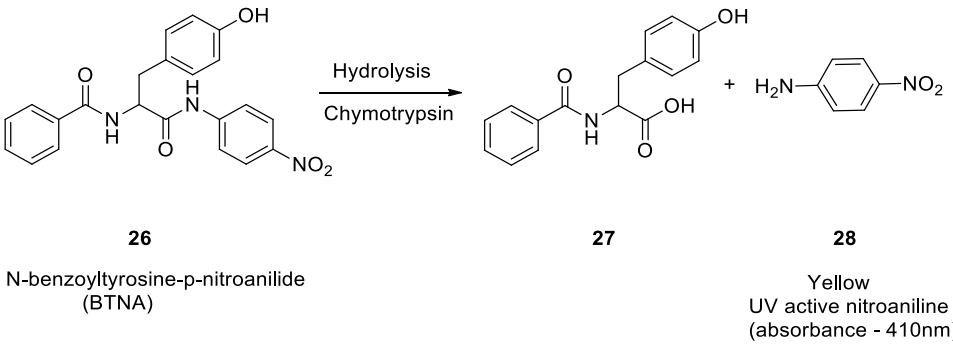

*Scheme 29: UV absorbent product from α-chymotrypsin enzyme catalysed hydrolysis of BTNA **26***

As mentioned before, upon hydrolysis BTNA **26** generates nitroaniline **28** that is yellow in colour (p-nitroaniline) and can be used to follow the hydrolysis over time, Scheme 29. Initial rates can then be determined from plots of nitroaniline **28** concentration versus time. Initially, a baseline/control was established for the activity of α-chymotrypsin in the absence of inhibitor, using BTNA **26** as the substrate. The reactions were carried out using 2.0 μM BTNA **26** and 0.4 μM α-chymotrypsin (pH = 7.46-phosphate buffer). For the control reaction, a typical reaction profile of nitroaniline **28** concentration (M) against time (s) was recorded in the absence of unfunctionalised GO **46** (Figure 85), and the rate or initial velocity (V) was calculated using linear regression over 2400 seconds (GraphPad Prism 7.03). [63]

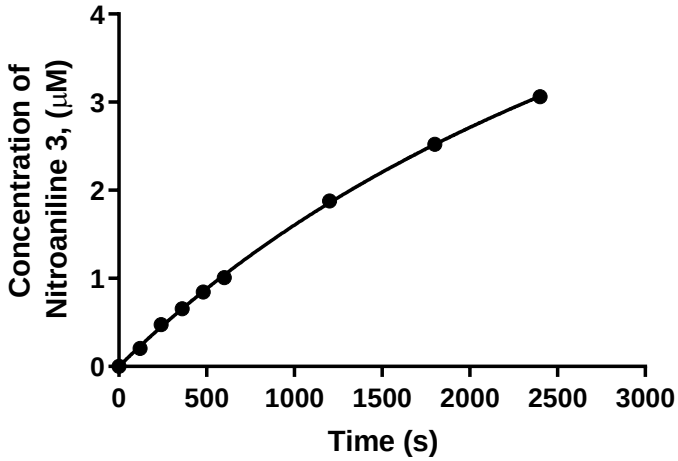

*Figure 85: Rate plots for the hydrolysis of 2 μM BTNA **26** (substrate) with the Chy (enzyme) at 1.0 μM without inhibitor called control reaction.*

Subsequently, the experiment was repeated in the presence of GO **46** (inhibitor). GO was initially added at a concentration of 0.06 μg/mL. This was prepared by pre-incubating Chy with GO **46** and the mixture was shaken for 24 hours prior to the assay. The reaction profiles show the initial velocity for the control (V_o) and for the experiments with added GO **46**. The reaction rates were 1.380×10^{-9} Ms^{-1} and 1.20×10^{-9} Ms^{-1}, respectively; thus, the presence of GO **46** decreases the reaction rate. The results obtained indicate that at a GO **46** concentration of 0.06 μg/mL, the reaction is inhibited by 13% as because of weak binding.

Therefore, it would be expected that higher levels of inhibition will be observed at a higher concentration of GO **46**. We decided to keep the final concentration of enzyme

and substrate at a ratio of 1:5 and enzyme concentration at 0.4 µM. The concentration of inhibitor was systematically increased from 0.06 to 0.12 µg/mL. It was observed the reaction rate inhibition increased from 13% to 23% when the concentration of inhibitor was doubled. Then, the experiment was carried out at inhibitor concentrations up to 0.24 µg/mL and 0.48 µg/mL. The data in Table 29 indicate that when concentration of GO **46** was increased, the initial velocity was reduced from 1.200 x 10^{-9} to 0.768 x 10^{-9} Ms^{-1} as a result of increasing binding from 13% to 44%.

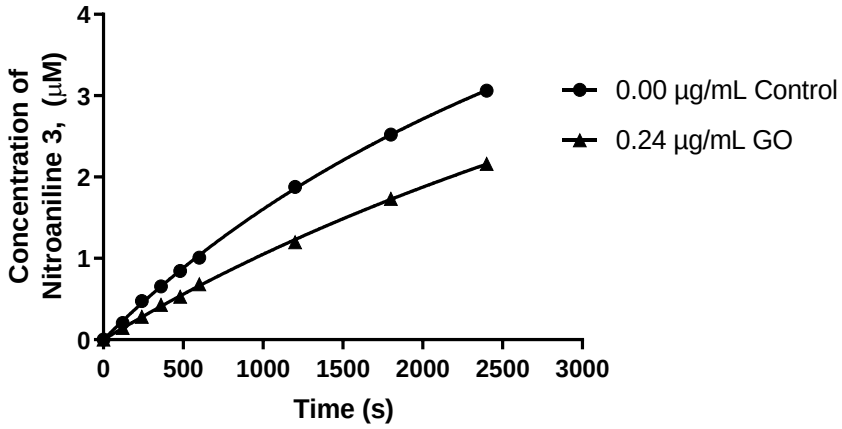

*Figure 86: Rate plots for the hydrolysis of 2 µM BTNA **26** (substrate) with the absence and presence of GO **46**.*

BTNA **26** [S], µM	Control 0.00 µg/mL GO **46**	0.06 µg/mL GO **46**	0.12 µg/mL GO **46**	0.24 µg/mL GO **46**	0.48 µg/mL GO **46**
	Initial velocity (V), nMs^{-1}				
2.0	1.380 (±0.571)	1.200 (± 0.502)	1.062 (±0.440)	0.948 (±0.0412)	0.768 (±0.0341)

*Table 29: Initial velocity data for the hydrolysis of 2.0 µM BTNA **26** (substrate) with the absence and presence of GO **46**.*

Therefore, we decided to use the five concentrations of GO **46** inhibitor shown in Table as our reference template. In further studies, the substrate concentration was increased to an enzyme: substrate ratio of 1:10 at an enzyme concentration of 0.4 µM. At this ratio, it was expected that the potential for collisions between enzyme and substrate would be increased, contributing to an increase in the rate of hydrolysis. This was confirmed by measuring the initial rates, which were 2.23 x 10^{-9} Ms^{-1} in the absence of GO **46** and which decreased gradually to 1.40 x 10^{-9} Ms^{-1} in the presence of GO **46** at the maximum concentration (0.48 µg/mL).

Enzyme: substrate ratios of 1:15 and 1:20 were selected for further experiments. These experiments were conducted at the same five concentrations of GO **46** (0, 0.06, 0.12, 0.24 and 0.48 µg/mL). For each of the GO **46** concentrations, the initial velocity data were obtained (Table 30). In all cases, the reaction profiles and initial velocities were reduced when compared to the reaction rate without GO **46** inhibitor. However, as the substrate concentration was increased, a minimal increase in the initial velocity was observed.

BTNA **26** [S], µM	Control 0.00 µg/mL GO **46**	0.06 µg/mL GO **46**	0.12 µg/mL GO **46**	0.24 µg/mL GO **46**	0.48 µg/mL GO **46**
	Initial velocity (V), nMs^{-1}				
2.0	1.380 (±0.571)	1.200 (± 0.502)	1.062 (±0.440)	0.948 (±0.0412)	0.768 (±0.0341)
4.0	2.230 (±0.872)	2.098 (±0.832)	1.890 (±0.770)	1.687 (±0.681)	1.400 (±0.650)
6.0	2.780 (±0.109)	2.580 (±0.902)	2.380 (±0.962)	2.100 (±0.863)	1.800 (±0.781)
8.0	3.240 (±0.217)	3.870 (±0.117)	2.700 (±0.110)	2.410 (±0.101)	2.119 (±0.803)

*Table 30: The summary of initial velocity data in the absence and presence of unfunctionalised GO **46**. Chy at 0.4 µM*

Then the data obtained was plotting in Mixed model inhibition using GraphPad Prism 7.03, Table 30 the data was fitted to Equation 1, which is the general rate equation that describes enzymatic reactions in the presence of an inhibitor (*as previously described in section 2.2.7, page 54*). In addition, the important α parameter can also be obtained with this model and is informative with respect to the mechanism of inhibition as shown in Scheme 30. [64]

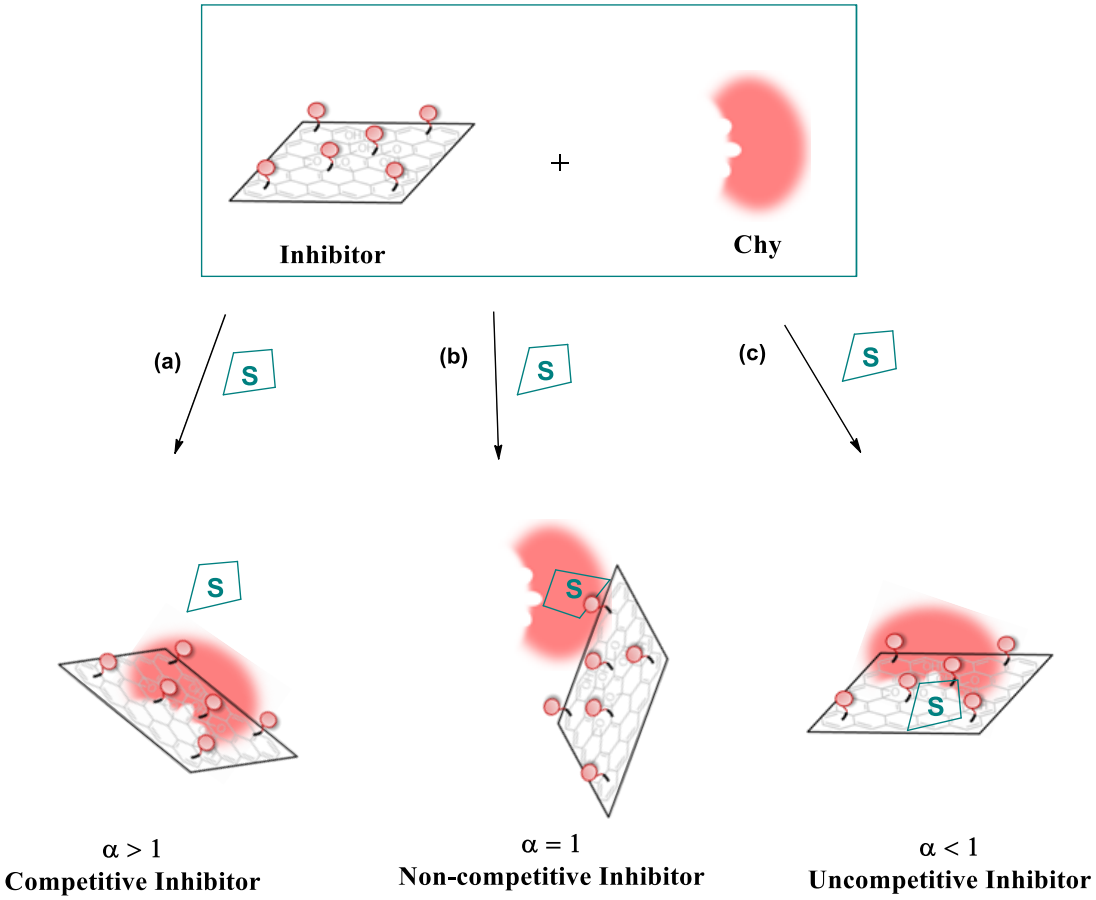

Scheme 30: The degree of inhibition (α) with respect to the mechanism inhibition, a) When α > 1, the inhibitor and substrate compete for the enzyme, this condition is referred to as competitive inhibition b) when α =1 is the condition in which the substrate binding to the enzyme is unaffected by the inhibitor called non-competitive inhibition, c) When α < 1, the inhibitor binds to the enzyme-substrate(ES) complex preventing formation of product corresponds to uncompetitive inhibitor.

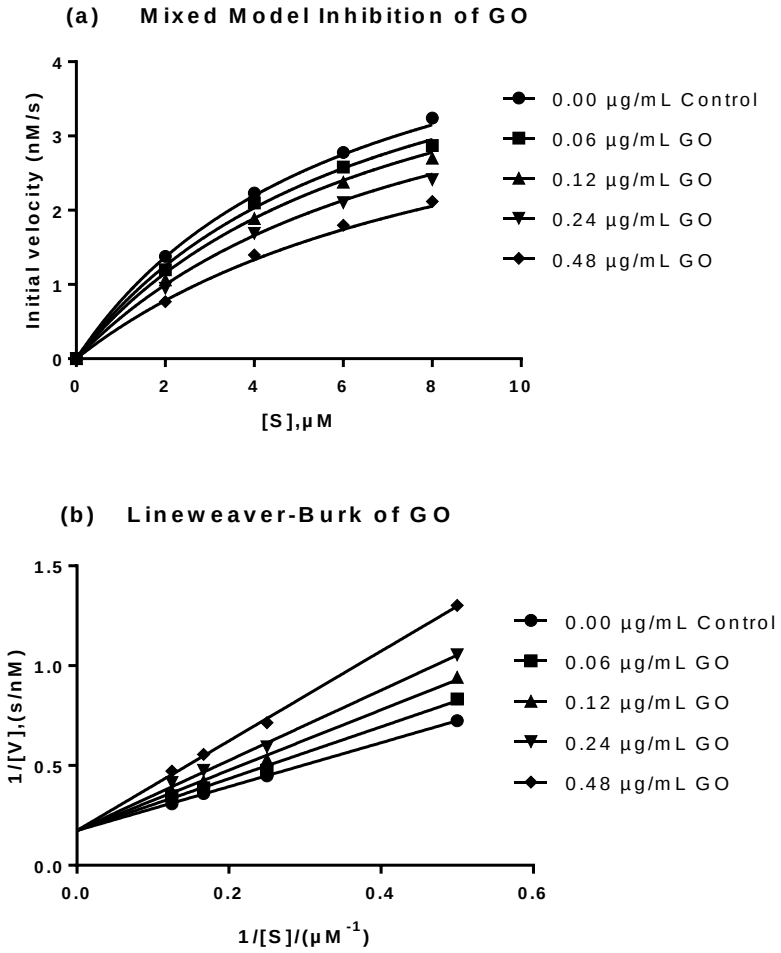

Figure 87: The mixed model inhibition of graphene oxide (GO) ***46*** *transformed into a Lineweaver-Burk plot and demonstrating a common y-intercept*

GO system / Kinetic inhibition data	Unfunctionalised GO **46**
V_{max}, nMs^{-1}	6.00 (± 0.050)
Alpha, α	3.74 (± 0.044)
K_i, µg/mL	0.53 (±0.004)
K_m, µM	6.13 (±0.013)

Table 31: Summary of kinetic parameters obtained from a linear fit of data for the unfunctionalised GO ***46****.*

The values of V_{max}, K_m, and K_i, as best-fit values from the GO **46** data set (Figure 87), are summarised in Table 31. The V_{max} obtained when it reached maximum velocity is 6.0 nMs^{-1} and the K_m of 6.13 μM is the concentration where the enzyme and the substrate bind. The α value is 3.74, which indicates a competitive inhibitor (more than 1). The results from the Lineweaver-Burk plot also show a competitive inhibitor as the same y-intercept was obtained for all GO concentrations. This indicates that the inhibitor can compete with the substrate in order to bind at the surface of the enzyme. The K_i value is 0.53 μg/mL which is provides information regarding the concentration of inhibitor needed to inhibit Chy's surface. Therefore, this value can be used as a reference to compare with functionalised GO.

The results from this study demonstrate that GO is a competitive inhibitor which agrees with De;[31] however, the actual value of α and K_i obtained were different; in their study, α is 3.94 and K_i is 2.71 μg/mL. For this reason, it was essential to study our GO first before comparing the effect of functionalised GO. As mentioned earlier, the different values of α and K_i obtained in our study vs that of De may be attributed to the use of a different substrate or variation in the GO preparation method used**.** Nevertheless, the important K_i value was obtained, and this is needed for studying binding affinity. Thus, the smaller value of K_i means that a smaller amount of inhibitor is needed in order to inhibit the activity of Chy. With this information, we can compare directly which inhibitors are better than others.

4.3.2 Inhibition using GO functionalised with oligomeric systems

As previously mentioned, the simplest method for preparing functionalised GO is to react it with non-protected amino acids. Attention was focused on preparing the aromatic amino acids, tyrosine and phenylalanine. These possess a similar flexibility and a thick layer. A simple kinetic assay was carried out in order to study the importance of functionality. The experiments were repeated using an enzyme: substrate ratio of 1:5 and a concentration of 0.48 μg/mL in an oligomeric system with tyrosine and phenylalanine.

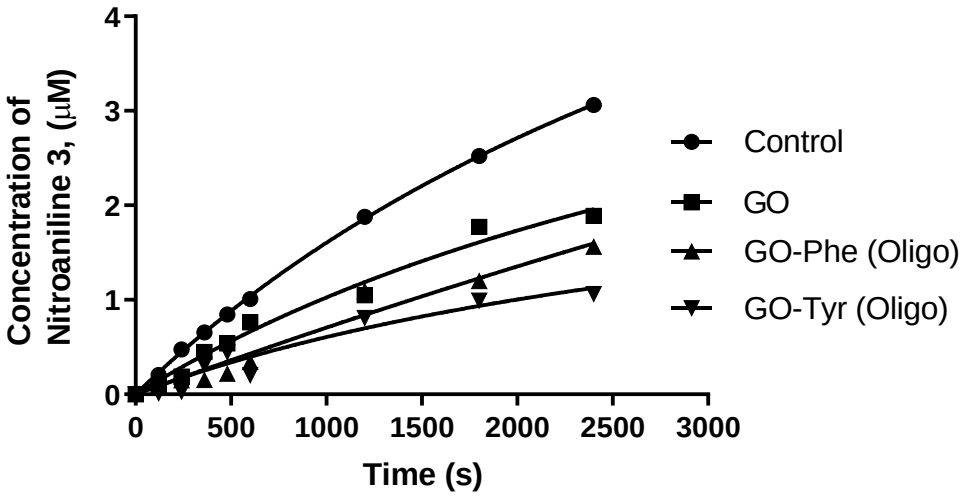

Figure 88: Rate plots to hydrolyse 8 μM of substrate (BTNA) at 0.48 μg/mL of GO and Oligomeric GO. Chy at 0.4 μM

The data shown in Figure 88 illustrate the hydrolysis performance both in the absence and presence of functionalised GO. It is apparent that the functionalised GO binds better because it inhibits the rate of hydrolysis of BTNA **26** better than simple GO **46**. GO-Tyr (Oligo) **49** and GO-Phe (Oligo) **50** both provide additional π-π interactions which is why these may bind and inhibit better than GO. However, GO-Tyr (Oligo) **49** performs best due to the additional hydrogen bonding provided by the phenolic OH, which can interact with the residues around entrance to the enzyme active site. This additional interaction contributes to the better stability of the GO complex as compared with GO-Phe. This inhibitor sits at the active site entrance and blocks the approach of BTNA **26**. As a result, the highest affinity between GO inhibitor and Chy results in the most effective inhibition. This explains why GO-Tyr is the most effective inhibitor in this study.

This simple study demonstrated that the oligomeric system and tyrosine are most effective at binding with the Chy enzyme. Therefore, the next goal was compared the oligomeric and monomeric systems of tyrosine. Both methods (oligomeric and monomeric) present advantages and disadvantages and more research would be required to verify which was best. Therefore, the experiment was carried out with the same measurements used for unfunctionalised GO **46** (*refer section 4.3.1*). The results in Table 32 and Lineweaver Burk Plot (Figure 89) were obtained to study the mode of inhibition of GO-Tyr (Oligo) **49**. The typical binding profile for the mode of inhibition

was observed and a common y-intercept in the Lineweaver Burk Plot showed that GO-Tyr (Oligo) **49** is a competitive inhibitor.

BTNA **26** [S],µM	Control 0.00 µg/mL GO-Tyr (Oligo) **49**	0.06 µg/mL GO-Tyr (Oligo) **49**	0.12 µg/mL GO-Tyr (Oligo) **49**	0.24 µg/mL GO-Tyr (Oligo) **49**	0.48 µg/mL GO-Tyr (Oligo) **49**
	Initial velocity (V), nMs^{-1}				
2.0	1.380 (±0.571)	1.150 (±0.48)	0.877 (±0.043)	0.770 (±0.041)	0.620 (±0.012)
4.0	2.230 (±0.872)	1.940 (±0.760)	1.743 (±0.680)	1.480 (±0.620)	1.120 (±0.500)
6.0	2.780 (±0.109)	2.320 (±0.970)	2.210 (±0.930)	1.870 (±0.750)	1.408 (±0.650)
8.0	3.240 (±0.217)	2.755 (±0.113)	2.420 (±0.108)	2.170 (±0.101)	1.730 (±0.42)

*Table 32: The summary of initial velocity data in the absence and presence of oligomeric tyrosine system (GO-Tyr) **49**. Chy at 0.4µM.*

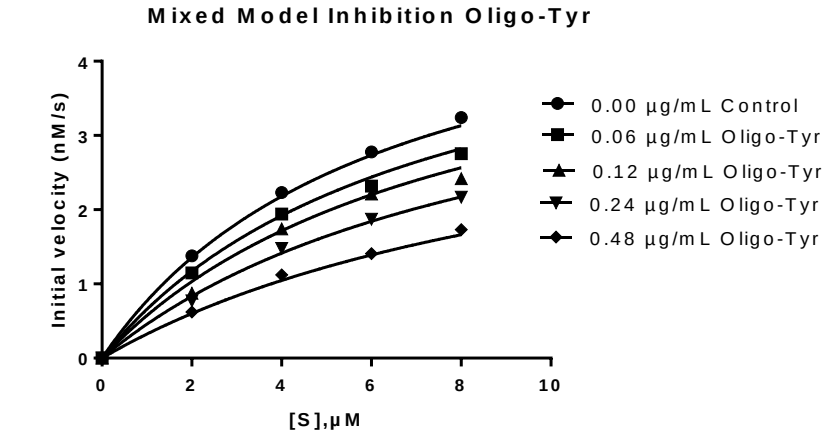

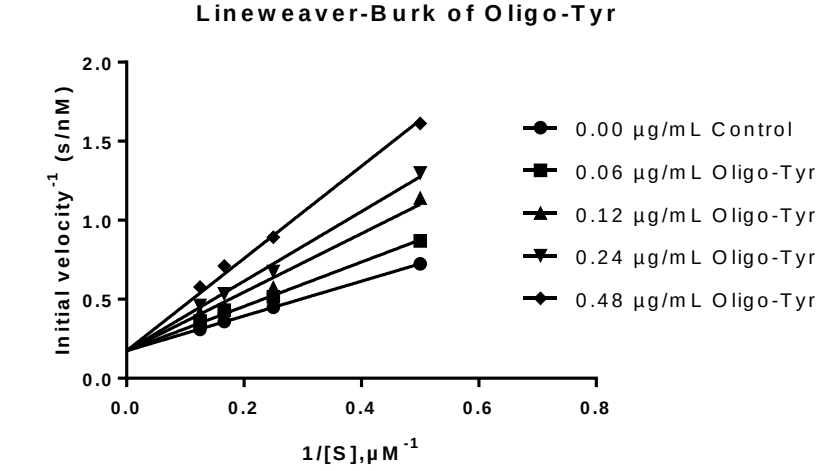

*Figure 89: Mixed mode inhibition and Lineweaver-Burk plots for GO-Tyr (Oligo) **49***

4.3.3 Inhibition using GO functionalised with a monomeric tyrosine

This system examines whether or not a single layer of tyrosine is able to bind to Chy better than the oligomeric systems or unfunctionalised GO **46**. Analogous measurements to those use for the unfunctionalised GO **46** were used. This permitted investigation of which layer demonstrates the most effective inhibition before and after functionalisation. Table 33 shows the data for experiments with various substrate and GO-Tyr concentrations. The Lineweaver-Burk plot (Figure 90) shows that a common y-intercept was obtained, indicating competetive inhibition. The value of α = 4.84, and K_i was reduced to 0.14 µg/mL after functionalisation as shown Table 34. The results indicate that of GO-Tyr (Mono) **48**, has a greater binding affinity to inhibit the activity of Chy when compared to unfunctionalised GO **46**. It can be assumed that the lack of movement for monomeric tyrosine leads to stronger binding to Chy. Moreover, monomeric tyrosine may enhance the hydrophobic interactions further between the enzyme and GO **46** (less steric crowding). As a result, GO-Tyr (mono) **48** possesses greater inhibitory activity when compared with unfunctionalised GO **46** or the oligomeric GO system **49**.

BTNA **26** [S], µM	Control 0.00 µg/mL GO-Tyr (Mono) **48**	0.06 µg/mL GO-Tyr (Mono) **48**	0.12 µg/mL GO-Tyr (Mono) **48**	0.24 µg/mL GO-Tyr (Mono) **48**	0.48 µg/mL GO-Tyr (Mono) **48**
	Initial velocity (V), nMs^{-1}				
2.0	1.380 (±0.571)	1.071 (±0.48)	0.759 (±0.42)	0.510 (±0.039)	0.368 (±0.029)
4.0	2.230 (±0.872)	1.740 (±0.78)	1.443 (±0.70)	0.960 (±0.062)	0.708 (±0.050)
6.0	2.780 (±0.109)	2.160 (±0.970)	1.822 (±0.890)	1.270 (±0.810)	0.968 (±0.066)
8.0	3.240 (±0.217)	2.650 (±0.121)	2.110 (±0.113)	1.560 (±0.94)	1.165 (±0.25)

*Table 33: The summary of initial velocity data in the absence (Chy only) and presence of monomeric tyrosine system (GO-Tyr Mono) **48**.*

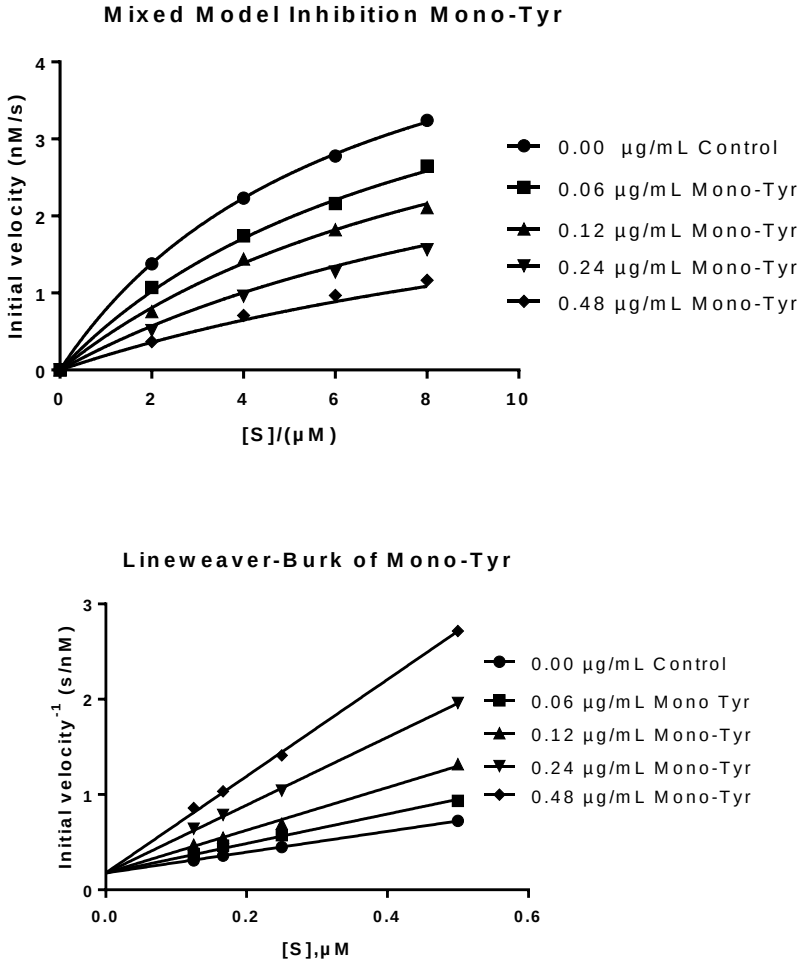

Figure 90: Mixed mode inhibition and Lineweaver-Burk plots for GO-Tyr (Mono) ***48****. Chy at 0.4 µM.*

GO system / Kinetic inhibition data	Unfunctionalised GO **46**	Functionalised GO GO-Tyr (Mono) **48**
V_{max} , nMs^{-1}	6.00 (± 0.050)	6.00 (±0.033)
Alpha, α	3.74 (± 0.044)	4.84 (±0.012)
K_i , µg/mL	0.53 (±0.004)	0.14 (±0.011)
K_m , µM	6.13 (±0.013)	6.36(±0.022)

Table 34: Summary of kinetic parameters obtained from a linear fit of data for unfunctionalised GO ***46*** *and GO-Tyr (Mono)* ***48.***

4.3.4 Comparison of monomeric and oligomeric Tyrosine systems at the surface of GO

In the previous section we discussed the inhibition properties of the oligo and monomeric GO-Tyr systems. In general terms, both of these systems have advantages and disadvantages (flexibility-cooperativity, mobility etc.). However, deciding which is best based on a single data set (GO-Tyr) is not possible, and more research needs to be carried out. Nevertheless, it is still useful to compare the systems directly (Figure 91) at maximum concentration of substrate and inhibitor, 8.0 µM and 0.48 µg/mL respectively. These concentrations were selected due to the anticipation that the strongest binding can be observed. As can be seen, the typical profile was obtained and a decreased rate of reaction for the monomeric system suggests that it is better than the oligomeric system.

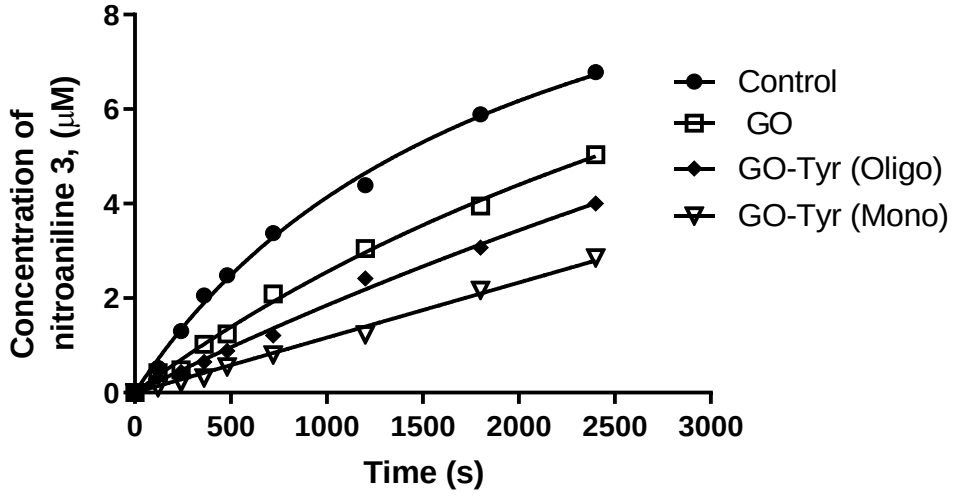

Figure 91: Rate plots for the hydrolysis at 8.0 µM of BTNA 26 and 0.48 µg/mL of inhibitor

The data in Table 35 summarises the results and shows the important parameters for both systems. The V_{max} obtained for the systems (unfunctionalised GO **46** and functionalised GO) showed the same V_{max} (unchanged) at 6.00 nMs^{-1}, and the K_m value gradually increased from 6.13 µM for unfunctionalised to 6.22 µM GO-Tyr (Oligo) **49** and 6.36 µM of GO-Tyr (Mono) **48** as a result of weaker binding between the BTNA **26** and the Chy. Here, we can conclude from α values, Lineweaver-Burk plots and other information (V_{max} unchanged and K_m increased) that in all of the system studied the GO **46** and functionalised GO inhibitors demonstrate competitive inhibition. It also can be

observed that the α value increased from 3.74 for unfunctionalised GO **46**, to 4.08 for GO-Tyr (Oligo) **49** and further increased to 4.84 for GO-Tyr (Mono) **48**.

GO system / Kinetic inhibition data	Unfunctionalised	Functionalised	
	GO **46**	GO-Tyr (Oligo) **49**	GO-Tyr (Mono) **48**
V_{max} , nMs^{-1}	6.00 (±0.050)	6.00 (±0.014)	6.00 (±0.033)
Alpha, α	3.74 (±0.044)	4.08 (±0.008)	4.84 (±0.012)
K_i , µg/mL	0.53 (±0.004)	0.31 (±0.016)	0.14 (±0.011)
K_m , µM	6.13 (±0.013)	6.22 (±0.017)	6.36(±0.022)

*Table 35: Summary of kinetic parameters obtained from a linear fit of data for unfunctionalised GO **46**, functionalised GO-Tyr (Oligo)**49** and GO-Tyr (Mono) **48**.*

Also, Table 35 demonstrates that when GO-tyr mono or oligo is bound to the enzyme, K_i decreases from the original K_i for the unfunctionalised GO, which confirms that functionalised GO can exhibit different enzyme binding and inhibition activity. The K_i value of 0.14 µg/ml obtained with the monomeric system is lower than the oligomeric system, despite the fact that oligomeric structure provides a flexible spacer. (Figure 92).

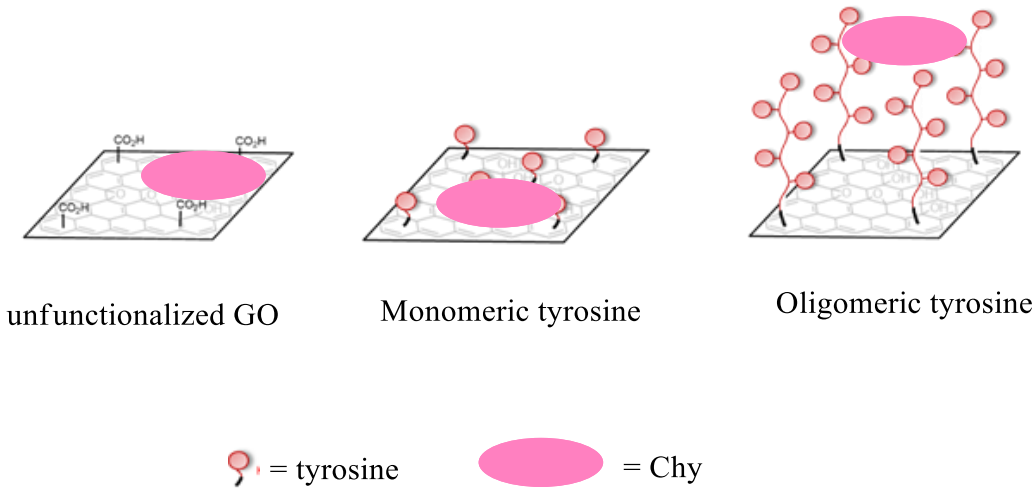

Figure 92: Illustration of the binding relationship between GO, monomeric and oligomeric of tyrosine with Chy

Therefore, it could be predicted that the oligomeric structure is flexible with a high degree of freedom to move and this may facilitate strong binding and the ability to bind to any sites on the protein. In contrast, the monomeric system produced does not have a spacer and its lack of movement and flexibility could limit binding. However, this rigid structure could also provide selectivity (due the fixed position of the amino acid functionality). In addition, there may be space on the surface of GO that is free from the

steric effects involved in the oligomeric system and that allows additional hydrophobic interaction. Although interactions with the monomeric amino acids may be weaker than those of the oligomer, the possibility of additional hydrophobic binding may provide a reason for the enhanced binding observed for the monomer.

Another explanation could be that the oligomeric system can interact with the GO surface in a cooperative way (π-π stacking from the aromatic groups). If this occurs, then it may make it difficult for a protein to compete with these interactions. This could be another explanation for why the monomeric system binds best. A final explanation is that the two systems can interact with the protein in a way that alters its structure or even denatures the protein. If the oligomeric system does this to a greater extent, then its binding to the protein will be weaker.

4.3.5 Effect of binding on Chy structure over time and temperature

Previous research has demonstrated that unfunctionalised GO **46** has no effect on the structure of bound Chy. Although some denaturation was observed over time, this was attributed to the protein aging in solution, as opposed to a direct consequence of complexation with GO. [31] However, to confirm these findings with the functionalised GO used in this study, the same experiments were repeated and studied using Circular Dichroism (CD). By comparing the spectra of only native Chy solution with the Chy/GO complex solution, any structural differences could be identified.

Experiments were carried out after a 1 hour incubation and concentrations of 0.4 μM and 0.48 μg/mL for the protein and GO systems respectively. All measurements were carried out at 37°C and at pH 7.35. The spectra obtained, which are shown in Figure 93, unfunctionalised and functionalised GO have no characteristic peaks. Furthermore, clearly show that none of the GO systems have an effect on the spectra, and therefore no effect on the structure of the protein. The experiments were repeated after 24 and 36 hours, and no changes in the spectra were observed. Therefore, the GO systems inhibit enzymatic activity without denaturing the protein. This means that the GO sheets can adapt their structure sufficiently to match the surface curvature of the protein. [111] As well as monitoring the structures over time, we also studied the effect of heat on the structure of Chy in the presence and absence of the GO. Experiments were performed at the same concentrations and pH. The samples were heated up and the intensity of the peak at 230 nm was monitored with respect to temperature. The results in Figure 94 indicated no differences in extent of denaturation with respect to temperature, generating similar plots. Therefore, binding of the GO systems do not destabilise or stabilise the protein structures.

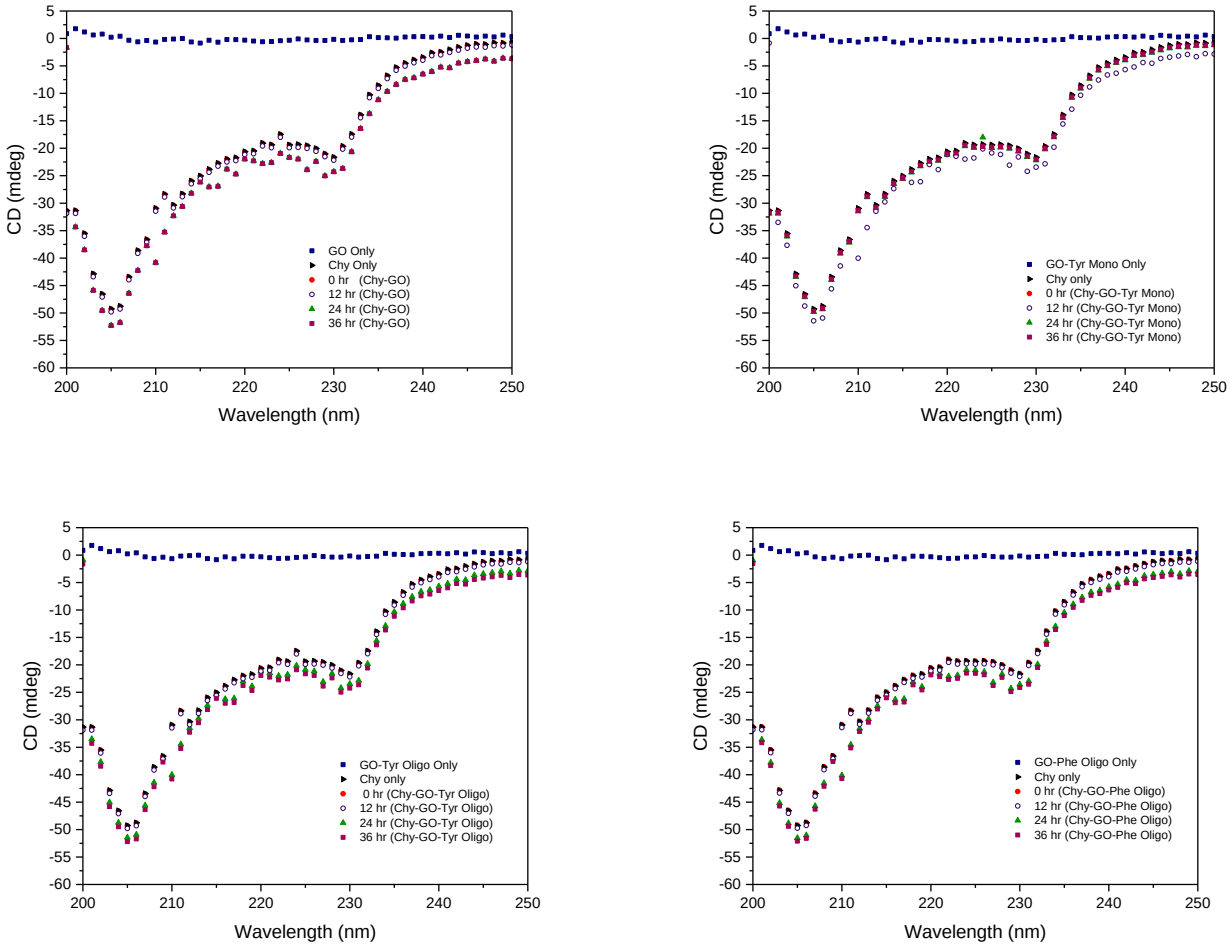

*Figure 93: CD spectra of Chy(0.4 μM) with GO **46** and functionalised GO **48-50** (0.48 μg/mL) over time*

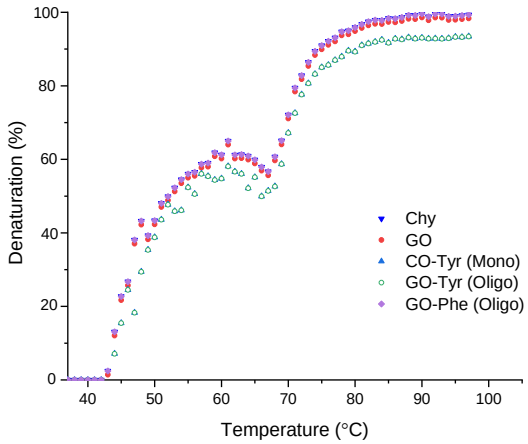

Figure 94: Temperature profiles of percentage denaturation of Chy alone and when bound to unfunctionalised or functionalised GO at 230 nm.

4.4 Conclusions

Although we knew that graphene oxide could bind strongly to the surface of proteins, we wanted to determine if a functionalised GO could bind proteins more strongly than a corresponding unfunctionalised GO. As well as improving binding, it may be possible (in the future) to introduce selectivity via functionalisation. The functionality selected for our initial study, was the amino acid tyrosine. Tyrosine is one of the few amino acids known to be important with respect to protein-protein binding and protein-surface binding. As well as determining how a specific functional group may influence binding, we also wanted to know if the extent of functionalisation (in regards of surface thickness and any spacer effect provided by the oligomer) was an important parameter with respect to protein binding. As such, we successfully synthesised graphene oxide with an oligomeric layer of tyrosine using non-protected tyrosine and an EDC coupling methodology and a single synthetic step. A monomeric functionalised graphene oxide was also synthesised using a slight variation of the same method. The process involved two steps, the first of which involved the same EDC mediated addition of C-protected tyrosine. A second step hydrolysed and removed the protecting group to yield GO with a monomeric layer of tyrosine. All of the GO systems were able to inhibit the function of chymotrypsin.

Kinetic analysis indicated that the monomeric system inhibited the best and therefore bound the strongest, with a K_i value of 0.14 μg/mL. This is almost 4 times better than GO alone (K_i 0.53 μg/mL) and double the affinity of the oligomeric functionalised GO (K_i 0.31 μg/mL). In addition, the kinetic analysis confirmed all systems bound and inhibited chymotrypsin via the same competitive binding mechanism. As such, any differences in binding affinity/inhibition are not related to differences in the mode or mechanism of binding. When analysing the reasons for the differences in binding, we conclude that the oligomeric system binds and inhibits less well (than the monomeric functionalised GO), due to unfavourable interactions between the aromatic units of the oligomeric chain and the graphene oxide surface. Consequently, protein binding is in competition with this strong intramolecular binding and must be overcome before the amino acids can bind cooperatively to the protein surface.

Although the same intramolecular interactions occur for the monomeric system, they are monomolecular and not cooperative. As a result, the intramolecular interaction between the amino acids and GO are much weaker and can be easily broken by the protein when it binds to the amino acids using stronger intermolecular cooperative interactions. Therefore, when designing GO based systems for protein or polyvalent binding, it is important to take into account any intramolecular cooperative effects, that will weaken any intermolecular interactions. Overall, we have demonstrated that functionalised GO can bind to chymotrypsin with high affinity and this affinity can be moderated by the level of oligomerisation. In an effort to obtain new protein ligands and enzyme inhibitors that are more selective with respect to their binding, we are currently exploiting the methodology and results to design and construct new GO inhibitors.

4.5 Experimental

4.5.1 Instrumentation

RAMAN spectrometer
Raman spectra of samples were recorded from 500 to 3500 cm^{-1} on a Renishaw inVia Raman Microscope using a green laser operating at wavelength of 514.5 nm and laser power at 20 mV.

X-ray photoelectron spectrometer (XPS)
X-ray photoelectron spectroscopy measurements were performed using monochromatic Al-kα radiation (hν = 1486.69 eV). CasaXPS v 2.3.16 software was used to record curve fitting and to calculate the atomic concentrations.

Thermogravimetric analysis (TGA)
Thermogravimetric Analysis (TGA) were performed using a Perkin Elmer Pyris in the range of 25°C - 800°C. and analysed using origin software.

X-ray diffractometer (XRD)
XRD patterns were collected using a Bruker, D8 Advanced diffractometer with a copper target at the wave length of λ CuKα = 1.54178 Å and a tube voltage of 40 kV and tube current of 35 mA, in the range of 5–100° at the speed of 0.05°/min

Elemental Analysis (EA)
The elements analysed using a Vario MICRO Cube CHN/S analyser and solid samples were used.

Scanning Electron Microscope (SEM)
The samples were analysed by a JEOL-7001F operated at 15 kV. Solid samples were used for the SEM and EDX analysis.

Circular Dichroism Spectrometer (CD)
The protein solution was analysed by a Jasco (Model J-810) at the wavelength 200-250 nm. The result obtained was studied using origin software.

* *Characterisations of graphene oxide materials have been discussed in section 4.2 (page 136)*

Synthesis of Graphene Oxide (GO) 46

Graphite flakes **45** (3.0 g, 1.0 eq) was mixed to the 9:1 mixture of cool concentrated H_3PO_4/ H_2SO_4 (40: 360 mL) and added to 18.0 g of $KMnO_4$ (6.0 eq), a slight exotherm (around 40 °C) produced. The reaction was stirred and refluxed at 50 °C for 24 hours. The reaction was allowed to cool at room temperature. The mixture reaction was poured onto ice (500 mL) with 3 mL of 30% H_2O_2. The crude product was centrifuged (4000 rpm, 30 min) and the supernatant produced was decanted off. The crude product was then washed several times with 400 mL of water, 400 mL of 30% HCl, and 400 mL of ethanol until the pH of the crude product was constant. Diethyl ether (400 mL) was added to coagulate and the suspension formed was filtered. The precipitate obtained on the filter was vacuum-dried for 24 hours at room temperature. The product (5.8 g) obtained as a dark brown solid.

4.5.2 Synthesis of Functionalised Graphene Oxide

Graphene Oxide - Tyr-OCH_3 (Methyl ester) 47

GO (0.20 g, 1 eq) was dispersed in deionised water (100 mL) and was sonicated with ultrasonic oscillation for 3 hours. The mixture was added to the 10eq of L-tyrosine methyl ester (2.0 g, 12 mmol), DMAP (2.93 g, 24.0 mmol) and followed by triethylamine (3.67 g, 36.0 mmol) and EDC.HCl (4.64 g, 24.0 mmol). The reaction mixture was stirred and refluxed at 75 °C for 24 hours. The reaction was allowed to cool at room temperature. The crude product was washed with brine (100 mL x 3). The filtrate was centrifuged for 45 minutes (4000 rpm) and the supernatant produced was decanted off. The precipitate produced was washed again with 2 L of water and ethanol and dried at 60 °C. The product (0.40 g) obtained as a black solid.

Graphene Oxide - Tyr (Mono-Deprotection) 48

GO (0.20 g, 1 eq) was dispersed in 100 ml of deionised water and was sonicated with ultrasonic oscillation for 4 hours. The mixture was mixed with 20 mL of KOH (2 M) and refluxed at 75 °C for 24 hours. The reaction mixture was stirred and allowed to cool at room temperature. 20 mL of sulfuric acid (2 M) was added and sonicated again with ultrasonic oscillation for another 4 hours. The crude product was washed with brine solution (100 mL x 4) and dried with Mg_2SO_4. The crude product was filtered and dried at 60 °C. The product (0.33g) obtained as a black powder.

Graphene Oxide - Tyr (Oligo) 49

GO (0.20 g, 1 eq) was dispersed in deionised water (100 mL) and sonicated with ultrasonic oscillation for 4 hours. The mixture was added to the excess of L-tyrosine and DMAP (2.93 g, 24.0 mmol), and followed by triethylamine (3.67 g, 36.0 mmol) and EDC.HCl (4.64 g, 24.0 mmol). The reaction mixture was stirred and refluxed at 75 °C for 24 hours. The reaction mixture was allowed to cool at room temperature and washed with brine (100 mL x 4). The filtrate was centrifuged for 45 minutes (4000 rpm) and the supernatant produced was decanted off. The precipitate formed was washed again with water and ethanol. The product was dried at 60 °C and (0.41 g) of product obtained as a black solid.

Graphene Oxide - Phe (Oligo) 50

GO (0.20 g, 1 eq) was dispersed in deionised water (100 mL) and sonicated with ultrasonic oscillation for 4 hours. The mixture was added to the excess of L-phenylalanine and DMAP (2.93 g, 24.0 mmol), and followed by triethylamine (3.67 g, 36.0 mmol) and EDC.HCl (4.64 g, 24.0 mmol). The reaction mixture was stirred and refluxed at 75 °C for 24 hours. The reaction was allowed to cool to room temperature and washed with brine (100 mL x 3). The filtrate was centrifuged for 45 min (4000 rpm) and the supernatant produced was decanted off. The precipitate formed was washed again with water and ethanol. The product was dried at 60 °C and (0.44 g) of product was obtained as a black solid.

4.5.3 The inhibition of *α*-chymotrypsin using graphene Oxide

General procedure:

All of the specimens were dissolved in 5 mM of phosphate buffer (pH 7.4) at 25 ºC. GO prepared with different concentration (0.15, 0.30, 0.60 and 1.20 μg/mL), and were incubated with 1.0×10^{-6} M Chy for 24 hours prior to assay. For control experiment, the cuvette began with Chy and buffer solution (1.0 mL *α*-chymotrypsin and 1.0 mL phosphate buffer) or 2.0 mL protein-GO/functionalised solution and was added with 0.5 mL BTNA **26**. Hydrolysis of the BTNA **26** substrate was monitored by recording the 4-nitroaniline absorbance at λ = 410 nm at 120 second intervals for a period of 2400 s.

Assay of GO-Chymotrypsin Activity

The enzyme activity was measured at final BTNA **26** (substrate) concentrations of 2.0 μM, 4.0 μM, 6.0 μM and 8.0 μM at different concentration of GO/functionalised GO. All experiments were performed at an enzyme final concentration of 0.4 μM. Initial velocity for each GO/substrate combination was obtained by linear fittings of 4-nitroaniline production over the time using Graphpad prism 7.0. Initial velocity conditions were observed in all cases. All absorption readings are recorded at least three times. The data obtained was plotted and analysed using the Mixed mode inhibition model and transformed into Lineweaver-burk plot.

Chapter 5

Conclusion

5.0 Conclusion

Having studied dendrimers and graphene oxide, it can be concluded that is possible to functionalise the macromolecules to increase protein affinity. GO's layer can be covalently functionalised, while the dendrimers can be functionalised using a non-covalent method. All the inhibitor systems were investigated in order to find their optimum binding and the data that was obtained confirmed our predictions. These predictions were based on the work of Thorn and Bogan regarding the general population of amino acids throughout a protein and at their surface. [12]

The data summarised in Table 36 shows that GO and functionalised GO are the best and strongest inhibitors. However, higher binding is not always preferable, and it is more important for the inhibitor to be specific and selective when binding to the surface of the enzyme. Therefore, our aim was not to inhibit the protein, but rather to develop a method for increasing selectivity.

Inhibitor	Molecular weight ($gmol^{-1}$)	α	K_i (µM) / $\mu moldm^{-3}$	K_i (µg/ml)
*GO **46**	n/a	3.74 (±0.044)	n/a	0.53
GO-Tyr (Mono) **48**	n/a	4.84 (±0.012)	n/a	0.14
*G3.5-COOH **12**	5562	2.57 (± 0.002)	0.31	1.72
G3.5-COOH-Tyr **24**	7746 (estimated)	3.02 (±0.002)	0.19	1.47

Table 36:The Kinetic parameters as a comparison for unfunctionalised or functionalised (GO and dendrimer) to inhibit Chy.

GO is very hard to functionalise and it is impossible to control where on the surface each amino acid goes. The study did not attempt to bind GO with another protein and it was anticipated that the GO might not be selective. It is likely that GO can inhibit any type of positively charged protein, since it has layers of negatively charged groups on the surface. However, with respect to size and functionality, the dendrimers are both versatile and

controllable. Although dendrimer binding is weaker than that of GO, it seems likely that it is more selective and future work will investigate whether or not this is feasible.

Chapter 6

References

6.0 References

1. Chothia, C. & Janin, J. Principles of protein-protein recognition. *Nature* **256**, 705–708 (1975).
2. Hashimoto, M., Rockenstein, E., Crews, L. & Masliah, E. Role of protein aggregation in mitochondrial dysfunction and neurodegeneration in Alzheimer's and Parkinson's diseases. *NeuroMolecular Med.* **4**, 21–35 (2003).
3. Tao, S. C., Li, Y., Zhou, J., Qian, J., Schnaar, R. L., Zhang, Y., Goldstein, I. J., Zhu, H. & Schneck, J. P. Lectin microarrays identify cell-specific and functionally significant cell surface glycan markers. *Glycobiology* **18**, 761–769 (2008).
4. Whitford, D. *Proteins: Structure and Function*. (John Wiley and Sons Ltd, 2005).
5. Jones, S. & Thornton, J. M. Principles of protein-protein interactions. *Proc. Natl. Acad, Sci* **93**, 13–20 (1996).
6. Stefan, M. I. & Nove, N. Le. Cooperative Binding. *PLOS Comput. Biol.* **9**, 2–7 (2013).
7. Stites, W. Protein-protein interactions: interface structure, binding thermodynamics, and mutational analysis. *Chem. Rev.* **97**, 1233–1250 (1997).
8. Conte, L. Lo, Chothia, C. & Janin, È. The Atomic Structure of Protein-Protein Recognition Sites. *J. Mol. Biol.* **285**, 2177–2198 (1999).
9. Reichmann, D., Rahat, O., Cohen, M., Neuvirth, H. & Schreiber, G. The molecular architecture of protein-protein binding sites. *Curr. Opin. Struct. Biol.* **17**, 67–76 (2007).
10. Argos, P. An investigation of protein subunit and domain interfaces. *Protein Eng. Des. Sel.* **2**, 101–113 (1988).
11. Tsai, C. J., Lin, S. L., Wolfson, H. J. & Nussinov, R. Studies of protein-protein interfaces: a statistical analysis of the hydrophobic effect. *Protein Sci.* **6**, 53–64 (1997).
12. Bogan, A. A. & Thorn, K. S. Anatomy of hot spots in protein interfaces. *J. Mol. Biol.* **280**, 1–9 (1998).
13. Clarkson, T. & Wells, J. a. A hot spot of binding energy in a hormone-receptor interface. *Science* . **267**, 383–386 (1995).
14. Jain, R. K. & Hamilton, A. D. Protein surface recognition by synthetic receptors based on a tetraphenylporphyrin scaffold. *Org. Lett.* **2**, 1721–1723 (2000).
15. Yin, H. & Hamilton, A. D. Strategies for targeting protein-protein interactions with synthetic agents. *Angew. Chemie - Int. Ed.* **44**, 4130–4163 (2005).
16. Fry, D. C. Protein – Protein Interactions as Targets for Small Molecule Drug Discovery. **84**, 535–552 (2006).
17. D. Kuritzkes, S. K. and P. K. Fresh from the Pipeline: Maraviroc. *Nat. Rev. Drug Discov.* **7**, 15–16 (2008).
18. Arkin, M. R., Tang, Y. & Wells, J. A. Small-Molecule Inhibitors of Protein-Protein Interactions: Progressing toward the Reality Michelle. *Chem. Biol.* **21**, 1102–1114 (2014).
19. Alderton, W. K., Cooper, C. E. & Knowles, R. G. Nitric oxide synthases : structure , function and inhibition. *Biochem. J* **615**, 593–615 (2001).
20. Carrington, B., Myers, W. K., Horanyi, P., Calmiano, M. & Lawson, A. D. G. Natural

Conformational Sampling of Human TNF α Visualized by Double Electron-Electron Resonance. *Biophys. J.* **113**, 371–380 (2017).
21. Miller, S. E., Thomson, P. F. & Arora, P. S. Synthesis of Hydrogen-Bond Surrogate α-Helices as Inhibitors of Protein-Protein Interactions. in *Curr. Protoc. Chem. Biol* **6**, 101–116 (John Wiley & Sons, Inc, 2014).
22. Wang, D., Lu, M. & Arora, P. S. Inhibition of HIV-1 Fusion by Hydrogen-Bond-Surrogate-Based a Helices. *Angew. Chemie - Int. Ed.* **47**, 1879–1882 (2008).
23. Renner, C., Kusebauch, U., M. Löweneck, Milbradt, A. G. & Moroder, L. Azobenzene as photoresponsive conformational switch in cyclic peptides. *Chem. Biol. Drug Des.* **65**, 4–14 (2005).
24. Akio Ojida, Masa-aki Inoue, Yasuko Mito-Oka & Itaru Hamachi. Cross-Linking Strategy for Molecular Recognition and Fluorescent Sensing of a Multi-phosphorylated Peptide in Aqueous Solution. *J. Am. Chem. Soc.* **125**, 10184–5 (2003).
25. Leung, D. K., Yang, Z. & Breslow, R. Selective disruption of protein aggregation by cyclodextrin dimers. *Proc. Natl. Acad, Sci* **97**, 5050–5053 (2000).
26. Edgar, J. Biphenyls as Potential Mimetics of Protein alpha-Helix. *Bioorg. Med. Chem. Lett.* **12**, 891–893 (2002).
27. Nguyen, K. T., Syed, S., Urwyler, S., Bertrand, S., Bertrand, D. & Reymond, J.-L. Discovery of NMDA-Glycine Site Inhibitors from the Chemical Universe Database GDB. *ChemMedChem* **3**, 1520–1524 (2008).
28. Lee, J. H., Zhang, Q., Jo, S., Chai, S. C., Oh, M., Im, W., Lu, H. & Hyun-Suk Lim. Novel Pyrrolopyrimidine-Based α-Helix Mimetics: Cell-Permeable Inhibitors of Protein−Protein Interactions. *J. Am. Chem. Soc.* **133**, 676–679 (2010).
29. Guo, W., Wisniewski, J. A. & Ji, H. Hot spot-based design of small-molecule inhibitors for protein – protein interactions. *Bioorg. Med. Chem. Lett.* **24**, 2546–2554 (2014).
30. Srivastava, S., Verma, A., Frankamp, B. L. & Rotello, V. M. Controlled assembly of protein-nanoparticle composites through protein surface recognition. *Adv. Mater.* **17**, 617–621 (2005).
31. De, M., Chou, S. S. & Dravid, V. P. Graphene oxide as an enzyme inhibitor: Modulation of activity of α-chymotrypsin. *J. Am. Chem. Soc.* **133**, 17524–17527 (2011).
32. Ahmada, I., Mozhia, A., Yanga, L., Hana, Q., Lianga, X., Lia, C., Yanga, R. & Chen Wang. Graphene oxide-iron oxide nanocomposite as an inhibitor of Aβ 42 amyloid peptide aggregation. *Colloids Surfaces B Biointerfaces* **159**, 540–545 (2017).
33. Svenson, S. & Tomalia, D. A. Dendrimers in biomedical applications - Reflections on the field. *Adv. Drug Deliv. Rev.* **57**, 2106–2129 (2005).
34. Moiani, D., Salvalaglio, M., Cavallotti, C., Bujacz, A., Redzynia, I., Bujacz, G., Dinon, F., Pengo, P. & Fassina, G. Structural Characterization of a Protein A Mimetic Peptide Dendrimer Bound to Human IgG. *J. Phys. Chem* **113**, 16268–16275 (2009).
35. Chiba, F., Hu, T. C., Twyman, L. J. & Wagstaff, M. Dendrimers as size selective inhibitors to protein-protein binding. *Chem Commun* 4351–4353 (2008). doi:10.1039/b806517a

36. Kim, R. M., Manna, M., Hutchins, S. M., Griffin, P. R., Yates, A., Bernick, A. M., Chapman, K. T., Griffin, P. R., Yates, N. A., Bernick, A. M. Y. M. & Chapman, K. T. Dendrimer-Supported Combinatorial Chemistry Published. *Proc. Natl. Acad. Sci. U. S. A.* **93**, 10012–10017 (1996).
37. Li, J., Nowak, P. & Otto, S. Dynamic Combinatorial Libraries : From Exploring Molecular Recognition to Systems Chemistry. *J. Am. Chem. Soc* **135**, 9222–9239 (2013).
38. Huang, R. & Leung, I. K. H. Protein-Directed Dynamic Combinatorial Chemistry : A Guide to Protein Ligand and Inhibitor Discovery. *Molecules* **27**, 910 (2016).
39. Liu, R., Li, X. & Lam, K. S. Combinatorial Chemistry in Drug Discovery. *Curr. Opin. Chem. Biol.* **38**, 117–126 (2017).
40. Fletcher, S. & Hamilton, A. D. Targeting protein – protein interactions by rational design : mimicry of protein surfaces. *J. R. Soc. Interface* **3**, 215–233 (2006).
41. Toogood, P. L. Inhibition of Protein−Protein Association by Small Molecules: Approaches and Progress. *J. Med. Chem.* **45**, 1543–1558 (2002).
42. Babine, R. E. & Bender, S. L. Molecular Recognition of Protein − Ligand Complexes : Applications to Drug Design. *Chem. Rev.* **97**, 1359–1472 (1997).
43. Shaunak, S., Thomas, S., Gianasi, E., Godwin, A., Jones, E., Teo, I., Mireskandari, K., Luthert, P. *et al.* Polyvalent dendrimer glucosamine conjugates prevent scar tissue formation. *Nat. Biotechnol.* **22**, 977–984 (2004).
44. Palen, E. The Enzyme Kinetic Activity of Chymotrypsin : Temperature and pH Effects , Determination of K m , V max , and Inhibitor Effects. 1–11 (2011).
45. Torchilin, V. P. Drug targeting. *Eur. J. Pharm. Sci.* **11**, S81–S91 (2000).
46. Abbasi, E., Aval, S., Akbarzadeh, A., Milani, M., Nasrabadi, H., Joo, S., Hanifehpour, Y., Nejati-Koshki, K. & Pashaei-Asl, R. Dendrimers: synthesis, applications, and properties. *Nanoscale Res. Lett.* **9**, 247 (2014).
47. Tsou, L. K., Jain, R. K. & Hamilton, A. D. Protein surface recognition by porphyrin-based receptors. *J. Porphyr. Phthalocyanines* **08**, 141–147 (2004).
48. Nanoparticles, A. A. G., You, C., De, M., Han, G. & Rotello, V. M. Tunable Inhibition and Denaturation of r -Chymotrypsin with Fabrication of Amino Acid-Functionalized Gold Nano-. 12873–12881 (2005).
49. Gao, W. The chemistry of graphene oxide. *Graphene Oxide Reduct. Recipes, Spectrosc. Appl.* 61–95 (2015).
50. Jha, A. N., Vishveshwara, S. & Banavar, J. R. Amino acid interaction preferences in proteins. *Protein Sci.* **19**, 603–616 (2010).
51. Gilles, P., Wenck, K., Stratmann, I., Kirsch, M., Smolin, D. A., Schaller, T., De Groot, H., Kraft, A. & Schrader, T. High-Affinity Copolymers Inhibit Digestive Enzymes by Surface Recognition. *Biomacromolecules* **18**, 1772–1784 (2017).
52. Ciolkowski, M., Rozanek, M., Bryszewska, M. & Klajnert, B. The influence of PAMAM dendrimers surface groups on their interaction with porcine pepsin. *Biochim. Biophys. Acta - Proteins Proteomics* **1834**, 1982–1987 (2013).
53. Munro, P. D., Jackson, C. M. & Winzor, D. J. Consequences of the non-specific binding of a protein to a linear polymer: Reconciliation of stoichiometric and equilibrium titration data for the thrombin-heparin interaction. *J. Theor. Biol.* **203**, 407–418 (2000).

54. Smith, K. & Twyman, L. J. A comparison of dendrimers and hyperbranched polymers for the encapsulation of poorly soluble drugs. **MChem**, (University of Sheffield, 2012).
55. Ficker, M., Petersen, J. F., Hansen, J. S. & Christensen, J. B. Guest-host chemistry with dendrimers-binding of carboxylates in aqueous solution. *PLoS One* **10**, 1–12 (2015).
56. Esfand, R. & Tomalia, D. a. Poly(amidoamine) (PAMAM) dendrimers: From biomimicry to drug delivery and biomedical applications. *Drug Discov. Today* **6**, 427–436 (2001).
57. Tomalia, D. A., Baker, H., Dewald, J., Hall, M., Kallos, G., Martin, S., J. Roeck, J. R. & Smith, P. A New Class of Polymers: Starburst-Dendritic Macromolecules. *Polym. J.* **17**, 117–132 (1985).
58. Khurana, K. & Twyman, L. J. Exploring a new methodology for drug delivery using non covalent chemistry. (University of Sheffield, 2015).
59. Chandrudu, S., Simerska, P. & Toth, I. Chemical Methods for Peptide and Protein Production. *Molecules* **18**, 4373–4388 (2013).
60. Sheehan, J. C. & Hess, G. P. A New Method of Forming Peptide Bonds. *J. Am. Chem. Soc.* **77**, 1067–1068 (1955).
61. Pande, S. & Crooks, R. M. Analysis of poly(amidoamine) dendrimer structure by UV-Vis spectroscopy. *Langmuir* **27**, 9609–9613 (2011).
62. Kesharwani, P., Jain, K. & Jain, N. K. Dendrimer as nanocarrier for drug delivery. *Prog. Polym. Sci.* **39**, 268–307 (2014).
63. Copeland, R. A. A Practical Introduction to Structure, Mechanism, and Data Analysis. in *Analytical Biochemistry* **291**, 278 (Wiley-Blackwell, 2001).
64. Berg, J., John, M., Tymoczko., L. & Stryer., L. *Biochemistry*. (W.H. Freeman and Company, 2007).
65. Paul F. Cook, W. W. C. *Enzyme Kinetics and Mechanism*. (Garland Science, 2007).
66. Garrett, R. H. & Charles M. Grisham. *Biochemistry*. *Brooks Cole, a divisin 0f Cengage Learning . Inc* (2013).
67. Chiba, F. & Twyman, L. J. Effect of Terminal-Group Functionality on the Ability of Dendrimers to Bind Proteins. *Bioconjug. Chem.* **28**, 2046–2050 (2017).
68. Wenck, K., Koch, S., Renner, C., Sun, W. & Schrader, T. A noncovalent switch for lysozyme. *J. Am. Chem. Soc.* **129**, 16015–16019 (2007).
69. Wang, M. & Twyman, L. J. Investigating the Inhibition of Protein-Protein Interactions by PAMAM Dendrimers. (University of Sheffield, 2014).
70. Morgan, M. T., Nakanishi, Y., Kroll, D. J., Griset, A. P., Carnahan, M. a., Wathier, M., Oberlies, N. H., Manikumar, G., Wani, M. C. & Grinstaff, M. W. Dendrimer-encapsulated camptothecins: Increased solubility, cellular uptake, and cellular retention affords enhanced anticancer activity in vitro. *Cancer Res.* **66**, 11913–11921 (2006).
71. Yavuz, B., Pehlivan, S. B. & Unlu, N. Dendrimeric systems and their applications in ocular drug delivery. *ScientificWorldJournal.* **2013**, 732340 (2013).
72. Yung-Chi, C. & Prusoff, W. H. Relationship between the inhibition constant (KI) and the concentration of inhibitor which causes 50 per cent inhibition (I50) of an enzymatic reaction. *Biochem. Pharmacol.* **22**, 3099–3108 (1973).

73. Woody, R. W. & Dunker, A. K. *Aromatic and Cystine Side-Chain Circular Dichroism in Proteins.* (Springer, Boston, MA, 1996).
74. Chiba, F., Mann, G. & Twyman, L. J. Investigating possible changes in protein structure during dendrimer-protein binding. *Org Biomol Chem* **8**, 5056–5058 (2010).
75. Battistuzzi, G., Loschi, L., Borsari, M. & Sola, M. Effects of nonspecific ion-protein interactions on the redox chemistry of cytochrome c. *J. Biol. Inorg. Chem.* **4**, 601–607 (1999).
76. Allhorn, M. & Klapyta, A. Redox properties of the lipocalin a 1 -microglobulin : Reduction of cytochrome c , hemoglobin , and free iron. *Free Radic. Biol. Med.* **38**, 557–567 (2005).
77. Yamaguchi, Y., Kato, N., Azuma, H., Nagasaki, T. & Ohkanda, J. Protein recognition of hetero-/homoleptic ruthenium(II) tris(bipyridine)s for a-chymotrypsin and cytochrome c. *Bioorg. Med. Chem. Lett.* **22**, 2354–2358 (2012).
78. Yang, D., Shin, J., Choi, M. & De, C. L. Cytochrome c assembly on fullerene nanohybrid metal oxide ultrathin films. *RSC Adv.* **6**, 19173–19181 (2016).
79. Braun, M., Atalick, S., Guldi, D. M., Lanig, H., Brettreich, M., Burghardt, S., Hatzimarinaki, M., Ravanelli, E., Prato, M., Eldik, R. Van & Hirsch, A. Electrostatic Complexation and Photoinduced Electron Transfer between Zn-Cytochrome c and Polyanionic Fullerene Dendrimers. *Chem. Eur. J* **9**, 3867–3875 (2003).
80. Chigu, N. L. & Hirosue, S. Cytochrome P450 monooxygenases involved in anthracene metabolism by the white-rot basidiomycete Phanerochaete chrysosporium. *Appl. Microbiol Biotechnol* **87**, 1907–1916 (2010).
81. Clark-ferris, K. K. & Fisher, J. Topographical mimicry of the enzyme binding domain of cytochrome c. *J. Am. Chem. Soc.* **107**, 5007–5008 (1985).
82. Aya, T. & Hamilton, A. D. Tetrabiphenylporphyrin-based receptors for protein surfaces show sub-nanomolar affinity and enhance unfolding. *Bioorganic Med. Chem. Lett.* **13**, 2651–2654 (2003).
83. Hamuro, Y., Calama, M. C., Park, H. S. & Hamilton, A. D. A Calixarene with Four Peptide Loops: An Antibody Mimic for Recognition of Protein Surfaces. *Angew. Chemie Int. Ed.* **36**, 2680–2683 (1997).
84. Park, H. S., Lin, Q. & Hamilton, A. D. Protein Surface Recognition by Synthetic Receptors: A Route to Novel Submicromolar Inhibitors for α-Chymotrypsin. *J Am Chem Soc* **121**, 8–13 (1999).
85. Douglas, R. & John, C. Mitochondria and apoptosis. *Science.* **281**, 1309–1312 (1998).
86. Martos, V., Castreño, P., Valero, J. & de Mendoza, J. Binding to protein surfaces by supramolecular multivalent scaffolds. *Curr. Opin. Chem. Biol.* **12**, 698–706 (2008).
87. Zhou, H., Baldini, L., Hong, J., Wilson, A. J. & Hamilton, A. D. Pattern Recognition of Proteins Based on an Array of Functionalized Porphyrins. *J Am Chem Soc* **128**, 2421–2425 (2006).
88. Crowley, P. B., Ganji, P. & Ibrahim, H. Protein Surface Recognition : Structural Characterisation of Cytochrome c – Porphyrin Complexes. *ChemBioChem* **9**, 1029–1033 (2008).
89. Jain, R. K. & Hamilton, A. D. Designing Protein Denaturants : Synthetic Agents Induce Cytochrome c Unfolding at Low Concentrations and Stoichiometries. *Angew.*

Chem. Int. Ed. Engl **41**, 641–643 (2002).
90. Parr, G. R. & Robert F. Pasternack. The Interaction of Some Water-Soluble Porphyrins and Metalloporphyrins with Human Serum AIbumin. *Bioinorg. Chem.* **7**, 277–282 (1977).
91. Robert F. Pasternack, Gillies, S. & Julia P. Stromsted. Substitution reactions of a water-soluble metalloporphyrin with azide and 1,1,3,3-tetramethyl-2-thiourea. *Bioinorg. Chem.* **8**, 33–44 (1978).
92. Paul, D., Miyake, H., Shinoda, S. & Tsukube, H. Proteo-Dendrimers Designed for Complementary Recognition of Cytochrome c : Dendrimer Architecture toward Nanoscale Protein Complexation. *Chem. Eur. J* **12**, 1328–1338 (2006).
93. Adler, A. D.; Longo, F. R.; Finarelli, J. D.; Goldmacher, J.; Assour, J.; Korsakoff, L. J. Condensation of Pyrrole with Benzaldehyde Under Adler Conditions; Tetraphenylporphyrins. *Org. Chem* **32**, 476–476 (1967).
94. Andre Geim - Facts". Nobelprize.org. Nobel Media AB 2014. No Title. Available at: http://www.nobelprize.org/nobel_prizes/physicslaureates/2010/geim-facts.html. (Accessed: 3rd August 2018)
95. Luo, Q., Dong, Z., Hou, C. & Liu, J. Protein-based supramolecular polymers: progress and prospect. *Chem. Commun.* **50**, 9997–10007 (2014).
96. Yan, M., Liang, Q., Wan, W., Han, Q., Tan, S. & Ding, M. Amino acid-modified graphene oxide magnetic nanocomposite for the magnetic separation of proteins. *RSC Adv.* **7**, 30109–30117 (2017).
97. Mallakpour, S., Abdolmaleki, A. & Borandeh, S. Fabrication of amino acid-based graphene-zinc oxide (ZnO) hybrid and its application for poly(ester-amide)/graphene-ZnO nanocomposite synthesis. *J. Thermoplast. Compos. Mater.* **30**, 358–380 (2017).
98. Rambabu, G. & Bhat, S. D. Amino acid functionalized graphene oxide based nanocomposite membrane electrolytes for direct methanol fuel cells. *J. Memb. Sci.* **551**, 1–11 (2018).
99. González-Domínguez, J. M., Gutiérrez, F. A., Hernández-Ferrer, J., Ansón-Casaos, A., Rubianes, M. D., Rivas, G. & Martínez, M. T. Peptide-based biomaterials. Linking l-tyrosine and poly l-tyrosine to graphene oxide nanoribbons. *J. Mater. Chem. B* **3**, 3870–3884 (2015).
100. Marcano, D., Kosynkin, D., Berlin, J. , Sinitskii, A., Sun, Z., Slesarev, A., Alemany, L. B., Lu, W. & Tour, J. M. Improved synthesis of graphene oxide. *ACS Nano* **4**, 4806–4814 (2010).
101. Azimi, S. Preparation and Application of Graphene Oxide/Functionalized Graphene Oxide Nanostructures as Antibacterial Agents. (Razii University, 2013).
102. Kumar, M., Swamy, B. E. K., Asif, M. H. M. & Viswanath, C. C. Preparation of alanine and tyrosine functionalized graphene oxide nanoflakes and their modified carbon paste electrodes for the determination of dopamine. *Appl. Surf. Sci.* **399**, 411–419 (2017).
103. Dimiev, A. M. & Tour, J. M. Mechanism of graphene oxide formation. *ACS Nano* **8**, 3060–3068 (2014).
104. Kumar, P., Kanaujia, P. K., Vijaya Prakash, G., Dewasi, A., Lahiri, I. & Mitra, A. Growth of few- and multilayer graphene on different substrates using pulsed

nanosecond Q-switched Nd:YAG laser. *J. Mater. Sci.* **52**, 12295–12306 (2017).
105. Graf, D. & Ensslin, K. Spatially Resolved Raman Spectroscopy of Single- and Few-Layer Graphene. *Solid State Phys.* **7**, 1–6 (2006).
106. Arthi G, P. B. & BD, L. A Simple Approach to Stepwise Synthesis of Graphene Oxide Nanomaterial. *J. Nanomed. Nanotechnol.* **06**, 2–5 (2015).
107. Meng, H., Sui, G. X., Fang, P. F. & Yang, R. Effects of acid- and diamine-modified MWNTs on the mechanical properties and crystallization behavior of polyamide 6. *Polymer (Guildf).* **49**, 610–620 (2008).
108. Kuilla, T., Bhadra, S., Yao, D., Kim, N. H., Bose, S. & Lee, J. H. Recent advances in graphene based polymer composites. *Prog. Polym. Sci.* **35**, 1350–1375 (2010).
109. Hedstrom, L. Serine protease mechanism and specificity. *Chem. Rev.* **102**, 4501–4523 (2002).
110. Copeland, R. A. Evaluation of Enzyme Inhibitors in Drug Discovery: A Guide for Medicinal Chemists and Pharmacologists. in 25–55 (John Wiley & Sons, Inc, 2005).
111. Dobson, C. M. The fundamental mechanism of protein folding. *Nature* **426**, (2003).